REACTION KINETIC STUDY OF NONCATALYZED HYDROTHERMAL LIQUEFACTION OF ORGANIC WASTE MODEL COMPOUNDS

A Thesis

Presented to the Faculty of the Graduate School

of Cornell University

in Partial Fulfillment of Requirements for the Degree of

Master of Science

by

Huiyong Li

August 2018

ABSTRACT

My research addresses how cellulose in waste biomass was converted into biochemical products through hydrothermal liquefaction (HTL). In HTL experiments, aqueous product samples were collected at different reaction times, separated by vacuum filtration, and analyzed by High Performance Liquid Chromatography (HPLC). Exponentially Modified Gaussian (EMG) model was applied to fitting the HPLC curves of the standards under different concentrations. The EMG model corresponded well with each curve with mean percent error (MPE) values less than 3%. Overlapping HPLC signals were observed and resolved computationally using the superposition of EMG functions. To simulate HTL reaction kinetics, various reaction pathway schemes were proposed based on the experimental findings. Best-fit reaction kinetic parameters were derived from an optimization of the errors of reaction kinetic modeling. The reaction kinetics will help entrepreneurs and researchers optimally produce selective commodity biochemical from waste biomass to provide alternatives to the petrochemical industry.

BIOGRAPHICAL SKETCH

Huiyong Li was born and raised in Guangzhou, China. Graduating from Guangya High School in Guangzhou, he was interested in developing alternatives to fossil fuels, as he wanted to resolve the pollution of atmosphere and Pearl River, the mother river of Guangzhou. Huiyong majored in energy engineering at South China University of Technology (SCUT). He was an international transfer student in the Rutgers-SCUT 2+2 Transfer Program in 2014. He graduated *summa cum laude* from Rutgers, the State University of New Jersey in May of 2016 with a Bachelor of Science Degree in Chemical Engineering. He also earned a Bachelor of Engineering Degree in Energy Engineering and Automation from South China University of Technology in July of 2016. After college graduation, he became a student in the Master of Science Program in Chemical Engineering at Cornell University. For his undergraduate research in developing computational tools to systematically evaluate the thermodynamic and structural behaviors of supercritical oxygen molecules, he published a paper, "Widom Line, Dynamical Crossover and Percolation Transition of Supercritical Oxygen via Molecular Dynamics Simulations", in *the Journal of Chemical Physics* in January 2018. Furthermore, he contributed to the pest control study at SCUT with two publications in *the Chinese Journal of Pest Control* and *International Journal of Food Engineering* respectively. Motivated by solving the global energy crisis, Huiyong is now focused on the conversion chemistry from waste biomass into biofuels and biochemicals at Cornell University. He plans to continue researching biofuels as a PhD student at Washington University in St. Louis later in Fall 2018.

ACKNOWLEDGEMENTS

I would like to express great appreciation to the people and institutions along the way to my MS graduation at Cornell. Thanks to my family for always caring about my situation in the United States and financially supporting me through my study. Thanks to the Chemical and Biomolecular Engineering Department at Cornell University for admitting me into such an inclusive and extraordinary program and providing great resources through my MS study. Thanks to Dr. Borja Cantero-Tubila and Dr. Roy Posmanik for their experimental work for mentoring my research. I also want to thank Prof. Jefferson Tester for serving as my committee chair with his precious advice on reaction kinetic modeling and his continuous support in this thesis process. Furthermore, I want to express my appreciation for the other members of my committee, Prof. Fengqi You and Prof. Matthew Reid, who helped me with the computational solutions for overlapping HPLC signals and provided me with encouragement throughout this research. I also would like to thank the English Language Support Office and the Knight Writing Institute of Cornell University for providing extraordinary assistance in improving my writing, speaking, and presentation skills. Thanks to Prof. Yee Chiew for motivating me to become an independent researcher when I conducted research on supercritical oxygen at Rutgers University. Thanks to my colleagues at Cornell for being great friends of me: Xiang, Ivan, Kartikay, Ventkesh, Rui, Zhiping, Arna, Andrea, etc. During my extracurricular time, the Cornell Badminton Club and Tennis Club are really amazing for providing me with sufficient support and excellent facilities. All my diligence, toughness, gratitude and other characteristics come from the love and support of my friends, my family, my teachers and my colleagues. Thank you to everyone who has helped me along the way.

TABLE OF CONTENTS

LIST OF FIGURES

LIST OF TABLES

LIST OF ABBREVIATIONS

The table below describes the significant abbreviations and acronyms in this thesis.

Abbreviation	Meaning
A	*Area* (a parameter in the Exponentially Modified Gaussian Model)
AA	Acetic Acid
Cellulose-300	The Hydrothermal Liquefaction Experiments using Cellulose as the feedstock with a preset reaction temperature of 300°C
EMG	Exponentially Modified Gaussian
Er	Erythrose
FA	Formic Acid
Fa	Formaldehyde
Fu	Furfural (also Named as 2-Furfuraldehyde)
G_1 or G1	Cellulo-Monomers
G_{11} or G11	Glucose
G_{12} or G12	Fructose
G_2 or G2	Cellobiose
G_3 or G3	Cellotriose
G_4 or G4	Cellotetraose
GA	Glycolaldehyde
Glucose-275	The Hydrothermal Liquefaction Experiments using Glucose as the Feedstock with a Preset Reaction Temperature of 275°C
Glucose-300	The Hydrothermal Liquefaction Experiments using Glucose as the Feedstock with a Preset Reaction Temperature of 300°C
G_n	Cellulose
HMF	5-Hydroxymethylfurfural
HPLC	High Performance Liquid Chromatography
HTL	Hydrothermal Liquefaction
k	Reaction Rate Constant

LA	Levulinic Acid
Levulinic-300	The Hydrothermal Liquefaction Experiments using Levulinic Acid as the Feedstock with a Preset Reaction Temperature of 300°C
min	Minute
MPE	Mean Percent Errors
SA	Succinic Acid
SSE	Sum Squared Error
t_R	Retention Time (a Parameter in the Exponentially Modified Gaussian Model)
UDP	Undefined Degradation Products

CHAPTER 1

BACKGROUND AND MOTIVATION

1.1 Introduction

Understanding the physiochemical behaviors of subcritical and supercritical water is crucial for the optimal production of biofuels and selective commodity biochemicals from waste biomass. This chapter encompasses a background about HTL, my motivation for studying the reaction kinetics of the HTL of cellulose and a literature review about previous HTL studies.

Supercritical water and subcritical water have aroused great interest from researchers in many fields for their distinctive phase behaviors (Yang & Li, 1999; Koomyart, *et al*., 2016; Kumar & Gupta, 2009; Cantero-Tubilla, *et al*., 2017; Patwardhan, *et al*., 2013). Although there were varieties of conventional methods to convert biomass into biochemicals, the hydrothermal processes gained favor for sustainability and viability due to the abundant existence of water in biomass. As ***Figure 1*** shows, the phase diagram of water for hydrothermal processing can be divided into three major parts, liquefaction, catalytic gasification and high-temperature gasification. HTL process is a thermochemical process in aqueous phase to convert macromolecules in biomass into biochemicals and bio-oil under high pressure and moderate temperature up to the critical temperature of water. Near the critical point, physiochemical properties of water, including its ionization constant and density, experience dramatic changes. For the ionization of water, proton hydration has been proposed as a complete chemical expression given by Error! Reference source not found. (Bandura & Lvov, 2006; Marshall & Franck, 1981).

$$2H_2O \Leftrightarrow H_3O^+ + OH^- \quad (\mathbf{1})$$

The researchers assumed that the short-range ion-water interactions are generated with the structural and energetic changes in the boundary region of bulk water upon the transfer of water molecules from the bulk water to a cavity that is created by the release of hydrogen and hydroxide ions. At the same time, long-range polarization interactions play a significant role in the interactions between the solvation complex and bulk water (Bandura & Lvov, 2006). The results of the calculation of negative logarithm (base 10) of ionization constants of water K_W corresponded well with the available experimental data and indicated that under the selected pressures between 0 and 50 MPa and selected temperatures between 150°C and 350°C, the minimum of $-\log_{10} K_W$ occurred at the point of 300°C and 50 MPa with a value of 10.89 (Bandura & Lvov, 2006). Previous studies have shown that in the experiments, $-\log_{10} K_W$ is linearly correlated with $\log_{10} \rho_W$ measured at a certain temperature and pressure (Bandura & Lvov, 2006; Marshall & Franck, 1981; Matsugami, Yoshida, & Hirata, 2014). The temperature effect of the ion product of substance water was caused using the empirical fitted expression for $-\log_{10} K_W$ by ***(2***, where A, B, C, D, E, F, and G were empirical constants, and ρ_W was measured experimentally (Marshall & Franck, 1981).

$$\log_{10} \frac{K_W}{(\frac{mol}{kg})^2} = A + \frac{B}{T} + \frac{C}{T^2} + \frac{D}{T^3} + (E + \frac{F}{T} + \frac{G}{T^2}) \cdot \log_{10} \frac{\rho_W}{\frac{g}{cm^3}} \quad (\mathbf{2})$$

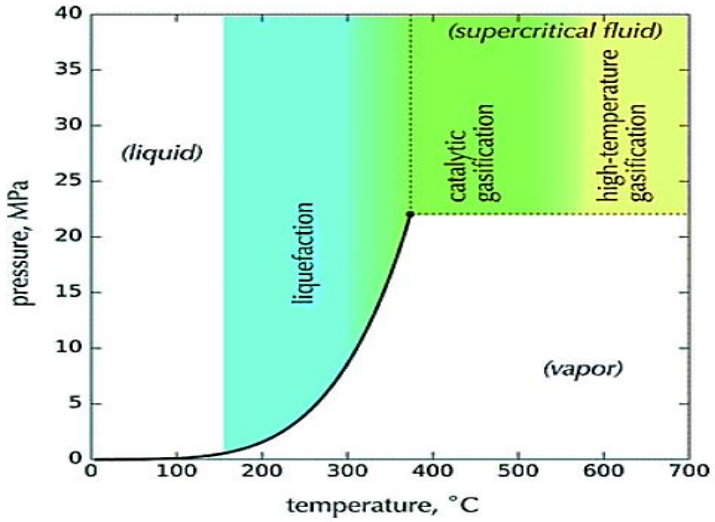

Figure 1: Phase diagram of water for hydrothermal processing of biomass (Peterson, *et al*., 2008).

The active ionization in the vicinity of the critical point provides a friendly environment for depolymerization of macromolecules in biomass. The ion effect on the structure and properties of bulk water was investigated to determine how ions could alter the hydrogen bonding in water molecules (Zhang & Cremer, 2006). Previous results showed that no long-range structure-making or structure-breaking in water molecules takes place in ionic solutions (Zhang & Cremer, 2006).

The biomass typically consists of 40–45 wt% cellulose as the most abundant natural macromolecule in biomass (Artemenko S., 2014). For most hydrocarbons, the vapor-liquid boundary begins to disappear near the critical point of water, maximizing the heat capacity and transport properties of soluble sugars (Artemenko S., 2014). The dissolution of cellulose in subcritical or supercritical water is a key step in the production of bio-oil and biochemical products during hydrothermal processes of biomass. In the experimental study of cellulose dissolution, it was concluded that cellulose dissolves in supercritical or subcritical water with the density of 800 kg/m^3 at the lowest dissolution temperature (Ogihara, 2005). With a higher density over 800 kg/m^3, drastically higher packing of cellulose caused elevated dissolution

temperature, thus restricting its access to bulk water (Ogihara, 2005). Researchers detected various essential biochemical products in subcritical and supercritical water, such as levulinic acid and HMF, at the residence times of 3-60 minutes (Knez, Škerget, & Pavlovič, 2013). The quick depolymerization from cellulose to soluble oligomers and monomers was observed, and the yields of bio-oil, aqueous, and gaseous products were derived at various residence times under different temperatures and pressures (Knez, Škerget, & Pavlovič, 2013). In this research project, the choice of model compounds were based on the natural abundance of cellulose in biomass and the role of glucose in the degradation pathways of cellulose. The reaction conditions, including temperature, pressure, residence time, and reactor atmosphere, were determined according to the phase behaviors of subcritical water in previous studies in the hydrothermal processing of biomass (Kumar & Gupta, 2009; Cantero-Tubilla, *et al*., 2017; Bandura & Lvov, 2006; Peterson, *et al*., 2008; Matsugami, Yoshida, & Hirata, 2014; Ogihara, 2005; Knez, Škerget, & Pavlovič, 2013).

1.2 Motivation

1.2.1. Biofuel Production for a Sustainable Future

Biofuels are derived from biomass through thermochemical and biochemical processes. They are widely considered to be an environmentally friendly substitute for fossil fuel. Similar to fossil fuels, biofuels have varieties of forms, including biodiesel, biochar, bioethanol, biogas and biocrude, which have already been commercially produced. Biofuels can be categorized based on the type of feedstock. First-generation biofuels are generated from edible feedstocks, such as sugarcane and corn. Although the first-generation biofuels account for the majority of commercial biofuels, today they have severely affected the food industry and thus have become

unsustainable for energy production (Bhatia, Kim, Yoon, & Yang, 2017). To seek for a sustainable solution, scientists have been studying non-edible feedstock for second-generation biofuel production. Novel pretreatment methods of raw biomass, such as microwave irradiation and sonication, have enabled gaseous products and soluble chemicals to be produced from cellulose and hemicellulose fraction in waste biomass (Bhatia, Kim, Yoon, & Yang, 2017). However, Bhatia *et al.*'s study did not include much information about hydrothermal processing while hydrothermal processing helps eliminate dehydration processes in biomass pretreatment processes, utilize the large heat potential of water to improve energy efficiency, and catalyze the depolymerization of macromolecules in biomass (Bhatia, Kim, Yoon, & Yang, 2017).

Aware of the adverse impacts of global warming, the United States is attempting to lower the carbon emissions by replacing fossil fuels with renewable energies. In the United States, food industry generates 36 million tons of food waste annually where a large amount of sugars, phenolic compounds and fatty acids are discharged (Posmanik, Cantero, Malkani, Sills, & Tester, 2017). The storage and disposal of food waste have caused environmental issues, such as contamination of soil and underground waters, and release of unpleasant odors to the neighborhood. To help solve the energy and environmental problems, the cellulose, lignin, and hemicellulose in the food residues can be hydrothermally processed for the production of biofuels and biochemicals. Standing out among thermochemical conversion methods, hydrothermal processes utilize a water phase under the subcritical and supercritical conditions and thus eliminate the energy requirements and costs of the dehydration steps in waste treatment. As outlined in **Chapter 2**, the goal of my research is to simulate the HTL reaction kinetics of the cellulose decomposition by investigating the reaction chemistry in the HTL of model compounds for organic wastes, including cellulose, glucose and levulinic acid. Based on a literature review,

reaction pathway schemes for the HTL experiments will be proposed in **Chapter 6** to understand the reaction chemistry and product evolution. **Chapter 7** is about the results and discussions.

1.2.2 Dilemma for HTL Reaction Kinetic Modeling

Few HTL studies have provided a thorough evaluation of analytical measurements and uncertainties in reaction kinetic modeling. Earlier in our group at Cornell, we demonstrated the effects of feedstock composition on the bio-oil carbon yields ranging from 10% to 80% on the effectiveness of hydrothermal processing of waste biomass. This study lacked adequate analysis of the aqueous products, which is crucial for understanding the formation of bio-oil (Posmanik, Cantero, Malkani, Sills, & Tester, 2017). Catalytic decomposition of fructose in subcritical water was explained by proposed reaction pathways from fructose to degradation products for reaction kinetic modeling (Asghari & Yoshida, 2007), but there remained several problems: first, their study did not consider glucose for isomerization kinetics, which could significantly affect the rate equation of the production of the degradation products; second, it did not examine the accuracy of the analytical measurements of HPLC; and third, uncertainties were not analyzed. Croce, *et al*. studied the HTL of combinations of organic waste model compounds examined the bio-oil products thoroughly in terms of analytical measurements and their elemental composition in comparison with that of petroleum crude oil. De Caprariis's research (de Caprariis, De Filippis, Petrullo, & Scarsella, 2017) focused on the effects of reaction temperature and biomass composition on bio-oil yield and its composition with a complete list of the aqueous products.

1.2.3 Availability of Experimental Data in Our Group at Cornell University

In our group, Dr. Roy Posmanik and Dr. Borja Cantero-Tubila used HPLC to analyze the product distribution in the aqueous products of the HTL experiments at various reactor residence times. The HPLC signals were recorded but not analyzed quantitively. They were further assessed through the HPLC signal modeling in my study, as described later in **Chapters 4** and **5**.

1.2.4 Scale-up Problems

Reaction kinetic modeling is the key to applying bench-scale experimental results to industrial processes using optimization tools. In the study by Tripodi, Compagnoni, Martinazzo, Ramis, and Rossetti, the integration of kinetic modeling with process simulation revealed the guidelines for system performance and therefore provided a solid basis for scaling up the process. The paper also compared the simulation data with the industrial data in catalytic ethanol reforming, concluding that formulation of the kinetic model for batch reactions in the inert-gas environment could be described using pseudo-homogeneous rate equations for the intermediates and products. Reaction rate constants under different reaction temperatures could be used to extrapolate the thermodynamic activation energy constants of various chemical reactions from the Eyring Equation. The thermodynamic activation energy constants are an essential input for process simulation of a preliminary plant design. Apart from thermochemical conversion of biomass to produce biofuels, research is also studying engineered metabolic pathways in cells using genetic and enzymatic tools (Albanez, Lovato, Zaiat, Ratusznei, & Rodrigues, 2016; Dias, Luz Jr., Mitchell, & Krieger, 2017). In those studies, first-order reaction rate kinetics are assumed for the chemical reactions in both batch reactors and plug flow reactors, while for plug flow reactors, transport of fluids was considered to obtain the mass balances in terms of flow rate

and reactor volume. Process optimization requires the assessment of the reaction rate constants for manufacturing the products of interest to determine reactor sizing parameters.

1.3 Previous Research

1.3.1 Product Yields

Researchers have been investigating on the HTL of various categories of biomass for decades. The mass yield of biocrude product could be achieved as high as 61%. Based on a literature review, the available experimental data with relatively high biocrude yields is selectively listed in ***Table 1***.

***Table 1**: Literature studies available on biomass conversion for production of bio-oil – reaction conditions, biocrude oil yield, its elemental composition (mass fraction) and its HHV value (MJ/kg) reported.*

Reference	Feedstock	T (°C)	Time (min)	Catalyst	Yield (%) [1]	HHV (MJ/kg)	Bio-Oil Elemental Composition (wt%)			
							C	H	O	N
(Croce, *et al.*, A Model Study to Unravel the Complexity of Bio-Oil from Organic Wastes, 2017)	Cellulose and tripalmitin	300	20	N/A	51	35.7	71.4	11.4	17.2	N/A
(de Caprariis, De Filippis, Petrullo, & Scarsella, 2017)	Natural hay	280	30	N/A	3 [6]	31.5	74.3	7.6	18.1	N/A
	Oak wood	320	30	N/A	2.8 [6]	27.5	69.4	6.3	24.2	N/A
	Walnut shell	320	30	N/A	2.7 [6]	28.5	71.2	6.3	22.5	N/A
	Cellulose	280	30	N/A	2 [6]	23.7	63	5	32	N/A
(Zhou, Schideman, Yu, & Zhang, 2013)	Algae series *Carboy*	300	30	N/A [2]	52.2	32.9	70.4	8.2	6.6	14.7
(Posmanik, *et al.*, 2018)	Carbohydrate-rich food waste	300	60	w/o, acid, or alkaline	22-30	32.5-35.4	70.6-74.1	8.1-9.2	13.4-17.8 [3]	2.8-4.2
	Digested cattle manure	300	60	w/o, acid, or alkaline	17-27	33.4-34.8	73-75.9	7.6-8.7	13.6-15.8	2.6-3.8

(Posmanik, Cantero, Malkani, Sills, & Tester, 2017)	Potato starch, bovine serum albumin, and linoleic acid	250-350	20 or 60	N/A	35-67 [4]	36.3 [5]	71-77	8.4-10	9.4-12.6	2.5-3.5
	Potato starch and linoleic acid	250-350	20 or 60	N/A	47-57 [4]	37 [5]	72-79	7-8	12-16	N/A
	Linoleic acid	250-350	20 or 60	N/A	38-77 [4]	32.5 [5]	68-75	9-11.4	12.8-24	N/A
(Li, *et al*., 2016)	Fermentation waste of corn stalks and ethanol	370	30	N/A	40.79	N/A	N/A	N/A	N/A	N/A
(Dote, Sawayama, Inoue, Minowa, & Yokoyama, 1994)	Botryococcus braunii microalgae strain	300	60	Na_2CO_3 (5%)	64	49	85.4	13.8	0 [3]	0.8
(Minowa, Yokoyama, Kishimoto, & Okakura, 1995)	Dunaliella tertiolecta microalgae strain	300	5	N/A	43.8	34	72.1	8.3	12.9	6.7
(Yang, Feng, Inamori, & Maekawa, 2004)	Microcystis viridis microalgae strain	340	30	Na_2CO_3 (5%)	33	28	63.3	7.6	19.7	7.1
(Garcı´a Alba, *et al*., 2012)	Desmodesmus sp. microalgae strain	375	5	N/A	49	35.4	74.5	8.6	10.5	6.3
(Matsui, *et al*., 1997)	Spirulina microalgae strain	350	60	N/A	61	26	57.3	7.4	28.5 [3]	6.8

(Duan & Savage, 2011)	Nannochloropsis sp. microalgae strain	350	60	Pd/C (50% daf)	57	38.6	73.4	10.8	8.5	3.9
(Singh, *et al*., 2015)	Deodar residue	280	15	KOH	34	N/A	N/A	N/A	N/A	N/A
	Pine wood residue	280	15	KOH	34	N/A	N/A	N/A	N/A	N/A
	Wheat straw residue	280	15	KOH	33	N/A	N/A	N/A	N/A	N/A
	Sugarcane bagasse	280	15	KOH	36	N/A	N/A	N/A	N/A	N/A
(Yin & Tan, 2012)	Cellulose	300	0 (7)	Hydrochloric acid	34	N/A	N/A	N/A	N/A	N/A
	Cellulose	300	0 (7)	N/A	28.4	N/A	N/A	N/A	N/A	N/A
	Cellulose	300	0 (7)	Sodium hydroxide	5.8	N/A	N/A	N/A	N/A	N/A

N/A: not applicable.
w/o: without.
(1) Yields are calculated on a dry mass basis unless specified.
(2) The algae series were cultivated in wastewater that could contain some catalysts for HTL processes.
(3) Oxygen content was calculated by difference (including the ash content).
(4) The yields were calculated on a carbon mass basis.
(5) Only average value under different reaction temperature is displayed here.
(6) Only heavy bio-oil recovered from solid product filtration was considered.
(7) The holding time was marked as the time under the preset temperature, which was 300°C at this point.

Previous efforts showed that either second-generation biomass, such as wood residue and digested dairy manure, or third-generation biomass, such as algae, could generate biocrude with HHV of 32-36 MJ/kg (Croce, *et al*., 2017; de Caprariis, De Filippis, Petrullo, & Scarsella, 2017; Zhou, Schideman, Yu, & Zhang, 2013; Posmanik, *et al*., 2018; Li, *et al*., 2016; Dote, Sawayama, Inoue, Minowa, & Yokoyama, 1994; Minowa, Yokoyama, Kishimoto, & Okakura, 1995; Yang, Feng, Inamori, & Maekawa, 2004; Garcı´a Alba, *et al*., 2012; Matsui, *et al*., 1997; Duan & Savage, 2011; Singh, *et al*., 2015; Yin & Tan, 2012). While HHV of anthracite coal was equal to 32.6 MJ/kg and that of petroleum coke was 31.3 MJ/kg, most of the biocrude product could be a potential competitor to some commercial solid fuels in energy production (Engineering Toolbox, 2003). Biocrude oil could be further upgraded into biodiesel or bioethanol via oxygen removal, thus having a HHV value of 40.5 MJ/kg that is close to diesel fuel (45.6 MJ/kg) (Engineering Toolbox, 2003).

To mimic the contents of commercial fossil fuels, formation of contents in biocrude oil should be comprehensively investigated. The key factors affecting biocrude formulation include feedstock composition, reaction temperature, residence time of reactor, and catalyst. With the evolution of time, there were three stages of the biomass conversion observed (Peterson, *et al*., 2008; Posmanik, Cantero, Malkani, Sills, & Tester, 2017; López Barreiro, Prins, Ronsse, & Brilman, 2013; Asghari & Yoshida, 2007; Yin & Tan, 2012): decomposition of macromolecules into oligomers and monomers, further degradation into small-chain molecules, and repolymerization and condensation of the small molecules to solid and bio-oil products. The composition of the biomass feedstock is important in determining the biocrude yield and biocrude composition.

From ***Table 1***, we find that algae tend to have higher biocrude yields with a broader range of HHV, and the Dote's study (Dote, Sawayama, Inoue, Minowa, & Yokoyama, 1994) showed that the biocrude product could have the hydrocarbon composition. This indicates that lipids may be friendlier to the biofuel production than carbohydrates and protein. It is also interesting that a combination of model compounds, such as a mixture of starch, linoleic acid, and bovine serum albumin in an earlier study (Posmanik, Cantero, Malkani, Sills, & Tester, 2017), could achieve higher biocrude yields with lower oxygen content. Some retro-aldo reactions between lipids and carbohydrates were proven to be advantageous for the formulation of precursors of biofuels (Peterson, *et al*., 2008; Bhatia, Kim, Yoon, & Yang, 2017; Croce, *et al*., 2017). There are also a large number of HTL studies of lignocellulosic biomass, such as wood residues and dairy manure. According to the experimental results cited (Posmanik, Cantero, Malkani, Sills, & Tester, 2017; Croce, *et al*., 2017; de Caprariis, De Filippis, Petrullo, & Scarsella, 2017; Li, *et al*., 2016), lignocellulosic biomass was relatively easy to pretreat for producing higher yields of biocrude compared to protein-rich biomass. Cellulose and starch were frequently treated as the model compounds for studying the HTL of sugar-rich biomass, because cellulose and starch were the most abundant natural sugars in biomass, mostly in agricultural wastes, and they both were easier to be milled to have a larger contact area. From ***Table 1***, the maximum yields for biocrude production always occur at temperatures in the range of 280-300°C for cellulosic biomass. At a pressure of around 30 MPa that is suitable for practical process operation, the ion dissociation reached its maximum at around 300°C with a relatively high density to encourage the interactions between water molecules and biomolecules under HTL conditions. High pressures can lead to operational problems and more leaking issues, while lower pressures would lower densities and water may be present as vapor.

1.3.2 Modeling HPLC Signals

Liquid chromatography has changed significantly since its development in separating chemical components from the 1940s, and in the last decade, scientists have worked on improving efficiency of liquid chromatography by introducing HPLC. With the tools of spectrometry, researchers have been able to identify different components via retention time values and peak shape. The accuracy and precision of HPLC signals are crucial to identifying the chemical components and allocating area under the HPLC peak to the concentration of the identified component using calibration curves and linear regression between the area under the HPLC peak and the concentrations of HPLC standards. Various analytical methods have been employed to analyze the accuracy and precision of HPLC signals (Thekkudan, Rutan, & Carr, 2010; Wahab, Patel, & Armstrong, 2017; Li J. , 2002; Baeza-Baeza, Torres-Lapasió, & García-Álvarez-Coque, 2011; Jin, *et al*., 2008). In the study of peak quantification in comprehensive two-dimensional liquid chromatography in time (Thekkudan, Rutan, & Carr, 2010), a Gaussian model was used for estimating area in each dimension under the HPLC curves, and the researchers found that the percent relative standard deviation was kept below 5%. The theoretical background of Gaussian model was demonstrated in previous studies (Thekkudan, Rutan, & Carr, 2010; Wahab, Patel, & Armstrong, 2017; Li J. , 2002; Baeza-Baeza, Torres-Lapasió, & García-Álvarez-Coque, 2011). In liquid chromatography, when the absorption isotherm is linear, peak broadening issues in ideal chromatography plots influence all analyte molecules with the same probability. For example, without differentiating molecules in various parts of the peak, the peak shape has a Gaussian distribution. However, in real liquid chromatography, there were fronting, tailing, and asymmetry issues of the curves due to the suspension of some analyte particles in chromatography. To better describe the separation efficiency with those difficulties,

researchers applied various mathematical models with modification of the simple Gaussian model, including the empirically transformed Gaussian, polynomial modified Gaussian, generalized exponentially modified Gaussian, and hybrid function of Gaussian and truncated exponential functions (Wahab, Patel, & Armstrong, 2017; Li J. , 2002). The models are respectively displayed in ***(3*** - ***6*** below.

$$f(t) = \frac{H''}{\{1+\lambda_L \exp[k_L(t_L - t)]\}^{(t_L/t)^\alpha} + \{1+\lambda_T \exp[k_T(t - t_T)]\}^{(t/t_T)^\beta} - 1} \quad \textbf{(3)}$$

$$f(t) = \frac{H_m \sigma_0}{\sigma} \exp\left[-\left(\frac{t - t_m}{\sigma}\right)^2 \right] \quad \textbf{(4)}$$

$$f(x) = \frac{a_0}{2a_3} \exp\left[\frac{a_2^2}{2a_3^2} + \frac{a_1 - x}{a_3}\right]\left[\operatorname{erf}\left(\frac{x - a_1}{2^{1/2}a_2} - \frac{a_2}{2^{1/2}a_3}\right) + 1\right] \quad \textbf{(5)}$$

$$f(t) = \begin{cases} H \exp\left(\dfrac{-(t - t_m)^2}{2\sigma^2 + \tau(t - t_m)}\right), & 2\sigma^2 + \tau(t - t_m) > 0 \\ 0, & 2\sigma^2 + \tau(t - t_m) \le 0 \end{cases} \quad \textbf{(6)}$$

The generalized Exponentially Modified Gaussian (EMG) model was the most popular function used for curve fitting of HPLC signals (Li J. , 2002). In ***(5***, the EMG model (Li J. , 2002) was derived by convoluting a Gaussian function with the resultant of two exponential m functions of different time constants, where a_0 is peak area denoted as *A* or *Area* in this thesis; a_1 is retention time denoted as t_R in this thesis; a_2 is the width of Gaussian denoted as *Width* in this thesis; a_3 is exponential damping factor denoted as *D* in this thesis; erf is the error function.

Wahab, Patel, and Armstrong describe issues associated with chromatography data in fronting, tailing, and asymmetry. They carried out peak shape analysis using different cut-off

criteria for the peak height and concluded that the upper section of HPLC curve above 80% peak height had the perfect Gaussian shape. They also described a noteworthy departure from perfect Gaussian for the HPLC signals below the 20% peak height. However, with the correction of error function of I_i in EMG model, the deviation from the simplified Gaussian model could be well described. The EMG model has been successfully applied in a variety of systems (Thekkudan, Rutan, & Carr, 2010; Wahab, Patel, & Armstrong, 2017; Li J. , 2002; Baeza-Baeza, Torres-Lapasió, & García-Álvarez-Coque, 2011).

Due to the close retention time values, there were overlapping HPLC signals in a "shoulder" type observed as shown in ***Figure 2*** below.

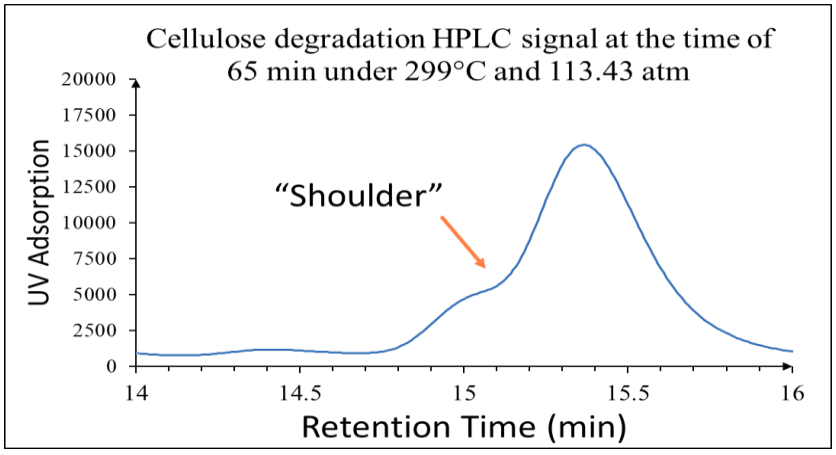

***Figure 2**: A representative diagram of overlapping issues in our hydrothermal experiments, where x-axis is retention time in minutes and y-axis is HPLC signal.*

There were successful computational solutions to the overlapping HPLC signals (Goodman & Brenna, 1994; Kong, *et al*., 2005; Cavanillas, Serrano, Di´az-Cruz, Ariño, & Esteban, 2016; Felinger, 1994). In the Goodman's study of curve fitting for overlapping peaks in GC-MS analysis (Goodman & Brenna, 1994), different models including EMG were used for simulations to find the best fit of chromatography signals. The results showed that EMG model

accounted for the largest regression statistical parameter R^2 with the R^2 value equal to 0.99948, and the largest F-statistic value of 41864, which indicated 95% confidence level in t-test. This excellent curve fitting of chromatographic data using the EMG model was also demonstrated in Cavanillas' project about signal fitting of highly asymmetric voltammograms (Cavanillas, Serrano, Di´az-Cruz, Ariño, & Esteban, 2016). The experimental voltammetric data was well reproduced with a relatively small mean percent deviation equal to 1.1%. The overlapped peaks were also well resolved in those studies (Goodman & Brenna, 1994; Kong, *et al*., 2005; Cavanillas, Serrano, Di´az-Cruz, Ariño, & Esteban, 2016; Felinger, 1994), and a typical deconvolution is shown in ***Figure 3***.

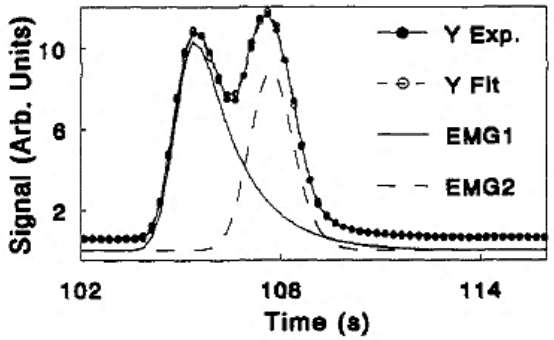

Figure 3*: Best fit for the application of the EMG/EMG function combination to a 1:1, 70% valley chromatogram (Goodman & Brenna, 1994).*

1.3.3 Reaction Pathway Schemes and Reaction Kinetic Modeling

In earlier research, concentrations of compounds of interest were derived from a linear regression of the area values under the HPLC peaks using a standardized correlation of areas with known standard concentrations. Concentrations of the identified chemical components were used for further analysis including reaction kinetic modeling. The reaction kinetic modeling results were able to demonstrate the microscopic chemical conversion for cellulose under the HTL conditions.

To better understand the chemistry of conversion from cellulose to the value-added products, reaction pathway schemes are required for the reaction kinetic modeling. At elevated temperatures and pressures, water is an outstanding reaction medium to enable the oxygen-removal reactions. As cellulose is the most natural abundant macromolecule with a polyol structure, cellulosic biomass has a large potential for production of renewable biofuels. Many studies have shown the success of producing essential chemicals in laboratories, such as HMF as a building block for bio-based products and a starting material for generating biofuels (Roman-Leshkov, Barrett, Liu, & Dumesic, 2007). In subcritical or supercritical water, cellulose was observed in many studies to decompose via rapid hydrolysis into monosaccharides mainly including glucose and fructose by the cleavage of 1, 4-glycosidic bonds (Peterson, *et al*., 2008; Knez, Škerget, & Pavlovič, 2013; Yin & Tan, 2012; Croce, *et al*., Mass Spectrometry and Nuclear Magnetic Resonance Spectroscopy Study of Carbohydrate Decomposition by Hydrothermal Liquefaction Treatment: A Modeling Approach on Bio-oil Production from Organic Wastes, 2015; Kröger, Hartmann, & Klemm, 2013; Amarasekara & Wiredu, 2014; Lin, *et al*., 2015). Glucose was isomerized into fructose via Lobry de Bruyn, Alberda van Ekenstein transformation with a lower reaction rate than the degradation of glucose or fructose (Peterson, *et al*., 2008). However, the reverse formation of glucose from fructose did not seem important as fructose degraded much faster than glucose, as observed in the Antal's study (Antal Jr, Mok, & Richards, 1990). Under the influence by active hydrogen ions and hydroxide ions, glucose and fructose further decomposed into furans, carboxyl acids, and aldehydes. Researchers have identified varieties of those degradation products, and all the degradation products detected are listed in ***Table 2***.

Table 2: *Cellulose and glucose degradation products detected in previous studies with the specification of reaction conditions.*

Name of the degradation product	References	T (°C)	P (MPa)	Catalyst
Cellotetraose	[54]	25-240	N/A	H_2SO_4
Cellotriose	[54]	25-240	N/A	H_2SO_4
Cellobiose	[52], [54]	25-240[54] 200-230[52]	N/A	H_2SO_4
Glucose	[13], [50], [51], [52], [54]	220-300[13] 130-200[50] 250-300[51] 25-240[54] 200-230[52]	N/A[13],[50],[52],[54] 12-20[51]	N/A[13],[51] 1-(1-propylsulfonic)-3-methylimidazolium chloride[50] H_2SO_4[52],[54]
Fructose	[13], [50], [51], [52], [54]	220-300[13] 130-200[50] 250-300[51] 25-240[54] 200-230[52]	N/A[13],[50],[52],[54] 12-20[51]	N/A[13],[51] 1-(1-propylsulfonic)-3-methylimidazolium chloride[50] H_2SO_4[52],[54]
HMF	[13], [50], [51], [52], [53], [54]	220-300[13] 130-200[50] 250-300[51] 25-240[54] 200-230[52] 200-250[53]	N/A[13],[50],[52],[54] 12-20[51] 34.5[53]	N/A[13],[51] 1-(1-propylsulfonic)-3-methylimidazolium chloride[50] H_2SO_4[52],[53],[54]
Fufrural	[47], [51], [53]	250-350[47] 250-300[51] 200-250[53]	5-1[54][7] 12-20[51] 34.5[53]	N/A[47],[51] H_2SO_4[53]
Levulinic acid	[50], [52], [53], [54]	130-200[50] 25-240[54] 200-230[52]	N/A[50],[52],[54] 34.5[53]	1-(1-propylsulfonic)-3-methylimidazolium chloride[50] H_2SO_4[52],[53],[54]
Lactic acid	[53]	200-250[53]	34.553	H_2SO_4
Acetic acid	[51], [52], [53], [54]	250-300[51] 25-240[54] 200-230[52] 200-250[53]	N/A[52],[54] 12-20[51] 34.5[53]	N/A[51] H_2SO_4[52],[53],[54]
Formic acid	[51], [52], [53], [54]	250-300[51] 25-240[54] 200-230[52] 200-250[53]	N/A[52],[54] 12-20[51] 34.5[53]	N/A[51] H_2SO_4[52],[53],[54]
Succinic acid	[55]	180	1	Ru
Glycolaldehyde	[53]	200-250[53]	34.553	H_2SO_4

N/A: not applicable.
Symbol [13] refers to Reference (Knez, Škerget, & Pavlovič, 2013).
Symbol [47] refers to Reference (Croce, *et al*., Mass Spectrometry and Nuclear Magnetic Resonance Spectroscopy Study of Carbohydrate Decomposition by Hydrothermal Liquefaction Treatment: A Modeling Approach on Bio-oil Production from Organic Wastes, 2015).
Symbol [50] refers to Reference (Amarasekara & Wiredu, 2014).
Symbol [51] refers to Reference (Lin, *et al*., 2015).
Symbol [52] refers to Reference (Xiang, Lee, & Torget, 2004).
Symbol [53] refers to Reference (Antal Jr, Mok, & Richards, 1990).
Symbol [54] refers to Reference (SriBala & Vinu, 2014).
Symbol [55] refers to Reference (Podolean, *et al*., 2016).

Among the degradation products, lactic acid was produced from glucose via intermediates including glyceraldehyde and pyruvaldehyde through benzylic acid rearrangement dehydration (Yin & Tan, 2012). This reaction and the retro-aldol formation of glycolaldehyde from glucose via erythrose are alkaline pathways. HMF was observed to be mostly derived from fructose, and it could be rehydrated to form levulinic acid and formic acid with the help of hydrogen ions. Detailed conversion pathways from cellulose are depicted in ***Figure 4*** and **Figure 5** below with the types of the reactions indicated and the molecular structures labeled respectively.

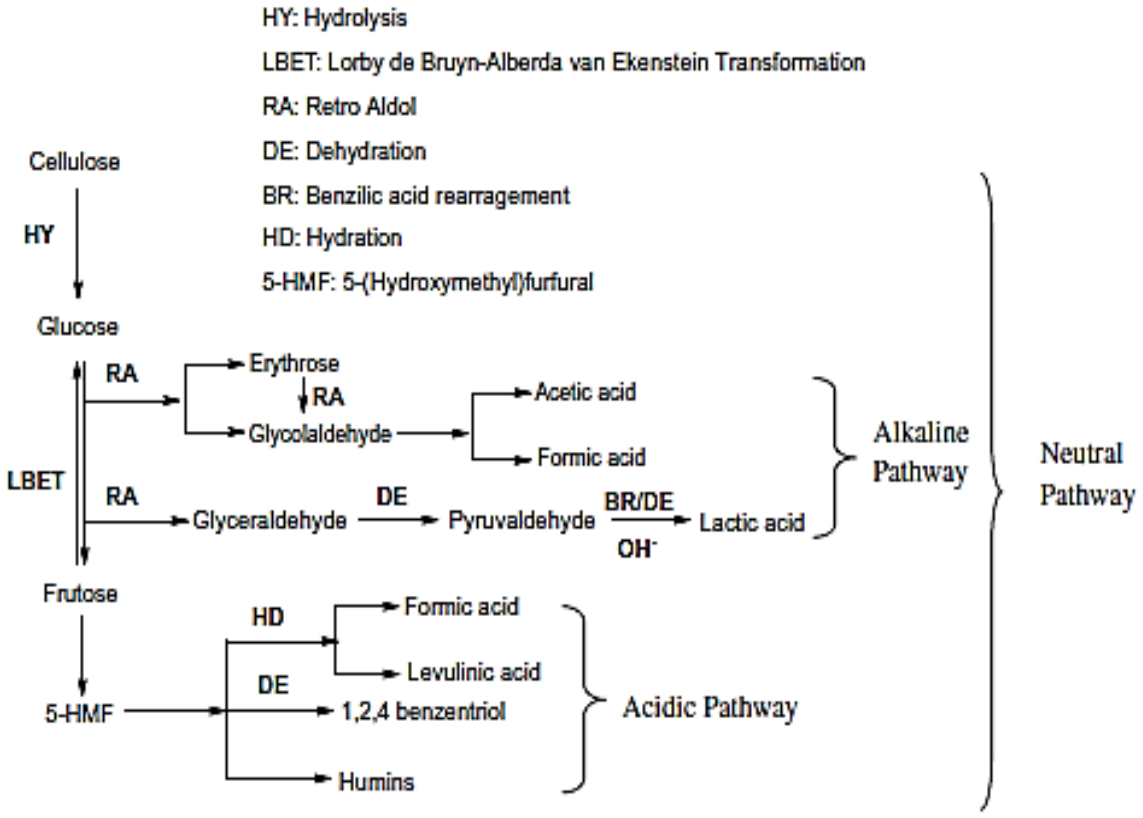

Figure 4*: Degradation pathways of hydrothermal decomposition of cellulose with names of reactions marked (Yin & Tan, 2012).*

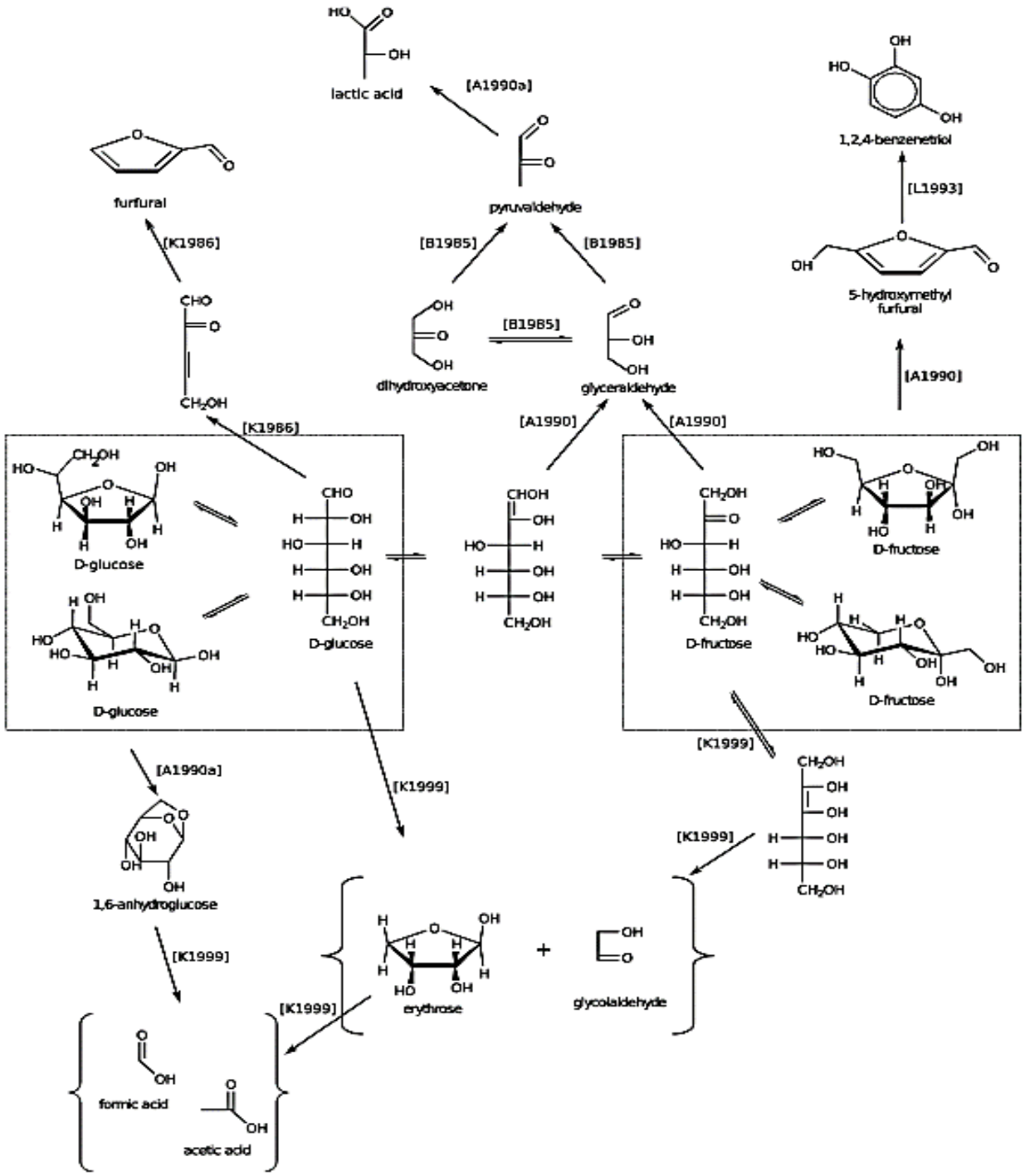

Figure 5*: Structural representation of mapping conversion pathways for the degradation of D-glucose and D-fructose, where the references are: [B1985] = (Bonn, Rinderer, & Bobleter, 2006); [K1986] = (Krishna, et al., 1986); [A1990] = (Antal Jr, Mok, & Richards, 1990); [A1990a] = (Antal Jr, Mok, & Richards, Four-carbon model compounds for the reactions of sugars in water at high temperature, 1990); [L1993] = (Luijkx, van Rantwijk, & van Bekkum, 1993); [K1999] = (Kabyemela, Adschiri, Malaluan, & Arai, 1999); and [J2004] = (Jin, Zhou, Enomoto, Moriya, & Higashijima, 2004).*

1.4 Organization of the Thesis Documentation

Following **Chapter 1**, **Chapter 2** introduces the overall objectives of this study and approaches that I use in my research. In **Chapter 3**, we describe the experimental protocols for our HTL study. Based on our experimental results, we further analyze the experimental HPLC signals using the EMG model in **Chapters 4** and **5**. After the experimental findings are concluded for the reaction kinetic modeling, the uncertainties are evaluated based on the projected reaction pathway schemes from cellulose to the identified degradation products in **Chapter 6**. Results and discussion of the kinetic modeling are given in **Chapters 7**. **Chapter 8** encloses the conclusions and provides recommendations for future HTL work.

CHAPTER 2

OBJECTIVES AND APPROACHES

2.1 Scope and Objectives

As mentioned in **Chapter 1**, one important obstacles in the commercialization of biorefinery processes is the scale-up of bench-scale studies. The emerging biorefinery industries require careful evaluation of available methods of utilizing waste biomass as a commercial feedstock. As for thermochemical biomass conversion methods, there remains large space for optimizing biofuel production using the tool of reaction kinetic modeling. This study establishes differential forms of mole balances around each identified chemical species based on the projected chemical reactions. Least square fitting will be applied for calculating simulated EMG parameters and chemical reaction rate constants. The objectives of this research can be summarized in three categories:

1. Demonstrating the accuracy of HPLC analysis and deconvoluting complex HPLC chromatographs using mathematical tools (EMG model);
2. Explaining reaction selectivity through proposed reaction pathway schemes and chemical reaction mechanisms;
3. Providing insights for selective production of biochemicals and bio-oil based on the modeling results.

2.2 Approaches

Using the experimental protocol and analytical techniques as described in **Chapter 3**, I was able to identify chemical species in the aqueous products from HTL treatment. To accurately

characterize the HPLC peak features, the EMG model was used to simulate the HPLC signals using different cut-off thresholds for specified HPLC peaks. A linear relationship was validated between the concentration of the identified chemical species and the area under each HPLC peak using HPLC standards. Thus, the concentrations of the identified compounds in the HTL experiments could be determined. However, there are overlapping signals detected in the HPLC analysis results due to the close retention time values of many of the chemical species. It is to computationally resolve these overlapping signals with very low error values based on a literature review. **Chapters 4** & **5** present the results and discussions about the HPLC signal modeling and the deconvolution of HPLC complex signals.

As mentioned in **Chapter 1**, there are three stages observed in the depolymerization of cellulose: decomposition from cellulose to cellulo-monomers through cellulo-oligomers, dehydration and decarbonylation of cellulo-monomers to form the identified degradation products, and condensation and repolymerization of the short-chain products. Under the Three-Stage assumption, the chemical reactions involved at each stage are used as a basis for the reaction kinetic modeling. This study proposes several chemical reaction pathway schemes for the HTL of cellulose to the identified degradation products. There remain uncertainties of the conversion pathways due to the complexity of HTL reaction chemistry. The preliminary reaction kinetic modeling results in this research will quantify reaction selectivity among the proposed chemical reactions and compare the reaction rate constants with the findings in other HTL studies. These results serve as a key to understanding the underlying chemistry of biomass conversion under HTL conditions into the value-added products. To demonstrate the product evolution, different chemical reaction pathway schemes are proposed in **Chapter 6**.

CHAPTER 3

EXPERIMENTAL SETUP

3.1 Rationale behind Selection of Model Substances

The substances selected for this research were chosen to mimic their composition of lignocellulosic biomass. Lignocellulosic biomass feedstock mainly includes woody residues, animal manure and grasses. Generally, 25%-70% of those residues are cellulose, which usually accounts for the largest proportion in lignocellulosic biomass. To mimic the realistic composition of cellulose in biomass, the initial concentration of cellulose used in this study was set to be 50g/L deionized (DI) water. Researchers have shown that cellulosic feedstock to the bio-oil yields can be as high as 60% on a dry mass basis (Croce, *et al*., 2017). In general in this research, cellulose was studied as the major model compounds for understanding the degradation of cellulosic biomass under HTL conditions. In addition, glucose was an important model compound for explaining its role as an intermediate in the degradation pathways of cellulose. As an essential product in biochemical industries, levulinic acid was treated as feedstock to evaluate the stability of carboxylic acids under hydrothermal conditions. As earlier studies have reported that cellulose and glucose were very reactive under HTL conditions (e.g., Zhang & Cremer, 2006), we were interested in exploring the decomposition behavior of cellulose and glucose under such circumstances. As is shown in ***Figure 6***, at a temperature between 270°C and 300°C and an elevated pressure, the ionization constant of water (K_W) reaches its maximum, with a value of around 10^{-11} that is almost 1000 times greater than under room temperature and ambient pressure. We used maximized ionization of water conditions as the reaction temperature and pressure for this study. To have a basic idea of the HTL reaction mechanisms, we conducted

noncatalyzed experiments with a careful evaluation of precision and uncertainties of the analytical and mathematical tools.

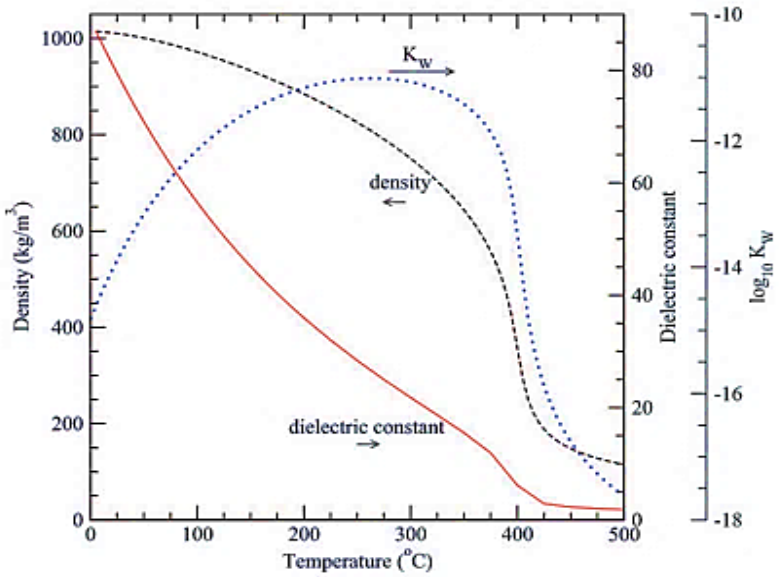

***Figure 6**: Density (Wagner & Pruss, 2002), static dielectric constant (Archer & Wang, 1990) and ion dissociation constant (K_w) (Bandura & Lvov, 2006) of water at 30 MPa as a function of temperature. The dielectric constant of water drops drastically as water is heated, and approaches that of a (room-temperature) non-polar solvent at supercritical conditions (Peterson, et al., 2008).*

HTL studies in our group were primarily focused on migration of chemical elements from biomass to biofuels (Cantero-Tubilla, *et al*., 2017; Posmanik, Cantero, Malkani, Sills, & Tester, 2017), detection of the intermediates in the conversion pathways from cellulose to value-added products (Asghari & Yoshida, 2007; Croce, *et al*., 2015, 2017), and the time evolution of the product distribution in different phases around the bioreactor (Posmanik, *et al*., 2018; Xiang, Lee, & Torget, 2004; SriBala & Vinu, 2014). In the degradation pathways from cellulose, the intermediates were found mostly as cellulo-oligomers such as cellobiose and cellotriose, cellulo-monomers, such as glucose and fructose, and aldehydes like glycolaldehyde. However, previous

research on HTL reaction kinetics modeled the degradation of cellulose or glucose via only a few chemical reactions using relatively simplified assumptions.

3.2 Equipment and Materials

The experimental work was performed by Dr. Roy Posmanik and Dr. Borja Cantero-Tubilla. More information can be found in the publication (Cantero-Tubilla, *et al*., 2017) and his thesis (Cantero-Tubilla, 2017). In this section, I will briefly summarize the equipment and materials they used for setting up their experiments to provide a basis for the experimental protocols described in the next section.

The HTL experiments were conducted in a 316 stainless steel, 1000-mL bolted closure reactor (Autoclave Engineers, Inc., Erie, PA). Feed streams were pumped into the reactor using a high-pressure pump connected with a gas tank (Thar Process, Inc., Pittsburgh, PA). To mix the contents inside the reactor, a refrigerated magnetically controlled shaft and impeller was attached to the batch reactor. The reactor was also equipped with a porous metal diffuser for maximizing the contact area between the gas feed and the aqueous feed inside it. To keep track of the reactor temperature, a type-K thermocouple (Nickel-Chromium/Nickel-Aluminum) was imbedded inside the batch reactor. As for reactor pressure measurements, a pressure gauge (Duro United Instruments, Inc., Northvale, NJ) and a pressure transducer (Model 280E Setra Systems, Inc., Boxborough, MA) were set inside a port of the reactor. To heat up the reactor to the preset temperature, an electrical heating jacket with a thermocouple was used. A Sentinel Series control system (Autoclave Engineers, Inc., Erie, PA) was applied to monitor the heating rate and mixing speed. Venting valves and a back-pressure regulator were applied for decompressing the batch

reactor with the heating tape covered to prevent the lines from freezing. Tap water was used for quenching the reactor after HTL experiments. A chromatograph showing the internal components of the reactor is given in ***Figure 7***.

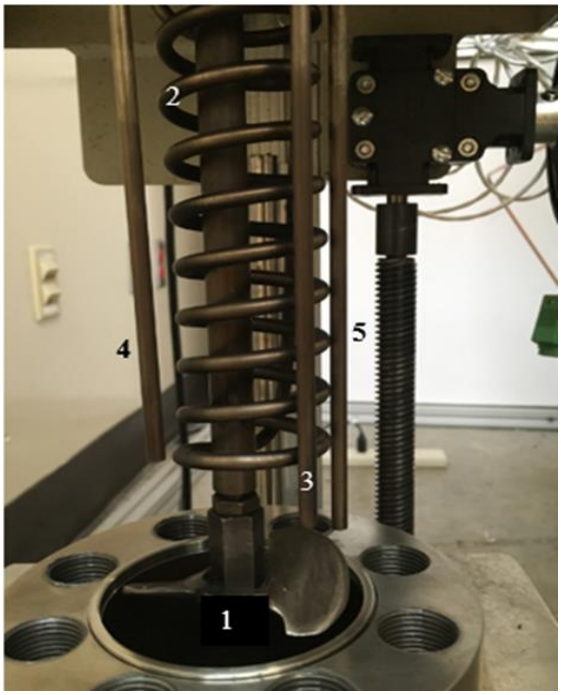

Figure 7*: Fitting inside the reactor: 1) Stirrer with propeller, 2) heat exchanger coil for reaction quenching, 3) thermo-well for thermo-par, 4) gas inlet, 5) sampling line (Cantero-Tubilla, 2017).*

For kinetic experiments, product samples in different phases were collected using output ports located at different internal positions in the reactor. With regards to liquid extraction, the volume of the products was maximized for sample collection. The temperature of collection lines was lowered down using two 3-meter copper coil heat exchangers submerged in an ice bath in the place before decompression. After the sample temperature was cooled down, a ball-valve was used to decrease the pressure and sample was collected at the end of the outlet piping line. A photograph of the reactor with sampling line schemes is given in ***Figure 8***.

Figure 8*: Pictures of the reactor used for studying the kinetic of HTL of model compounds. Enlarged stem of exhaust valves (1) was applied for safe operation. Heat exchangers (2) was used to quench sample before depressurization with ball valve (3), and sample collection (4). Pressure transducer (5) was attached to the feed lines. Pressure transducer (6) was directly connected to a port of the reactor (Cantero-Tubilla, 2017).*

There were some safety issues to note here. The clogging of the sampling line with high pressures may cause severe damage to the batch reactor and will further lead to explosion. To ensure the safe operation of the experiments, the decomposition valves were modified with enlarged stems and isolated with polycarbonate panels. Furthermore, the potential of the existence of the solid products in the liquid product sampling line was minimized by ensuring

adequate time of the cooling and decompression. To prevent cross contamination between consecutive experiments, repeated treatments with acetone and DI water were used to flush out the contents inside the reactor and the lines after every experiment. Details of the experimental protocols and biomass feedstocks are discussed in the next section.

3.3 Experimental Protocols

The schematic of the HTL process is shown in ***Figure 9***. The blue line represents the tap water used to cool down the stirrer and quench the reactor. In the HTL experiments, the water was kept flowing through the stirrer to stay at lower temperatures. After the reaction terminated at a specified reaction time, the ball valve on the green line was turned on to let water through the coil heat exchanger into the reactor to cool it down. The purple lines refer to the feed lines of the batch reactor. The model compounds used in this study, fibrous cellulose powder CF11, glucose powder and levulinic acid solution, were purchased from Whatman, LLC. To mimic realistic biomass concentrations, the concentrations of cellulose, glucose and levulinic acid were set to 50 g/L or 5 wt% in DI water with a total volume of 700mL. The dilute concentrations ensured the safe operation when solid products were relatively unlikely to be generated or were presenting in small amount. The model feedstocks were loaded into the reactor after the reactor was filled with pressurized N_2 gas at a pressure higher than 100 psig using the purple line equipped with a three-way valve. Then the reactor was heated up to the temperature setpoint of 300°C or 275°C and pressurized with liquid water to a pressure of 5-20 MPa using the thermocouple and the pump respectively on purple lines. The monitoring system connected to the purple lines kept track of reactor temperature and pressure. The reactor temperature and

pressure profile for different cases, where for example, *Cellulose 300°C Case* represents that in the HTL experiments, cellulose was the feedstock and the preset reactor temperature was 300°C, also named especially for Cellulose-300 Case, as shown in ***Figure 10***, ***Figure 11***, *and* ***Table 3*** below. In Glucose-300 and Glucose-275 Cases, glucose was the feedstock of the batch reactor with the controlled steady-state reaction temperature of 300°C and 275°C respectively. For the Levulinic-300 Case, levulinic acid was loaded into the reactor when the steady-state temperature was 300°C.

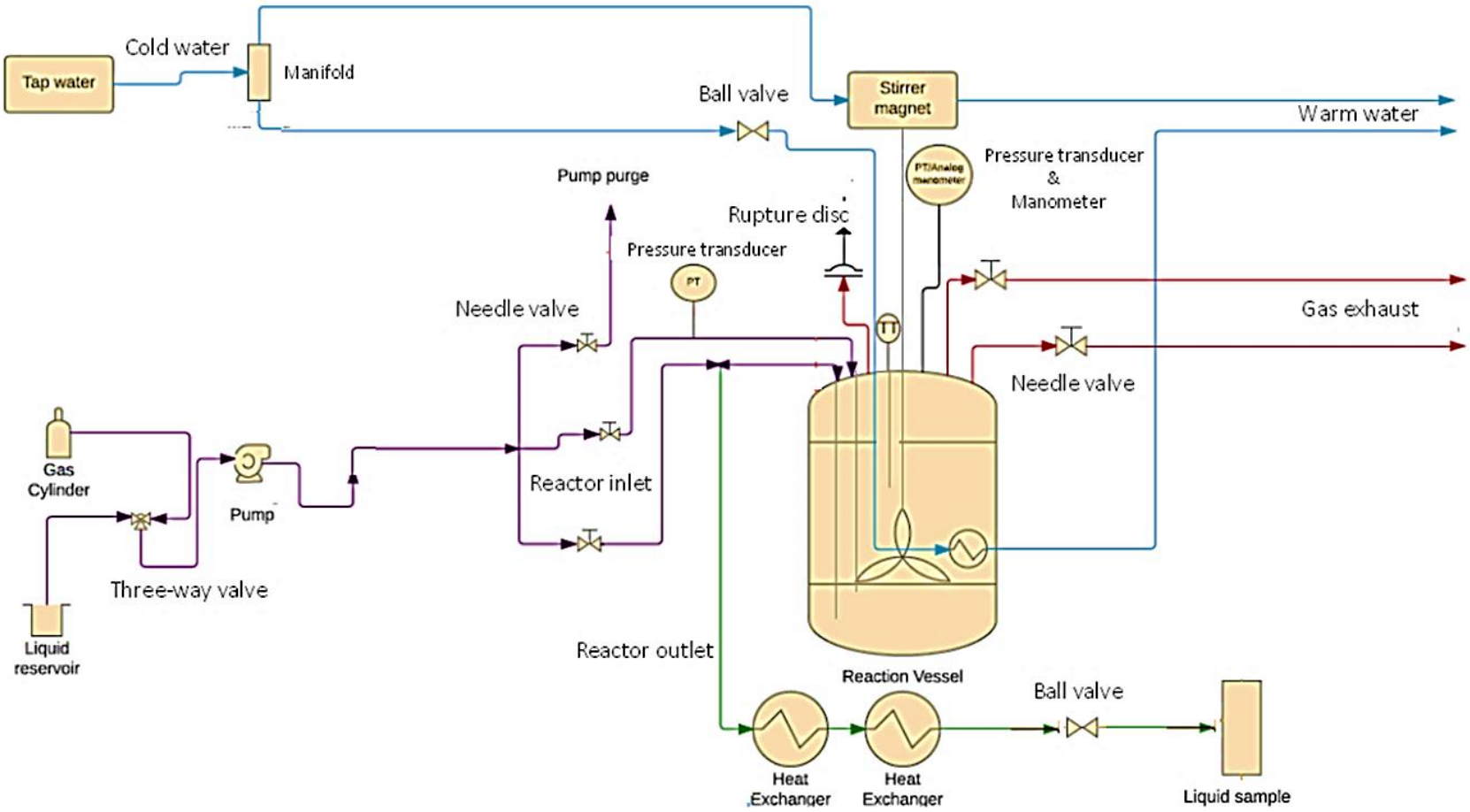

***Figure 9**: Schematic of the reactor system used to study the kinetic of the HTL process of model compounds* (Cantero-Tubilla, 2017).

a) Cellulose 300˚C

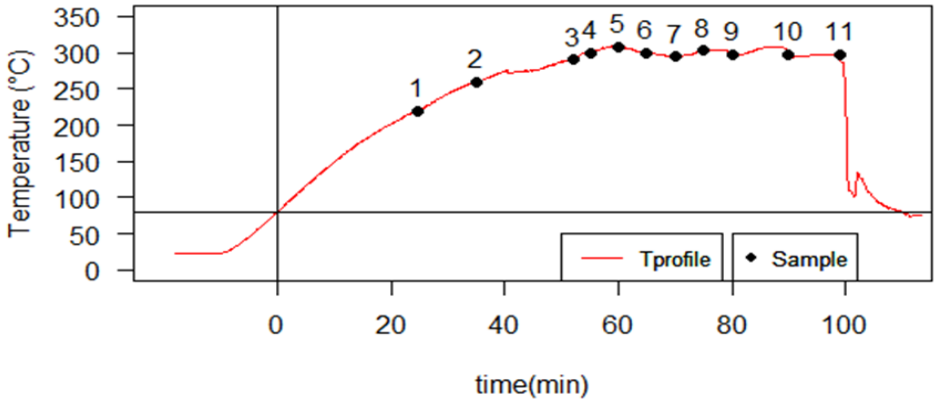

b) Glucose 300˚C

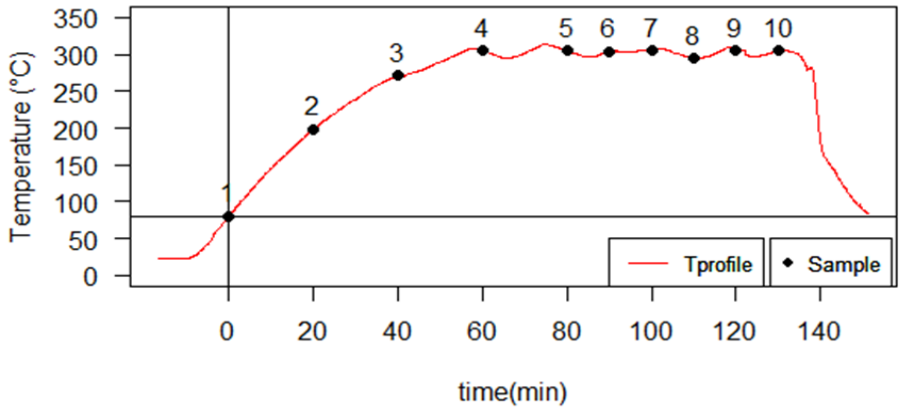

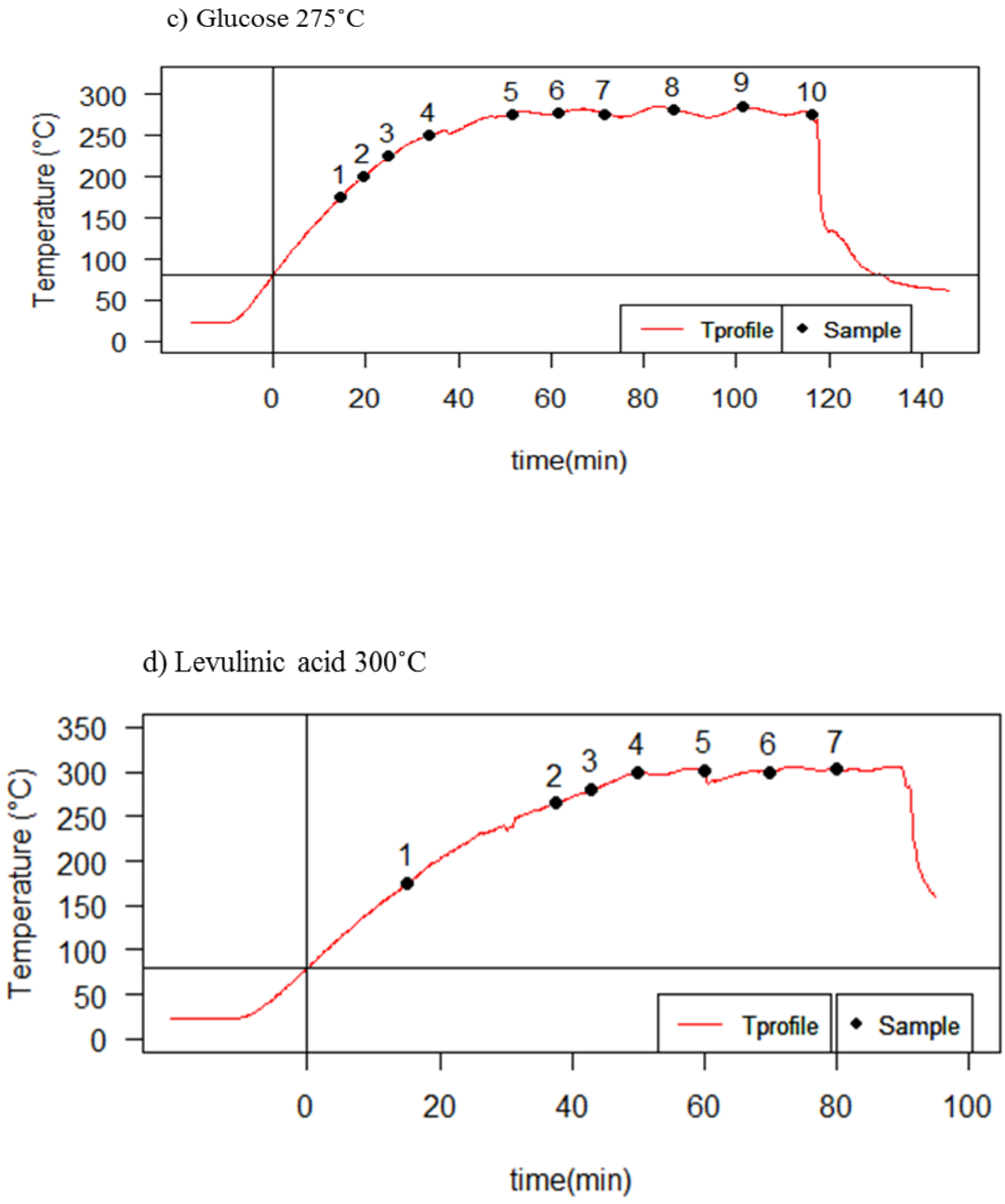

***Figure 10**: Temperature profiles for kinetics experiments for model compounds: a) Cellulose 300˚C. b) Glucose 300˚C. c) Glucose 275˚C. d) Levulinic acid 300˚C. The black dots represent sample collection conditions (Cantero-Tubilla, 2017).*

a) Cellulose 300˚C

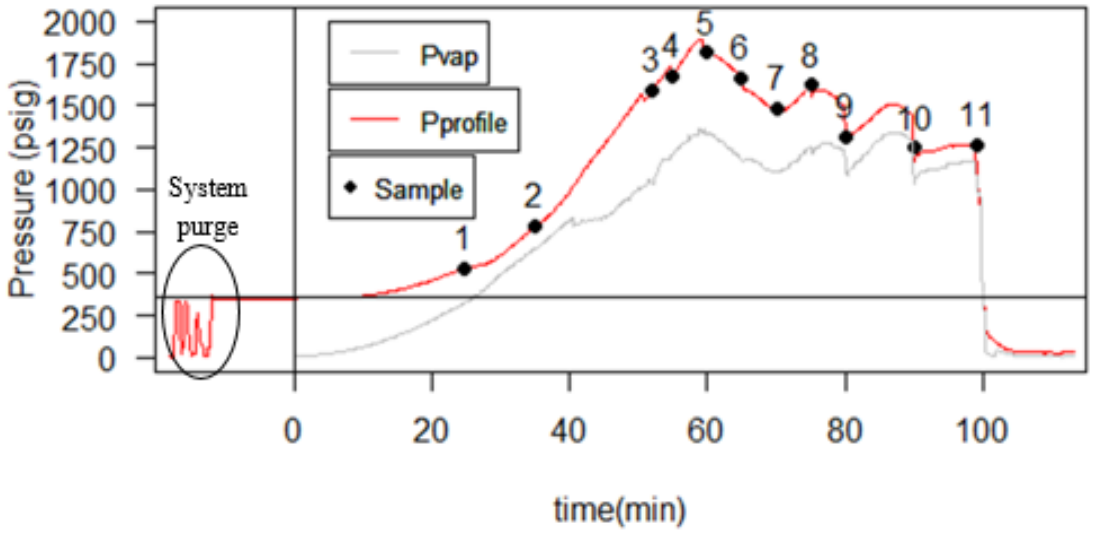

b) Glucose 300˚C

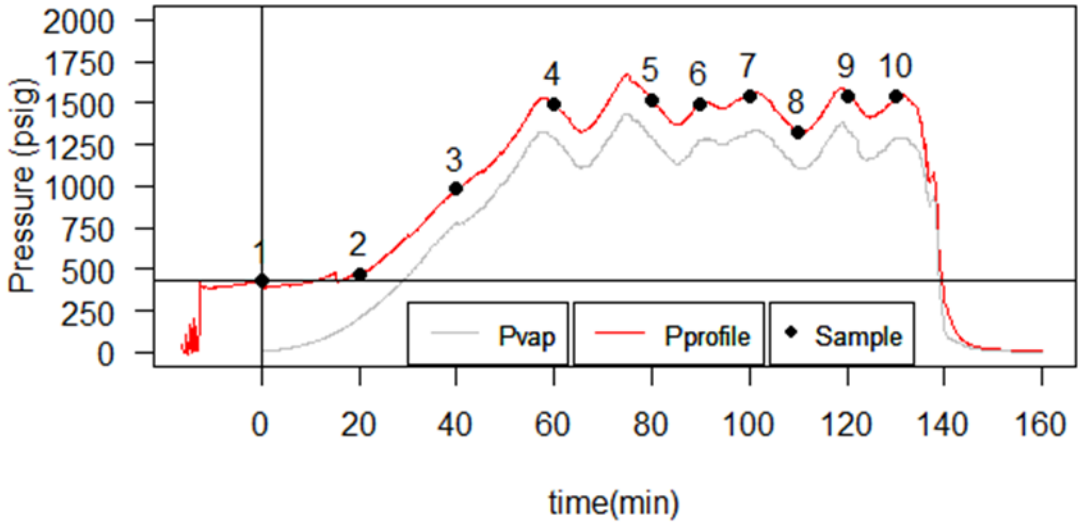

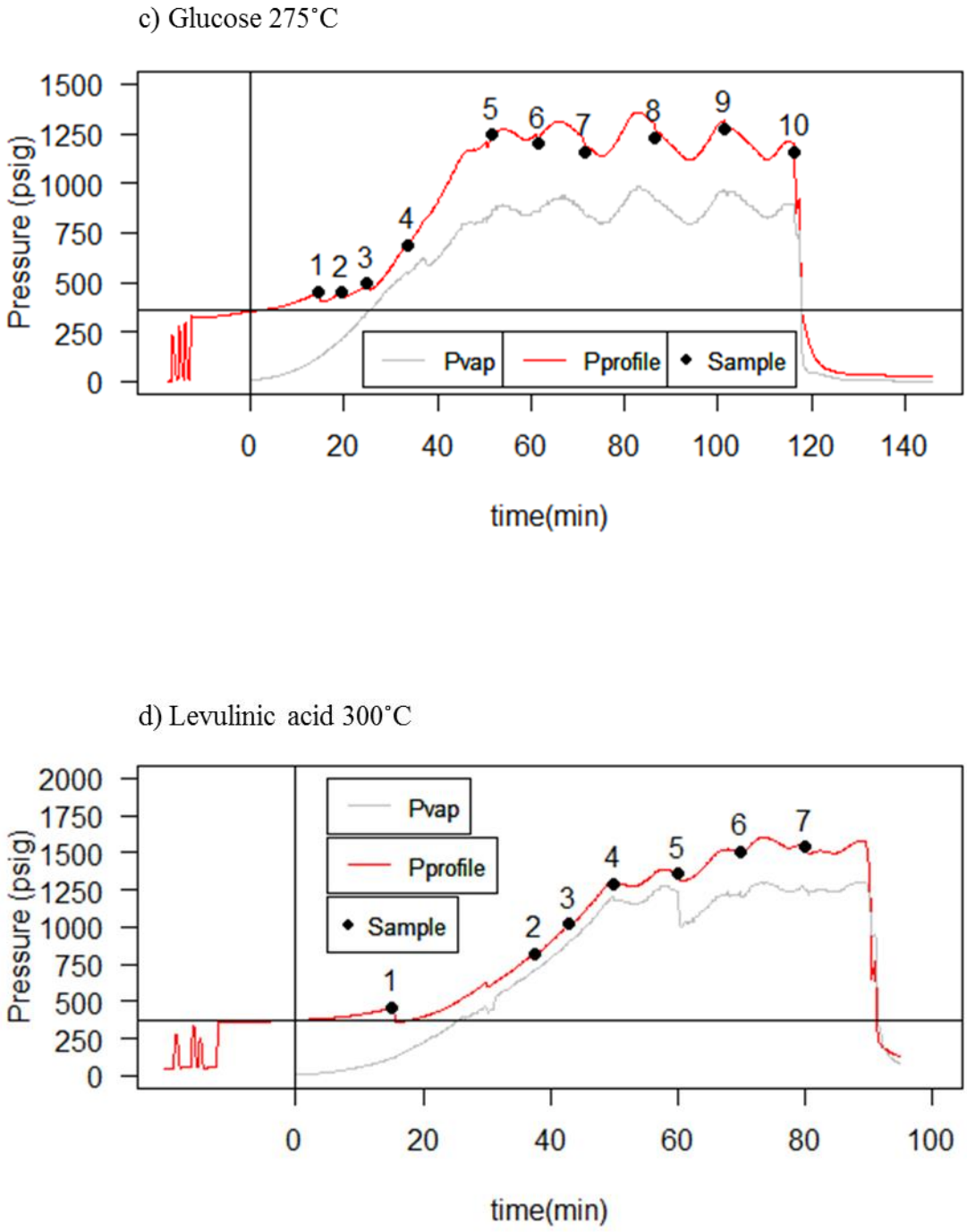

Figure 11*: Pressure profiles for kinetics experiments for model compounds: a) Cellulose 300˚C. b) Glucose 300˚C. c) Glucose 275˚C. d) Levulinic acid 300˚C. The black dots represent sample collection conditions (Cantero-Tubilla, 2017).*

Table 3*: The temperature and pressure profiles with sampling conditions tabularized for each experiment conducted. (Cantero-Tubilla, 2017).*

	Cellulose 300˚C			**Glucose 300˚C**		
Sampling #	Time (min)	T (˚C)	P (psig)	Time (min)	T (˚C)	P (psig)
	0	80	354	0	80	428
1	24.7	220	533	20	198	469
2	35	260	784	40	271	981
3	52	290	1589	60	305	1497
4	55	300	1678	80	305	1521
5	60	308	1812	90	304	1494
6	65	299	1667	100	305	1546
7	70	294	1482	110	294	1323
8	75	303	1620	120	305	1541
9	80	298	1314	130	305	1543
10	90	297	1250			
11	100	298	1266			
	Glucose 275˚C			**Levulinic aicd 300˚C**		
Sampling #	Time (min)	T (˚C)	P (psig)	Time (min)	T (˚C)	P (psig)
	0	80	354	0	80	375
1	14.67	175	451	15.2	175	457
2	19.5	200	449	37.5	265	821
3	25	225	492	42.8	280	1017
4	33.5	250	690	50	300	1288
5	51.5	275	1242	60	302	1357
6	61.5	277	1198	70	300	1505
7	71.5	276	1159	80	303	1538
8	86.5	281	1232			
9	101.5	285	1275			
10	116.5	275	1156			

Product samples were collected at the designated reactor times after cooling and decompression using a sample volume of 25 mL from the green line in the schematic. The first sample of the experiments at the specified reaction time was discarded. This protocol was repeated to collect samples for HPLC and elemental analysis. The red lines in the schematic were used for depressurizing the reaction system to exhaust the pressurized gas and ensure the safe operation. The temperature and pressure profiles were recorded after the temperature reached 80 ˚C. After depleting the reaction volume, the heating was stopped, and the reactor was quenched in this cooling coils. At least 100 mL dead volume of liquid existed in the reactor after each

experiment. DI water and acetone were used to flush the reaction system immediately after the experiments to ensure better washouts. Details about HPLC analysis are included in the next section.

3.4 Analytical Techniques

After the product samples were removed from the reactor, they were quenched in an ice bath and filtered using pre-weighted filter papers (Whartman No.1) to isolate any solid products that formed. The pH values of the liquid phase were measured by an Accumet AB150 probe (Fisher Scientific Inc., Hampton, NH). Then the liquids were further filtered using syringe filters and centrifuged for HPLC analysis (Shimadzu,Columbia Inc., MD). The HPLC equipment had a refractive index detector while the samples were first eluted at 0.6mL/min through an HPX-87H Bio-Rad Aminex column (BioRad, Hercules Inc., CA) at a temperature of 65˚C. The mobile phase used in HPLC was 5mM sulfuric acid solution in nanopure water. Each run in the HPLC lasted for 60 minutes. The HPLC analysis has been proven viable to identify sugars, carboxylic acids, aldehydes, and carbonyl compounds by previous studies (Asghari & Yoshida, 2007; Yin & Tan, 2012). We were able to identify 13 chemical species based on the peak features of the HPLC signals in this study. The HPLC signals were modeled using the EMG model (see **Chapters 4** and **5)**.

CHAPTER 4

MODELING HPLC PEAK SIGNALS IN THE HPLC STANDARDS

4.1 Simulation Procedure

As discussed in **Chapter 1**, the EMG model has been widely used for modeling signals of chromatography including HPLC (Cavanillas, Serrano, Di´az-Cruz, Ariño, & Esteban, 2016; Baeza-Baeza, Torres-Lapasió, & García-Álvarez-Coque, 2011; Felinger, 1994). In **Chapter 3**, we discussed the viability of detecting the degradation products of cellulose using HPLC. In this phase of our research, we cenoided 16 chemical species potential degradation products during HTL of cellulose based on earlier experimental studies. The chemical species were cellotetraose, cellotriose, cellobiose, glucose, fructose, HMF, glycolaldehyde, furfural, lactic acid, malonic acid, succinic acid, formic acid, acetic acid, butyric acid, levulinic acid, and acetone. Using the EMG model to describe a HPLC peak, the retention time value, t_R, which refers to the parameter a_1 in ***(5***, is the most important parameter in the EMG model.

Among HPLC peaks in the HTL experiments of cellulose, glucose or levulinic acid, the peaks at the retention time of around 10 min and 21.15 min representing malonic acid and butyric acid respectively were not observed. Therefore, we did not model the HPLC signals for malonic acid and butyric acid in the HPLC standards. Furthermore, as we used acetone for washing off the reaction system after every HTL experiment, the modeling of HPLC peaks for acetone was also not included. Therefore, we did modeling using EMG model only for 13 chemical species, which were cellotetraose, cellotriose, cellobiose, glucose, fructose, HMF, furfural, succinic acid, levulinic acid, formic acid, acetic acid, glycolaldehyde, and lactic acid in the HPLC standards.

Different concentrations of the species were prepared in a 10 mL solution using MilliQ water. As the residues from the HPLC analysis may have an impact on the accuracy of the next ones, the samples were centrifuged for 10 seconds before being placed on the tray for analysis. Furthermore, in a series of HPLC tests for a chemical species, we started with the highest concentration, took a proportion of the last sample and mixed it with a certain amount of MilliQ DI water for the next sample. For example, if we had analyzed a 10 mL solution with the concentration of 25 mmol (mM) for the first HPLC analysis, in the second HPLC analysis we took 8 mL out of the 10 mL solution and mixed this 8 mL with 2 mL of MilliQ water for a solution with the concentration of 20 mM. We repeated this protocol for all the 13 chemical species and to minimize the mean percent errors (MPEs) between the detected HPLC signals and the simulated HPLC signals around the identified peaks. The expression of calculating MPEs is shown in ***7*** below, where *abs* refers to taking the absolute value of the result in the parenthesis; N_p is the number of points determined by the HPLC adsorption frequency, which is $\frac{1}{120}$ min in this study; $HPLC\ Signal_{i,simulated}$ refers to the value of the simulated HPLC signal at the point i; $HPLC\ Signal_{i,detected}$ refers to the value of the detected HPLC signal at the point i. After an optimization of the EMG parameters, a sensitivity analysis of EMG parameters was conducted to determine the most sensitive EMG parameter. To compare the confidence level of the simulated EMG parameters, threshold to divide different sections of the peak signals was chosen to be 10%, 30%, 50%, and 70% of the maximum HPLC signal. The simulated EMG parameters were estimated as the averages of the parameters acquired at different cutoff levels at the same confidence level. A representative modeling result of the HPLC signals near the peak retention time for this particular chemical species in HPLC standards is plotted in ***Figure 12***.

$$MPE = \frac{\sum_{i=1}^{i=Np} abs(\frac{HPLC\ Signal_{i,simulated} - HPLC\ Signal_{i,detected}}{HPLC\ Signal_{i,detected}})}{N_p} \times 100\ (\%) \qquad (7)$$

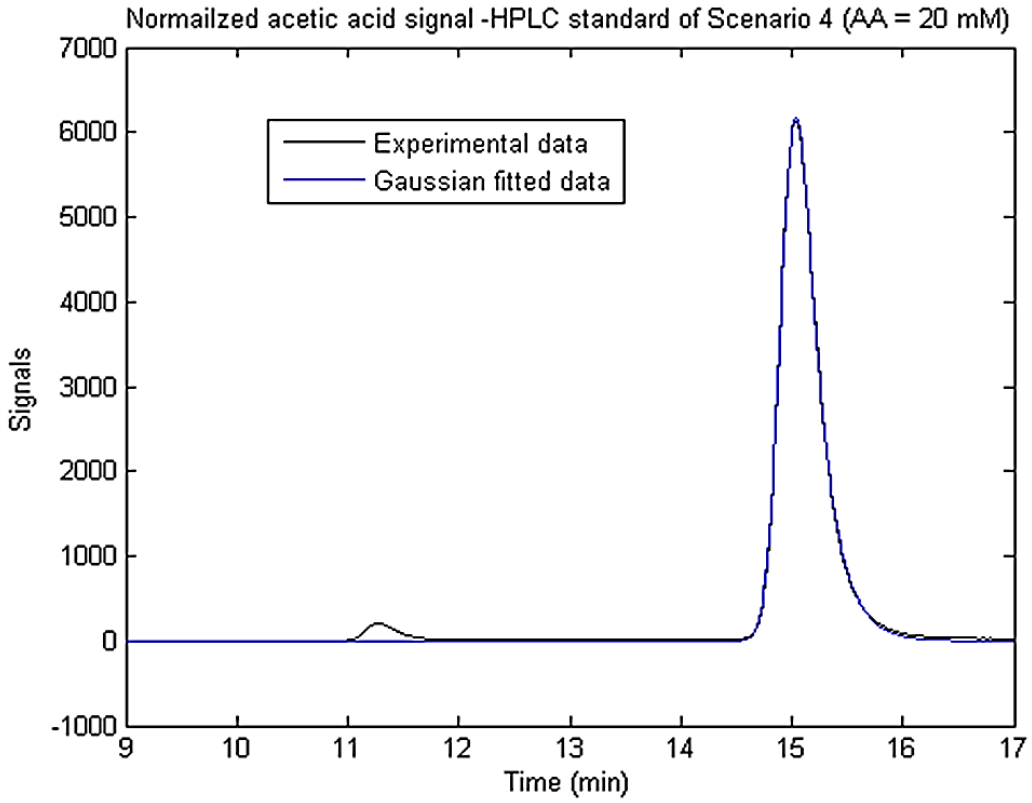

***Figure 12**: Plots of simulated HPLC signal (blue curve) in the standard of acetic acid at the concentration of 20 mM as a function of retention time compared to the detected HPLC signals (black curve).*

The simulated retention time values of all the identified HPLC peaks were within 0.1 min from the observed retention time values. The mean percent error in simulated results for the cases was calculated to be lower than 1% for all the data measured. In the other standards, the MPE values were generally below 1%. These results served as a solid basis for the reaction kinetic modeling and the solutions to the overlapping issues in HPLC signals.

Similarly, when the MPE values for the HPLC standards were minimized, the simulated EMG parameters of the chemical species at different concentrations were finalized. With the variations in concentrations, a sensitivity analysis of the regressed EMG parameters was conducted using piecewise linear interpolation between the consecutive points for different concentrations of specific species. For example, two points $A_1(x_i, y_i)$ and $A_2(x_{i+1}, y_{i+1})$ were given representing two individual simulated EMG parameters under different concentrations of the chemical species A, where y could be any parameter of the four EMG parameters and x was the value of concentrations. In the sensitivity analysis, the scenario at the lowest concentration of the chemical species was chosen as the base scenario. Assuming that the behavior of the parameters remained constant between any two consecutive points, a linear interpolation could be applied starting from the point in the base scenario to calculate the "piecewise" slope as $\frac{y_{i+1}-y_i}{x_{i+1}-x_i}$, also named as "gradient change" in this thesis. The calculated gradient change values for different EMG parameters were used directly to determine the most sensitive parameter. If the gradient change values were calculated to be close to 0, this parameter was considered insensitive to the variation of concentrations. That parameter was then chosen as a variable with minimum and maximum constraints in the HPLC signal modeling for the HTL experiments. On the contrary, if the gradient change values of an EMG parameter were all larger than 100, it was assumed that the parameter should be set as an independent variable only with nonnegative constraints in the modeling. The results of the HPLC signal modeling for the HPLC standards will be presented in the following section of this chapter. Overlapping issues of the HPLC signals are discussed in **Section 4.5**.

4.2 Results of Characterizing HPLC Curves in Standards

Based on the rationale discussed in the previous section, the EMG model was used to simulate the identified HPLC peak signals. The MPE values were successfully minimized in all cases. The ranges of the concentrations of different chemical species in the HPLC standards are shown in ***Table 4*** below.

Table 4*: Preparing different concentrations of the thirteen-chemical species in HPLC standards.*

Component	Minimum Concentration of the Component (mM)	Maximum Concentration of the Component (mM)	Component	Minimum Concentration of the Component (mM)	Maximum Concentration of the Component (mM)
Glucose	5.00	250.00	Formic acid	5.00	25.00
Fructose	5.00	25.00	Lactic aicd	5.00	100.00
Cellotetraose	2.34	37.50	Glycolaldehyde	5.00	100.00
Cellotriose	1.88	30.00	Succinic aicd	5.00	25.00
Cellobiose	12.50	100.00	Levulinic aicd	5.00	100.00
HMF	5.00	25.00	Acetic acid	5.00	100.00
Furfural	5.00	100.00			

After the MPE values were minimized by the *fmincon* function in *Matlab*®, the simulated EMG parameters and MPE values for each chemical species are summarized below in ***Table 5***-***Table* 9**. From the simulation results, I find that the simulated retention time values are all close to the observed experimental retention time values. The calculated MPEs are all below 5%, while most of them are smaller than 1%. This indicates that the EMG model accurately describes the HPLC peak signals maybe due to the high-resolution feature of HPLC analysis. With the simulated values, sensitivity analysis of these parameters were conducted to determine the concentration-sensitive parameters. More details will be shown in the next section. Lactic acid HPLC signals were modeled around the major peak at the retention time value of around 12.75

min as the lactic acid HPLC signal itself had three peaks detected at different retention time values. More details about modeling the HPLC signals are in **Section 4.5.2**.

Table 5*: Retention time values for the identified chemical species in the HPLC standards.*

Component	Observed Experimental Values		Simulated Values in EMG Model		
	Minimum Retention Time (min)	Maximum Retention Time (min)	Mean Retention Time (min)	Minimum Retention Time (min)	Maximum Retention Time (min)
Glucose	9.146	9.530	9.091	9.067	9.127
Fructose	9.853	9.869	9.796	9.776	9.807
Cellotetraose	6.394	6.406	6.337	6.330	6.349
Cellotriose	6.691	6.699	6.633	6.627	6.639
Cellobiose	7.377	7.384	7.294	7.284	7.300
Formic acid	13.798	13.801	13.698	13.688	13.702
Lactic aicd	12.736	12.744	12.657	12.651	12.669
Glycolaldehyde	12.722	12.736	12.643	12.634	12.653
Succinic aicd	11.427	11.438	11.341	11.331	11.350
Levulinic aicd	15.326	15.380	15.236	15.213	15.288
Acetic acid	15.032	15.043	14.939	14.927	14.955
HMF	28.113	28.183	27.972	27.933	28.020
Furfural	41.577	41.900	41.583	41.325	41.670

Table 6*: Simulated Area values for the identified chemical species in the HPLC standards.*

Component	Mean *Area* Value	Minimum *Area* Value	Maximum *Area* Value
Glucose	89322	4357	265312
Fructose	13015	4251	22367
Cellotetraose	44851	6427	120850
Cellotriose	26430	4056	69343
Cellobiose	78994	20837	173368
Formic acid	1122	408	1868
Lactic aicd	7973	1341	25144
Glycolaldehyde	16617	2451	49129
Succinic aicd	6293	2168	10600
Levulinic aicd	13321	2059	43430
Acetic acid	4340	726	13601
HMF	11965	3804	19574
Furfural	15871	5788	56890

***Table 7**: Simulated peak width values for the identified chemical species in the HPLC standards.*

Component	Mean *Width* Value	Minimum *Width* Value	Maximum *Width* Value
Glucose	0.0806	0.0736	0.0855
Fructose	0.0820	0.0808	0.0852
Cellotetraose	0.0656	0.0626	0.0670
Cellotriose	0.0709	0.0693	0.0719
Cellobiose	0.0864	0.0818	0.0906
Formic acid	0.1049	0.1026	0.1071
Lactic aicd	0.1052	0.0957	0.1177
Glycolaldehyde	0.0947	0.0875	0.0977
Succinic aicd	0.0948	0.0929	0.0981
Levulinic aicd	0.1142	0.1045	0.1187
Acetic acid	0.1106	0.1020	0.1151
HMF	0.1898	0.1870	0.1924
Furfural	0.2679	0.2571	0.2745

***Table 8**: Simulated damping factor values, D, for the identified chemical species in the HPLC standards.*

Component	Mean *D* Value	Minimum *D* Value	Maximum *D* Value
Glucose	0.1396	0.1179	0.1615
Fructose	0.1318	0.1230	0.1485
Cellotetraose	0.1273	0.1170	0.1403
Cellotriose	0.1227	0.1203	0.1274
Cellobiose	0.1933	0.1782	0.2128
Formic acid	0.2052	0.1962	0.2409
Lactic aicd	0.1451	0.1238	0.1606
Glycolaldehyde	0.1597	0.1414	0.1758
Succinic aicd	0.1778	0.1717	0.1886
Levulinic aicd	0.2070	0.1701	0.2290
Acetic acid	0.1859	0.1545	0.2048
HMF	0.3050	0.2835	0.3518
Furfural	0.4615	0.4011	0.5844

***Table 9**: Mean Percent Error values for the identified chemical species in the HPLC standards.*

Component	Minimum *Mean Percent Error* (%)	Maximum *Mean Percent Error* (%)
Glucose	0.0027	2.3243
Fructose	0.0021	0.7729
Cellotetraose	0.0073	3.3620
Cellotriose	0.0251	1.2163
Cellobiose	0.0066	4.0266
Formic acid	0.0030	4.6303
Lactic aicd	0.0010	4.4857
Glycolaldehyde	0.0015	2.7359
Succinic aicd	0.0016	2.7156
Levulinic aicd	0.0014	1.4697
Acetic acid	0.0015	1.0017
HMF	0.0031	4.3537
Furfural	0.0028	2.6430

4.3 Sensitivity Analysis of the EMG Parameters

Section 4.1 provided the rationale of choosing the concentration-sensitive parameters as independent variables in the EMG model to model the HPLC peak signals of the identified chemical species in our HTL experiments. We identified the base scenario for each chemical species as the one with the lowest concentrations, as presented in ***Table 10***. Given the simulation results of the EMG parameters, gradient change values were calculated for comparison among the regressed EMG parameters using the gradient formula $\frac{y_{i+1}-y_i}{x_{i+1}-x_i}$ as described in **Section 4.1**. The gradient change values for the EMG parameters are shown below in ***Table 11*** - ***Table* 14**.

***Table 10**: Base scenarios in the sensitivity analysis of the EMG parameters.*

Component	Concentration of the Component (mM)	*Area* Value	Retention Time Value	*Width* Value	*D* Value
Glucose	5.00	4454	9.078	0.0833	0.1475
Fructose	5.00	4319	9.800	0.0814	0.1292
Cellotetraose	2.34	6663	6.337	0.0642	0.1282
Cellotriose	1.88	4086	6.629	0.0714	0.1222
Cellobiose	12.50	21414	7.296	0.0891	0.1932
Formic acid	5.00	414	13.69	0.1056	0.2192
Lactic aicd	5.00	1343	12.65	0.1054	0.1535
Glycolaldehyde	5.00	2457	12.65	0.0976	0.1537
Succinic aicd	5.00	2192	11.35	0.0973	0.1792
Levulinic aicd	5.00	4886	15.23	0.1171	0.2101
Acetic acid	5.00	730	14.93	0.1146	0.1972
HMF	5.00	3811	28.02	0.1920	0.2859
Furfural	15.00	8567	41.64	0.2710	0.4336

***Table 11**: Sensitivity analysis results of the parameter Area.*

Component	Minimum Gradient Change	Maximum Gradient Change
Glucose	828.46	884.95
Fructose	849.79	880.59
Cellotetraose	3096.78	3243.86
Cellotriose	2283.11	2417.31
Cellobiose	1666.73	1725.50
Formic acid	68.14	72.11
Lactic aicd	246.62	255.89
Glycolaldehyde	447.26	507.43
Succinic aicd	395.41	413.04
Levulinic aicd	379.41	416.50
Acetic acid	130.76	135.05
HMF	700.19	760.53
Furfural	557.46	586.57

***Table 12**: Sensitivity analysis results of the retention time parameter t_R.*

Component	Minimum Gradient Change	Maximum Gradient Change
Glucose	-0.000979	0.000321
Fructose	-0.001055	0.000855
Cellotetraose	-0.000767	0.000210
Cellotriose	0.000317	0.002420
Cellobiose	-0.000582	0.000026
Formic acid	0.000157	0.001391
Lactic aicd	0.000037	0.000765
Glycolaldehyde	-0.000686	0.000664
Succinic aicd	-0.001284	-0.000331
Levulinic aicd	-0.000636	0.001245
Acetic acid	-0.000097	0.000979
HMF	-0.006028	-0.003912
Furfural	-0.007823	-0.003750

***Table 13**: Sensitivity analysis results of the peak width parameter.*

Component	Minimum Gradient Change	Maximum Gradient Change
Glucose	-0.000061	0.000037
Fructose	-0.000019	0.000181
Cellotetraose	0.000048	0.000588
Cellotriose	-0.000072	0.000034
Cellobiose	-0.000141	0.000068
Formic acid	-0.000184	-0.000044
Lactic aicd	-0.000136	0.000255
Glycolaldehyde	-0.000172	-0.000032
Succinic aicd	-0.000412	-0.000190
Levulinic aicd	-0.000226	0.000012
Acetic acid	-0.000247	-0.000076
HMF	-0.000270	-0.000173
Furfural	-0.000401	-0.000164

***Table 14**: Sensitivity analysis results of the parameter D.*

Component	Minimum Gradient Change	Maximum Gradient Change
Glucose	-0.000133	0.000155
Fructose	-0.000002	0.000569
Cellotetraose	-0.000695	0.000054
Cellotriose	-0.000068	0.000074
Cellobiose	-0.000094	0.000121
Formic acid	-0.003199	-0.000874
Lactic aicd	-0.000587	-0.000202
Glycolaldehyde	-0.000101	0.001865
Succinic aicd	-0.000381	-0.000048
Levulinic aicd	-0.000653	0.000446
Acetic acid	-0.000804	-0.000124
HMF	0.000317	0.002000
Furfural	0.001397	0.002773

From the sensitivity analysis results for t_R, *Width* and *D* respectively in ***Table 12*** - ***Table 14***, the variations are found to be very small approaching zero. This indicates that for specified parameters t_R, *Width* and *D* can be treated as concentration-insensitive variables in the HPLC signal modeling. Thus, the minimum and maximum of the parameters will be constrained by the values listed in ***Table 5***,

Table 7, and ***Table* 8**. Furthermore, the scale of gradient change values for parameter *A* appears to be much larger than that of others, at least 10^5 times the value of the other parameters. Therefore, it is safely concluded that the parameter *A* is the most concentration-sensitive and considered as the only concentration-sensitive parameter among the four EMG parameters.

4.4 Linear Calibration Curves of Concentrations versus Parameter A

Based on the finding that the parameter *A* is the most concentration-sensitive parameter among the four EMG parameters, the relationship between the simulated parameter *A* and the concentrations of the chemical species need to be quantified. Linear regression was considered as the primary choice, with each line passing through the origin point (0, 0). Thus, this results in the linear regression to have only one parameter, the slope of the line. With only one variable to fit in regression, the degree of freedom was maximized to be more data-driven. It was found that for all the identified species, simulated parameter *A* was perfectly linear versus the concentration. The regression coefficients R^2 and the slope values of the calibration curves are shown in ***Table 15***.

Table 15*: Parameters of the fitted regression curves for the HPLC standards.*

Component	Regression Coefficient R^2	Slope of the Linear Regression Curves (mM^{-1})
Glucose	0.9997	842
Fructose	0.9996	8670
Cellotetraose	0.9998	3109
Cellotriose	1.0000	2278
Cellobiose	0.9999	1679
Formic acid	0.9984	74
Lactic aicd	0.9998	252
Glycolaldehyde	0.9995	483
Succinic aicd	0.9997	418
Levulinic aicd	0.9997	413
Acetic acid	0.9998	134
HMF	0.9984	755
Furfural	0.9950	572

The R^2 values are within 0.999 of 1.0 validating the linear relationship between the simulated EMG parameter *A* and concentrations of the chemical species. A representative calibration curve is presented in ***Figure 13*** below. The regressed slope values will be used as a basis for solving overlapping issues described in the next section. Furthermore, the slope can be reversibly used for calculating the concentrations of the identified chemical species from simulated parameter *A* in the HTL experiments when the MPE values of the experimental HPLC signal modeling are optimized.

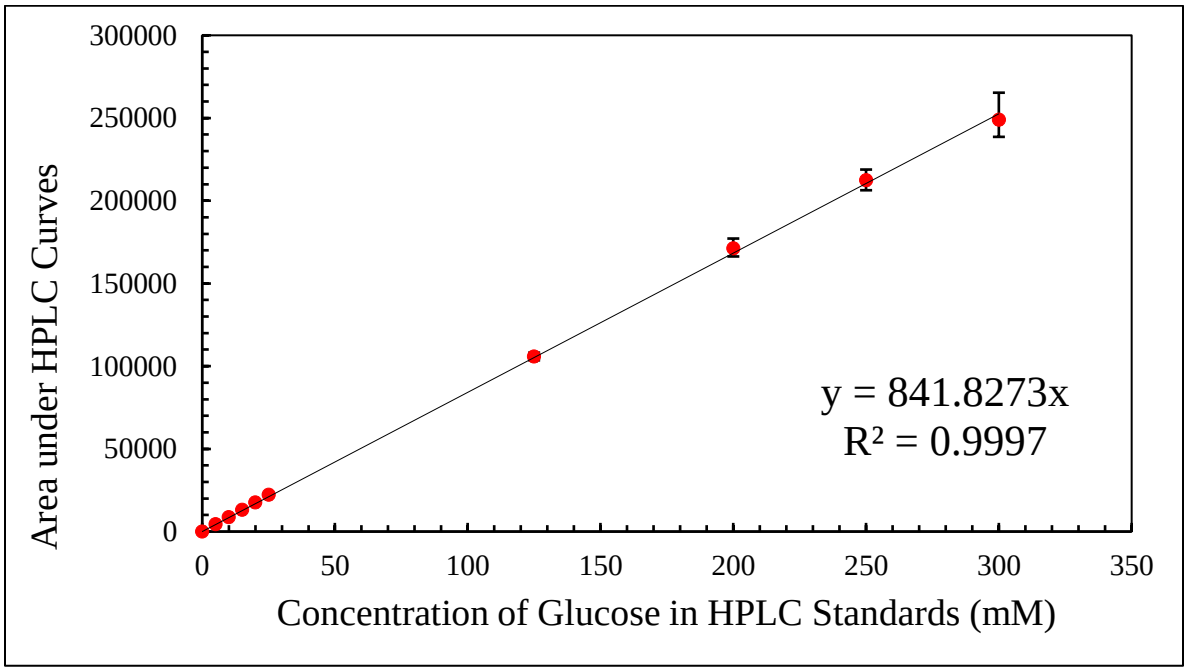

Figure 13*: The Calibration Curve between the Parameter Area and the Concentrations of Glucose in the HPLC Standards.*

4.5 Deconvolution of the Overlapping HPLC Signals

The EMG model has been evaluated to be consistent in the standards for individual identified chemical species. However, as the retention time values of two species get close to

each other, there are some overlapping HPLC signals. As is shown in ***Figure 14*** below, the "shoulder-like" peak shape indicates that there is another hidden peak at a retention time value of around 15.1 min, which corresponds to acetic acid based on the HPLC standards. With these similar retention times, we need to deconvolute the overlapping signals.

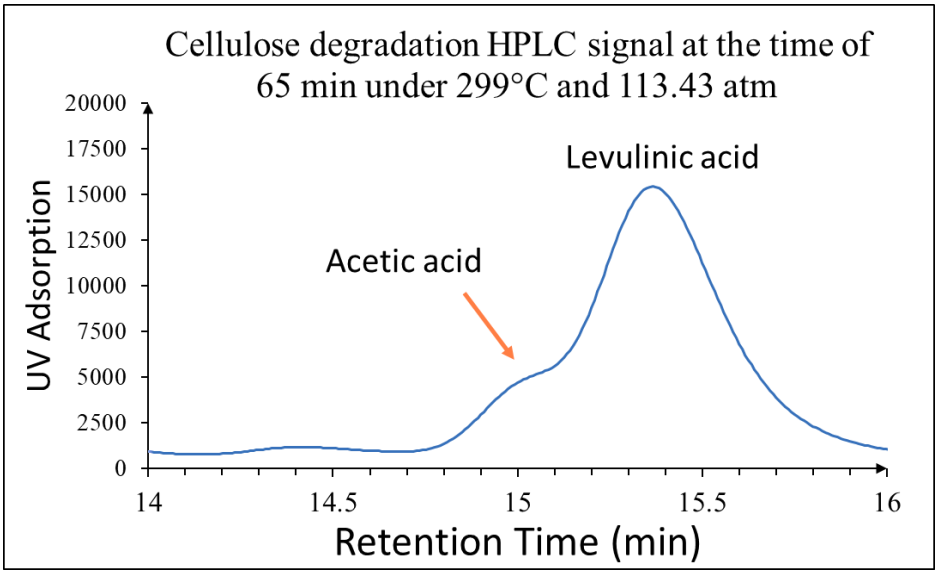

Figure 14*: Overlapping HPLC Signals Observed in the Cellulose-300 HTL Experiments.*

Previous approaches to resolving overlapping signals have already been successfully applied the superposition of the EMG models for gas chromatography data (Goodman & Brenna, 1994; Felinger, 1994). And a few studies included the deconvolution of overlapping HPLC signals using the EMG model. As the EMG model shows extraordinary correspondence with the HPLC peak signals for realistic chromatography results, the high-resolution feature of HPLC may help keep the individual HPLC signals of the overlapping species in its original shape behind the overlapping signals. Therefore, under this assumption, the superposition of the EMG models for each species can be applied to solving the overlapping issues. In our HTL

experiments, there were two groups of overlapping species identified: the first group was levulinic acid and acetic acid, while the other one was lactic acid and glycolaldehyde.

4.5.1 Levulinic Acid Overlapping with Acetic Acid

The overlapping signals in ***Figure 14*** can be deconvoluted into two HPLC curves with peaks at the retention time values of around 15.1 min and 15.4 min correspondingly. Scenarios of mixtures of levulinic acid and acetic acid are presented in ***Table 16***. A deconvolution example of the overlapping HPLC signals is shown in ***Figure 15***.

Table 16*: Preparation of Different Combinations of Levulinic Acid and Acetic Acid.*

Case	Concentration of Levulinic Acid in the Mixture (mM)	Concentration of Acetic Acid in the Mixture (mM)
1.1	12.50	12.50
1.2	25.00	25.00
1.3	50.00	50.00
1.4	50.00	12.50
1.5	12.50	5.00
1.6	5.00	50.00
1.7	5.00	12.50

Table 17*: Deconvolution Results of the Parameter A for Levulinic Acid.*

Case	Parameter *A* of Levulinic Acid	Mean Value of the Calculated Concentration of Levulinic Acid (mM)	Deviation from the Realistic Concentration of Levulinic Acid (%)
1.1	5223	12.64	1.11
1.2	9652	23.35	-6.59
1.3	19995	48.38	-3.24
1.4	20561	49.75	-0.50
1.5	5239	12.68	1.41
1.6	1961	4.74	-5.11
1.7	2143	5.19	3.71

***Table 18**: Deconvolution Results of the Parameter A for Acetic Acid.*

Case	Parameter *A* of Acetic Acid	Mean Value of the Calculated Concentration of Acetic Acid (mM)	Deviation from the Realistic Concentration of Acetic Acid (%)
1.1	1600	11.94	-4.46
1.2	3006	22.44	-10.25
1.3	5970	44.56	-10.88
1.4	1516	11.32	-9.46
1.5	622	4.65	-7.08
1.6	6733	50.26	0.51
1.7	1644	12.27	-1.84

***Table 19**: The Ranges of Mean Percent Error Values for the Deconvolution Results.*

Case	Minimum Mean Percent Error (%)	Maximum Mean Percent Error (%)
1.1	0.0011	0.9787
1.2	0.0045	0.7098
1.3	0.0066	0.8886
1.4	0.0030	1.9438
1.5	0.0075	4.0892
1.6	0.0011	0.7312
1.7	0.0181	1.6071

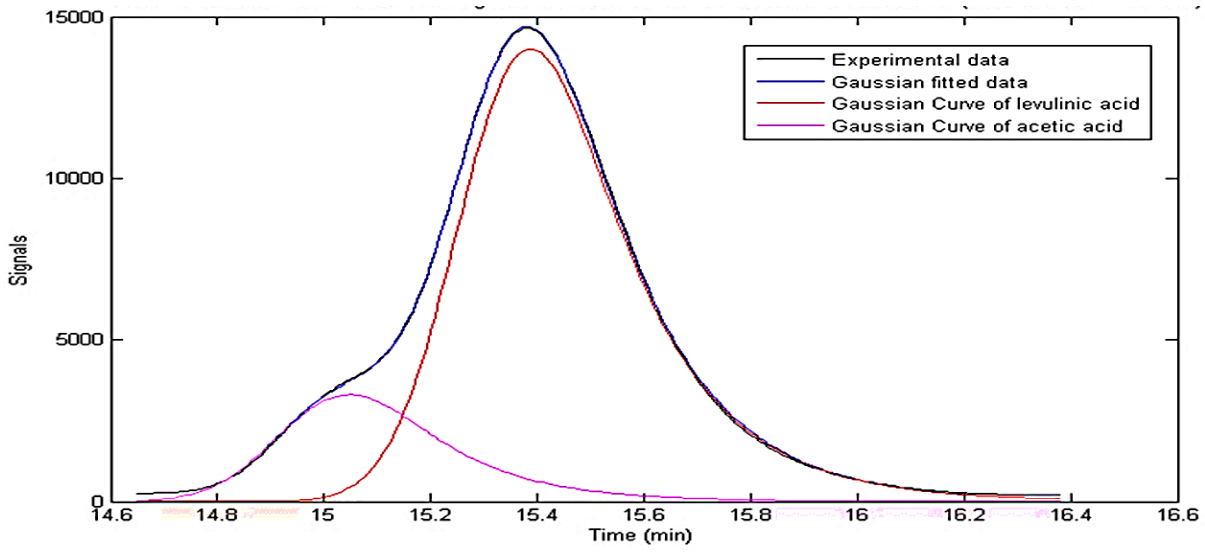

***Figure 15**: Deconvolution of the overlapping signals in Scenario **1.3**.*

In the optimization of the deconvolution, the constraints for the EMG parameters were all satisfied, and the MPE values were consistently low that were comparable to the MPE values in the HPLC standards for individual species. From the linear calibration curves of levulinic acid and acetic acid, we were able to calculate the simulated concentrations of levulinic acid and acetic acid respectively based on the deconvoluted parameter *A* values. The deviation from the expected value of concentration of levulinic acid and acetic acid was generally well below 10%. This provided sufficient confidence in deconvoluting the overlapping signals of levulinic acid and acetic acid in the observed HPLC signal response of the HTL experiments. For HTL experiments, additional details about the deconvolution of experimental overlapping signals are in **Chapter 5**.

4.5.2 Lactic Acid Overlapping with Glycolaldehyde

The rationale behind deconvoluting the lactic acid and glycolaldehyde HPLC peaks is different. The HPLC standards for lactic acid contained three peaks, while other species had only one major peak. The EMG parameters of lactic acid and glycolaldehyde are close, leading to overlapping signals that are difficult to deconvolute simply using superposition. The concentration combinations of the two species in the standards are listed in ***Table 20*** below.

Table 20*: Preparation of Different Combinations of Lactic Acid and Glycolaldehyde.*

Scenario	Concentration of Lactic Acid in the Mixture (mM)	Concentration of Glycolaldehyde in the Mixture (mM)
2.1	5.00	50.00
2.2	5.00	12.50
2.3	12.50	12.50
2.4	12.50	50.00
2.5	25.00	25.00

When the constraints of the retention time parameter t_R, as well as the *Width* and *D* parameters, were satisfied and MPE values were minimized below 5%, the optimized parameter *A* values were used to calculate the simulated concentrations of lactic acid and glycolaldehyde. However, although the MPE values satisfied the confidence level that the other HPLC standards achieved, the simulated concentrations of glycolaldehyde and lactic acid failed to match the realistic ones. One failed example is shown in ***Figure 16*** below.

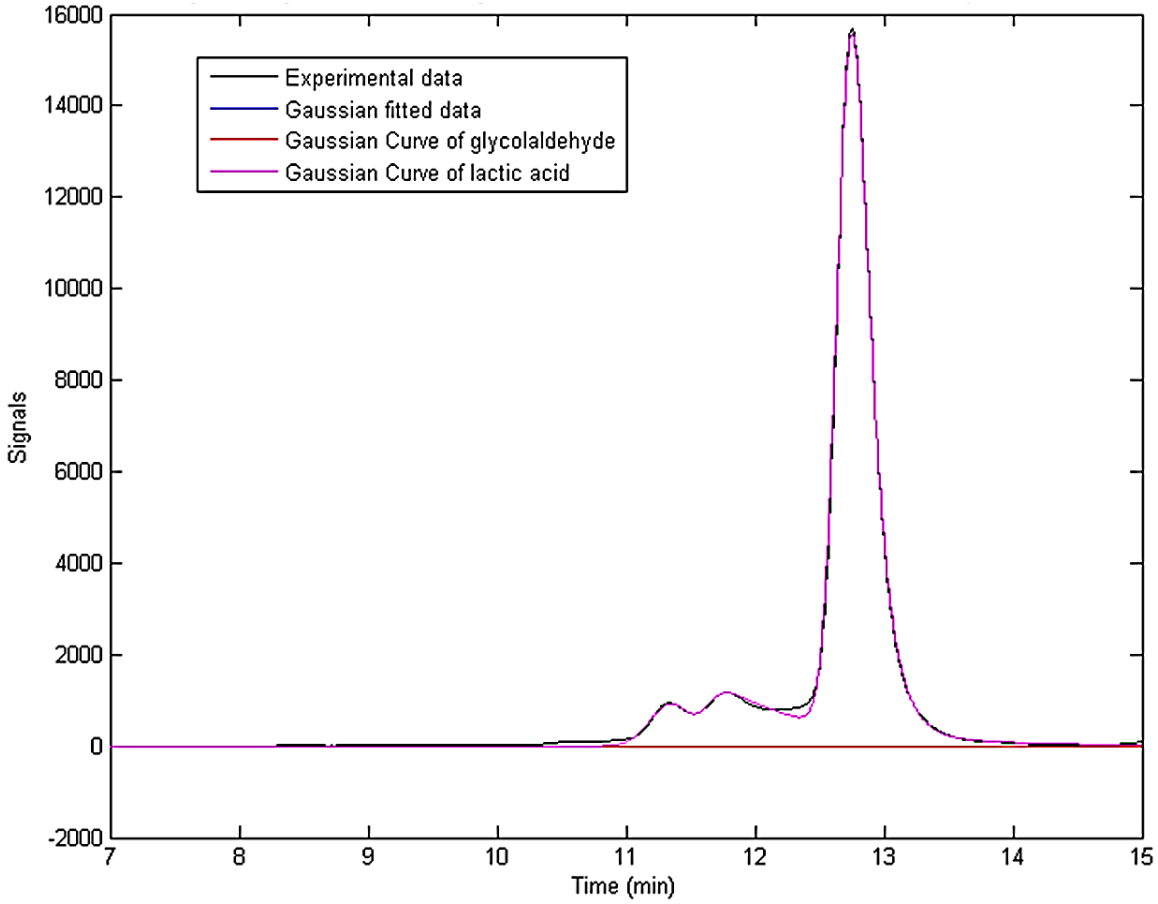

Figure 16*: Deconvoluted HPLC Signals of Lactic Acid and Glycolaldehyde in Scenario* ***2.3*** *using Superposition.*

From ***Figure 16*** above, the deconvoluted HPLC curve of glycolaldehyde stayed around 0, which indicated that the simulated concentration of glycolaldehyde was approximately 0.

Contradictorily, the realistic concentration of glycolaldehyde in the mixture in this scenario was prepared to be 12.5 mM. Furthermore, there were other failures in using superposition in the other cases. Thus superposition was an effective solution to solving overlapping signals of lactic acid and glycolaldehyde.

Based on the fact that the pure lactic acid HPLC signals had three peaks observed, we examined the peak height relationships among the three peaks. The retention time and peak height values are recorded below in ***Table 21***.

Table 21: *Observed Retention Time Values and Peak Height at the Peaks of Lactic Acid HPLC Signals in HPLC Standards.*

Concentration of Lactic Acid (mM)	Retention Time of the First Peak (min)	First Peak Value in HPLC Signals	Retention Time of the Second Peak (min)	Peak Value in HPLC Signals	Retention Time of the Third Peak (min)	Third Peak Value in HPLC Signals
5.00	11.300	573	11.725	542	12.742	3494
10.00	11.308	863	11.733	969	12.750	6744
15.00	11.300	1179	11.725	1411	12.742	10157
20.00	11.308	1428	11.733	1826	12.742	13370
25.00	11.308	1758	11.733	2288	12.742	16800
50.00	11.308	3023	11.742	4452	12.742	35778
100.00	11.325	6126	11.750	8975	12.750	71509

From the observed peak features, it is found that the distribution of retention time values of the peaks remains about the same regardless of lactic acid concentration. This indicates that the appearance of the peaks is consistent in observed retention time values even when the concentrations of lactic acid changed significantly. Furthermore, the ratios between the peak heights seem to be exponentially related, as a summary of the peak height ratios is shown in ***Table 22*** below. The peak ratios between the peak heights at different retention time values with

concentrations of lactic acid were correlated using different mathematical models, including linear, polynomial, exponential and power functions. All four models had to satisfy the condition that the regression curve should go through the origin point (0, 0).

***Table 22**: Peak Height Ratios at the Peaks of Lactic Acid HPLC Signals in the HPLC Standards.*

Concentration of Lactic Acid (mM)	Peak Ratio of First Peak Value to Third Peak Value	Peak Ratio of Second Peak Value to Third Peak Value	Peak Ratio of First Peak Value to Second Peak Value
5.00	0.1640	0.1551	1.0572
10.00	0.1280	0.1437	0.8906
15.00	0.1161	0.1389	0.8356
20.00	0.1068	0.1366	0.7820
25.00	0.1046	0.1362	0.7684
50.00	0.0845	0.1244	0.6790
100.00	0.0857	0.1255	0.6826

After trials of the mathematical models proposed for relationships between peak ratios or peak heights and concentrations, power models were found to have the largest R^2 regression coefficients for the regression between the first peak heights at the retention time value of around 11.3 min and concentrations of lactic acid. Linear relationship was found to be the best fit to the major peak heights at the retention time value of around 12.75 min. The models for the regression between the peak ratios did not have a higher R^2 regression coefficient than the best regression case of peak heights versus concentration values. The regression results of the peak heights versus concentration values of lactic acid in the HPLC pure standards are plotted in ***Figure 17*** - ***Figure* 20** below.

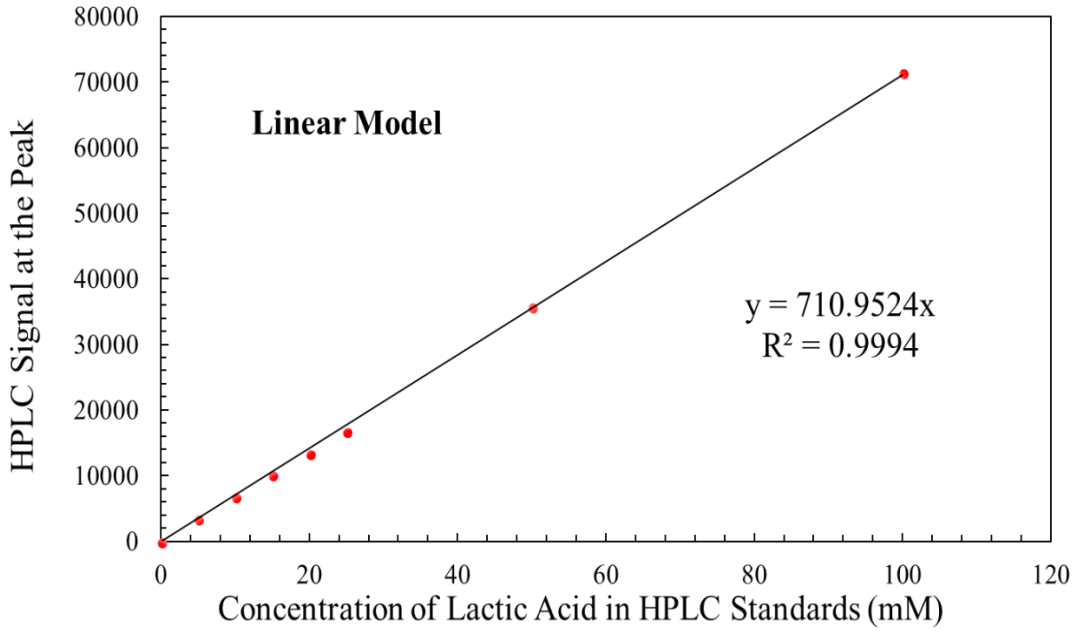

***Figure 17**: Linear Regression Curve between the Major Peak Height and the Concentration of Lactic Acid in the HPLC Standards.*

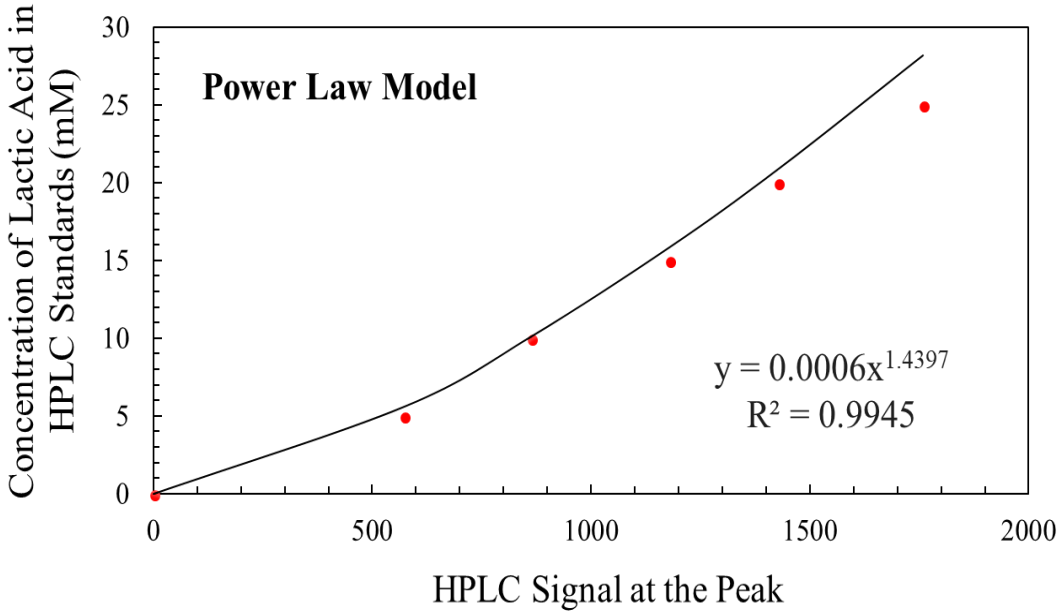

***Figure 18**: Regression Curve between the First Peak Height and the Concentration of Lactic Acid in HPLC Standards using Power Law Model.*

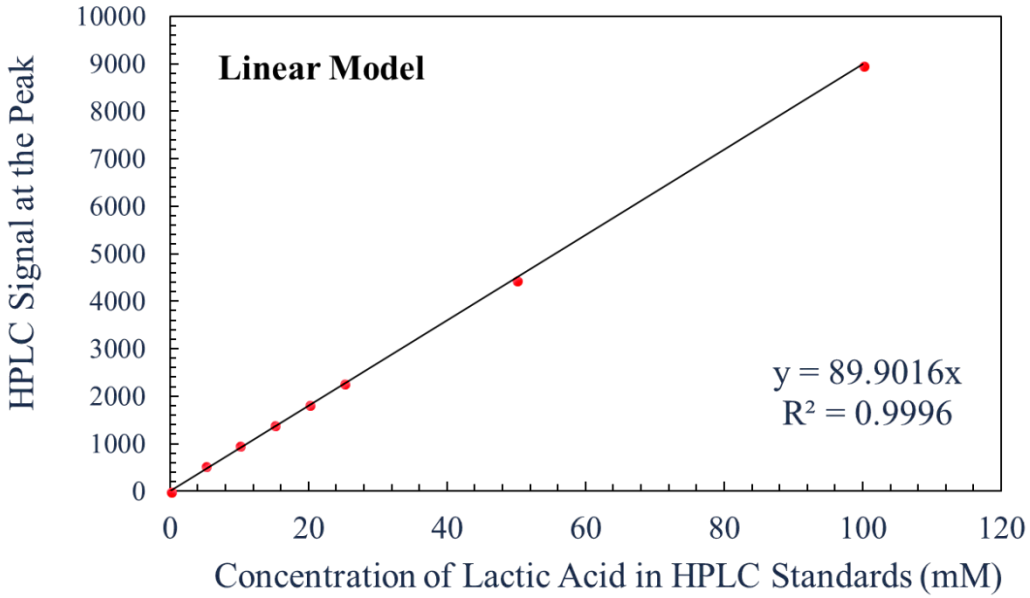

***Figure 19**: Linear Regression Curve between the Second Peak Height and the Concentration of Lactic Acid in the HPLC Standards.*

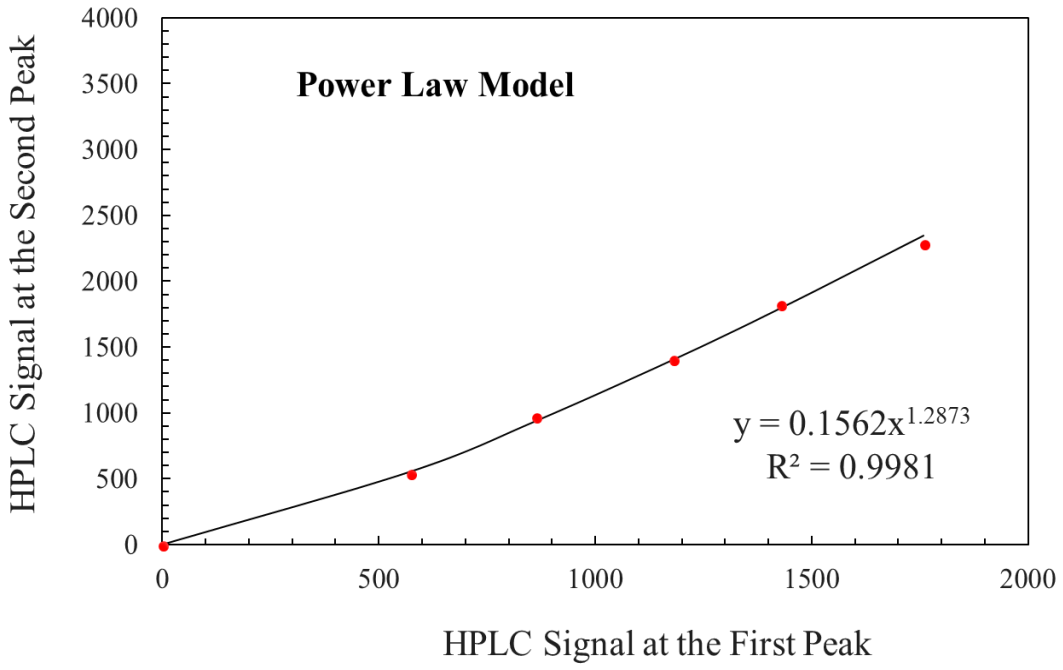

***Figure 20**: Regression Curve between the Second Peak Height and the First Peak Height of Lactic Acid in the HPLC Standards using Power Law Model.*

From ***Figure 17*** and ***Figure* 19**, the selection of x-axis is of equal convenience between the first peak heights and the concentration values. One alternative of the regression model between the first peak values and the concentrations is shown above in ***Figure 18***. The R^2 regression coefficient in the cases using linear model is the highest among the four models, very close to 1. Therefore, in this study I choose the linear model as the regression model for first peak heights versus concentration values of lactic acid in the HPLC standards.

The regression test is similar to the one we do for the calibration curves. The parameters of the modeled power curves or linear regression curves were used to evaluate the concentrations of lactic acid in the solutions where lactic acid and glycolaldehyde could be mixed, assuming that the peak ratios of lactic acid HPLC signals were not affected by the tailing of the HPLC curves of glycolaldehyde. Therefore, I managed to derive the simulated concentrations of lactic acid in the mixtures. With the concentration values, the EMG parameter *A* were calculated using the calibration curves of lactic acid as mentioned in **Section 4.4**. With the constraints of all four EMG parameters of lactic acid and all EMG parameters except *A* of glycolaldehyde, the superposition of the two EMG models can be applied for deconvoluting the overlapping HPLC signals. With MPE values minimized, the simulated concentrations of lactic acid and glycolaldehyde are summarized below in ***Table 23*** and ***Table 24***. After a series of deconvolution work, the simulated concentration values were compared to the realistic ones that were used for the preparation of the mixtures of lactic acid and glycolaldehyde in the HPLC standards. From ***Table 23*** and ***Table 24***, a higher confidence level was typically reached for lactic acid and glycolaldehyde at higher concentrations. Yet it is the best solution that we can offer for deconvoluting lactic acid and glycolaldehyde signals at this time. Further improvements of the deconvolution of overlapping signals of lactic acid and glycolaldehyde may include the

supplementation of other mathematical models or modeling the peak heights using other functions.

***Table 23**: Comparison of the Calculated Concentrations and the Realistic Concentrations of Lactic Acid in the Mixtures of Lactic Acid and Glycolaldehyde.*

Scenario	Calculated Concentration of Lactic Acid using Power Model (mM)	Realistic Concentration of Lactic Acid (mM)	Deviation from the Realistic Value (%)
2.1	6.58	5.00	31.61
2.2	5.41	5.00	8.28
2.3	14.87	12.50	18.99
2.4	14.27	12.50	14.15
2.5	22.61	25.00	-9.57

***Table 24**: Comparison of the Calculated Concentrations and the Realistic Concentrations of Glycolaldehyde in the Mixtures of Lactic Acid and Glycolaldehyde.*

Scenario	Calculated Concentration of Glycolaldehyde using Power Model (mM)	Realistic Concentration of Glycolaldehyde (mM)	Deviation from the Realistic Value (%)
2.1	49.62	50.00	-0.75
2.2	10.23	12.50	-18.18
2.3	14.35	12.50	14.79
2.4	53.46	50.00	6.92
2.5	32.79	25.00	31.14

The deconvolution results of lactic acid mixing with glycolaldehyde were used for determining whether lactic acid was present in the HTL experiments. If lactic acid HPLC signals were verified based on the peak features for the first peak and the second peak, the regression curves in this section can be used to calculate the realistic concentration values of lactic acid in the experiments. As we can see the precision of HPLC signals is crucial for reaction kinetic modeling to demonstrate the underlying reaction mechanisms for HTL, MPE values together

with the EMG parameters t_R, *Width* and *D* can be used as criteria for justifying the accuracy of the identified HPLC peak signals. In the next chapter, the modeling results of HPLC peak signals for the HTL experiments of cellulose, glucose and levulinic acid will be presented based on the HPLC signal modeling results developed in **Chapter 4**.

Chapter 4 systematically evaluated the identified HPLC peaks that mostly occurred in the previous HTL studies of cellulose. However, there are still many unidentified degradation products of cellulose and many other overlapping scenarios. In the future study, more chemical species in the degradation pathway should be identified to supplement the reaction kinetics of HTL of cellulose presented in this study.

CHAPTER 5

MODELING HPLC SIGNALS IN THE HTL EXPERIMENTS

5.1 Cellulose-300 Scenario

Guided by the experimental protocol as described in **Chapter 3**, the aqueous product samples from the Cellulose-300 HTL experiment were sent to HPLC analysis for identifying the HTL degradation products. From **Chapter 4**, the HPLC signals in the HTL experiments can be characterized based on the HPLC standards. After MPE values are minimized, the values of EMG parameter *A* at different reaction times will be used to derive the concentration profiles of the identified species using the calibration curves and regression curves. With the experimental HTL concentration profiles, stages of product evolution will be discussed.

5.1.1 Results of Modeling the HPLC Signals

The HPLC peak signals for the Cellulose-300 Scenario were identified based on the observed retention time values. Chromatography plots of HPLC analysis are displayed in ***Figure 21***, where a red star represents the overlapping HPLC signals of levulinic acid mixed with acetic acid; the regions where the retention time values are between 6 and 8 min are zoomed in where any cellulo-oligomers were detected; the x-axis of the chromatography plots is retention time in unit of minutes and the y-axis is HPLC UV adsorption signal. With the identification results in Cellulose-300 Scenario, the HPLC signals were modeled using the EMG model with different cutoff criteria for the peak heights following the same modeling protocols in **Chapter 4**. The simulated EMG parameters for the HPLC experimental peak signals for Cellulose-300 Scenario are given in ***Table 32*** - ***Table*** **51** in **Appendix A**.

Cellulose (50g/L) with compressed N_2 with steady-state reactor temperature as 300 ˚C

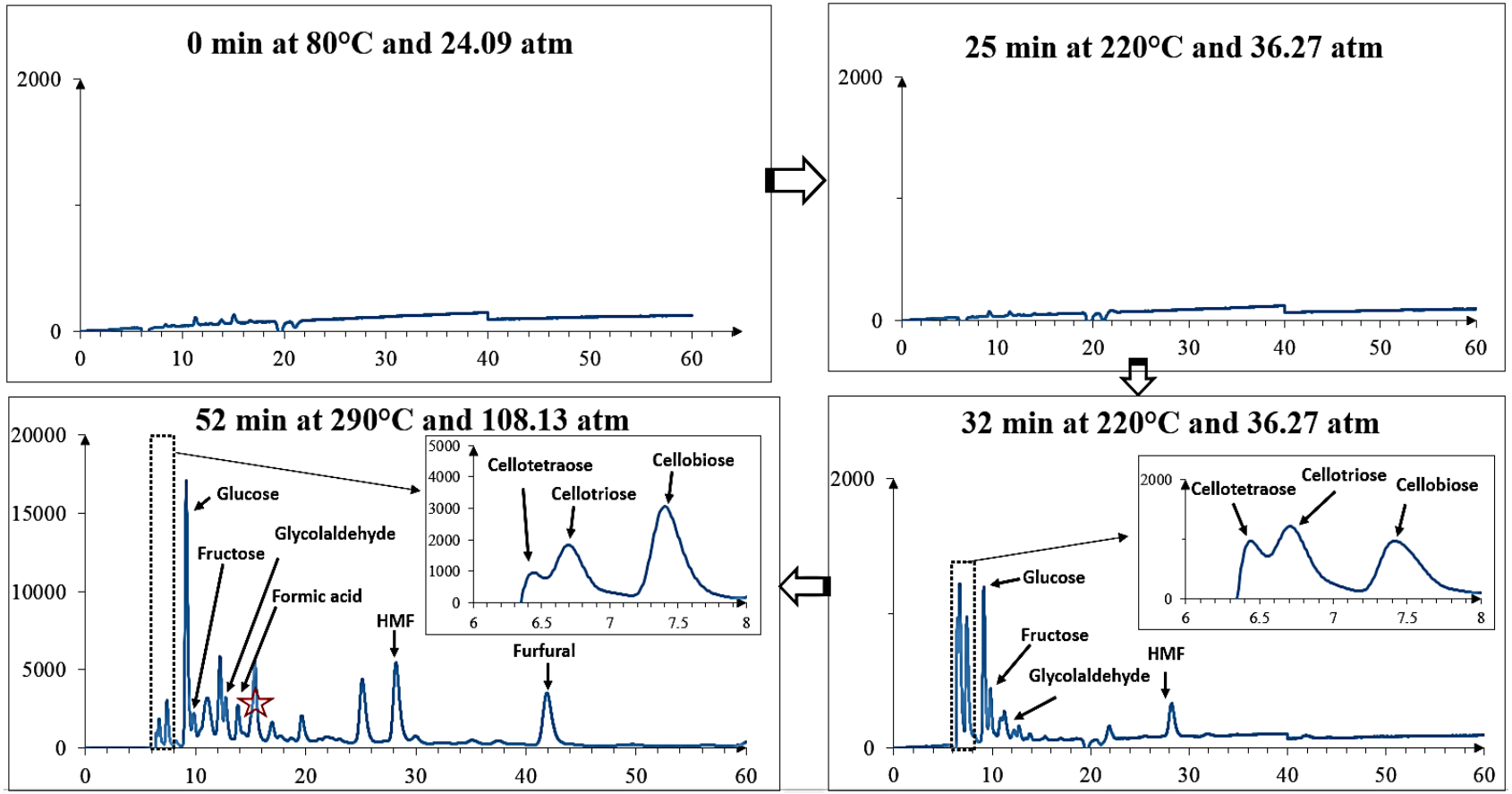

(a) When reaction time is 0 min, 25 min, 32 min and 52 min;

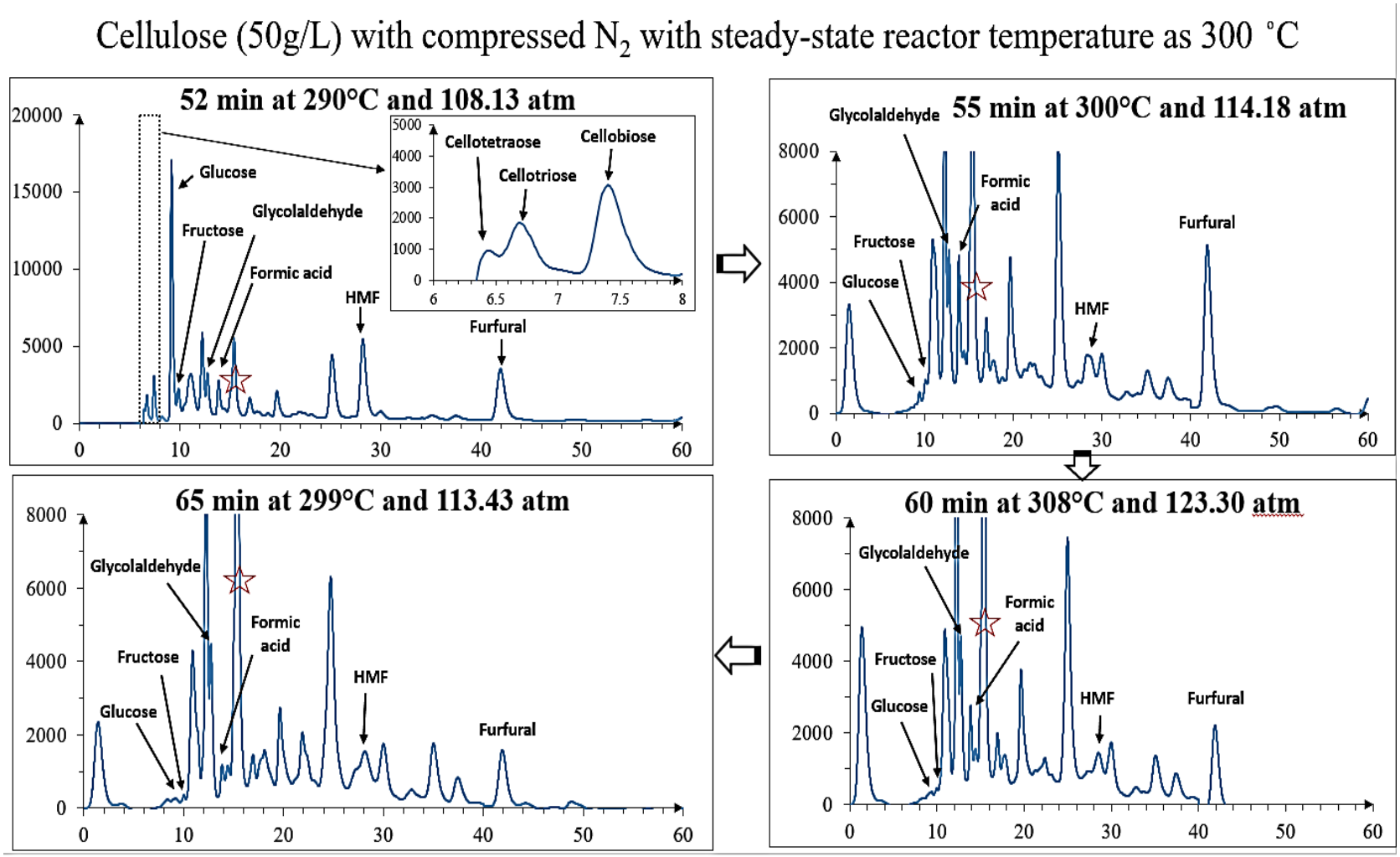

(b) When reaction time is 52 min, 55 min, 60 min and 65 min;

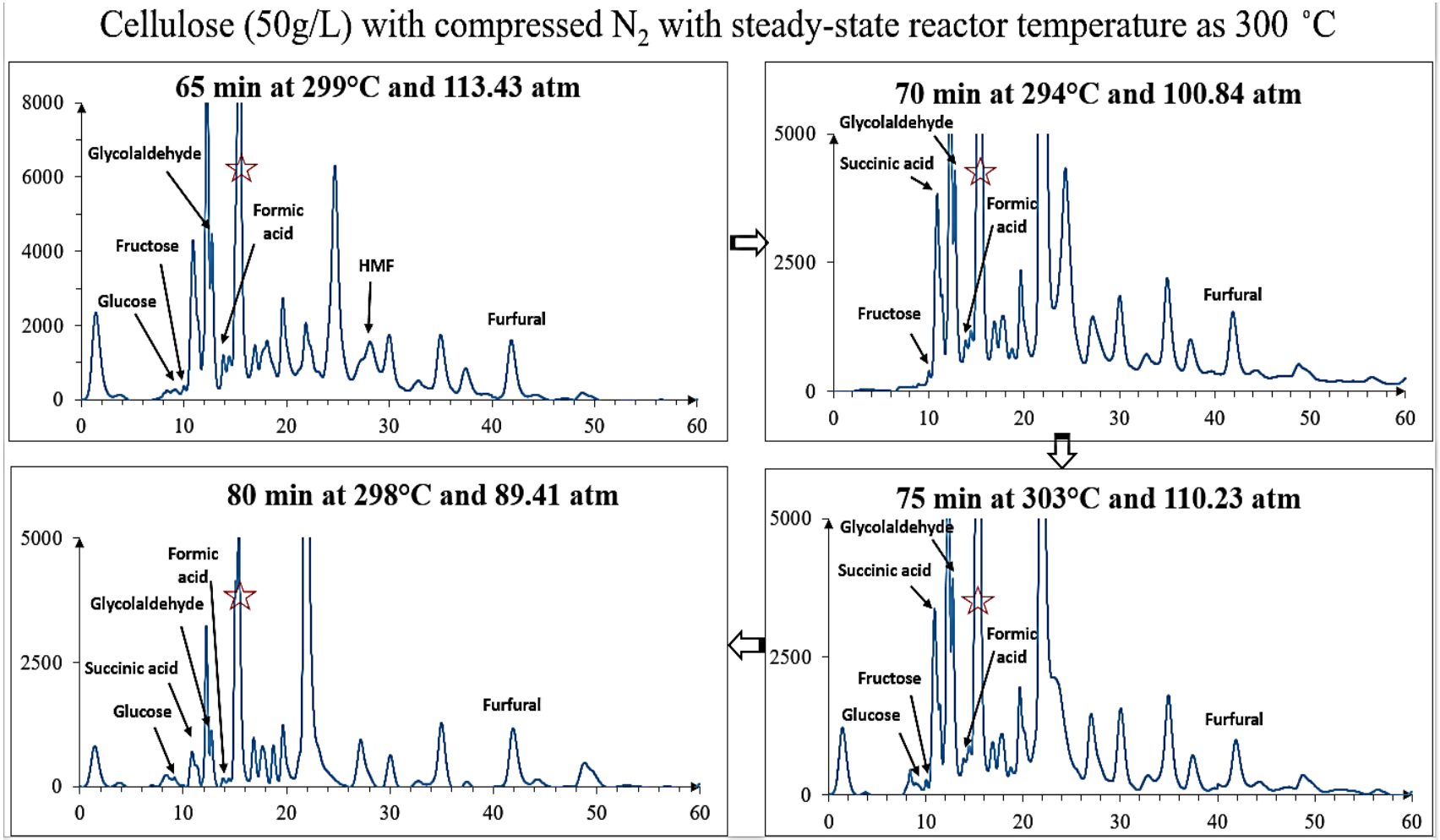

(c) When reaction time is 65 min, 70 min, 75 min and 80 min;

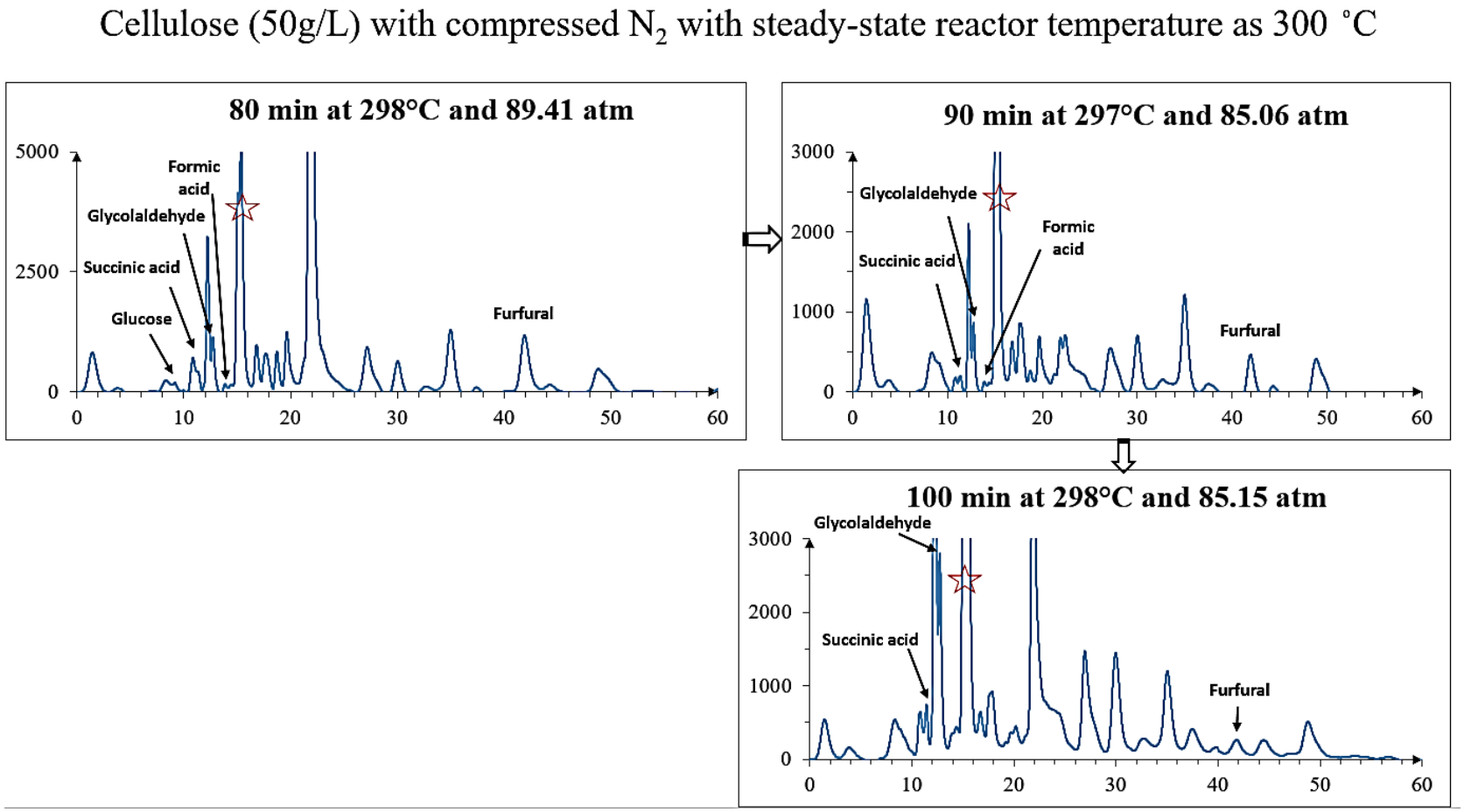

(d) When reaction time is 80 min, 90 min and 100 min.

Figure 21*: Chromatography plots of HPLC analysis with the identified chemical species labeled in Cellulose-300 Scenario.*

The chromatography plots in ***Figure 21*** show how the peak signals in Cellulose-300 Scenario evolve with reaction time. These HPLC peaks were identified based on the HPLC standards. There remain some peaks unidentified, which might play a significant role in the cellulose degradation mechanisms under HTL conditions. The identified HPLC peaks were modeled using the protocol that I describe in **Chapter 4**. In general, the simulated MPE values in this scenario were close to the ones in the HPLC standards. The peaks that had larger MPE values were mostly affected by the baseline fluctuation of the chromatography plots. Apart from the baseline effect, those peaks might overlap with the adjacent peaks that were unidentified. With the minimized MPE values, the simulated EMG parameters in this scenario are given in ***Table 32*** - ***Table* 55** in the **Appendix A**. The existence of lactic acid was excluded in the HPLC peak signals around the retention time values of approximately 12.74 min. The calculated major peak height values using the approach in **Section 4.5.2** did not match with the ones observed in the chromatography plots, as shown in ***Table 54*** and ***Table* 55**. Therefore, the lactic acid was not identified for the peaks around the retention time values of 12.74 min. Instead, glycolaldehyde was identified based on the HPLC standards when the fitting of the HPLC peak signals showed much smaller MPE errors than the overlapping cases of lactic acid mixing with glycolaldehyde. The simulated EMG parameters A were used for deriving the concentration profiles with error bars determined by the simulated parameters that gave the same group of MPE values (Group 1: <3%; Group 2: 3% - 8%; Group 3: 8% - 15%; Group 4: >15%).

From the chromatography plots of Cellulose-300 Scenario, three key findings were determined:

1) Generally there were three stages in the cellulose degradation under HTL conditions: ***Stage 1*** was the decomposition of cellulose into cellulo-oligomers (cellotriose, cellobiose and cellotetraose) and cellulo-monomers (glucose and fructose); ***Stage 2*** was further degradation of cellulo-monomers into aldehydes (e.g., HMF, furfural and glycolaldehyde) and carboxylic acids (e.g., succinic acid, levulinic acid, acetic acid and formic acid); ***Stage 3*** was the condensation and repolymerization of short-chain molecules. This Three-Stage hypothesis has also been concluded in previous studies (Croce, *et al*., 2017; Peterson, *et al*., 2008). From a literature review, I was able to establish a few chemical reaction pathway schemes for the HTL of cellulose, which are introduced in **Chapter 6**. After the reaction kinetic modeling according to the proposed HTL reaction networks, modeling results will be discussed, and recommendations will be provided for the HTL process optimization in **Chapter 7**.
2) The HPLC signals for some carboxylic acids were neither increasing nor decreasing significantly with the reaction time evolving. The stability of levulinic acid were analyzed in Levulinic-300 Scenario to test out how the carboxylic acids performed under HTL conditions.
3) The experimental HPLC signals for some unidentified chemicals were also evolving with reaction time. This can be further investigated in the future work using other analytical techniques, such as GC/MS.

5.1.2 Product Evolution Profile

Using the calibration curves, the experimental concentration profiles were derived from the simulated values of EMG parameter *A*. The simulated experimental concentration profiles are

plotted in **Appendix G**. To visually understand the macroscopic evolution for Cellulose-300 Scenario, the product evolution profiles are plotted in ***Figure 22*** and ***Figure* 23**.

Notably, the reason why I separated glycolaldehyde from HMF and Furfural was that the generation of glycolaldehyde may come from both glucose and fructose in ***Stage 2***, but the generation of furan aldehydes (e.g., HMF and furfural) was only found to originate from fructose in the HTL literature (Peterson, *et al*., 2008). More discussions about the degradation patterns are given in **Section 5.5** by comparison with the results in other scenarios.

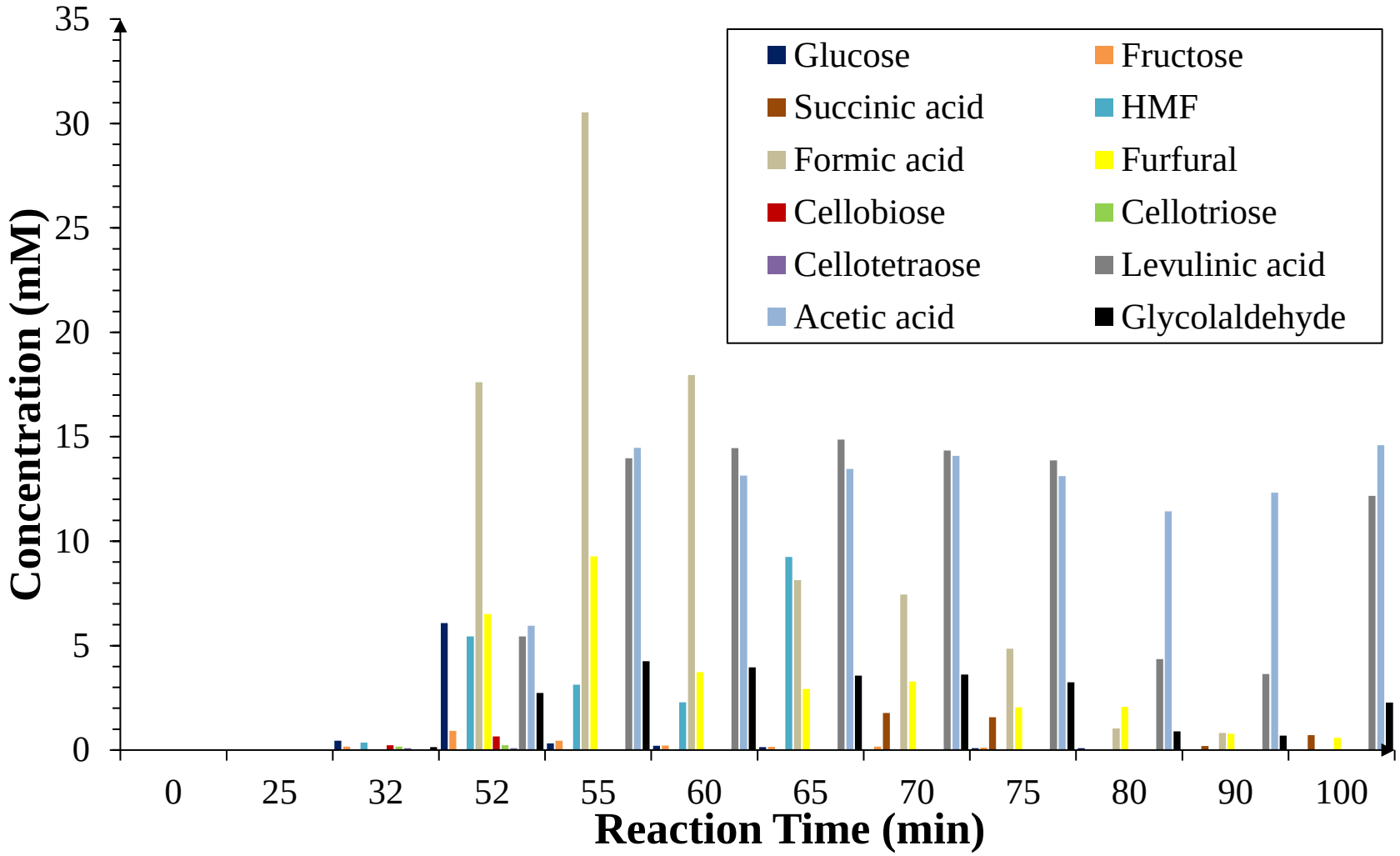

***Figure 22**: Evolution of the identified chemical species in Cellulose-300 Scenario.*

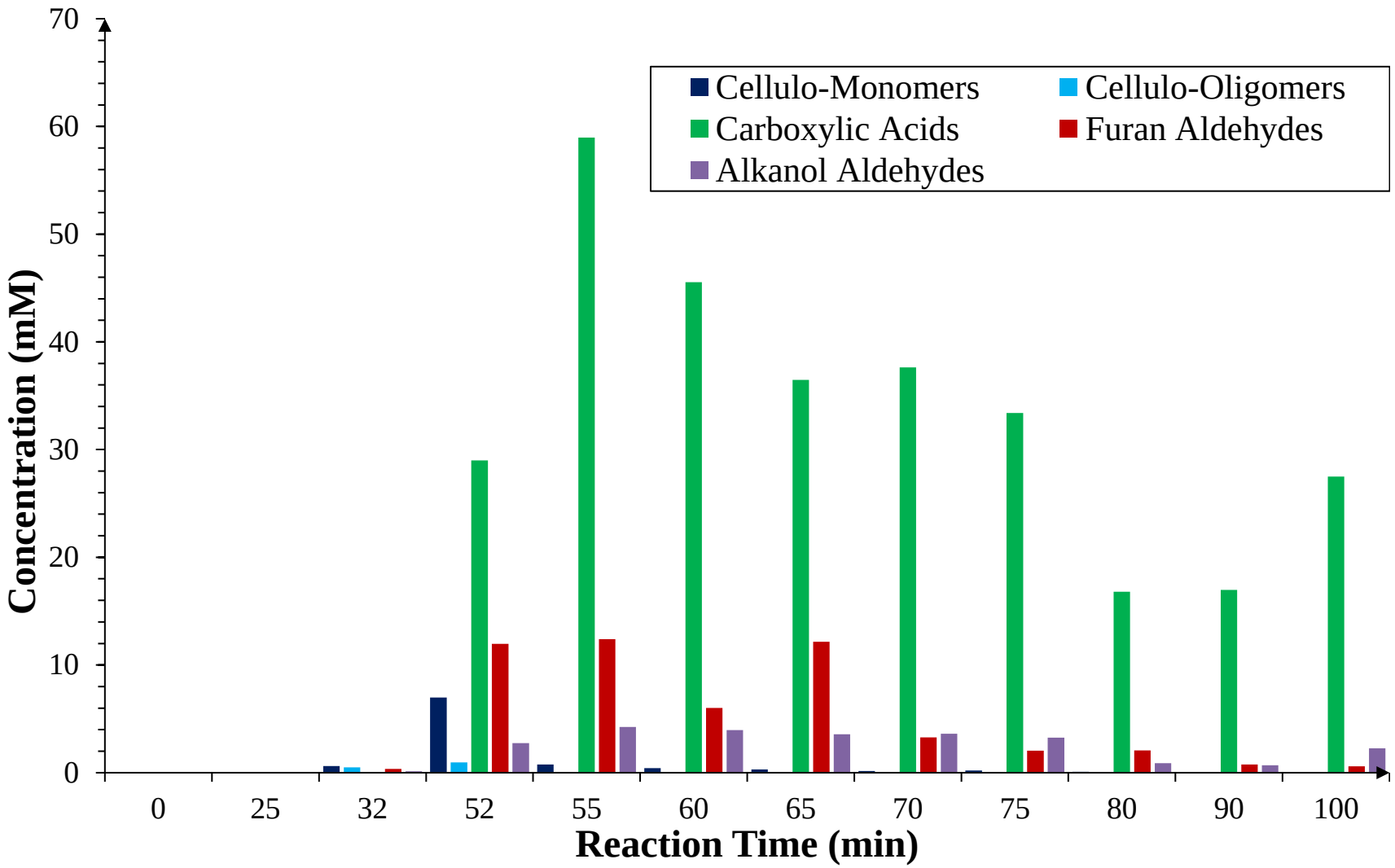

***Figure 23**: Evolution of the identified chemical groups in Cellulose-300 Scenario.*

5.2 Glucose-275 Scenario

5.2.1 Results of Modeling the HPLC Signals

Following the same simulation protocol used in **Section 5.1**, the simulated EMG parameters *A* and MPE values in Glucose-275 Scenario are given in ***Table 56*** - ***Table* 79** in **Appendix B**. Using the power law and linear models, the major peak height values around the retention time of 12.73 min were identified for glycolaldehyde when the entire peak height of the HPLC signals at the retention time value of approximately 11 min could not match lactic acid HPLC standards, because the estimated major peak height was at least 15 times larger than the observed major peak height values. It was concluded that there may be an unidentified chemical species for the peaks at the retention time of 11 min. The chromatography plots of HPLC signals for the aqueous products in Glucose-275 Scenario are presented below in ***Figure 24***.

With the evolution of reaction time, it is found that the degradation mechanisms in this scenario also coincides with the Three-Stage hypothesis proposed in Cellulose-300 Scenario. Succinic acid is not reported based on the HPLC analysis results. The unidentified peaks also evolve with the reaction time in this scenario, which shows the same trend as Cellulose-300 Scenario. From the chromatography plots in ***Figure 24***, some carboxylic acids remained constant or fluctuated a little after 116.5 min of the HTL experiments.

Glucose (50g/L) with compressed N_2 with steady-state reactor temperature as 275 °C

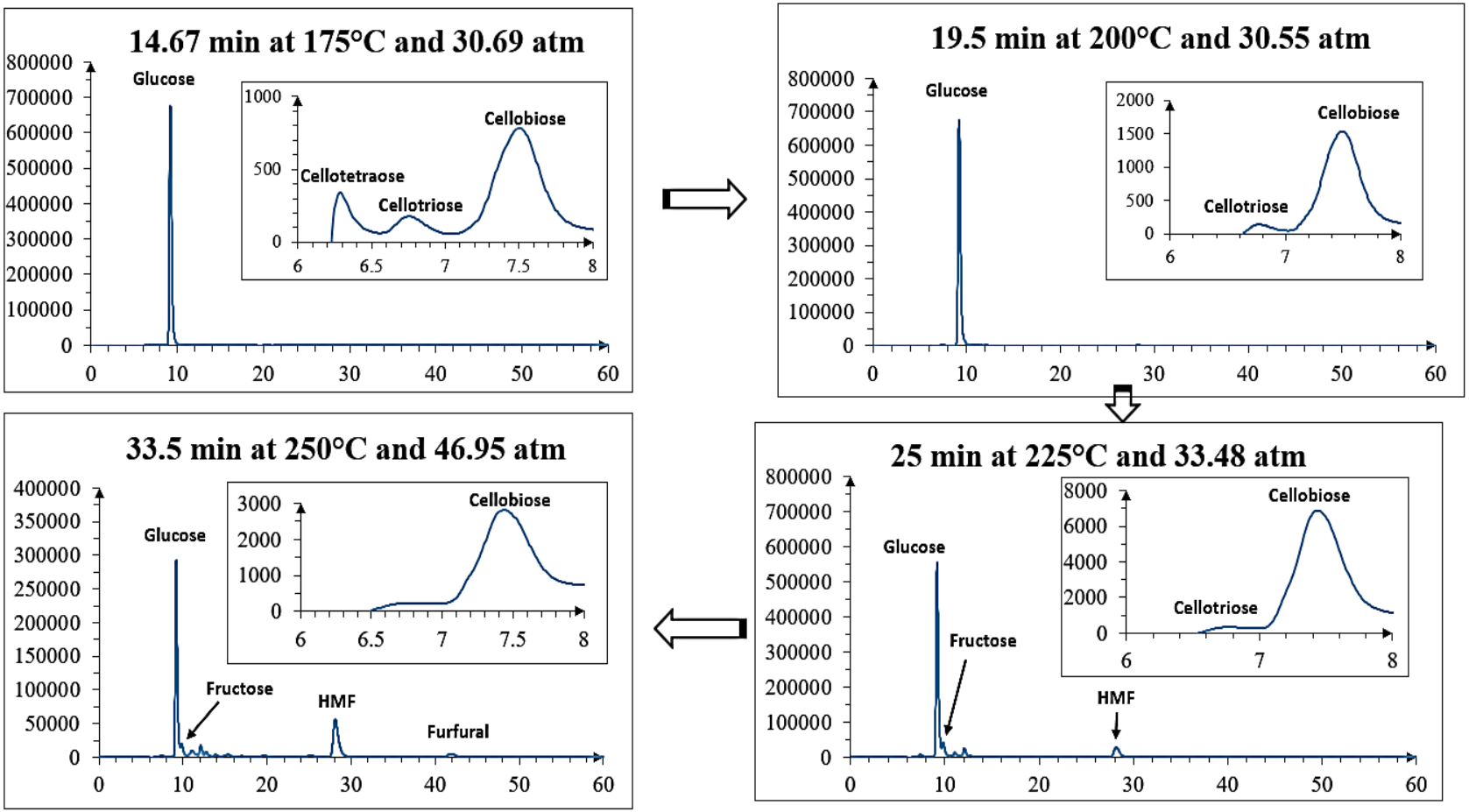

(a) When reaction time is 14.67 min, 19.5 min, 25 min and 33.5 min;

Glucose (50g/L) with compressed N_2 with steady-state reactor temperature as 275 °C

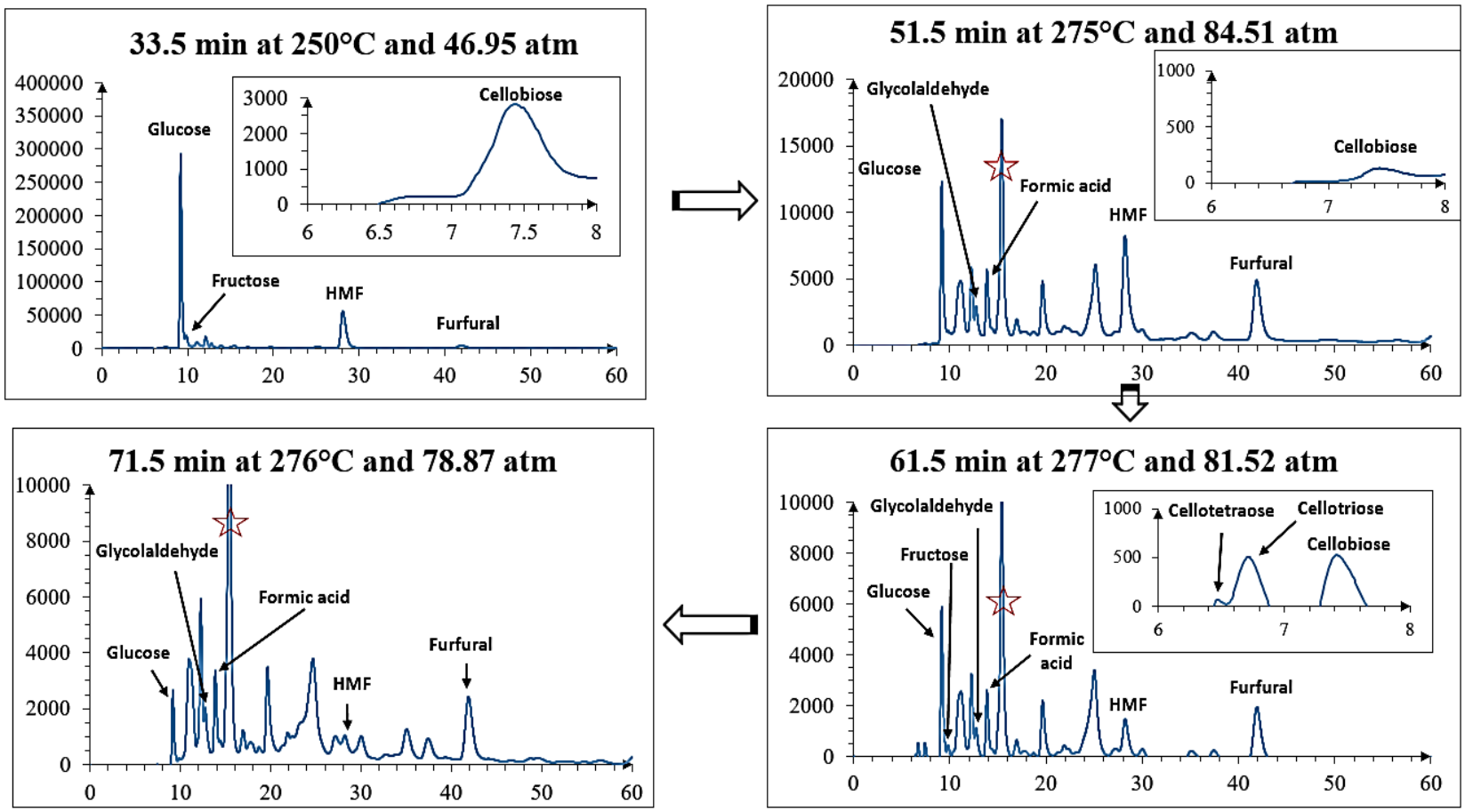

(b) When reaction time is 33.5 min, 51.5 min, 61.5 min and 71.5 min;

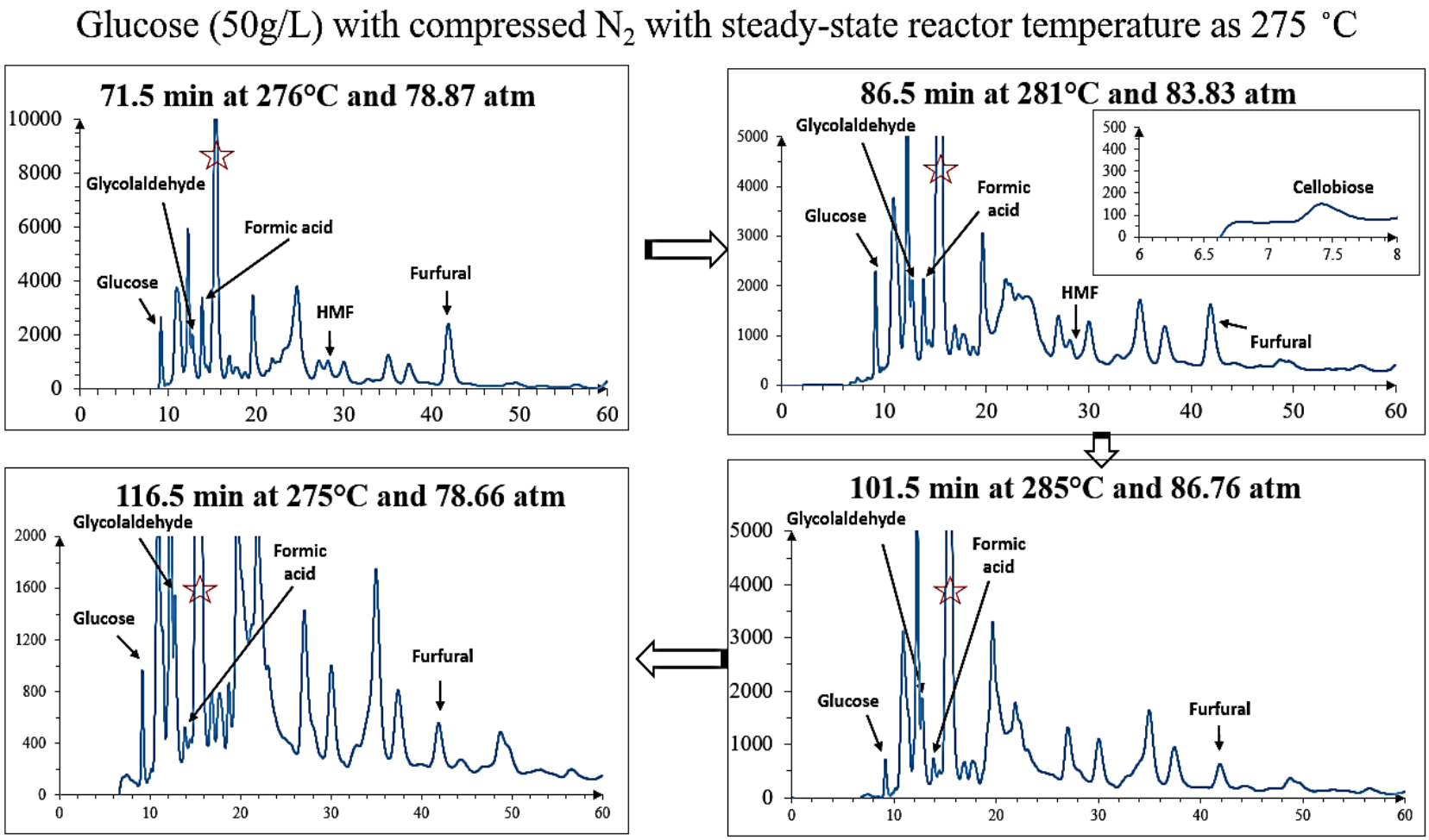

(c) When reaction time is 71.5 min, 86.5 min, 101.5 min and 116.5 min.

***Figure 24**: Chromatography plots of HPLC analysis with the identified chemical species labeled in Glucose-275 Scenario.*

5.2.2 Product Evolution Profile

With the simulated values of EMG parameter *A*, the concentration profiles were derived from the linear relationship between the EMG parameter *A* and concentration of the identified chemical species. The product evolution of chemical species and chemical groups in Glucose-275 Scenario is plotted in ***Figure 25*** and ***Figure* 26**.

Notably, the colors I use for the identified chemical species or chemical groups in all HTL scenarios were kept the same. In this scenario, glucose is the feedstock and the degradation mechanisms are found to be somewhat altered that will be discussed together with the reaction kinetic modeling results in **Chapter 7**. From the product evolution profiles in ***Figure 25*** and ***Figure* 26**, the exponential behavior of cellulo-monomers was consistent with the previous findings under HTL conditions (Xiang, Lee, & Torget, 2004; Kabyemela, Adschiri, Malaluan, & Arai, 1999). It is also interesting to note that the reaction time for the maximal production of furan aldehydes in Glucose-275 Scenario did not correspond with the time for the maximal generation of alkanol aldehydes. The overall product evolution patterns are concluded at the end of **Chapter 5**.

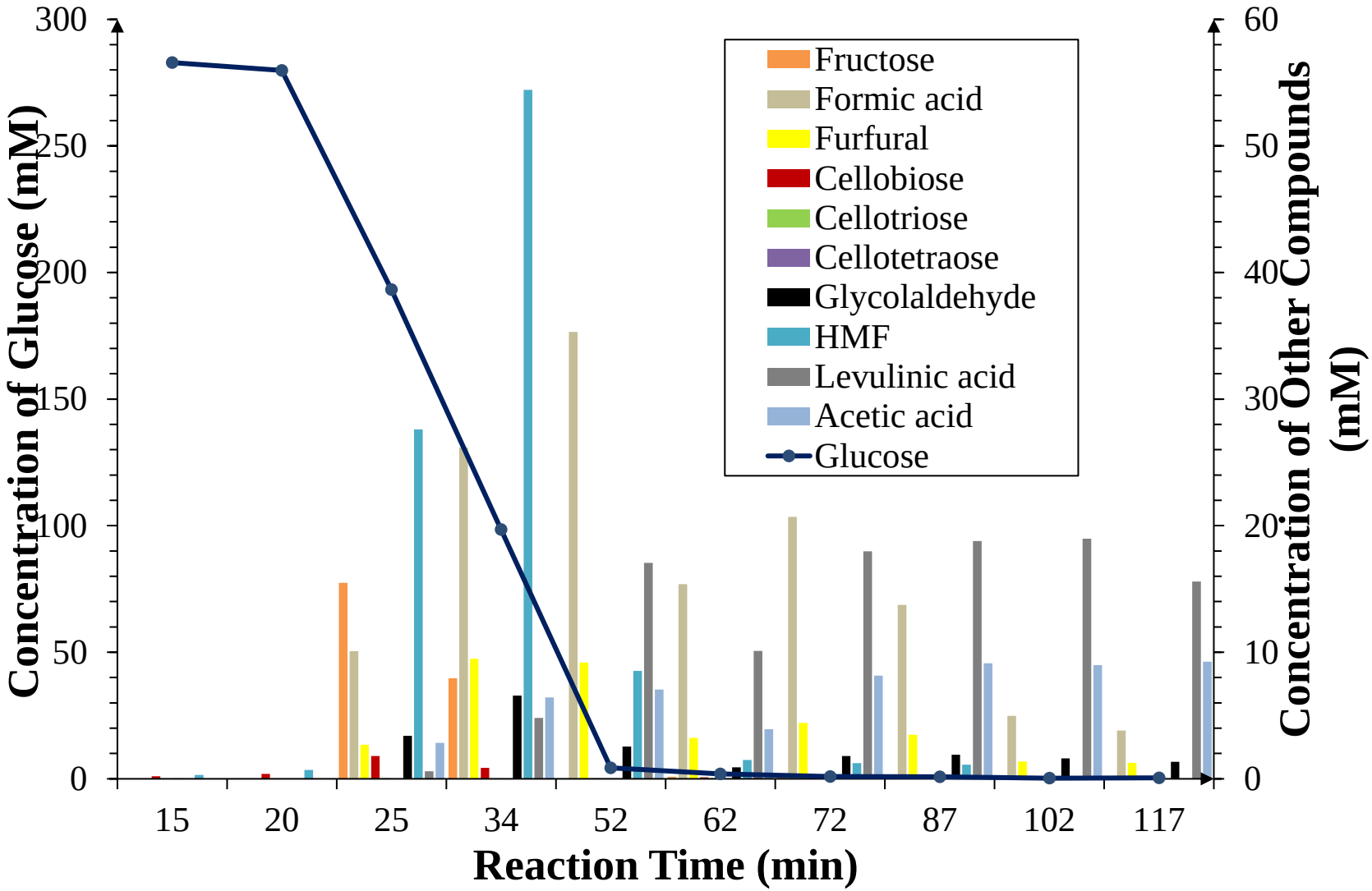

***Figure 25**: Evolution of the chemical species in Glucose-275 Scenario.*

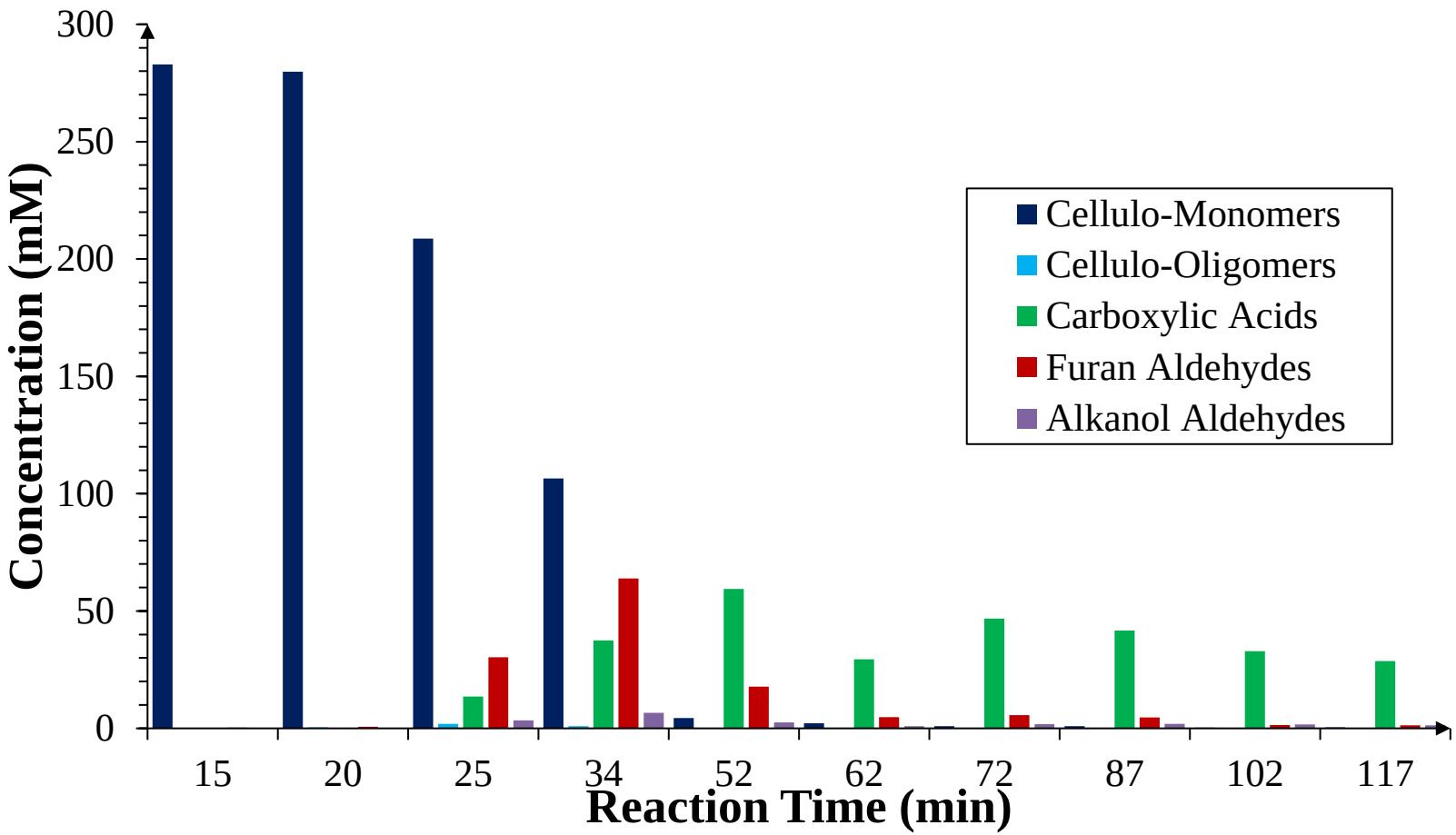

Figure 26: *Evolution of the chemical groups in Glucose-275 Scenario.*

5.3 Glucose-300 Scenario

5.3.1 Results of Modeling the HPLC Signals

This scenario was designed for examining the roles of glucose in the degradation pathways of cellulose under HTL conditions. The simulated concentration profiles for this scenario serve as an implementation for understanding the HTL reaction mechanisms for cellulose. The optimal EMG parameter Area and MPE values are given in ***Table 80***– ***Table* 103** in **Appendix C**. The chromatography plots of HPLC analysis of the aqueous products in Glucose-300 Scenario are shown in ***Figure 27***.

5.3.2 Product Evolution Profile

Based on the simulated concentrations, the product evolution for Glucose-300 Scenario are plotted in ***Figure 28*** and ***Figure* 29**. The exponential behavior of glucose degradation was consistent with Cellulose-300 and Glucose-275 Scenarios. It was also found that part of the identified carboxylic acids kept constant or fluctuated a little after 140 min of HTL reaction time. No cellotetraose was detected at all reaction times in Glucose-300 Scenario. It may be due to the rapid degradation of glucose under such HTL conditions, which led to the quick disappearance of cellotetraose within the first 20 min. It was inferred that the maximum of production of carboxylic acids could also be derived within shorter reaction times than Glucose-275 Scenario.

Glucose (50g/L) with compressed N_2 with steady-state reactor temperature as 300 °C

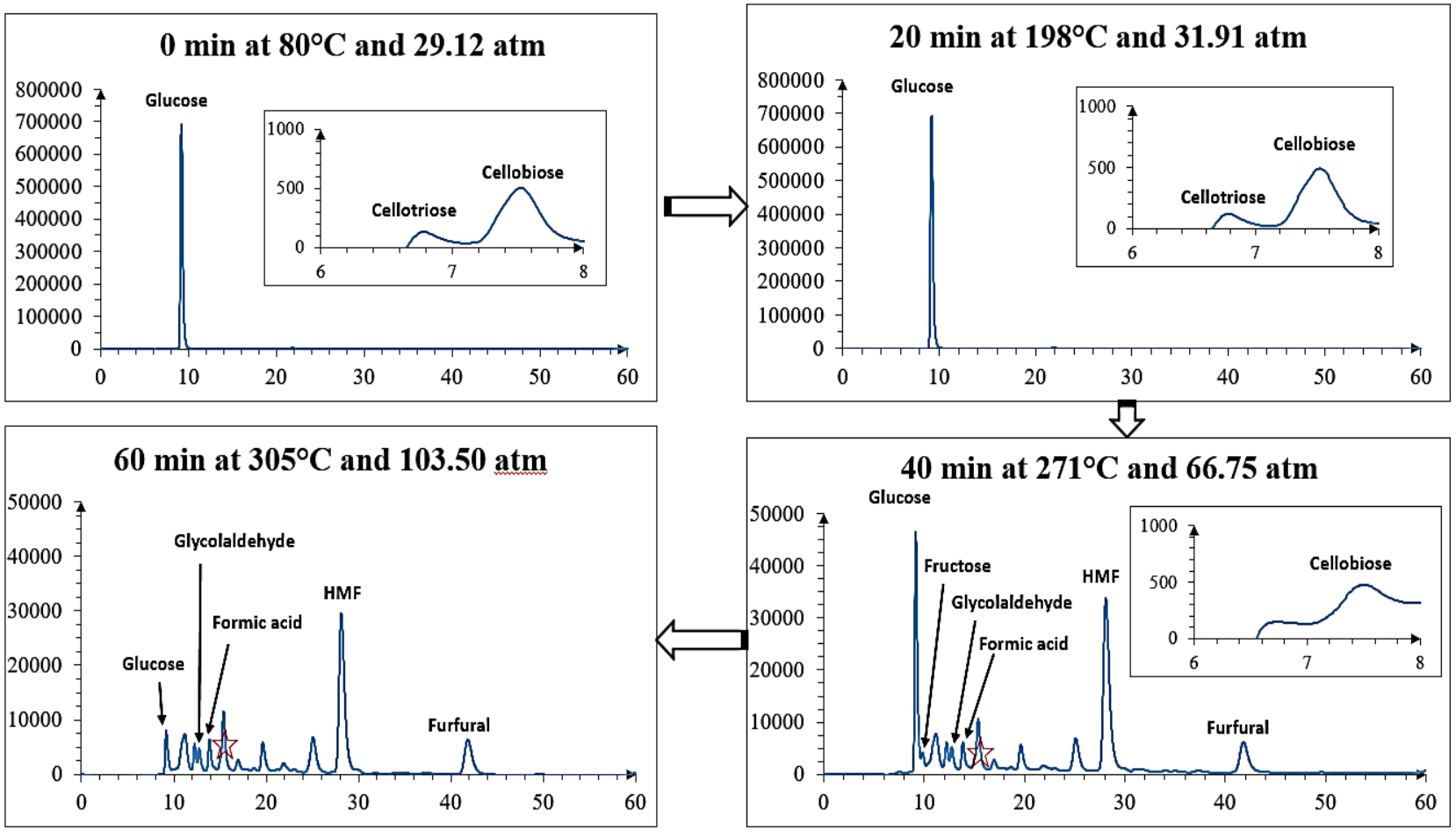

(a) When reaction time is 0 min, 20 min, 40 min and 60 min;

Glucose (50g/L) with compressed N_2 with steady-state reactor temperature as 300 ˚C

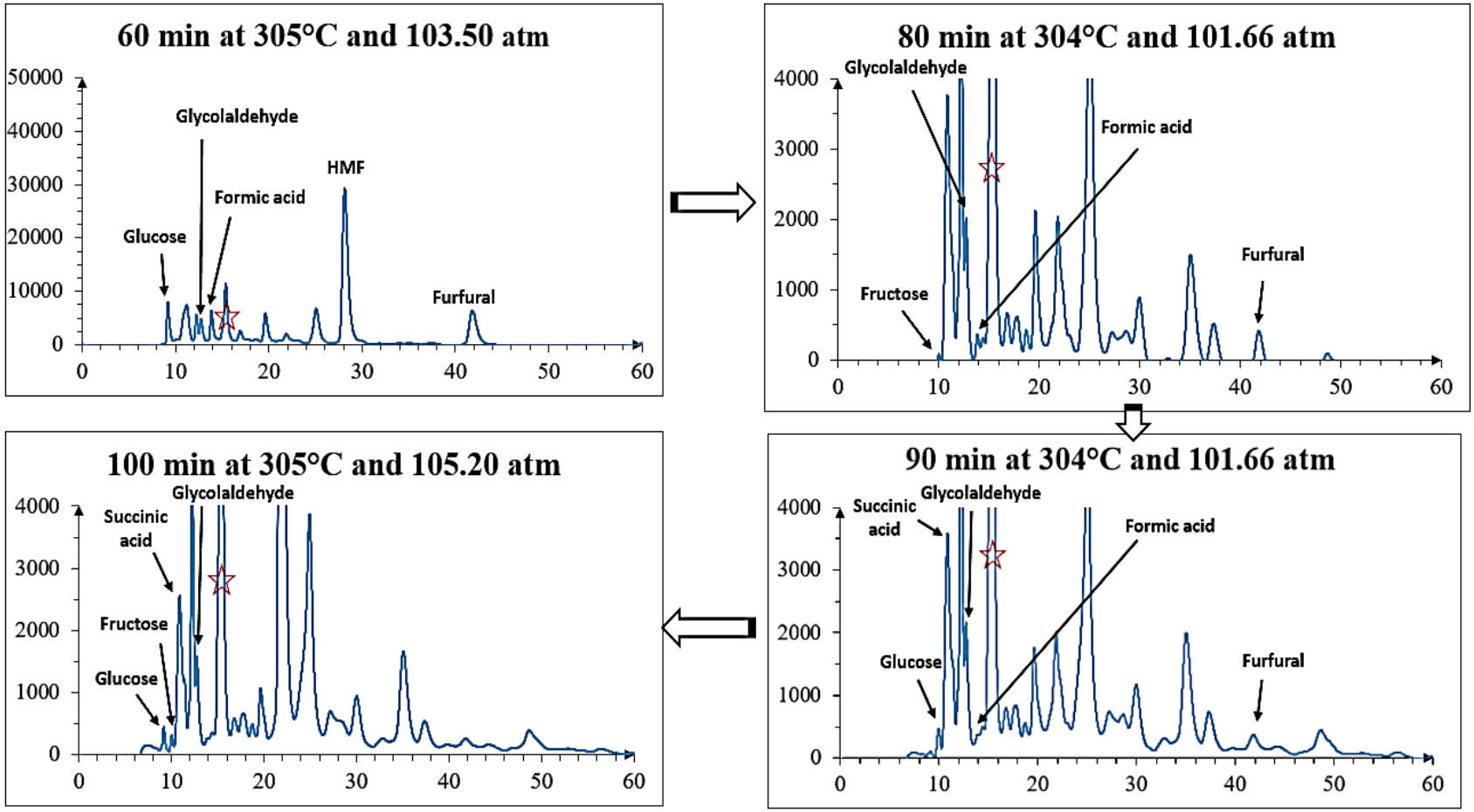

(b) When reaction time is 60 min, 80 min, 90 min and 100 min;

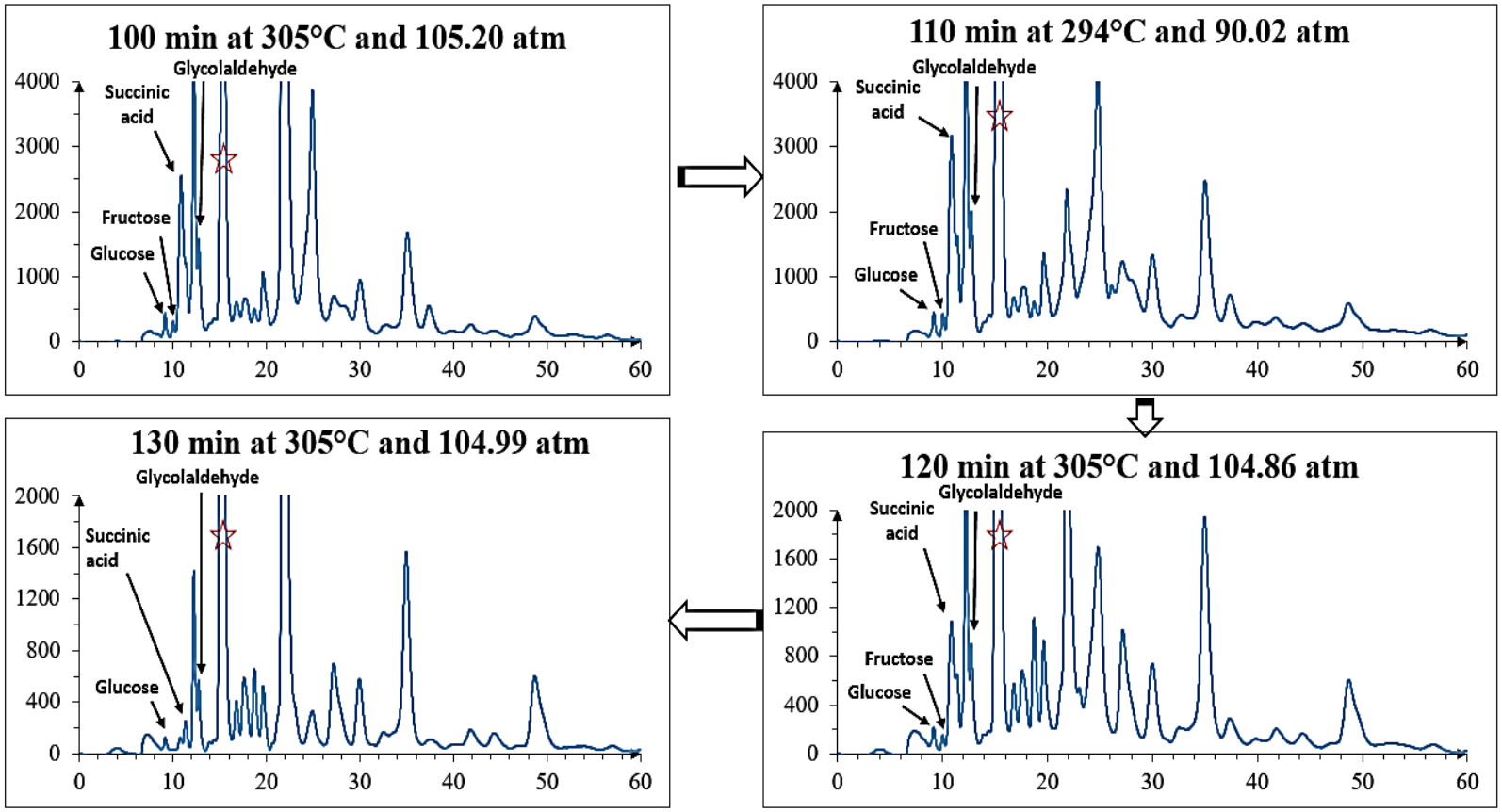

(c) When reaction time is 100 min, 110 min, 120 min and 130 min.

***Figure 27**: Chromatography plots of HPLC analysis with the identified chemical species labeled in Glucose-300 Scenario.*

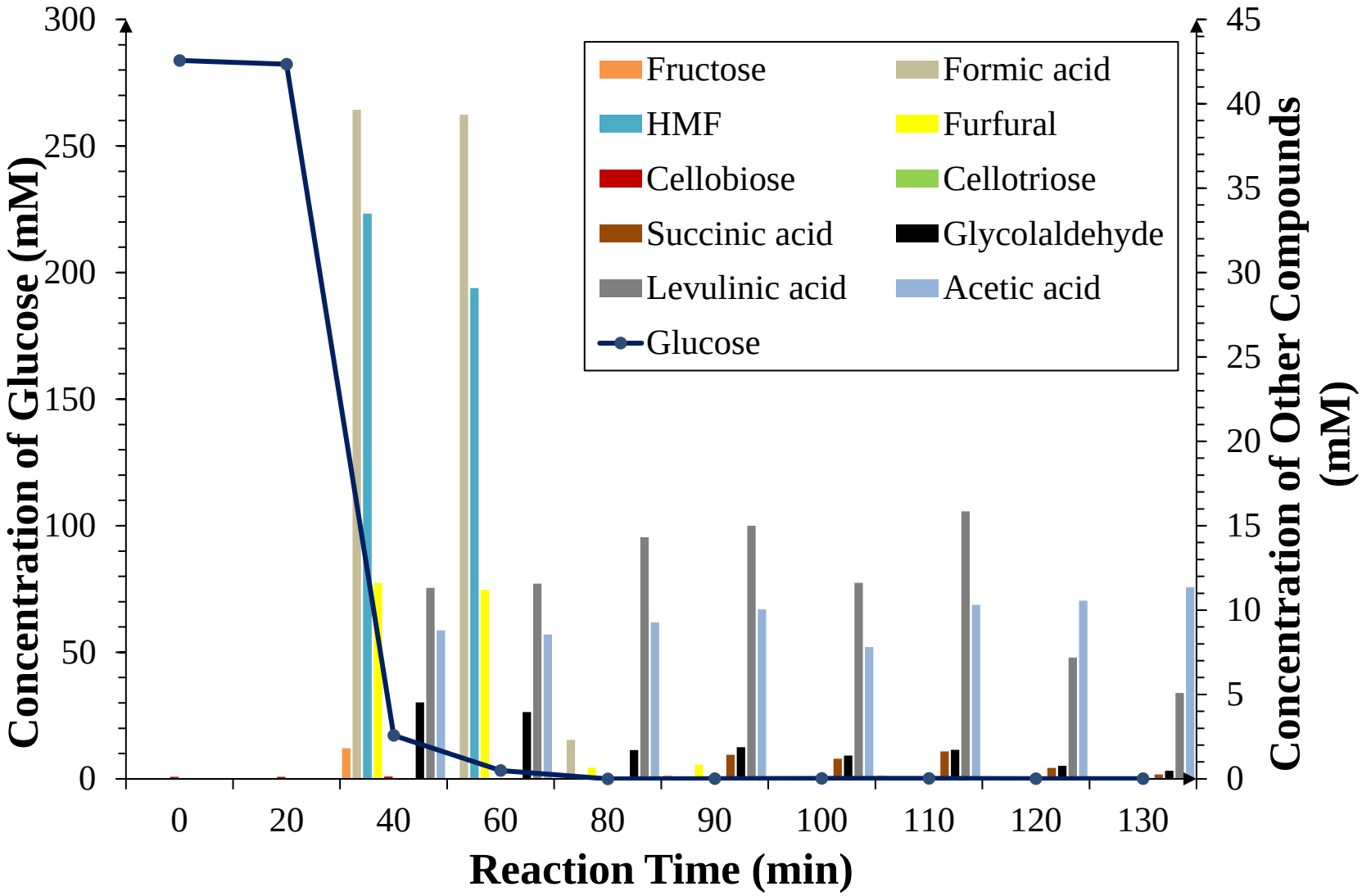

Figure 28: *Evolution of the chemical species in Glucose-300 Scenario.*

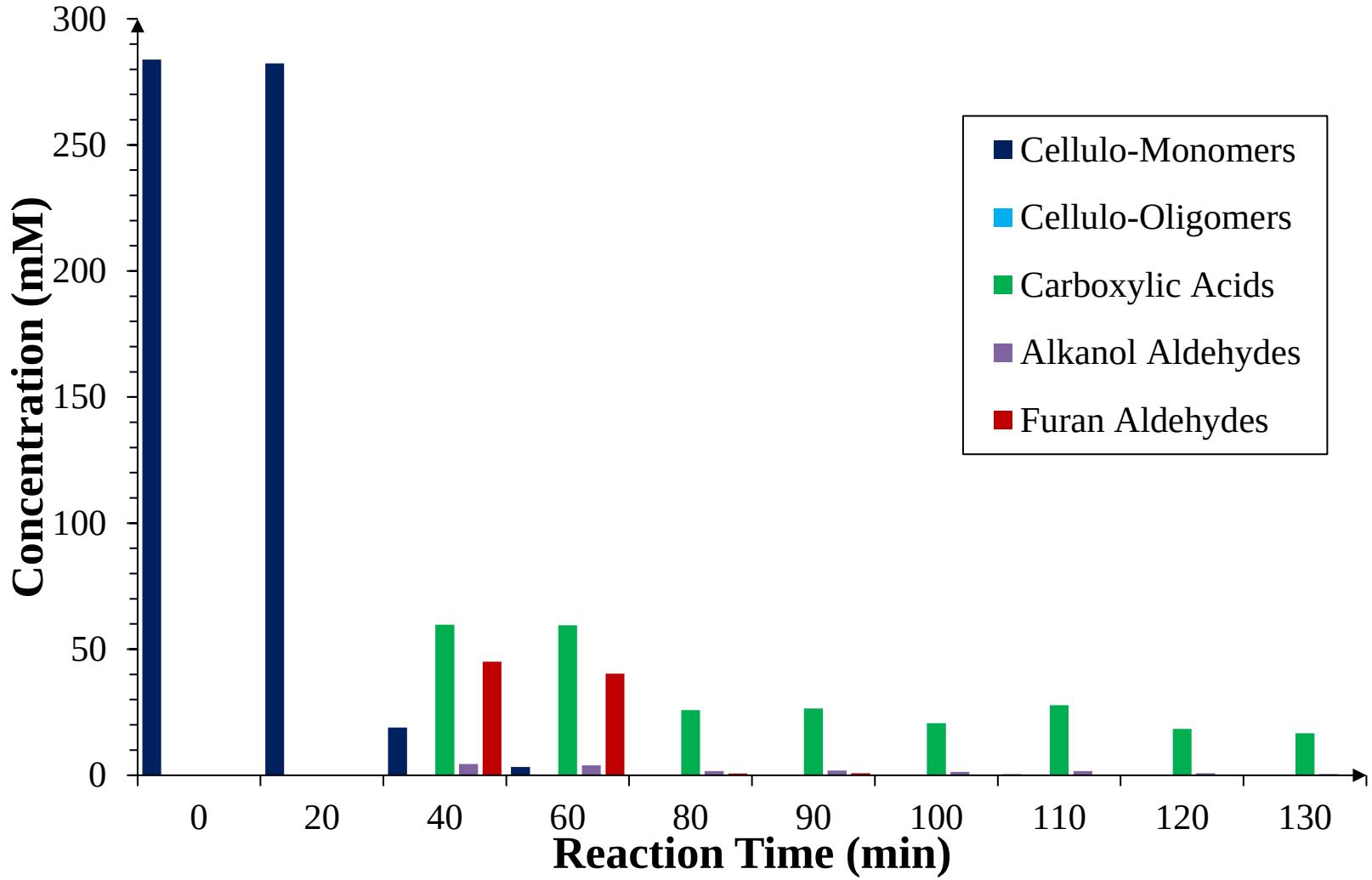

Figure 29: *Evolution of the chemical groups in Glucose-300 Scenario*

5.4 Levulinic-300 Scenario

5.4.1 Results of Modeling the HPLC Signals

The simulated EMG parameters *A* and MPEs in Levulinic-300 Scenario are presented in ***Table 104*** and ***Table* 105** in **Appendix D**. From the chromatography plots in ***Figure 30***, the HPLC peak signals around the retention time value of approximately 15.3 min were hardly changing with reaction time under the same reaction conditions of Cellulose-300 Scenario and Glucose-300 Scenario. The unchanged values of the signals for levulinic acid indicated that the stability of levulinic acid under the HTL conditions in Cellulose-300, Glucose-275 and Glucose-300 Scenarios were validated. This is used for understanding the reaction mechanisms for producing the carboxylic acids from cellulose in the reaction kinetic modeling, which will be discussed in **Chapter 7**.

5.4.2 Product Evolution Profile

Based on the detected HPLC signals, the EMG model was used to derive the parameter *A* for levulinic acid, and it was the only compound identified in this scenario. The evolution of levulinic acid is plotted in ***Figure 31***. The stability of levulinic acid will be further investigated in **Chapters 6** and **7**.

Levulinic acid (50g/L) with compressed N_2 with steady-state reactor temperature as 300 °C

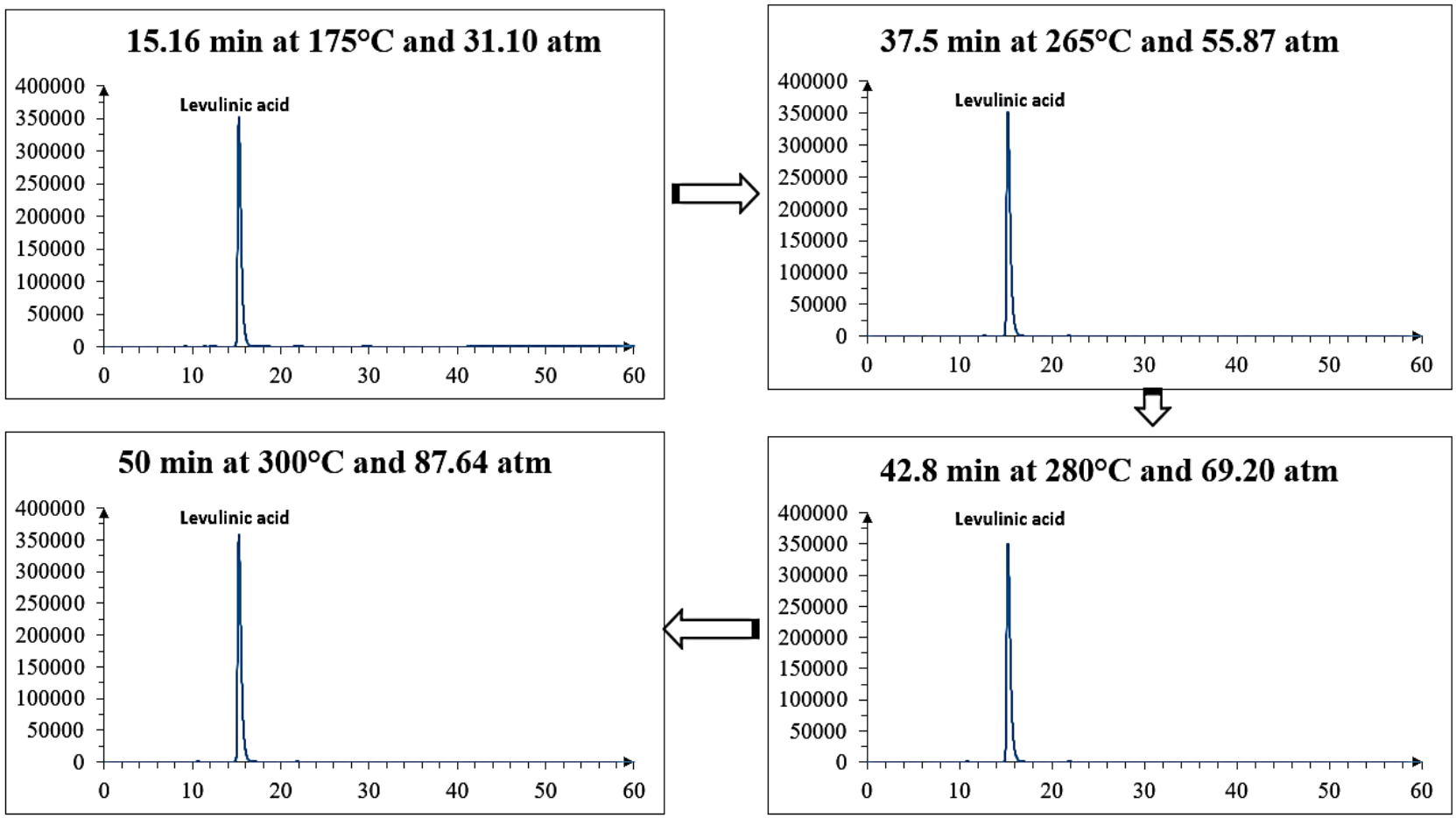

(a) When reaction time is 15.16 min, 37.5 min, 42.8 min and 50 min;

Levulinic acid (50g/L) with compressed N_2 with steady-state reactor temperature as 300 ˚C

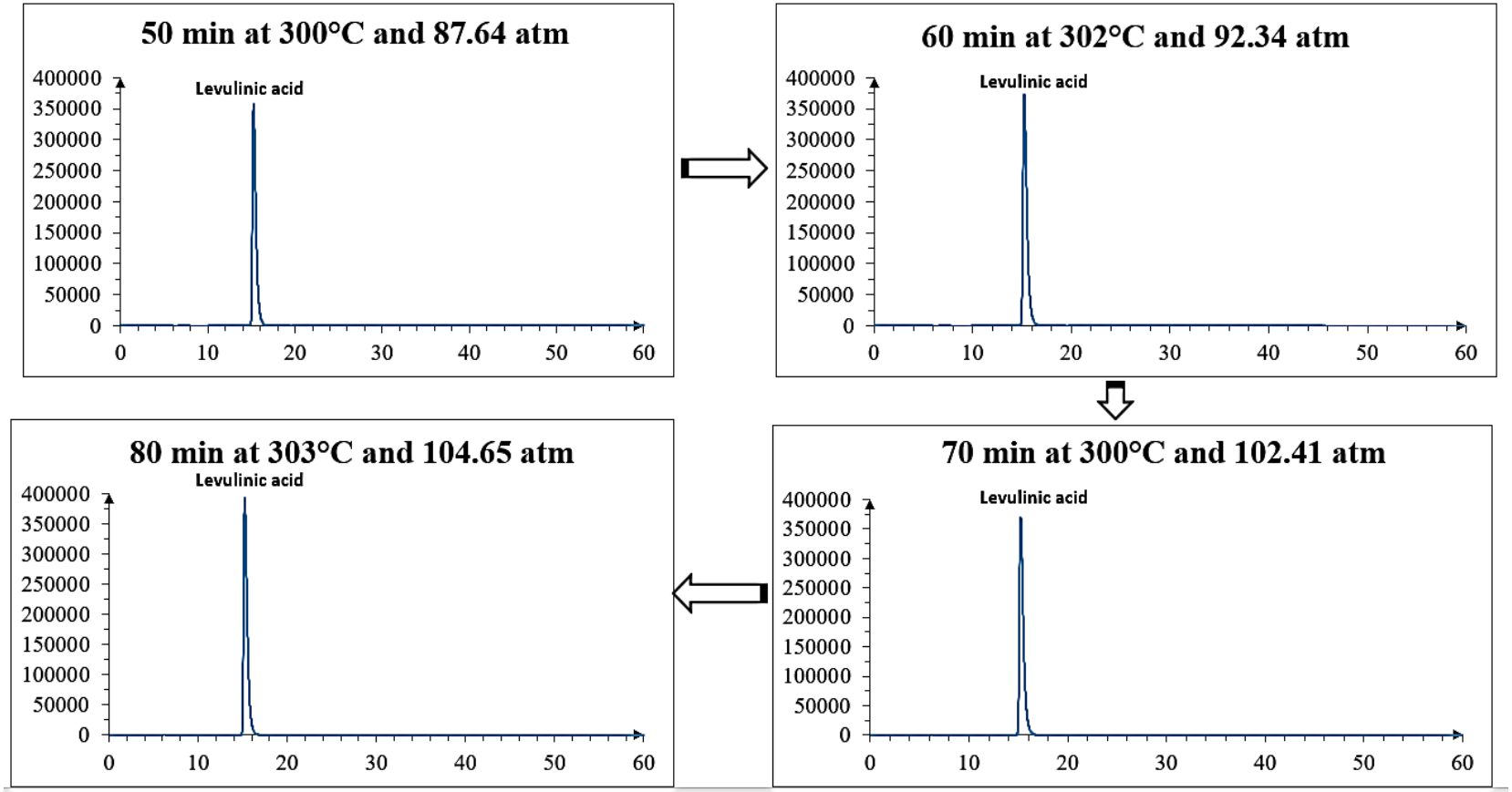

(b) When reaction time is 50 min, 60 min, 70 min and 80 min.

***Figure 30**: Chromatography plots of HPLC analysis with the identified chemical species labeled in Levulinic-300 Scenario.*

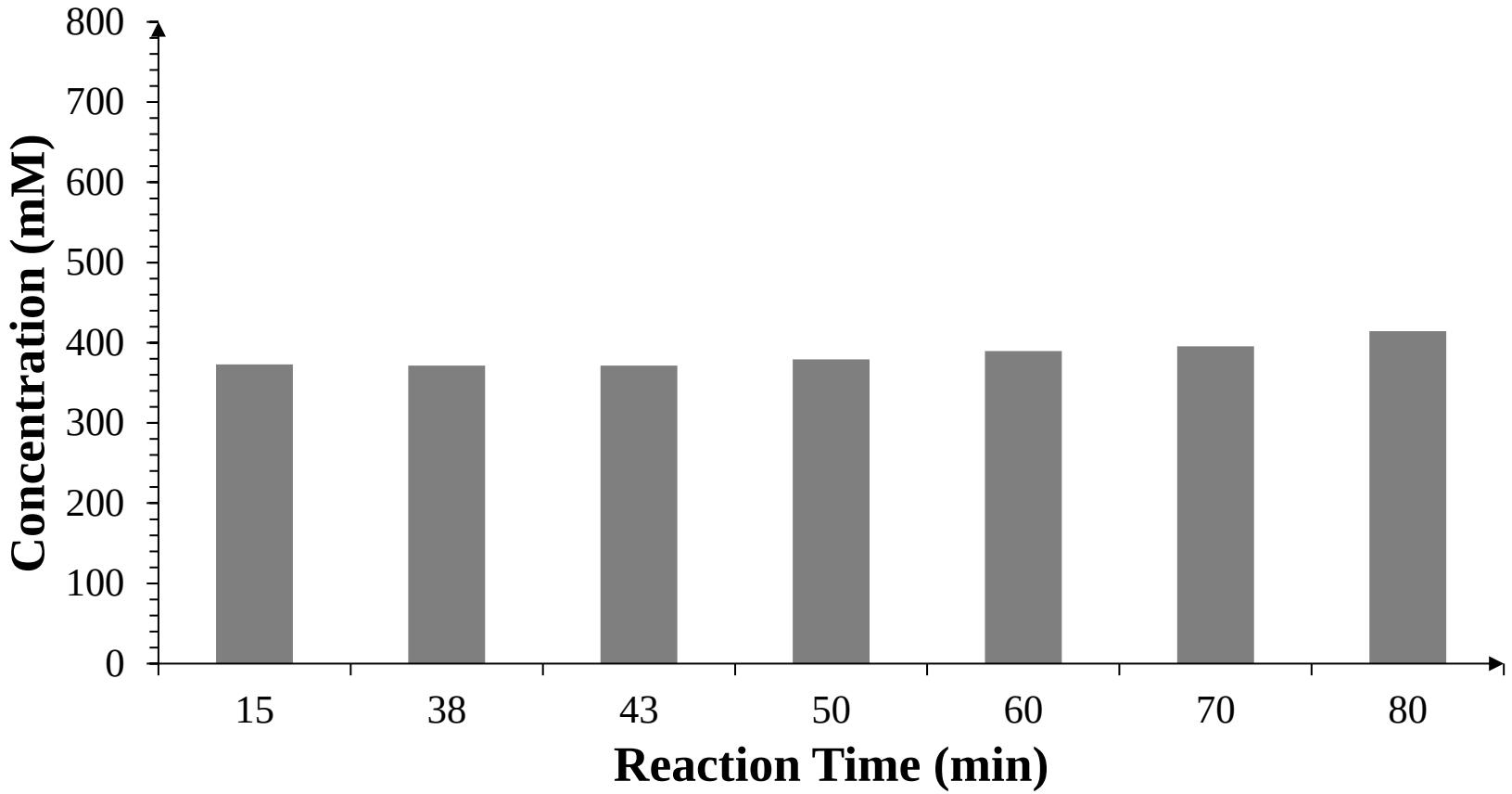

Figure 31: *Evolution of levulinic acid in Levulinic-300 Scenario.*

5.5 General Conclusions of HTL Product Evolution

Understanding the reaction stages in the HTL experiments is very crucial for the proposal of reaction pathway schemes for the degradation of cellulose under HTL conditions. There are many similarities among the product evolution in Cellulose-300, Glucose-275 and Glucose-300 Scenarios. Starting from the initial point with a reaction temperature of 80°C, the degradation was accelerated by the increase of heating rate, as observed by the vanishing of glucose and cellulose in those HTL scenarios. Looking through the product evolution plots for chemical species and chemical groups in ***Figure 22***, ***Figure* 23**, ***Figure* 25**, ***Figure* 26**, ***Figure* 28** and ***Figure* 29**, at the very early stage of decomposition of the feedstock, varieties of cellulo-oligomers and cellulo-monomers were detected and vanished rapidly under HTL conditions, denoted as ***Stage 1***. As for cellulo-oligomers, cellotetraose was not detected at all reaction times in Glucose-300 Scenario. The degradation patterns with the evolution of reaction time for ***Stage 1*** in all three HTL scenarios coincided with each other.

For ***Stage 2***, the evolution of carboxylic acids and aldehydes varied quite differently for the three HTL scenarios. Following the degradation routes from cellulo-monomers to short-chain products, including aldehydes and carboxylic acids, the ratios of molar concentrations of glucose to carboxylic acids were much smaller than the cases in Glucose-275 Scenario and Glucose-300 Scenario. This may be because in ***Stage 1***, the conversion from cellulo-oligomers to glucose was only a small proportion, or under such reaction conditions, other unidentified reactions were favored to cause the low ratios in the scenarios that used glucose as the feedstock. In Glucose-275 Scenario, succinic acid was not observed at all reaction times. In Glucose-300 and Cellulose-300 Scenario, the formation and degradation of succinic acid was corresponding with that of levulinic acid. With the degradation of HMF, succinic acid was formulated. The relationships of

succinic acid, levulinic acid and HMF are further discussed in more details in **Chapter 6**. For furfural, its maximal concentration appeared after the point at the maximal concentration of HMF, which validated the possibility of decarbonylation from HMF to furfural together with the formulation of formic acid via acid-catalyzed reactions. In all scenarios, the concentration variations for glycolaldehyde coincided with the decomposition of glucose and fructose.

The situation for the small-chain carboxylic acids was quite dissimilar in those three scenarios. Formic acid had two equal peak concentrations when the difference in Glucose-300 Scenario, while it had only one peak concentration in the other two HTL scenarios. The concentration profiles of acetic acid in all scenarios reached its platinum at the late stage. From the product evolution profiles, it was found that the levulinic acid experienced its second accumulation period after a long reaction time. It is significant to figure out the balances between production of levulinic acid from cellulo-monomers and degradation of levulinic acid through the reaction networks for the HTL of cellulose or glucose. In the following chapter, detailed reaction mechanisms are introduced. Based on earlier HTL studies, the chemical reaction pathway schemes are projected in several cases. The reaction kinetic modeling through the proposed reaction pathways are demonstrated in **Chapter 7**, where uncertainties are assessed with regards to HPLC analysis and reaction kinetic modeling. With a careful evaluation of the kinetic modeling results, discussions about HTL reaction mechanisms and recommendations for HTL process optimization are given.

CHAPTER 6

CHEMICAL REACTION PATHWAY SCHEMES FOR THE HTL EXPERIMENTS

6.1 Overview of Reaction Networks for HTL

The crystalline polymer structure of cellulose experiences severe deconstruction via the scission of glycosidic bonding catalyzed by the active ionization of water (SriBala & Vinu, 2014). The scission mechanisms described by SriBala and Vinu provide various alternatives of the ongoing chemical reactions that generate cellulo-monomers and cellulo-oligomers from cellulose. Two types of the scission of glycosidic bonding have been considered, end scission and random scission. Random scission is based on the assumption that the spatial distribution in cellulose molecules has no effect on the access of hydrogen ions to the glycosidic bonds, and thus there is an equal probability that each glycosidic bonding will be attacked by the hydrogen ions. Alternatively, in end scission, there is a significant difficulty for hydrogen ions to access the inner side of cellulose or long-chain cellulo-oligomers at the early stage of decomposition. Under this condition, the cleavage of glycosidic bonding follows a sequential order beginning from the ends of the cellulose molecules or long-chain cellulo-oligomers. However, under HTL conditions, the dramatic change in the physiochemical properties of water may help the oligomers to diffuse into the places with higher concentrations of hydrogen ions. With the increased exposure to hydrogen ions, the scission of cellulo-oligomers may favor random mechanism. In this study, both scission mechanisms were investigated via proposed chemical reactions for reaction kinetic modeling. The chemical reactions between the identified cellulo-oligomers and cellulo-monomers are shown below in ***(8*** **-** **(14**:

$$H(C_6H_{10}O_5)_nOH+(\frac{n}{m}-1)H_2O \rightarrow \frac{n}{m} C_{6m}H_{10m+2}O_{5m+1}, \quad m, n \; and \; \frac{n}{m} = 1, 2, \; 3, or \; 4. \qquad (\mathbf{8})$$

$$C_{24}H_{42}O_{21} + H_2O \rightarrow C_{18}H_{32}O_{16} + C_6H_{12}O_6 \quad \textbf{(9)}$$

$$C_{24}H_{42}O_{21} + 2H_2O \rightarrow C_{12}H_{22}O_{11} + 2C_6H_{12}O_6 \quad \textbf{(10)}$$

$$C_{12}H_{22}O_{11} + 2H_2O \rightarrow 3C_6H_{12}O_6 \quad \textbf{(11)}$$

$$C_{18}H_{32}O_{16} + H_2O \rightarrow C_{12}H_{22}O_{11} + C_6H_{12}O_6 \quad \textbf{(12)}$$

$$C_{12}H_{22}O_{11} + H_2O \rightarrow 2C_6H_{12}O_6 \quad \textbf{(13)}$$

$$C_{24}H_{42}O_{21} + H_2O \rightarrow 2C_{12}H_{22}O_{11} \quad \textbf{(14)}$$

In the end scission, the access for hydrogen ions to the central glycosidic bond in cellotetraose is negligible compared to the other alternatives. Thus, ***(14*** was not considered for end scission, and ***(8*** - **(13** were included for both scission mechanisms.

As introduced in ***Figure 4*** and ***Figure*** **5** in **Chapter 1**, the isomerization between glucose and fructose undergoes LBET transformation in several forms of hexose monomers. Previous studies showed that the isomerization reaction favored the direction from glucose to fructose (Asghari & Yoshida, 2007; Kabyemela, Adschiri, Malaluan, & Arai, 1999). Surrounded by hydrogen ions, fructose can be further dehydrated into HMF via fructofuranosyl intermediates (Kabyemela, Adschiri, Malaluan, & Arai, 1999), as shown in ***(15*** below.

$$C_6H_{12}O_6 \rightarrow 3H_2O + C_6H_6O_3 \quad \textbf{(15)}$$

Following degradation of fructose into HMF, furfural can be produced from HMF together with formaldehyde via dehydroxylation reaction when the alcohol side chain in HMF is replaced by a hydrogen ion via p-electron interaction (Srokol, *et al*., 2004). The chemical reaction involved is shown below in ***(16***:

$$C_6H_6O_3 \rightarrow C_5H_4O_2 + CH_2O \quad \textbf{(16)}$$

Another degradation pathway of HMF is a hydration reaction to produce levulinic acid and formic acid as presented in ***(17*** (Asghari & Yoshida, 2007).

$$C_6H_6O_3 + 2H_2O \rightarrow C_5H_8O_3 + CH_2O_2 \qquad \textbf{(17)}$$

The cleavage of the hydrogen bonds in water molecules is expedited by the active ionization. But the reaction selectivity around a reactant will be further examined through the reaction kinetic modeling in **Chapter 7**. Glycolaldehyde together with erythrose can be formed in a reverse aldol condensation reaction via a hexose monomer with hydroxyl and carbonyl groups at the end of the molecule (Kabyemela, Adschiri, Malaluan, & Arai, 1999). Kabyemela *et al*. also assumed that glucose and fructose were able to produce formic acid and acetic acid via other undefined pathways. In this study, that assumption will also be evaluated in **Chapter 7**.

As succinic acid was not reported in HTL studies of glucose and fructose (Kabyemela, Adschiri, Malaluan, & Arai, 1999; Asghari & Yoshida, 2007), a novel method using a Ru^{III} catalyst proved to have high selectivity of succinic acid production via fumaric acid (Podolean, *et al*., 2016). However, fumaric acid was not identified as a significant compound in this study. Succinic acid can also be produced from levulinic acid using I_2/t-BuOK System via a series of oxidation and substitution reactions (Kawasumi, *et al*., 2017). This pathway is also evaluated in **Chapter 7**.

Based on a literature review of the possible ongoing chemical reaction products resulting from HTL, four cases of chemical reaction pathway schemes were proposed (see **Table 25**). In each case, a base scenario and a condensation scenario were included, while reverse reactions in the degradation of cellulo-oligomers and cellulo-monomers were only considered in the

condensation scenarios. After the reaction mixture reached the temperature steady-state setpoint, cellulo-oligomers were observed to almost vanish.

***Table 25**: Overview of Reaction Kinetic Modeling Cases*

Case	Contain both base scenario and condensation scenario?	End scission or random scission?	Glucose and fructose combined as cellulo-monomers?
1.1	✔	End scission	✕
1.2	✔	Random scission	✕
2.1	✔	End scission	✔
2.2	✔	Random scission	✔

More details regarding the assumptions and algorithm used for reaction kinetic modeling are given in **Chapter 7**. The next section presents the four cases with chemical reaction pathway schemes proposed for cellulose degradation under HTL conditions.

6.2 Optional Cases of HTL Chemical Reaction Networks

Case 1.1

Based on the general conclusions mentioned in **Section 5.5**, the degradation pathways for cellulose in subcritical water are assumed to consist of three stages. As shown below in ***Figure 32***, the orange and blue lines present the chemical reactions in ***Stage 1,*** the depolymerization of cellulose into cellulo-monomers via cellulo-oligomers. The other lines in other colors well demonstrate further degradation of cellulo-monomers into aldehydes and carboxylic acids in ***Stage 2***, degradation of cellulo-monomers to aldehydes and carboxylic acids. Unidentified degradation products are not plotted in the proposed reaction pathway schemes but are included in the reaction kinetic modeling. This reaction pathway scheme provides insights into the

evolution stages among the identified chemical species and chemical groups. Notably, the kinetic modeling results play a key role in the HTL process optimization.

Case 1.2

As mentioned in **Section 6.1**, the combined effect of cellulo-monomers will be evaluated based on the reaction selectivity results for production of aldehydes and carboxylic acids. End scission is considered in this case for the decomposition of cellulo-oligomers. The chemical reaction pathway scheme for **Case 1.2** and **Case 2.2** is displayed in ***Figure 33***. The significance of cellulo-monomers will be explained in **Chapter 7** by comparison of the kinetic modeling results.

Case 2.1

The only difference between this case and **Case 1.1** is that cellulo-oligomers undergoes random scission of glycosidic bonding, where another option is provided for the conversion from cellotetraose to cellbiose. The other reactions in **Case 1.1** are kept the same for the reaction kinetic modeling in this case.

Case 2.2

As demonstrated in **Section 6.1**, the only dissimilarity between **Case 1.2** and **Case 2.2** is the random scission mechanism considered for this case rather than **Case 1.2**.

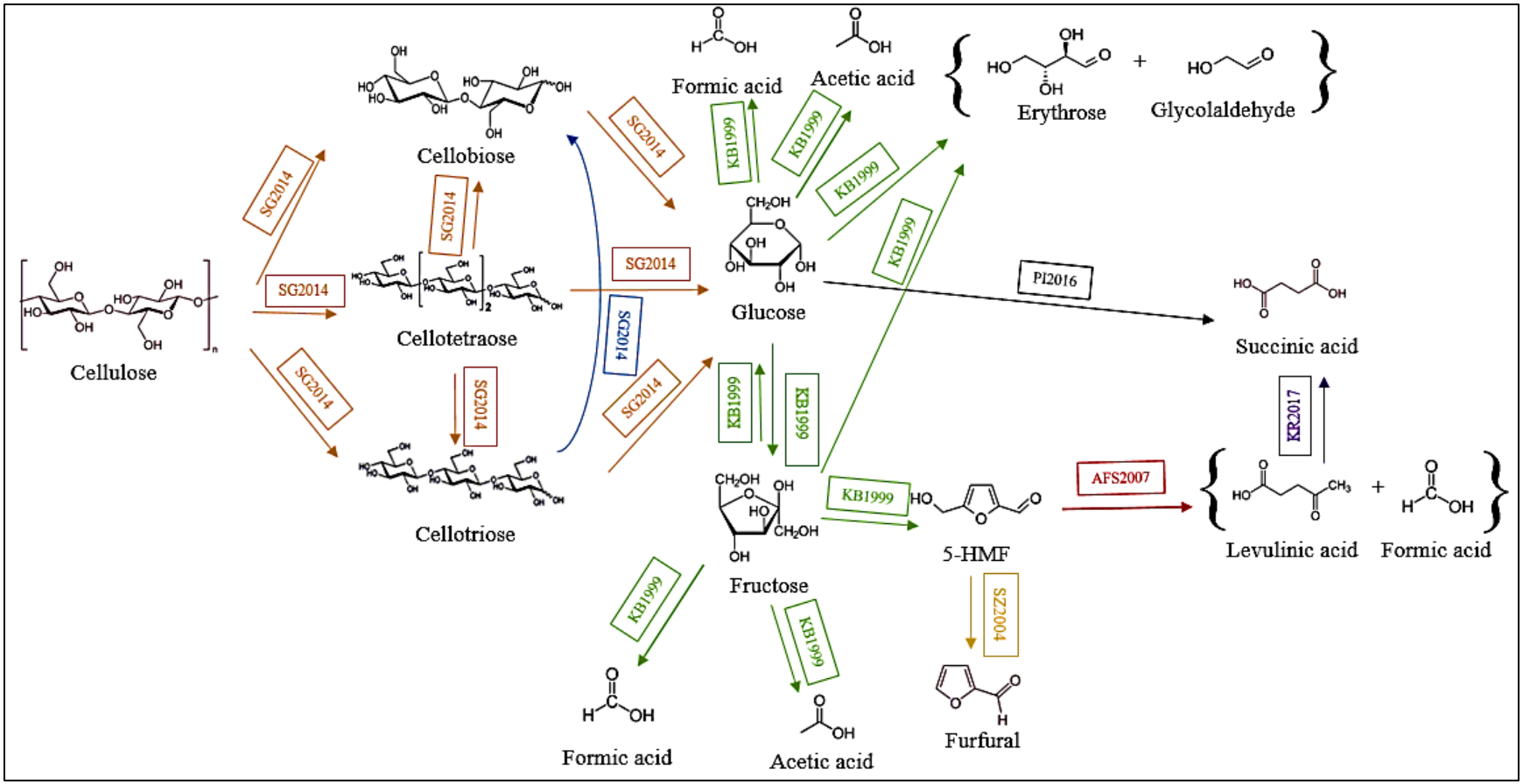

***Figure 32**: Proposed Chemical Reaction Pathway Scheme for **Case 1.1** and **Case 2.1**, where in the textbox for the sources of chemical reactions, SG2014 refers to (SriBala & Vinu, 2014); KB1999 refers to (Kabyemela, Adschiri, Malaluan, & Arai, 1999); PI2016 refers to (Podolean, et al., 2016); AFS2007 refers to (Asghari & Yoshida, 2007); KR2017 refers to (Kawasumi, et al., 2017); SZ2004 refers to (Srokol, et al., 2004); **Case 2.1** not only includes all the reactions considered in **Case 1.1**, but also considers the reaction that converts two units of cellobiose into one unit of cellotetraose and one unit of water molecule.*

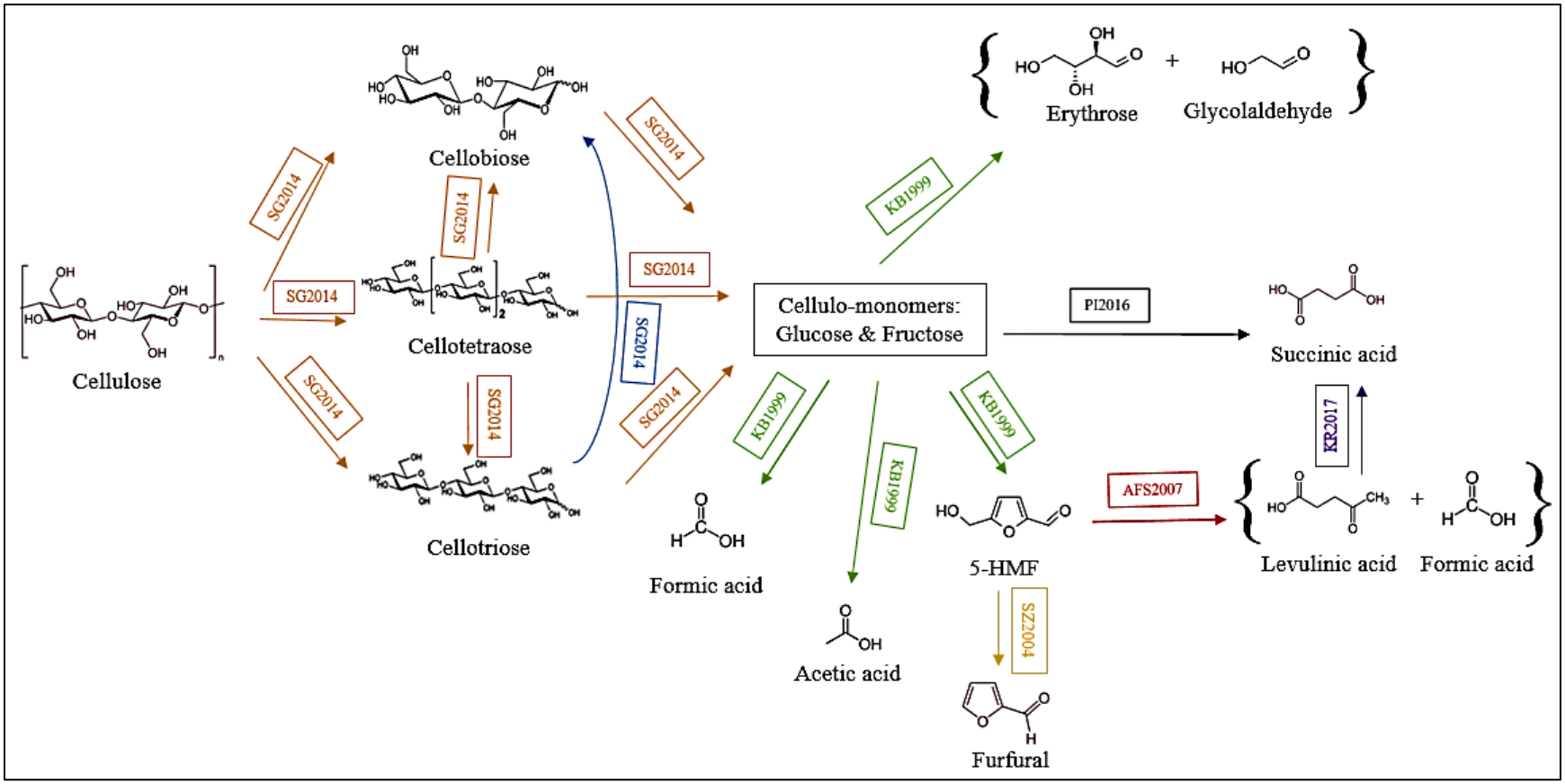

Figure 33: *Proposed Chemical Reaction Pathway Scheme for* ***Case 1.2*** *and* ***Case 2.2****, where in the textbox for the sources of chemical reactions, SG2014 refers to (SriBala & Vinu, 2014); KB1999 refers to (Kabyemela, Adschiri, Malaluan, & Arai, 1999); PI2016 refers to (Podolean, et al., 2016); AFS2007 refers to (Asghari & Yoshida, 2007); KR2017 refers to (Kawasumi, et al., 2017); SZ2004 refers to (Srokol, et al., 2004););* ***Case 2.2*** *not only includes all the reactions considered in* ***Case 1.2****, but also considers the reaction that converts two units of cellobiose into one unit of cellotetraose and one unit of water molecule.*

CHAPTER 7

REACTION KINETIC MODELING FOR THE HTL EXPERIMENTS

7.1 Assumptions for Reaction Kinetic Modeling

Only the concentration profiles under the steady-state temperature was simulated using the proposed reaction pathway schemes described in **Section 6.2**. A molar balance was analyzed for each identified chemical species in differential forms. The types of the material transfer for each chemical species mainly included diffusion, convection, and reaction. In the batch reactor, perfect mixing was assumed, and convective and diffusive mass transfer were neglected. Therefore, the variation of the concentrations was only due to the chemical reactions that were associated with that compound. First-order reaction kinetics was assumed for all reaction rate expressions. The stoichiometric coefficients of producing formic acid or acetic acid directly from glucose, fructose or cellulo-monomers were set to be 1. The reactant with the smallest stoichiometric coefficient was chosen as a basis for expressing the chemical reaction rate. The order of reaction kinetics of a specific reaction was not associated with the stoichiometric coefficients, but the reaction rate, whether consumption rate or production rate, was related to the stoichiometric relationships between the chemical species and the base reactant. When water participated in the HTL reactions, its concentration was not counted in the reaction rate expressions due to its plentiful presence. Differential forms of molar balance are given in the next section based on the kinetic modeling assumptions above. Reaction kinetic modeling was optimized via the simulation algorithm described in **Section 7.3** for plotting the simulated concentration profiles based on the reaction pathway schemes.

7.2 Differential Forms of Molar Balances

The general differential form of molar balance for an identified chemical species is given in ***(18***:

$$\frac{\partial <A>}{\partial t} = \sum_{i}^{Number\ of\ reactions\ that\ produced\ A} \frac{n_i}{m_i} k_{m_i B_i, n_i A} \cdot < B_i > - \sum_{j}^{Number\ of\ reactions\ that\ consumed\ A} k_{t_j A, s_j C_j} \cdot < A > \quad \textbf{(18)}$$

In ***(18***, the symbol $< A >$ represents the concentration of species A, and A can be any identified degradation products of cellulose; the variables $n_i, m_i, t_j\ and\ s_j$ and the chemical species B_i and C_i are given in ***(19*** and (**20**, assuming species B_i was the base reactant for the reactions that produced species A, and species A was the base reactant for the reactions that consumed species A. The subscript of the reaction rate constant $k_{m_i B_i, n_i A}$ includes names of reactants and products of the chemical reactions.

$$m_i B_i \rightarrow n_i A \quad \textbf{(19)}$$

$$t_j A \rightarrow s_j C_j \quad \textbf{(20)}$$

The involved chemical reactions together with the reaction rate constants for Cellulose-300, Glucose-275 and Glucose-300 Scenarios are given in ***Table 106*** in **Appendix E**. The differential forms of the molar balances around each identified chemical species in Cellulose-300 Scenario, Glucose-275 Scenario and Glucose-300 Scenario are presented in **Appendix F**.

7.3 Simulation Approach

For all cases of reaction kinetic modeling, the experimental profiles derived from the HPLC signal modeling were a major input. Sum squared errors between the simulated and experimental concentration profiles were used for determining the best combination of reaction rate constants for each case. The formula of calculating SSE is given below in ***(21***, where in the subscript, *i* and *j* denote the specific concentration of the species *i* at the reaction time of *j* min. The general simulation protocol is shown in ***Figure 34***. Upon the minimization of SSE values for all cases, the error distribution for each identified chemical species was calculated to evaluate the proposed chemical reaction pathway schemes. More details about the simulation errors are given in **Section 7.5**.

$$SSE = (Concentration_{i,j,simulated} - Concentration_{i,j,experimental})^2 \quad \textbf{(21)}$$

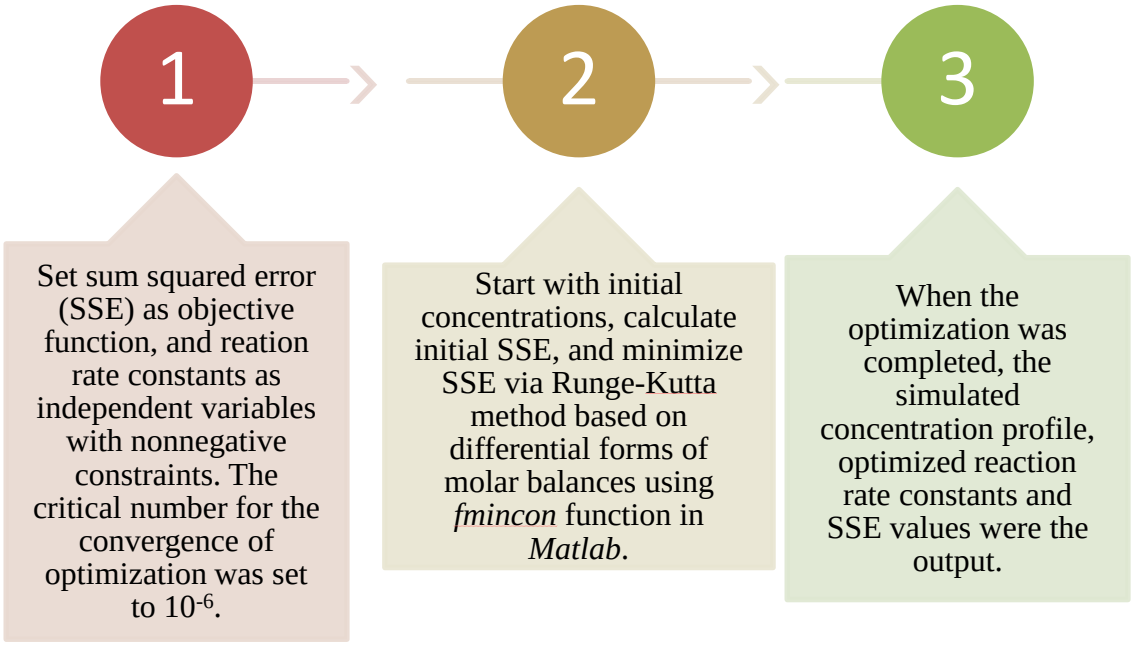

Figure 34*: Simulation algorithm of the reaction kinetic modeling in all cases.*

7.4 Results of the Reaction Kinetic Modeling

Different from the concentration profile as mentioned in **Chapter 5**, the simulated concentration profiles in this chapter for each chemical species were derived based on the chemical reaction pathway schemes proposed in **Chapter 6**. To clarify this dissimilarity, the former concentration profiles in **Chapter 5** were named as the simulated experimental concentration profiles. Additionally, the simulated concentration profiles in this chapter were continuous, while the simulated experimental profiles were discrete. The error distribution profiles described in **Section 7.5** were used for the uncertainty analysis of reaction kinetic modeling and HPLC analysis. The simulated concentration profiles Cellulose-300, Glucose-275 and Glucose-300 HTL experiments are plotted in ***Figure 41*** - ***Figure 77*** in **Appendix G**.

The simulated concentration plots of the identified chemical species are helpful for understanding the evolution patterns of the degradation products in the HTL experiments. The optimized reaction rate constants were compared not only within or among the HTL experiments to determine the best-fit case, but with earlier HTL research to conclude the evolution patterns in **Section 7.6**. The abbreviations used in this section are defined in the **List of Abbreviations**.

7.4.1 Cellulose-300 HTL Experiment

The role of cellulo-monomers was investigated through the proposed chemical pathway schemes where glucose and fructose were separated or combined. Best-fit scenarios were chosen based on the SSE values. For Cellulose-300 HTL Experiment, **Case 2.1** Condensation Scenario and **Case 2.2** Condensation Scenario were the best-fit scenarios, as given in ***Table 26*** and

Table 27. The reaction kinetic modeling results are assessed in **Section 7.6** to provide insights into the HTL reaction selectivity and product optimization.

***Table 26**: Simulated Reaction Rate Constants in the Reaction Kinetic Modeling of **Case 2.1** Condensation Scenario for Cellulose-300 HTL Experiment.*

Name of the Chemical Species	The Largest Reaction Rate Constant	Value (min^{-1})	The Second Largest Reaction Rate Constant	Value (min^{-1})	The Third Largest Reaction Rate Constant	Value (min^{-1})	The Fourth Largest Reaction Rate Constant	Value (min^{-1})	The Fifth Largest Reaction Rate Constant	Value (min^{-1})	The Sixth Largest Reaction Rate Constant	Value (min^{-1})
G_4	$k_{G_4,2G_2}$	360.8887	$k_{G_4,G_2 2G_{11}}$	150.6533	$k_{G_4,G_3 G_{11}}$	116.4066	$k_{G_4,UDP}$	0.0015				
G_3	$k_{G_3 G_{11},G_4}$	249.1061	$k_{G_3,G_2 G_{11}}$	113.8521	$k_{G_3,3G_{11}}$	106.1172	$k_{G_3,UDP}$	0.0033				
G_2	k_{2G_2,G_4}	26.5296	$k_{G_2,2G_{11}}$	22.7657	$k_{G_2 2G_{11},G_4}$	15.8714	$k_{G_2 G_{11},G_3}$	0.9384	$k_{G_2,UDP}$	0.0001		
G_{11}	$k_{G_{11},G_{12}}$	25.2455	$k_{G_{11},AA}$	2.1847	$k_{G_{11},FA}$	0.0071	$k_{G_{11},ErGA}$	0.0059	$k_{G_{11},UDP}$	0.0031	$k_{G_{11},SA}$	0.003
G_{11} *	$k_{G_3 G_{11},G_4}$	249.1061	$k_{G_2 2G_{11},G_4}$	31.7428	k_{3G_{11},G_3}	8.6264	$k_{G_2 G_{11},G_3}$	0.9384	k_{2G_{11},G_2}	0.0511		
G_{12}	$k_{G_{12},HMF}$	630.1213	$k_{G_{12},G_{11}}$	88.5009	$k_{G_{12},AA}$	83.1407	$k_{G_{12},ErGA}$	0.0723	$k_{G_{12},FA}$	0.0505	$k_{G_{12},UDP}$	0.034
HMF	$k_{HMF,G_{12}}$	822.8212	$k_{HMF,LAFA}$	41.1642	$k_{HMF,Fu}$	0.0007	$k_{HMF,UDP}$	0.0006				
Fu	$k_{Fu,UDP}$	0.0452										
LA	$k_{LAFA,HMF}$	21.5886	$k_{LA,UDP}$	0.0058	$k_{LA,SA}$	0.0055						
AA	$k_{AA,UDP}$	0.0019										
FA	$k_{LAFA,HMF}$	21.5886	$k_{FA,UDP}$	0.0635								
SA	$k_{SA,UDP}$	0.0768										
GA	$k_{GA,UDP}$	0.0082										

*****: This row of reaction rate constants was especially for the reactions that consumed glucose in condensation scenarios. Because there were many terms of reaction rate constants for glucose, the condensation rate constants for reactions where glucose was regarded as reactant were listed in a separate row.

***Table 27**: Simulated Reaction Rate Constants in the Reaction Kinetic Modeling of **Case 2.2** Condensation Scenario for Cellulose-300 HTL Experiment.*

Name of the Chemical Species	The Largest Reaction Rate Constant	Value (min^{-1})	The Second Largest Reaction Rate Constant	Value (min^{-1})	The Third Largest Reaction Rate Constant	Value (min^{-1})	The Fourth Largest Reaction Rate Constant	Value (min^{-1})	The Fifth Largest Reaction Rate Constant	Value (min^{-1})	The Sixth Largest Reaction Rate Constant	Value (min^{-1})
G_4	$k_{G_4,2G_2}$	481.2191	$k_{G_4,G_2 2G_1}$	9.1825	k_{G_4,G_3G_1}	8.0219	$k_{G_4,UDP}$	0.0001				
G_3	$k_{G_3G_1,G_4}$	118.4461	k_{G_3,G_2G_1}	26.3709	$k_{G_3,3G_1}$	0.0009	$k_{G_3,UDP}$	0.0002				
G_2	$k_{G_2 2G_1,G_4}$	207.4255	$k_{G_2,2G_1}$	52.1281	k_{2G_2,G_4}	26.5296	$k_{G_2G_1,G_3}$	8.5702	$k_{G_2,UDP}$	0		
G_1	$k_{G_1,HMF}$	129.028	$k_{G_1,AA}$	4.823	$k_{G_1,ErGA}$	0.0006	$k_{G_1,FA}$	0.0005	$k_{G_1,UDP}$	0.0003	$k_{G_1,SA}$	0
G_1*	$k_{G_2 2G_1,G_4}$	414.851	$k_{G_3G_1,G_4}$	118.4461	$k_{G_2G_1,G_3}$	8.5702	k_{3G_1,G_3}	0.0275	k_{2G_1,G_2}	0.0257		
HMF	k_{HMF,G_1}	57.2996	$k_{HMF,LAFA}$	11.0281	$k_{HMF,Fu}$	0.0002	$k_{HMF,UDP}$	0.0001				
Fu	$k_{Fu,UDP}$	0.0436										
LA	$k_{LAFA,HMF}$	0.0074	$k_{LA,UDP}$	0.0062	$k_{LA,SA}$	0.0058						
AA	$k_{AA,UDP}$	0.0015										
FA	$k_{FA,UDP}$	0.0653	$k_{LAFA,HMF}$	0.0074								
SA	$k_{SA,UDP}$	0.0844										
GA	$k_{GA,UDP}$	0.0076										

*****: This row of reaction rate constants was especially for the reactions that consumed cellulo-monomers in condensation scenarios. Because there were many terms of reaction rate constants for cellulo-monomers, the condensation rate constants for reactions where cellulo-monomers were regarded as reactant were listed in a separate row.

7.4.2 Glucose-275 HTL Experiment

For Glucose-275 HTL Experiment, **Case 1.1** Condensation Scenario and **Case 2.2** Condensation Scenario were the best-fit scenarios, as given in ***Table 28*** and ***Table* 29**.

7.4.3 Glucose-300 HTL Experiment

For Glucose-300 HTL Experiment, **Case 1.1** Condensation Scenario was the best-fit scenario, as presented in ***Table 30***. The accuracy of HTL reaction kinetic modeling for the three HTL scenarios are evaluated according to the error distribution in **Section 7.5**.

***Table 28**: Simulated Reaction Rate Constants in the Reaction Kinetic Modeling of **Case 1.1** Condensation Scenario for Glucose-275 HTL Experiment.*

Name of the Chemical Species	The Largest Reaction Rate Constant	Value (min^{-1})	The Second Largest Reaction Rate Constant	Value (min^{-1})	The Third Largest Reaction Rate Constant	Value (min^{-1})	The Fourth Largest Reaction Rate Constant	Value (min^{-1})	The Fifth Largest Reaction Rate Constant	Value (min^{-1})	The Sixth Largest Reaction Rate Constant	Value (min^{-1})
G_4	$k_{G_4,G_2 2G_{11}}$	5.1248	$k_{G_4,G_3G_{11}}$	5.1204	$k_{G_4,UDP}$	5.0335						
G_3	$k_{G_3G_{11},G_4}$	24.8896	$k_{G_3,3G_{11}}$	5.1596	$k_{G_3,G_2G_{11}}$	5.1029	$k_{G_3,UDP}$	5.0286				
G_2	$k_{G_2G_{11},G_3}$	25.4443	$k_{G_2 2G_{11},G_4}$	25.4031	$k_{G_2,2G_{11}}$	5.0667	$k_{G_2,UDP}$	5.035				
G_{11}	$k_{G_{11},AA}$	11.3753	$k_{G_{11},FA}$	8.4194	$k_{G_{11},UDP}$	7.7179	$k_{G_{11},G_{12}}$	0.0002	$k_{G_{11},ErGA}$	0		
G_{11} *	$k_{G_2 2G_{11},G_4}$	50.8062	$k_{G_2G_{11},G_3}$	25.4443	$k_{G_3G_{11},G_4}$	24.8896	k_{3G_{11},G_3}	24.3159	k_{2G_{11},G_2}	24.2181		
G_{12}	$k_{G_{12},UDP}$	6.3366	$k_{G_{12},FA}$	6.0943	$k_{G_{12},G_{11}}$	5.8149	$k_{G_{12},AA}$	5.8124	$k_{G_{12},HMF}$	4.259	$k_{G_{12},ErGA}$	1.4716
HMF	$k_{HMF,UDP}$	37.4221	$k_{HMF,LAFA}$	6.7799	$k_{HMF,Fu}$	1.8817	$k_{HMF,G_{12}}$	0.0001				
Fu	$k_{Fu,UDP}$	30.5111										
LA	$k_{LAFA,HMF}$	0.6541	$k_{LA,UDP}$	0								
AA	$k_{AA,UDP}$	0										
FA	$k_{FA,UDP}$	155.7331	$k_{LAFA,HMF}$	0.6541								
GA	$k_{GA,UDP}$	0.0116										

*****: This row of reaction rate constants was especially for the reactions that consumed glucose in condensation scenarios. Because there were many terms of reaction rate constants for glucose, the condensation rate constants for reactions where glucose was regarded as reactant were listed in a separate row.

***Table 29**: Simulated Reaction Rate Constants in the Reaction Kinetic Modeling of **Case 2.2** Condensation Scenario for Glucose-275 HTL Experiment.*

Name of the Chemical Species	The Largest Reaction Rate Constant	Value (min^{-1})	The Second Largest Reaction Rate Constant	Value (min^{-1})	The Third Largest Reaction Rate Constant	Value (min^{-1})	The Fourth Largest Reaction Rate Constant	Value (min^{-1})
G_4	$k_{G_4,2G_2}$	19.8302	k_{G_4,G_3G_1}	12.3215	$k_{G_4,G_2 2G_1}$	5.3651	$k_{G_4,UDP}$	0.0001
G_3	$k_{G_3G_1,G_4}$	20.9568	k_{G_3,G_2G_1}	6.6959	$k_{G_3,3G_1}$	5.0519	$k_{G_3,UDP}$	3.5543
G_2	$k_{G_2,2G_1}$	24.7242	$k_{G_2 2G_1,G_4}$	22.3908	$k_{G_2G_1,G_3}$	0.8989	$k_{G_2,UDP}$ k_{2G_2,G_4}	0.0004
G_1	$k_{G_1,HMF}$	0.1248	$k_{G_1,FA}$	0.0468	$k_{G_1,AA}$	0.0262	$k_{G_1,ErGA}$ $k_{G_1,UDP}$	0
G_1 *	$k_{G_2 2G_1,G_4}$	44.7816	$k_{G_3G_1,G_4}$	20.9568	$k_{G_2G_1,G_3}$	0.8989	k_{3G_1,G_3}, k_{2G_1,G_2}	0
HMF	k_{HMF,G_1}	0.2076	$k_{HMF,LAFA}$ $k_{HMF,Fu}$ $k_{HMF,UDP}$	0				
Fu	$k_{Fu,UDP}$	0.0413						
LA	$k_{LAFA,HMF}$ $k_{LA,UDP}$	0						
AA	$k_{AA,UDP}$	0						
FA	$k_{FA,UDP}$	0.0392	$k_{LAFA,HMF}$	0				
GA	$k_{GA,UDP}$	0.0119						

*: This row of reaction rate constants was especially for the reactions that consumed cellulo-monomers in condensation scenarios. Because there were many terms of reaction rate constants for cellulo-monomers, the condensation rate constants for reactions where cellulo-monomers were regarded as reactant were listed in a separate row.

***Table 30**: Simulated Reaction Rate Constants in the Reaction Kinetic Modeling of **Case 1.1** Condensation Scenario for Glucose-300 HTL Experiment.*

Name of the Chemical Species	The Largest Reaction Rate Constant	Value (min^{-1})	The Second Largest Reaction Rate Constant	Value (min^{-1})	The Third Largest Reaction Rate Constant	Value (min^{-1})	The Fourth Largest Reaction Rate Constant	Value (min^{-1})	The Fifth Largest Reaction Rate Constant	Value (min^{-1})	The Sixth Largest Reaction Rate Constant	Value (min^{-1})
G_3	$k_{G_3,UDP}$	19.8226	$k_{G_3,G_2G_{11}}$	19.6426	$k_{G_3,3G_{11}}$	19.5483						
G_2	$k_{G_2,UDP}$	19.8686	$k_{G_2,2G_{11}}$	19.4682	$k_{G_2G_{11},G_3}$	7.2259						
G_{11}	$k_{G_{11},AA}$	43.6794	$k_{G_{11},FA}$	29.7805	$k_{G_{11},UDP}$	27.8868	$k_{G_{11},G_{12}}$	2.8591	$k_{G_{11},SA}$	0.1245	$k_{G_{11},ErGA}$	0.0816
G_{11} *	$k_{G_2G_{11},G_3}$	7.2259	k_{3G_{11},G_3}	6.5128	k_{2G_{11},G_2}	6.5105						
G_{12}	$k_{G_{12},AA}$	24.5046	$k_{G_{12},FA}$	24.1725	$k_{G_{12},HMF}$	23.9792	$k_{G_{12},UDP}$	23.8096	$k_{G_{12},G_{11}}$	22.556	$k_{G_{12},ErGA}$	3.8508
HMF	$k_{HMF,LAFA}$	22.3901	$k_{HMF,G_{12}}$	7.3611	$k_{HMF,Fu}$	4.8288	$k_{HMF,UDP}$	3.0244				
Fu	$k_{Fu,UDP}$	3.3425										
LA	$k_{LAFA,HMF}$	8.5798	$k_{LA,UDP}$	0.0112	$k_{LA,SA}$	0.0032						
AA	$k_{AA,UDP}$	0										
FA	$k_{FA,UDP}$	91.2208	$k_{LAFA,HMF}$	8.5798								
SA	$k_{SA,UDP}$	0.0394										
GA	$k_{GA,UDP}$	0.0263										

*****: This row of reaction rate constants was especially for the reactions that consumed glucose in condensation scenarios. Because there were many terms of reaction rate constants for glucose, the condensation rate constant for reactions where glucose was regarded as reactant was listed in a separate row.

7.5 Error Distribution of Kinetic Modeling

The SSE values were used to evaluate how accurately the reaction kinetics was modeled based on the proposed chemical reaction pathways. Overall, the SSE values were acceptable with small discrepancy of concentrations for the identified chemical species. For each HTL experiment, error distribution is plotted for individual identified chemical species, as presented in ***Figure 35*** - ***Figure* 40**, based on the SSE formula given in **Section 7.3**. This section discusses the accuracy of reaction kinetic modeling for all cases, and in **Sections 7.6, 7.7 and 7.8**, further discussions about the HTL reaction chemistry, sources of uncertainties in the reaction kinetic modeling and future improvements are included. The abbreviations used in this section are defined in the **List of Abbreviations**.

7.5.1 Errors of the Reaction Kinetic Modeling for Cellulose-300 HTL Experiment

The SSE values for **Case 1.1** Base Scenario, **Case 1.1** Condensation Scenario, **Case 2.1** Base Scenario and **Case 2.1** Condensation Scenario were 328.06, 311.18, 328.14 and 307.45 correspondingly. The top five chemical species for the five largest error values were found to be HMF, formic acid, levulinic acid, acetic acid and furfural. These species were mostly involved in ***Stage 2*** of the cellulose degradation pathways. However, the error values for cellulo-monomers were much lower, indicating that the proposed chemical pathway schemes can serve as a basis for analyzing the degradation behaviors of cellulose, but the reaction orders may not all be first-order as assumed.

In **Case 1.2** Base Scenario, **Case 1.2** Condensation Scenario, **Case 2.2** Base Scenario and **Case 2.2** Condensation Scenario, the SSE values were 328.80, 314.89,

328.33 and 304.90 respectively. The top five chemical species with the largest errors remained the same. A sensitivity analysis of reaction order should be included in future work to examine the accuracy of predicting the reaction kinetics of the cellulose degradation. But the findings that are concluded in **Section 7.6** stay valid as it can be reproduced in the Glucose-300 HTL Experiment.

7.5.2 Errors of the Reaction Kinetic Modeling for Glucose-275 HTL Experiment

The SSE values for **Case 1.1** Base Scenario, **Case 1.1** Condensation Scenario, **Case 2.1** Base Scenario and **Case 2.1** Condensation Scenario were 991.96, 988.87, 991.96 and 988.87 correspondingly. In **Case 1.2** Base Scenario, **Case 1.2** Condensation Scenario, **Case 2.2** Base Scenario and **Case 2.2** Condensation Scenario, the SSE values were 215.80, 199.73, 241.22 and 196.99 respectively. The error distribution in ***Figure 37*** and ***Figure 38*** indicates that formic acid was the major cause for the deviation. Furthermore, from the kinetic modeling results of reactions that were associated with formic acid, HMF was only converted into furfural, and glucose decomposition did not gain favor over fructose from the simulated rate constants for formic acid production. However, the differences in the simulated rate constants between Cellulose-300 and Glucose-275 HTL Experiment were mainly due to the temperature effect. This effect can be further investigated under other reaction temperatures in the future work for deriving Arrhenius plots.

7.5.3 Errors of the Reaction Kinetic Modeling for Glucose-300 HTL Experiment

The SSE values for **Case 1.1** Base Scenario, **Case 1.1** Condensation Scenario, **Case 1.2** Base Scenario, and **Case 1.2** Condensation Scenario were 904.16, 61.60, 61.22 and 61.76 correspondingly. The error distribution is displayed in ***Figure 39*** and ***Figure 40***. The SSE values for **Case 1.1** Condensation Scenario, **Case 1.2** Base Scenario and **Case 1.2** Condensation Scenario were simulated to be much lower than the one of **Case 1.1** Base Scenario for Cellulose-300 HTL Experiment. Levulinic acid, formic acid and acetic acid were found to be the top three chemical species with the largest errors. The carboxylic acids were the most challenging chemical groups for reaction kinetic modeling due to the complexity of their formulation in the degradation pathways of cellulose. **Section 7.7** encompasses uncertainty analysis to assess the sources of simulation errors in this study.

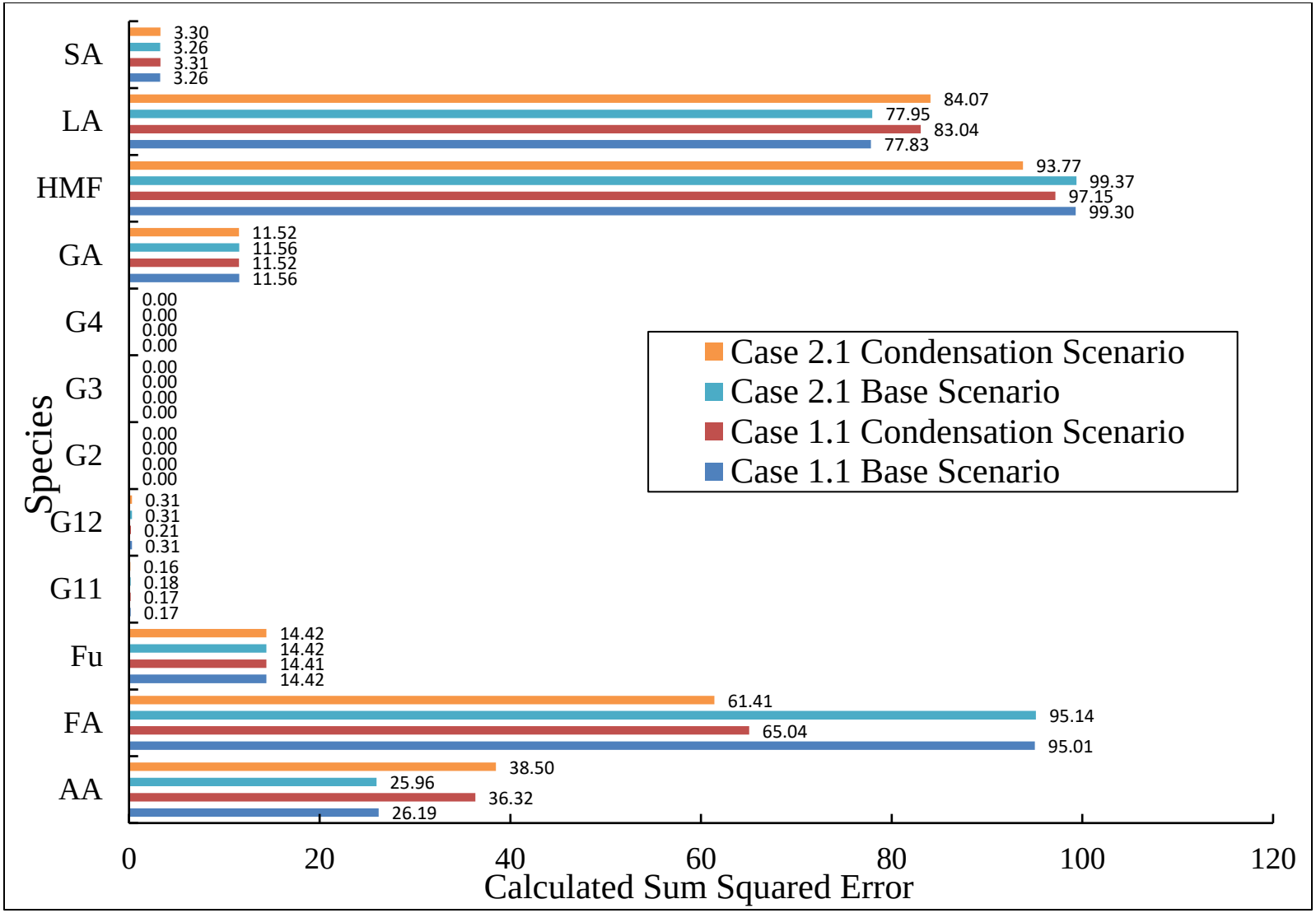

***Figure 35**: Error Distribution of the Reaction Kinetic Modeling among Species in **Case 1.1** & **Case 2.1** for Cellulose-300 HTL Experiment.*

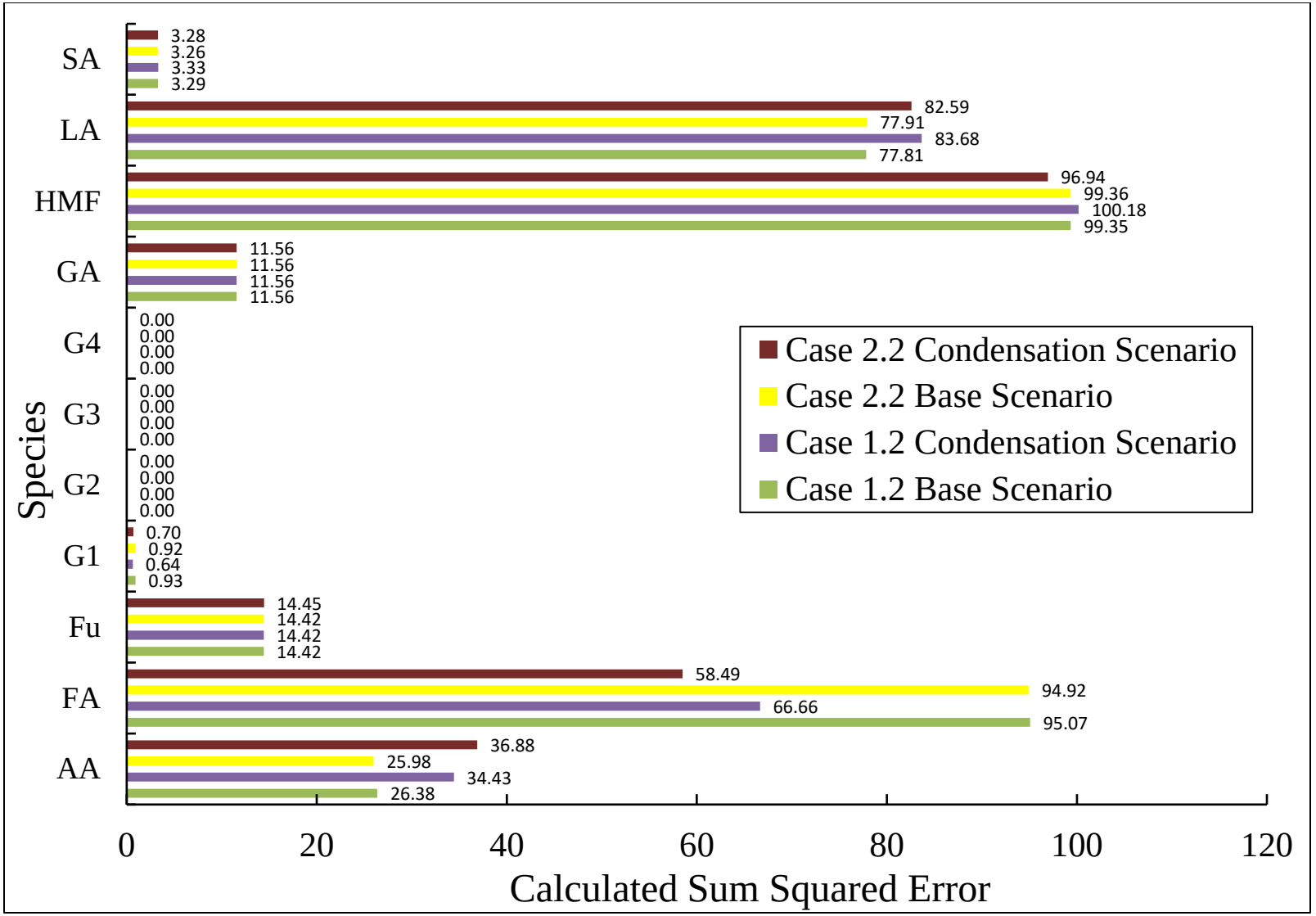

***Figure 36**: Error Distribution of the Reaction Kinetic Modeling among Species in **Case 1.2** & **Case 2.2** for Cellulose-300 HTL Experiment.*

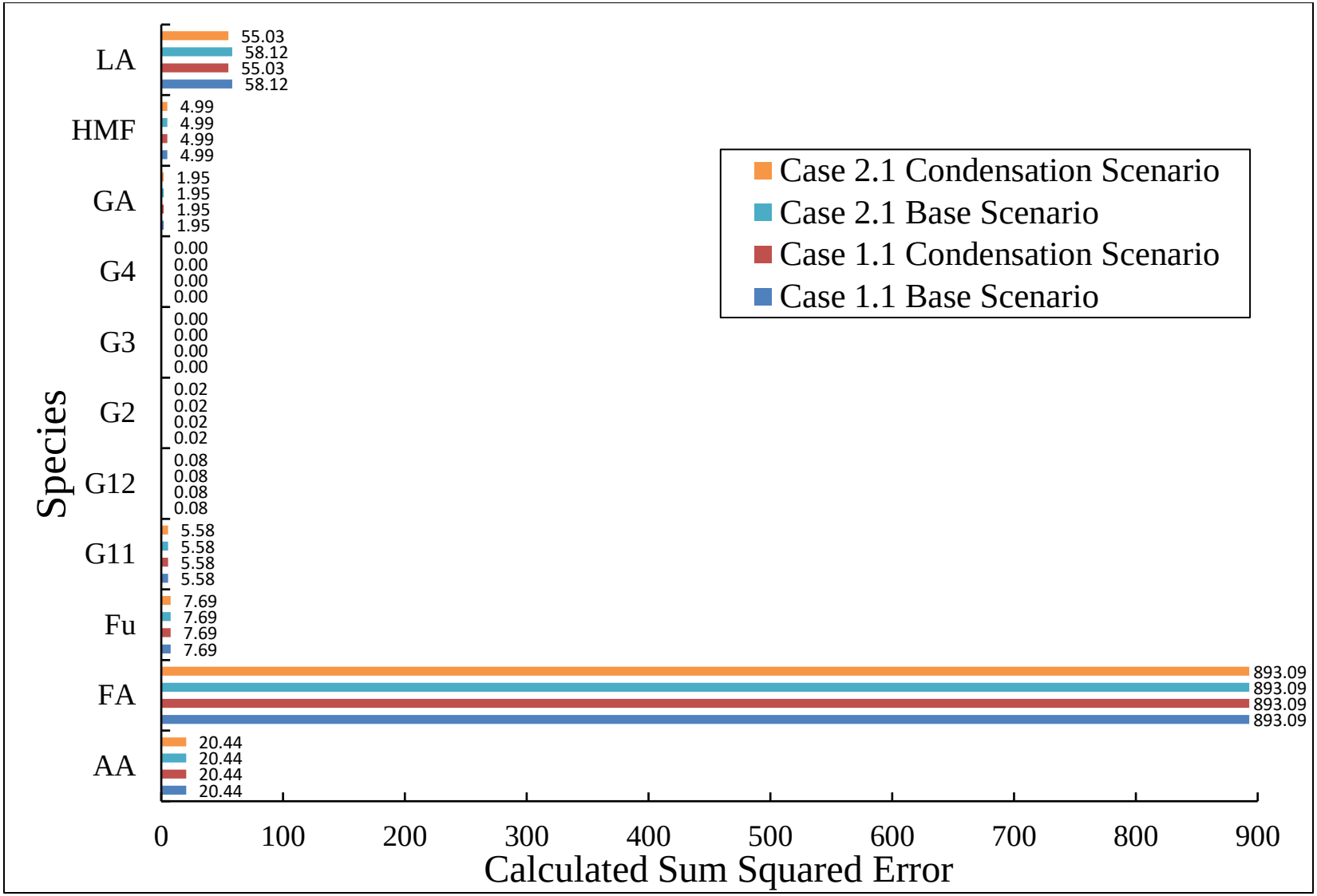

***Figure 37**: Error Distribution of the Reaction Kinetic Modeling among Species in **Case 1.1** & **Case 2.1** for Glucose-275 HTL Experiment.*

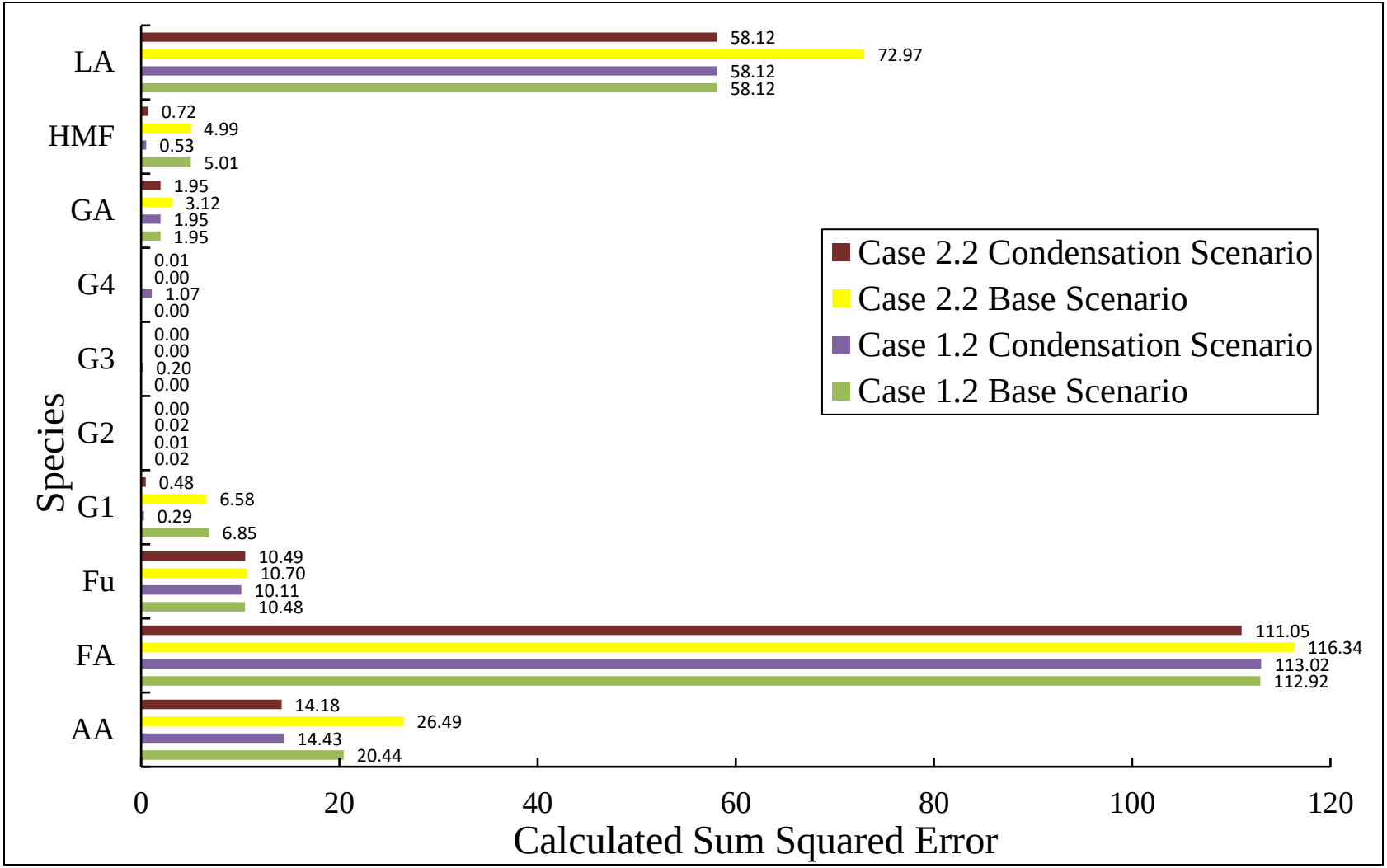

***Figure 38**: Error Distribution of the Reaction Kinetic Modeling among Species in **Case 1.2** & **Case 2.2** for Glucose-275 HTL Experiment.*

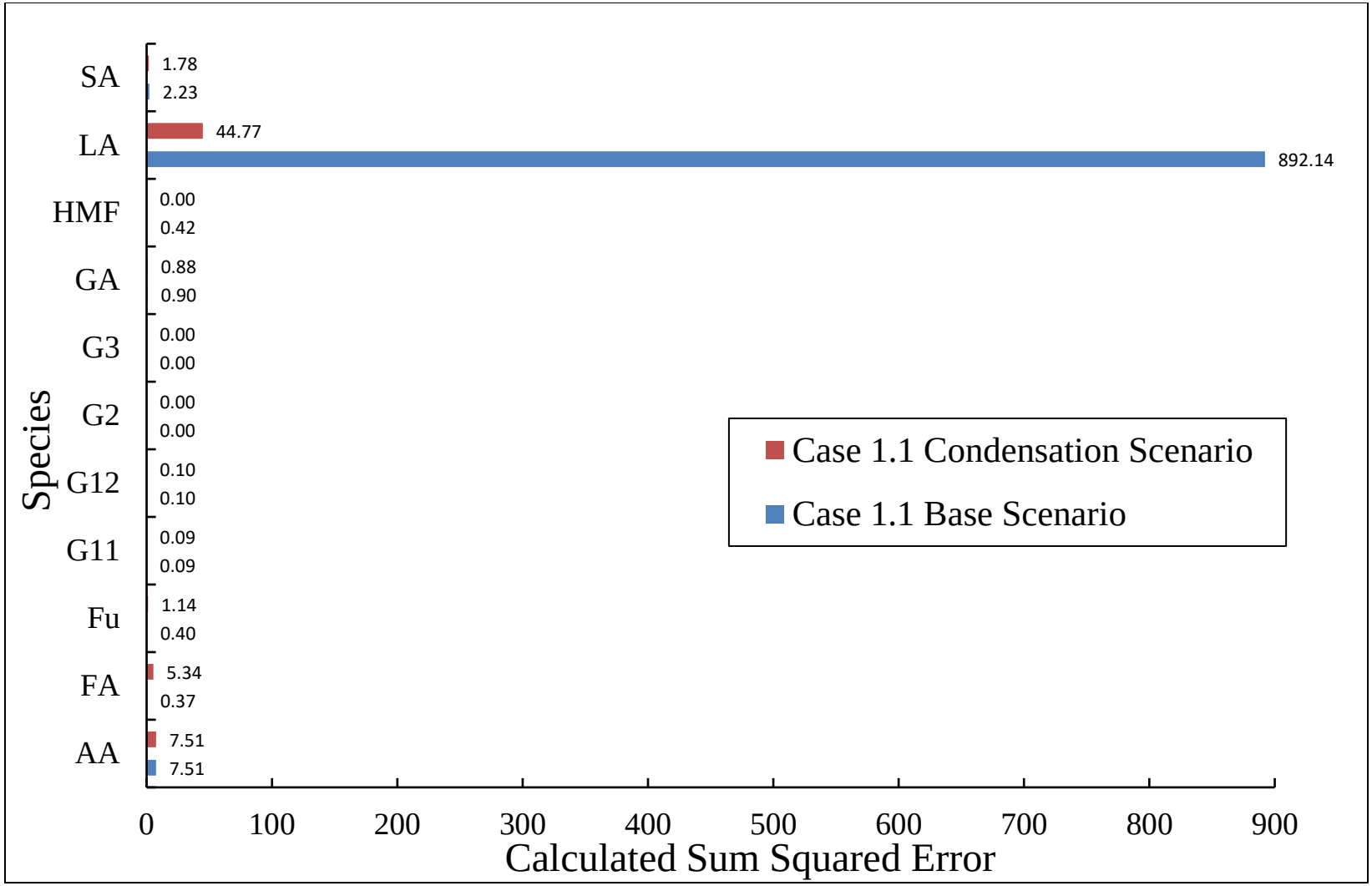

***Figure 39**: Error Distribution of the Reaction Kinetic Modeling among Species in **Case 1.1** for Glucose-300 HTL Experiment.*

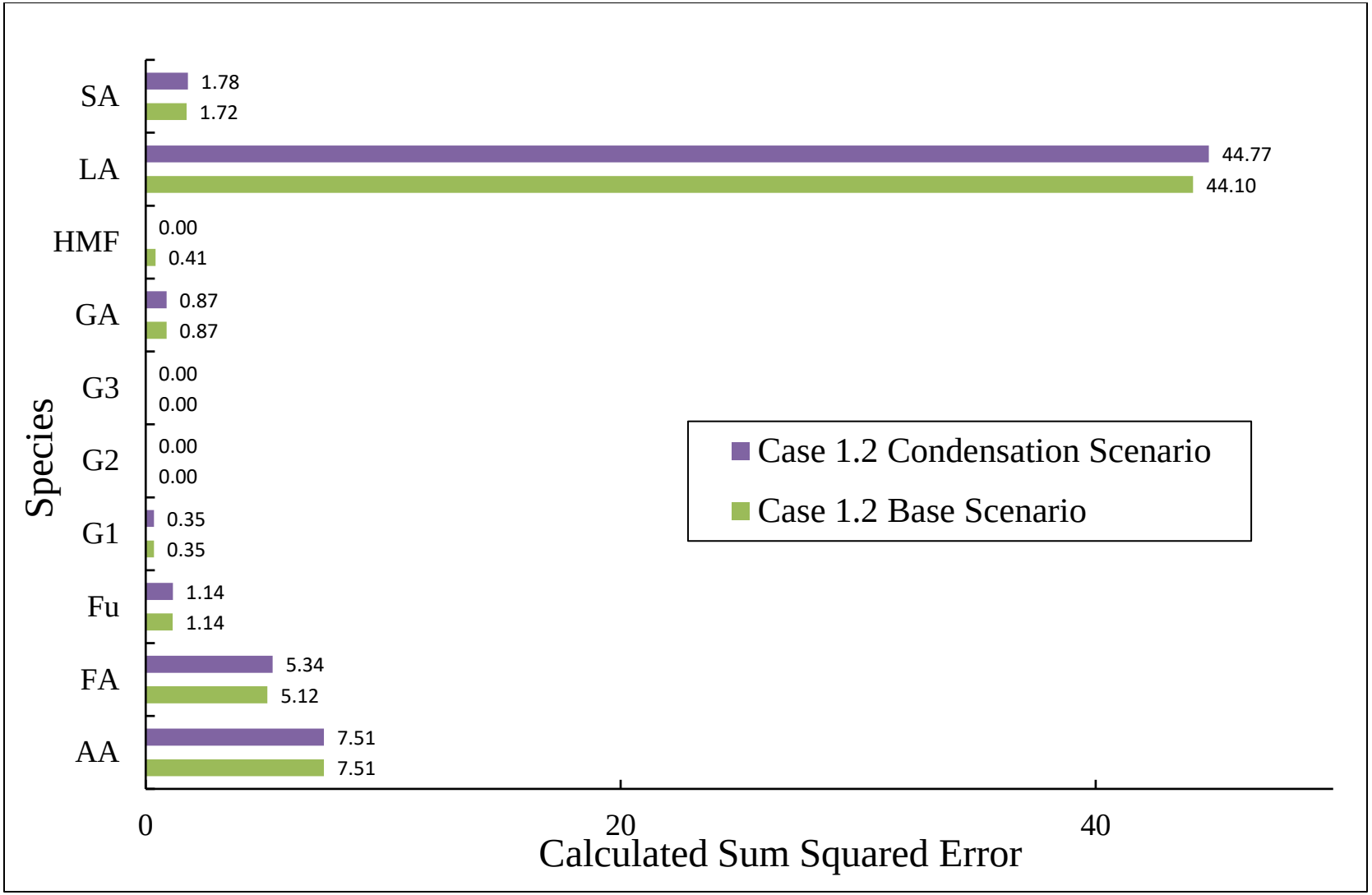

***Figure 40**: Error Distribution of the Reaction Kinetic Modeling among Species in **Case 1.2** for Glucose-275 HTL Experiment.*

7.6 Discussions of the Reaction Kinetic Modeling Results

The scales of reaction rate constants *k* for consuming a chemical species were compared for discussing HTL reaction selectivity and thus determining rate-limiting steps. The best-fit simulated reaction rate constants for all HTL experiments were also used for concluding the HTL product evolution patterns. The findings stated below were based on the simulation results in ***Table 26*** - ***Table* 30**, as well as the k values in earlier HTL studies.

7.6.1 Stage 1 and Stage 3

In ***Stage 1***, the rate constants for the reactions that involve cellulo-oligomers were the major focus. In ***Stage 3***, the rate constants for the reversible reactions that involve cellulo-oligomers and cellulo-monomers were the key focus. Generally, condensation and random scission scenarios were more preferred due to varieties of reaction pathways. For one mole of cellotetraose, under the end scission assumption of cellulo-oligomers, it was found that the rate for producing one mole of cellobiose together with two moles of glucose was slightly greater than that of generating one mole of glucose with one mole of cellotriose. That finding was consistent with what happens in the decomposition of cellotriose. Furthermore, in random scission scenarios, the rate of producing two moles of cellobiose from one mole of cellotetraose was much higher than other reaction rates around cellotetraose. The findings indicated higher possibility of simultaneous end scission from both ends of cellulo-oligomers than from one end. The findings stated above for cellotetraose stay valid in both Cellulose-300 and Glucose-275 HTL Experiments.

For the reactions that consumed cellotriose, the rehydration reaction to form cellotetraose had the highest reaction rate, whether glucose and fructose were separated. This finding repeated the same pattern for cellobiose. For the reactions that consumed cellobiose, the rehydration reaction rates to form cellotetraose or cellotriose were generally faster than degradation reaction rates. This finding implied that the significant barrier for the degradation reactions was in ***Stage 2*** as the trends for degradation from cellulo-oligomers into cellulo-monomers and their derivatives were not favored. Furthermore, the reaction rates for the same reaction in Cellulose-300 and Glucose-300 HTL Experiments were generally higher than those in Glucose-275 HTL Experiment due to temperature effects. As the errors for cellulo-oligomers were close to 0, the proposed chemical reaction pathways satisfied the mole balances around the identified cellulo-oligomers.

From ***Figure 22*** and ***Figure 23*** as mentioned in **Section 5.1.2**, there was a simultaneous decrease to note in the experimental concentration plots of furfural and HMF at the reaction time of 60 min in Cellulose-300 HTL Scenario. This may be caused by condensation or repolymerization reactions that were discussed in previous studies (Peterson, *et al*., 2008; Yin & Tan, 2012). The polymerization reactions may be included in the unidentified chemical reaction pathways, such as from HMF to solid or bio-oil products (Yin & Tan, 2012). However, in the environment where hydrogen ions and hydroxyl ions were particularly active, condensation reactions from aldehydes and carboxylic acids to cellulo-monomers or from cellulo-monomers to cellulo-oligomers in ***Stage 3*** become possible. The condensation reactions are given in **Appendix E**. From the results of reaction rate constants of **Case 1.1** Condensation Scenario for Cellulose-300 HTL Experiment, the reaction rate constants for the undefined reaction pathways were non-zero numbers, implying that the simulation values seemed more realistic with the

addition of condensation reactions. When glucose and fructose were not separated, the condensation rate constants were generally higher than those for the degradation rate constants. This polymerization pattern indicated the high possibility of other condensation reactions from degradation products to solid or bio-oil products.

7.6.2 Stage 2

For reactions that happened in ***Stage 2*** between cellulo-monomers and their derivatives, including aldehydes and carboxylic acids, fructose tended to degrade into acetic acid much faster than glucose with higher isomerization reaction rate to convert into glucose than that from glucose to fructose. The isomerization between glucose and fructose favored the direction from fructose to glucose over that from glucose to fructose. Fructose was found to be more volatile to degrade into carboxylic acids and aldehydes compared to glucose, where the degradation rate constants for fructose were generally higher than that for glucose. This was consistent with the high reactivity characteristics of fructose found in earlier studies (Kabyemela, Adschiri, Malaluan, & Arai, 1999). Especially for succinic acid, it could only be derived from levulinic acid based on the kinetic modeling results. The undefined conversion pathways from the identified chemical species have shown to be not existing, as the kinetic modeling was a data-driven optimization where the identified chemical species were primarily considered via the proposed chemical reaction networks. Looking among the scales of the reaction rate constants, the values for reactions in ***Stages 1 and 3*** were typically much larger than the reaction rate constants in ***Stage 2***, since many small-chain molecules originated from cellulo-oligomers and cellulo-monomers and the reaction stoichiometry may significantly cause the discrepancy of the rate constants.

Asghari and Yoshida proposed a degradation pathway from fructose to the identified degradation products, such as levulinic acid, formic acid, furfural and HMF, which were also identified in my research (Asghari & Yoshida, 2007). Their simulated reaction rate constants for the reactions producing levulinic acid and formic acid from HMF and generating furfural from HMF were consistent with the simulated rate constants in my study. This consistency provided a solid basis for validating the findings as described below for the reactions.

For HMF degradation, the rehydration reaction to form levulinic acid together with formic acid was more favored than the decarbonylation reaction to produce furfural along with formic acid. Explained by the Arrhenius Equation, at the same reaction temperature, the activation energy for the direct cleavage of C—C bonding between the ring and the ethanol side should be higher than that for cleavage of C—C bonding in hydrated straight-chain intermediates of HMF rehydration reaction. The rehydration mechanisms involved the addition of hydrogen and hydroxy group respectively onto the cathode-like and anode-like carbon atom in the C=C double bond, and then the reformation of hydroxy group under the influence of carbonyl group and ethanol oxygen. The inclination could also be explained by the stability of π-p interaction of the electron cloud areas in HMF molecules. This finding was validated by the kinetic modeling results as shown in ***Table 26*** and

***Table* 27**. The negligible values of the reaction rate constants for unidentified chemical reaction pathways indicated that the proposed reaction networks were able to precisely describe the evolution of cellulose degradation products.

7.7 Uncertainty Analysis

In **Section 7.5**, the error distribution described the inaccuracy of proposed chemical pathway schemes. However, this was traced back to the identification of peaks for chemical species in HPLC analysis as described in **Chapter 4** and **Chapter 5**. The MPE values for modeling HPLC signals in the HTL experiments were not as ideal as those in the HPLC standards. For example, the simulated MPE values could be as high as 30% at the reaction time of 55 min in Cellulose-300 HTL Experiment, as shown in ***Table 37*** in **Appendix A**. The deviation of modeling experimental HPLC signals came from the complication of multiple peaks in HPLC analysis when the retention time values of two chemical species were close. This inaccuracy was identified as a major source for SSE values in the reaction kinetic modeling.

Furthermore, in HPLC analysis, the undefined chemical species served as another main source for uncertainties in the degradation reaction kinetics. The role of the undefined chemical species could not be precisely evaluated for the degradation chemistry of cellulose under HTL conditions. In the assumptions for reaction kinetic modeling, first-order reaction kinetics was assumed for all proposed chemical reactions, but the realistic chemical reactions may undergo second-order or third-order reaction kinetics. Furthermore, the stoichiometry for some proposed undefined reactions remained unclear, while all the stoichiometric coefficients were assumed to follow 1:1 ratio. For example, for the undefined reactions that generated acetic acid from glucose, one mole of glucose can generate two moles of acetic acid from the aspect of chemical formulation. The variation of stoichiometry coefficients played a crucial role of describing the production rate of the product. Therefore, this disparity in the differential forms of molar balances resulted in a totally different best-fit combination of *k* values.

Future efforts require a full examination of the identification of experimental HPLC peaks, reaction orders, reaction stoichiometry among the identified chemical species, and

temperature effect for obtaining Arrhenius plots. The simulation results of this study can serve as a basis for the full examination from HPLC analysis to reaction kinetic modeling. Improvements of the modeling accuracy can be made based on the thorough assessment described in the previous sections.

7.8 Remarks on Conversion Efficiency and Carbon Balances of HTL Experiments

One of the key findings was that unlike protein and lipids, only carbohydrates can produce solid products under HTL conditions (Cantero-Tubilla, 2017). Solids were basically generated from condensation of small-chain aqueous degradation products (Cantero-Tubilla, 2017). This was consistent with the comparison results between base scenarios and condensation scenarios of the kinetic modeling results for HTL experiments. From the perspective of bio-oil products, the energy potential was analogical to commercial bio-ethanol, when carbohydrate-rich food wastes can be valorized to produce bio-oil products with higher energy density comparable to bio-diesel (Cantero-Tubilla, 2017).

The bio-crude derived in the HTL experiments was characterized into different groups. Alkenes, cyclic hydrocarbons, phenols, furans, long fatty acids, straight amides were detected in the bio-crude from HTL of manure and food waste. In this study, furans were identified in the aqueous product of Cellulose-300 HTL Experiment. Connections between the aqueous furans and bio-oil furans need further investigation. The abundant existence of cyclic hydrocarbons in bio-oil may be considerably related to the condensation of carboxylic acids and aldehydes in the aqueous product. In Shen's study, levoglucosan, HMF, furfural, hydroxylacetone, hydroxylacetaldehyde and some $C_{1\text{-}2}$ compounds were detected as the major components of the bio-oil product derived from thermal decomposition of cellulose (Shen & Gu, 2009). The

existence of HMF in bio-oil could result from the extraction of HMF from aqueous phase to bio-oil, while hydroxylacetone and hydroxylacetaldehyde may come from the hydration of the degradation products of cellulose in aqueous product. The abundant presence of levoglucosan was proposed to come from acetal reactions via the interactions between free hydroxyl radical on C-6 and the dislocated glucosidic bond on C-4 (Shen & Gu, 2009). There were still uncertainties in qualifying the reaction path from cellulose to value-added biochemical and bio-oil products. Future efforts should be taken to fully understand the evolution of the chemical species from aqueous phase to bio-oil.

As for the maximal carbon conversion (mole-based) of each identified chemical species, assuming cellulose molecules were all dissolved in subcritical water, the feedstock of Cellulose-300, Glucose-300, and Glucose-275 HTL Experiment had 1.85, 1.67 and 1.67 mol/L soluble carbon concentration respectively. The maximal carbon conversion was presented in ***Table 31*** below, where only mean concentration values were used to calculate the maximum carbon conversion efficiency. These conversion results were consistent with earlier studies that included a detailed investigation on HTL conversion of cellulose, cellulo-oligomers or cellulo-monomers (Asghari & Yoshida, 2007; Croce *et al*., 2017; He *et al*., 2017; Kabyemela, Adschiri, Malaluan, & Arai, 1999). With the HTL conversion efficiency data, it will be easier to understand the product evolution patterns and kinetic modeling results.

***Table 31**: Maximum Carbon Conversion Efficiency (Mole-Based) of the Identified Degradation Products in the HTL Experiments.*

Name of the degradation product	Reaction Time in Cellulose-300 HTL Experiment (min)	Maximum Carbon Conversion Efficiency (%)	Reaction Time in Glucose-275 HTL Experiment (min)	Maximum Carbon Conversion Efficiency (%)	Reaction Time in Glucose-300 HTL Experiment (min)	Maximum Carbon Conversion Efficiency (%)
Cellotetraose	35.00	0.11	14.67	0.04	-	-
Cellotriose	52.00	0.22	25.00	0.05	0.00	0.02
Cellobiose	52.00	0.42	25.00	1.30	40.00	0.10
Glucose	52.00	1.97	-	-	-	-
Fructose	52.00	0.30	25.00	5.56	40.00	0.65
HMF	65.00	3.00	33.50	19.56	40.00	12.04
Fufrural	55.00	2.51	33.50	2.84	40.00	3.47
Levulinic acid	65.00	4.02	101.50	5.68	110.00	4.75
Acetic acid	55.00	1.56	116.50	1.11	130.00	1.36
Formic acid	55.00	1.65	51.50	2.11	40.00	2.37
Succinic acid	70.00	0.38	-	-	90.00	0.34
Glycolaldehyde	55.00	0.46	33.50	0.79	40.00	0.54

CHAPTER 8

CONCLUSIONS AND FUTURE WORK

8.1 Conclusions

This thesis addressed reaction kinetic modeling for understanding the chemical pathways involved during the degradation of cellulose under HTL conditions using HPLC analysis. A set of HPLC standards were established to derive the standard EMG parameters as the references for modeling HPLC signals for HTL aqueous products. In the HPLC standards, MPE values between the detected and simulated HPLC signals were generally lower than 5% for the identified chemical compounds with a wide range of concentrations. Linear regression was successfully applied to describing the relationship between the simulated EMG parameter *A* and the concentration of the chemical compounds in the HPLC standards. In the experimental HPLC signal modeling, the best-fit EMG parameters were determined using the nonlinear regression method for minimizing MPE values. From the optimized EMG parameter *A* of each identified HPLC peak in the HTL experiments, the concentration of the identified chemical species is calculated via the linear relationship. The concentration plots of the identified chemical species were used to understand the chemical pathways, when products were divided into five categories based on functional groups, cellulo-oligomers, cellulo-monomers, furan aldehydes, alkanol aldehydes and carboxylic acids. The chemical pathways were modeled in reaction networks starting from cellulose. The study proposes various chemical reaction pathway schemes to simulate the reaction kinetics of cellulose degradation in HTL. Using nonlinear regression analysis, optimized reaction rate constants of the reaction kinetic modeling were used to predict HTL reaction selectivity and determine rate-limiting steps in various pathways.

In the HPLC signal modeling part, the overlapping signals of levulinic acid and acetic acid were effectively deconvoluted with errors that were comparable to the signals in the HPLC standards. All EMG parameters except parameter *A* were constrained according to the sensitivity analysis of the EMG parameters versus concentrations in the HPLC standards. But for the case where glycolaldehyde and lactic acid HPLC signals were overlapping, the superposition approach could not resolve the overlapping signals due to the proximity of their EMG parameters. In this case, the signals of lactic acid were separated first using regression analysis between the HPLC peak heights and the concentration of lactic acid. Then the overlapping signals were deconvoluted based on the superposition principle with the constraints of lactic acid EMG parameters. After resolution of the convoluted HPLC signals, the concentrations of the identified species were simulated for the reaction kinetic modeling to calculate the rate constants of proposed chemical reactions and therefore compare reaction selectivity.

In the reaction kinetic modeling, three stages of the product evolution were observed, including the depolymerization of cellulose into cellulo-monomers via cellulo-oligomers (***Stage 1***), degradation of cellulo-monomers to aldehydes and carboxylic acids (***Stage 2***), and condensation or repolymerization reactions involving the degradation products (***Stage 3***). According to the Three-Stage hypothesis, several chemical reaction pathway schemes were projected from cellulose to the value-added products. Based on the kinetic modeling assumptions, the role of cellulo-monomers in the degradation pathways of cellulose was evaluated in the scenarios where glucose and fructose were treated together as cellulo-monomers. The results showed that in most cases fructose was more reactive than glucose to decompose into carboxylic acids and aldehydes. Furthermore, fructose isomerized into glucose more rapidly than glucose, which demonstrated fructose's higher reactivity. In the scenarios

where glucose and fructose are not separated, the reaction rate constants indicated that the cellulo-monomers tended not to produce acetic acid and formic acid through undefined pathways, which contradicted the kinetic modeling results for the scenarios where glucose and fructose were separated. Furthermore, two mechanisms, the degradation mechanisms of cellulo-oligomer decomposition were investigated. Under the end scission assumption, the reaction rate of cleaving the glycosidic bonds in cellulo-oligomers from both ends was much higher than that from one end. In the random scission cases, the additional pathway from cellotetraose to cellobiose generally had the greatest reaction rate constant in ***Stage 1***. To categorize the magnitude of the simulated reaction rate constants in a descending order, in general, the *k* values for decomposition reactions of cellulo-oligomers were the largest. The comparison results of the magnitude of the best-fit reaction rate constants shows that ***Stage 2*** was the limiting stage in the degradation of cellulose. For HMF degradation, the dehydration reaction to form levulinic acid together with formic acid was more favored than the decarbonylation reaction to produce furfural along with formaldehyde.

The carbon yields of the identified products were used for understanding the product evolution. The yields of HMF were found to be the highest (around 20%) at the reaction time of 33.5 min in Glucose-275 HTL Experiment, and (around 12%) at the reaction time of 40 min in Glucose-300 HTL Experiment. In Cellulose-300 HTL Experiment, levulinic acid had the highest carbon yield, around 4%. Levulinic-300 HTL Experiment demonstrates the stability of levulinic acid under HTL conditions.

8.2 Future Work

Future work should include further investigation into the HTL reaction networks that pertain to carboxylic acid products as levulinic acid reacted with other chemical species. The decomposition of levulinic acid in HTL experiments of cellulose or glucose may be correlated with the production of succinic acid, but the mechanisms for generating succinic acid is not fully understood. From ***Table 31*** in **Section 7.8**, the reaction times of the maximal production of cellulo-oligomers, cellulo-monomers, aldehydes and carboxylic acids generally followed a sequential order from the longest to the shortest. This validated the Three-Stage hypothesis that the decomposition of cellulose chronologically generates cellulo-oligomers, cellulo-monomers, aldehydes and carboxylic acids in the aqueous phase.

To examine the mole balances in the aqueous phase, error distribution of the identified chemical species in the reaction kinetic modeling indicated that the molar balances around cellulo-oligomers, cellulo-monomers and aldehydes were adequately satisfied. However, the optimal simulated concentrations of carboxylic acids in the reaction kinetic modeling still need improvements. The error sources can be the unidentified HPLC peaks, first-order reaction kinetics and assumed reaction stoichiometry. This study provides insights in the evolution of value-added biochemicals that can be identified as the degradation products of cellulose under HTL conditions. Notably, the production of HMF or levulinic acid accounted for the largest carbon yield among the identified cellulose or glucose degradation products. In the future work, the combination of polar aprotic solvents and acids, as well as the decrease of cellulose loading and water content, may further improve the yields of HMF. As cellulose is the most naturally-abundant macromolecule in waste biomass, the HTL reaction kinetics uncovered in this research can help scientists optimize the production of selective commodity biochemicals from waste

biomass to help solve the environmental problems and offer alternatives to the petrochemical industry.

APPENDICES

Appendix A: HPLC Signal Modeling Results in Cellulose-300 Scenario

***Table 32**: Simulated Area Values for Identified Species in HPLC Signals in the Cellulose-300 Scenario at the reaction time of 32 min.*

Component	Mean Area Value	Minimum Area Value	Maximum Area Value
Cellotetroase	275.5075	263.8221	289.1403
Cellotriose	377.0399	369.2376	382.6604
Cellobiose	396.2067	383.7245	406.5820
Glucose	371.2493	368.5082	373.7828
Fructose	144.8111	142.2391	146.9325
Glycolaldehyde	68.7921	65.4888	70.4350
HMF	266.6021	258.9936	272.5629

***Table 33**: Simulated MPE Values for Identified Species in HPLC Signals in the Cellulose-300 Scenario at the reaction time of 32 min.*

Component	Mean Value of MPE (%)	Minimum Value of MPE (%)	Maximum Value of MPE (%)
Cellotetroase	5.3287	4.5884	6.0887
Cellotriose	1.2141	0.8696	1.3682
Cellobiose	3.7967	1.6673	6.1532
Glucose	0.1179	0.0219	0.3805
Fructose	6.3315	3.9667	8.7423
Glycolaldehyde	2.7364	1.9137	3.2201
HMF	2.0266	0.8332	2.8417

***Table 34**: Simulated Area Values for Identified Species in HPLC Signals in the Cellulose-300 Scenario at the reaction time of 52 min.*

Component	Mean Area Value	Minimum Area Value	Maximum Area Value
Cellotetroase	272.0248	261.1582	284.5177
Cellotriose	526.0957	518.2581	534.8852
Cellobiose	1087.5579	995.5544	1176.1775
Glucose	5114.5135	5065.8131	5183.3173
Fructose	794.8846	749.9514	824.0094
Glycolaldehyde	1321.9707	1294.9749	1353.6841
Formic acid	1308.1156	1299.8190	1316.6765
HMF	4110.7796	4075.3075	4163.0552
Furfural	3726.2428	3701.3869	3745.9857

***Table 35**: Simulated MPE Values for Identified Species in HPLC Signals in the Cellulose-300 Scenario at the reaction time of 52 min.*

Component	Mean Value of MPE (%)	Minimum Value of MPE (%)	Maximum Value of MPE (%)
Cellotetroase	3.8886	3.2876	4.5508
Cellotriose	0.9083	0.2222	1.6972
Cellobiose	3.1648	0.7877	7.1925
Glucose	0.3569	0.0078	2.1066
Fructose	5.0569	4.1003	5.6780
Glycolaldehyde	1.0807	0.6318	1.4150
Formic acid	2.6500	1.7691	3.5437
HMF	2.1461	0.0279	8.1404
Furfural	1.2052	0.0195	4.2437

***Table 36**: Simulated Area Values for Identified Species in HPLC Signals in the Cellulose-300 Scenario at the reaction time of 55 min.*

Component	Mean Area Value	Minimum Area Value	Maximum Area Value
Glucose	266.2933	219.4259	361.6728
Fructose	389.2755	351.1600	491.5581
Glycolaldehyde	2054.0828	1972.5160	2120.1214
Formic acid	2268.1846	2255.7065	2283.1789
HMF	2364.0151	2345.6664	2382.3588
Furfural	5306.0881	5271.4786	5359.7669

***Table 37**: Simulated MPE Values for Identified Species in HPLC Signals in the Cellulose-300 Scenario at the reaction time of 55 min.*

Component	Mean Value of MPE (%)	Minimum Value of MPE (%)	Maximum Value of MPE (%)
Glucose	21.3409	18.1942	23.2977
Fructose	29.4206	28.6564	29.7690
Glycolaldehyde	1.8641	1.4920	2.2156
Formic acid	2.2329	1.4710	3.0034
HMF	12.1840	12.1554	12.2126
Furfural	0.6472	0.0108	2.9081

***Table 38**: Simulated Area Values for Identified Species in HPLC Signals in the Cellulose-300 Scenario at the reaction time of 60 min.*

Component	Mean Area Value	Minimum Area Value	Maximum Area Value
Glucose	169.0896	169.0895	169.0896
Fructose	188.5427	184.4013	189.9232
Glycolaldehyde	1910.4368	1845.8288	1968.1885
Formic acid	1334.0513	1321.5072	1348.9310
HMF	1723.7882	1694.4476	1811.8093
Furfural	2136.5941	2116.0301	2154.9493

***Table 39**: Simulated MPE Values for Identified Species in HPLC Signals in the Cellulose-300 Scenario at the reaction time of 60 min.*

Component	Mean Value of MPE (%)	Minimum Value of MPE (%)	Maximum Value of MPE (%)
Glucose	42.2543	42.2543	42.2543
Fructose	23.6378	23.3630	23.7294
Glycolaldehyde	1.6866	1.4318	1.9212
Formic acid	3.0165	1.8338	4.2473
HMF	41.2408	41.1602	41.4824
Furfural	1.7680	0.0369	6.0877

***Table 40**: Simulated Area Values for Identified Species in HPLC Signals in the Cellulose-300 Scenario at the reaction time of 65 min.*

Component	Mean Area Value	Minimum Area Value	Maximum Area Value
Glucose	123.3495	119.6961	124.5675
Fructose	138.1009	130.5803	155.8402
Glycolaldehyde	1719.6701	1662.5817	1772.7224
Formic acid	604.1364	594.2192	609.7961
HMF	6979.7346	6979.7346	6979.7346
Furfural	1674.3077	1637.2184	1714.8180

***Table 41**: Simulated MPE Values for Identified Species in HPLC Signals in the Cellulose-300 Scenario at the reaction time of 65 min.*

Component	Mean Value of MPE (%)	Minimum Value of MPE (%)	Maximum Value of MPE (%)
Glucose	17.8664	17.4501	18.0056
Fructose	20.9102	20.5816	21.1045
Glycolaldehyde	1.7566	1.5627	1.9281
Formic acid	3.8689	3.8209	3.9088
HMF	6.4080	6.4080	6.4080
Furfural	2.6014	0.0981	11.9483

***Table 42**: Simulated Area Values for Identified Species in HPLC Signals in the Cellulose-300 Scenario at the reaction time of 70 min.*

Component	Mean Area Value	Minimum Area Value	Maximum Area Value
Fructose	148.1221	140.6436	170.5335
Succinic acid	744.7478	736.8746	754.7992
Glycolaldehyde	1748.5045	1694.9618	1794.3819
Formic acid	553.0929	540.0230	557.4495
Furfural	1881.4379	1858.6996	1910.7595

***Table 43**: Simulated MPE Values for Identified Species in HPLC Signals in the Cellulose-300 Scenario at the reaction time of 70 min.*

Component	Mean Value of MPE (%)	Minimum Value of MPE (%)	Maximum Value of MPE (%)
Fructose	21.5623	20.9080	21.7808
Succinic acid	5.7330	5.6022	5.8827
Glycolaldehyde	1.5276	1.3345	1.7461
Formic acid	12.5058	10.7467	13.0922
Furfural	0.9645	0.1975	1.7767

***Table 44**: Simulated Area Values for Identified Species in HPLC Signals in the Cellulose-300 Scenario at the reaction time of 75 min.*

Component	Mean Area Value	Minimum Area Value	Maximum Area Value
Glucose	77.9806	75.0969	79.2478
Fructose	96.4877	87.4895	113.0523
Succinic acid	657.1281	648.9610	670.9221
Glycolaldehyde	1568.5637	1533.9129	1608.1707
Formic acid	360.4833	352.6406	363.0979
Furfural	1169.8048	1157.9336	1187.5554

***Table 45**: Simulated MPE Values for Identified Species in HPLC Signals in the Cellulose-300 Scenario at the reaction time of 75 min.*

Component	Mean Value of MPE (%)	Minimum Value of MPE (%)	Maximum Value of MPE (%)
Glucose	9.6929	8.7217	10.1880
Fructose	19.0945	11.6055	26.3477
Succinic acid	6.2577	6.1561	6.5065
Glycolaldehyde	1.0974	0.9110	1.2230
Formic acid	12.4134	11.1145	12.8470
Furfural	1.8207	0.1646	4.2866

***Table 46**: Simulated Area Values for Identified Species in HPLC Signals in the Cellulose-300 Scenario at the reaction time of 80 min.*

Component	Mean Area Value	Minimum Area Value	Maximum Area Value
Glucose	72.9622	66.9037	76.9554
Glycolaldehyde	433.2146	427.6406	442.2343
Formic acid	76.9055	74.2254	78.9907
Furfural	1182.2776	1179.9951	1186.2760

***Table 47**: Simulated MPE Values for Identified Species in HPLC Signals in the Cellulose-300 Scenario at the reaction time of 80 min.*

Component	Mean Value of MPE (%)	Minimum Value of MPE (%)	Maximum Value of MPE (%)
Glucose	10.3794	9.4728	11.0706
Glycolaldehyde	0.5766	0.1776	0.7796
Formic acid	5.8072	3.2736	8.7833
Furfural	0.8583	0.0238	3.2811

***Table 48**: Simulated Area Values for Identified Species in HPLC Signals in the Cellulose-300 Scenario at the reaction time of 90 min.*

Component	Mean Area Value	Minimum Area Value	Maximum Area Value
Succinic acid	82.1051	76.1164	88.9537
Glycolaldehyde	330.6915	326.2472	337.3079
Formic acid	60.7620	58.9768	62.0816
Furfural	442.6838	430.6427	457.4930

***Table 49**: Simulated MPE Values for Identified Species in HPLC Signals in the Cellulose-300 Scenario at the reaction time of 90 min.*

Component	Mean Value of MPE (%)	Minimum Value of MPE (%)	Maximum Value of MPE (%)
Succinic acid	16.1159	15.9650	16.3796
Glycolaldehyde	0.9748	0.1064	1.6129
Formic acid	6.2139	5.9945	6.5569
Furfural	3.9168	0.3002	12.8554

***Table 50**: Simulated Area Values for Identified Species in HPLC Signals in the Cellulose-300 Scenario at the reaction time of 100 min.*

Component	Mean Area Value	Minimum Area Value	Maximum Area Value
Succinic acid	301.6710	294.6849	305.2565
Glycolaldehyde	1096.7863	1085.5705	1104.2302
Furfural	339.3166	331.1283	343.5748

***Table 51**: Simulated MPE Values for Identified Species in HPLC Signals in the Cellulose-300 Scenario at the reaction time of 100 min.*

Component	Mean Value of MPE (%)	Minimum Value of MPE (%)	Maximum Value of MPE (%)
Succinic acid	1.6361	1.0406	1.9539
Glycolaldehyde	0.6779	0.4379	0.8134
Furfural	5.1770	2.0131	7.2064

***Table 52**: Simulation Results of Area under the HPLC Curve in Deconvoluted HPLC Signals of Levulinic Acid and Acetic Acid in the Cellulose-300 Scenario.*

Reaction Time (min)	Simulated Mean Value Area under the HPLC Curve of Levulinic Acid	Simulated Minimum Value Area under the HPLC Curve of Levulinic Acid	Simulated Maximum Value Area under the HPLC Curve of Levulinic Acid	Simulated Mean Value Area under the HPLC Curve of Acetic Acid	Simulated Minimum Value Area under the HPLC Curve of Acetic Acid	Simulated Maximum Value Area under the HPLC Curve of Acetic Acid
52.00	2248.9671	2214.7242	2287.4204	797.5289	751.0260	839.4995
55.00	5774.8786	5774.8785	5774.8787	1937.8480	1937.8479	1937.8480
60.00	5973.9392	5951.0871	6012.6207	1760.1008	1640.7612	1888.6227
65.00	6145.2380	6123.6354	6166.8406	1803.6415	1744.5133	1862.7697
70.00	5924.7197	5773.9375	6038.5088	1886.6626	1741.2132	2097.3085
75.00	5729.5743	5666.1315	5799.6521	1757.3827	1675.2641	1847.7110
80.00	1798.4029	1791.4957	1803.7945	1531.1578	1526.2993	1534.7331
90.00	1503.2053	1501.8379	1504.5727	1651.1508	1649.6121	1652.6895
100.00	5032.0527	5007.7505	5056.3549	1955.2451	1928.7517	1981.7385

***Table 53**: Comparison of Mean Percent Error Values Using EMG Model Between Superposition of Levulinic Acid Together with Acetic Acid and the Scenario of Only Levulinic Acid in the Cellulose-300 Scenario.*

Reaction Time (min)	Curve Fitting Using Superposition of Levulinic Acid and Acetic Acid HPLC Signals			Curve Fitting Using Levulinic Acid HPLC Signals Only		
	Minimum Mean Percent Error (%)	Minimum Mean Percent Error (%)	Maximum Mean Percent Error (%)	Minimum Mean Percent Error (%)	Minimum Mean Percent Error (%)	Maximum Mean Percent Error (%)
52.00	0.1420	0.0025	0.8063	4.1814	0.0738	11.0255
55.00	0.1921	0.0025	1.3459	3.4413	0.0702	9.0288
60.00	1.1810	0.0027	6.3885	7.5048	0.0604	20.9841
65.00	0.8572	0.0030	5.9784	6.6469	0.0449	19.6623
70.00	0.0314	0.0024	0.0584	0.8860	0.0503	2.0754
75.00	0.4912	0.0025	4.1229	7.0650	0.0471	19.9096
80.00	0.2519	0.0080	1.2057	1.7608	1.6884	1.9299
90.00	0.3892	0.0105	2.0753	2.9054	1.1237	8.4720
100.00	0.4276	0.0025	1.9970	8.3983	0.0893	22.0572

***Table 54**: Observed and Expected Peak Features of the Peaks of Lactic Acid HPLC Signals in the Cellulose-300 Scenario.*

Reaction Time (min)	Retention Time of the First Peak (min)	First Peak Value in HPLC Signals	Expected Second Peak Value in HPLC Signals	Expected Major Peak Value in HPLC Signals	Expected Concentration of Lactic Acid (mM)
32.00	11.258	269	170	1343	1.89
52.00	11.067	3183	5956	47100	66.25
55.00	10.892	5309	12440	98376	138.37
60.00	10.900	4901	11087	87679	123.33
65.00	10.892	4295	9168	72505	101.98
70.00	10.875	3827	7765	61409	86.38
75.00	10.875	3364	6450	51004	71.74
80.00	10.867	710	687	5432	7.64
90.00	10.842	179	94	747	1.05
100.00	10.808	647	601	4752	6.68

Table 55*: Comparison between the Observed and Expected Retention Time Values and Peak Height at the Peaks of Lactic Acid HPLC Signals in the Cellulose-300 Scenario.*

Reaction Time (min)	Retention Time of the Second Peak (min)	Observed Second Peak Value in HPLC Signals	Expected Concentration of Lactic Acid (mM)	Retention Time of the Major Peak Value in HPLC Signals	Observed Major Peak Value in HPLC Signals	Expected Concentration of Lactic Acid (mM)
32.00	12.208	133	1.48	12.725	160	0.23
52.00	12.217	5868	65.27	12.733	3259	4.58
55.00	12.225	12214	135.86	12.733	4997	7.03
60.00	12.225	12598	140.13	12.725	4713	6.63
65.00	12.233	13026	144.89	12.725	4485	6.31
70.00	12.225	12445	138.43	12.733	4299	6.05
75.00	12.225	11933	132.73	12.733	3912	5.50
80.00	12.225	3226	35.88	12.733	1128	1.59
90.00	12.225	2108	23.45	12.733	862	1.21
100.00	12.225	8336	92.72	12.733	2807	3.95

Appendix B: HPLC Signal Modeling Results in Glucose-275 Scenario

***Table 56**: Simulated Area Values for Identified Species in HPLC Signals in the Glucose-275 Scenario at the reaction time of 14.67 min.*

Component	Mean Area Value	Minimum Area Value	Maximum Area Value
Cellotetroase	86.2785	55.6139	129.4652
Cellotriose	54.5583	53.8185	55.4678
Cellobiose	326.5395	314.3489	348.9759
Glucose	238171.9521	224569.7329	247801.5783
HMF	228.0381	219.0434	231.0363

***Table 57**: Simulated MPE Values for Identified Species in HPLC Signals in the Glucose-275 Scenario at the reaction time of 14.67 min.*

Component	Mean Value of MPE (%)	Minimum Value of MPE (%)	Maximum Value of MPE (%)
Cellotetroase	12.4686	7.5502	18.4025
Cellotriose	9.3162	6.1514	12.4515
Cellobiose	9.7689	5.3447	14.5511
Glucose	0.7368	0.1701	2.6551
HMF	8.7197	8.2919	8.8623

***Table 58**: Simulated Area Values for Identified Species in HPLC Signals in the Glucose-275 Scenario at the reaction time of 19.5 min.*

Component	Mean Area Value	Minimum Area Value	Maximum Area Value
Cellotriose	42.5261	39.6217	45.6347
Cellobiose	650.1182	634.5373	679.7558
Glucose	235547.5346	221957.6650	246102.8981
HMF	523.1868	514.0791	533.3870

***Table 59**: Simulated MPE Values for Identified Species in HPLC Signals in the Glucose-275 Scenario at the reaction time of 19.5 min.*

Component	Mean Value of MPE (%)	Minimum Value of MPE (%)	Maximum Value of MPE (%)
Cellotriose	5.9048	3.6607	8.1515
Cellobiose	9.7665	4.7051	15.3566
Glucose	0.6210	0.1191	2.4083
HMF	3.2890	1.0051	7.2201

***Table 60**: Simulated Area Values for Identified Species in HPLC Signals in the Glucose-275 Scenario at the reaction time of 25 min.*

Component	Mean Area Value	Minimum Area Value	Maximum Area Value
Cellotriose	113.7263	111.4327	117.6496
Cellobiose	3040.2123	3007.9790	3082.0653
Glucose	162658.3936	158700.8546	168150.1558
Fructose	13468.7146	13116.6995	13749.7068
Glycolaldehyde	1639.3297	1529.0030	1715.6529
Formic acid	748.9266	714.1561	766.1378
HMF	20858.4646	20398.1664	21384.2214
Furfural	1536.8544	1513.4531	1578.9196

***Table 61**: Simulated MPE Values for Identified Species in HPLC Signals in the Glucose-275 Scenario at the reaction time of 25 min.*

Component	Mean Value of MPE (%)	Minimum Value of MPE (%)	Maximum Value of MPE (%)
Cellotriose	14.2667	14.2415	14.3276
Cellobiose	4.9929	2.9623	7.3742
Glucose	0.9398	0.0190	5.3721
Fructose	2.6365	2.3175	2.8710
Glycolaldehyde	2.7582	2.5575	3.0551
Formic acid	7.7376	7.3802	7.9383
HMF	0.1541	0.0148	0.4916
Furfural	0.8732	0.0793	1.9095

***Table 62**: Simulated Area Values for Identified Species in HPLC Signals in the Glucose-275 Scenario at the reaction time of 33.5 min.*

Component	Mean Area Value	Minimum Area Value	Maximum Area Value
Cellobiose	1265.3317	1238.3585	1292.8386
Glucose	82940.2749	82204.1283	84024.4005
Fructose	6907.0908	6814.2357	7140.4957
Glycolaldehyde	3183.0963	3112.0511	3258.5626
Formic acid	1945.1719	1912.5285	1980.4107
HMF	41121.4984	40509.6775	41460.4624
Furfural	5425.3887	5375.8473	5502.3165

***Table 63**: Simulated MPE Values for Identified Species in HPLC Signals in the Glucose-275 Scenario at the reaction time of 33.5 min.*

Component	Mean Value of MPE (%)	Minimum Value of MPE (%)	Maximum Value of MPE (%)
Cellobiose	7.1163	3.5976	12.1776
Glucose	0.5319	0.0149	2.6646
Fructose	6.9296	6.7688	7.3306
Glycolaldehyde	1.0179	0.2404	1.5793
Formic acid	4.9122	3.0940	6.7683
HMF	0.5486	0.1426	1.9839
Furfural	1.4686	0.0113	5.7215

***Table 64**: Simulated Area Values for Identified Species in HPLC Signals in the Glucose-275 Scenario at the reaction time of 51.5 min.*

Component	Mean Area Value	Minimum Area Value	Maximum Area Value
Cellobiose	60.3217	59.5720	60.8808
Glucose	3667.1808	3623.9991	3750.5670
Glycolaldehyde	1227.1949	1179.0526	1259.9692
Formic acid	2624.0665	2564.2793	2723.4064
HMF	6438.3406	6403.2259	6518.4424
Furfural	5262.7968	5212.4205	5347.2550

***Table 65**: Simulated MPE Values for Identified Species in HPLC Signals in the Glucose-275 Scenario at the reaction time of 51.5 min.*

Component	Mean Value of MPE (%)	Minimum Value of MPE (%)	Maximum Value of MPE (%)
Cellobiose	12.3144	7.3375	17.3011
Glucose	0.9808	0.0060	4.3186
Glycolaldehyde	2.1926	1.7115	2.5951
Formic acid	3.7218	1.7378	6.0069
HMF	0.4220	0.0595	1.1029
Furfural	2.2965	0.0218	8.8379

***Table 66**: Simulated Area Values for Identified Species in HPLC Signals in the Glucose-275 Scenario at the reaction time of 61.5 min.*

Component	Mean Area Value	Minimum Area Value	Maximum Area Value
Cellotetroase	17.5535	15.9804	20.0185
Cellotriose	133.7266	124.3685	142.2627
Cellobiose	198.1701	182.7043	210.4639
Glucose	1659.0190	1648.6535	1677.1684
Fructose	131.9042	130.5371	133.3439
Glycolaldehyde	443.7609	438.7897	445.9033
Formic acid	1142.0127	1054.2136	1218.4317
HMF	1119.5376	1094.7068	1140.0140
Furfural	1846.9274	1817.6278	1877.4528

***Table 67**: Simulated MPE Values for Identified Species in HPLC Signals in the Glucose-275 Scenario at the reaction time of 61.5 min.*

Component	Mean Value of MPE (%)	Minimum Value of MPE (%)	Maximum Value of MPE (%)
Cellotetroase	2.5981	0.8830	3.4539
Cellotriose	6.4916	0.8186	19.6817
Cellobiose	6.9509	1.2035	18.6652
Glucose	0.6627	0.0162	2.8065
Fructose	4.0966	2.3816	5.7563
Glycolaldehyde	0.8563	0.4072	1.0180
Formic acid	5.0832	2.0324	9.0635
HMF	1.2710	0.5153	2.2714
Furfural	2.3624	0.1071	7.8946

***Table 68**: Simulated Area Values for Identified Species in HPLC Signals in the Glucose-275 Scenario at the reaction time of 71.5 min.*

Component	Mean Area Value	Minimum Area Value	Maximum Area Value
Glucose	759.4918	753.8934	767.0476
Fructose	74.2398	73.1668	74.5975
Glycolaldehyde	875.3203	851.1725	894.1484
Formic acid	1538.2165	1491.9886	1600.2059
HMF	933.8609	906.2918	949.0624
Furfural	2533.4326	2516.0152	2555.3933

***Table 69**: Simulated MPE Values for Identified Species in HPLC Signals in the Glucose-275 Scenario at the reaction time of 71.5 min.*

Component	Mean Value of MPE (%)	Minimum Value of MPE (%)	Maximum Value of MPE (%)
Glucose	0.6034	0.0144	2.1712
Fructose	8.2625	7.9655	8.3615
Glycolaldehyde	3.6441	3.2323	4.1679
Formic acid	5.0971	2.2778	8.4283
HMF	10.1405	9.8823	10.3273
Furfural	1.9330	0.0322	6.9130

***Table 70**: Simulated Area Values for Identified Species in HPLC Signals in the Glucose-275 Scenario at the reaction time of 86.5 min.*

Component	Mean Area Value	Minimum Area Value	Maximum Area Value
Cellobiose	68.5672	65.5136	69.7407
Glucose	704.5079	695.1052	727.6483
Fructose	131.9746	131.9746	131.9746
Glycolaldehyde	920.1555	892.0221	940.8410
Formic acid	1021.0511	1013.1530	1027.1090
HMF	849.2733	823.5058	857.8626
Furfural	1992.8477	1954.6039	2034.4009

***Table 71**: Simulated MPE Values for Identified Species in HPLC Signals in the Glucose-275 Scenario at the reaction time of 86.5 min.*

Component	Mean Value of MPE (%)	Minimum Value of MPE (%)	Maximum Value of MPE (%)
Cellobiose	4.6072	3.9213	4.8918
Glucose	0.1657	0.0057	0.9471
Fructose	26.5774	26.5774	26.5774
Glycolaldehyde	4.0170	3.5106	4.6108
Formic acid	4.1282	2.7494	5.5282
HMF	12.2018	11.8803	12.3089
Furfural	3.6499	0.2954	8.8482

***Table 72**: Simulated Area Values for Identified Species in HPLC Signals in the Glucose-275 Scenario at the reaction time of 101.5 min.*

Component	Mean Area Value	Minimum Area Value	Maximum Area Value
Glucose	203.7513	202.6764	206.2333
Fructose	100.0551	79.0957	147.3843
Glycolaldehyde	782.8790	764.6138	797.4390
Formic acid	370.2781	364.7957	373.1656
Furfural	785.6889	765.4183	801.2836

***Table 73**: Simulated MPE Values for Identified Species in HPLC Signals in the Glucose-275 Scenario at the reaction time of 101.5 min.*

Component	Mean Value of MPE (%)	Minimum Value of MPE (%)	Maximum Value of MPE (%)
Glucose	0.3991	0.0176	2.1192
Fructose	42.3622	37.2591	45.3174
Glycolaldehyde	2.4644	2.2887	2.7621
Formic acid	4.6587	4.6505	4.6789
Furfural	2.1143	0.5804	3.1694

***Table 74**: Simulated Area Values for Identified Species in HPLC Signals in the Glucose-275 Scenario at the reaction time of 116.5 min.*

Component	Mean Area Value	Minimum Area Value	Maximum Area Value
Glucose	294.5380	290.9037	303.9223
Fructose	115.1543	106.8720	140.0011
Glycolaldehyde	651.2413	631.8790	665.8032
Formic acid	282.8147	277.0594	285.3139
Furfural	720.7508	690.2935	737.0059

***Table 75**: Simulated MPE Values for Identified Species in HPLC Signals in the Glucose-275 Scenario at the reaction time of 116.5 min.*

Component	Mean Value of MPE (%)	Minimum Value of MPE (%)	Maximum Value of MPE (%)
Glucose	3.6321	0.0069	14.9697
Fructose	45.5084	44.6381	45.7986
Glycolaldehyde	2.2574	1.9940	2.5571
Formic acid	11.6447	11.5319	11.6990
Furfural	6.2653	1.9744	9.7134

***Table 76**: Simulation Results of Area under the HPLC Curve in Deconvoluted HPLC Signals of Levulinic Acid and Acetic Acid in the Glucose-275 Scenario.*

Reaction Time (min)	Simulated Mean Value Area under the HPLC Curve of Levulinic Acid	Simulated Minimum Value Area under the HPLC Curve of Levulinic Acid	Simulated Maximum Value Area under the HPLC Curve of Levulinic Acid	Simulated Mean Value Area under the HPLC Curve of Acetic Acid	Simulated Minimum Value Area under the HPLC Curve of Acetic Acid	Simulated Maximum Value Area under the HPLC Curve of Acetic Acid
25.00	244.1294	167.5680	270.6730	381.6148	376.5804	395.9855
33.50	1985.1126	1968.3046	2005.4848	862.4569	791.5786	902.6683
51.50	7053.5599	7004.7242	7102.3954	944.5077	772.4109	1116.6045
61.50	4174.2719	4174.2697	4174.2739	525.1891	525.1857	525.1929
71.50	7428.8804	7428.8804	7428.8805	1091.6539	1091.6536	1091.6543
86.50	7760.0701	7738.2914	7781.8488	1224.0394	1181.8045	1266.2743
101.50	7840.4176	7840.4155	7840.4192	1205.1546	1205.1535	1205.1561
116.50	6439.2724	6399.3387	6479.2062	1238.7242	1224.8150	1252.6331

***Table 77**: Comparison of Mean Percent Error Values Using EMG Model Between Superposition of Levulinic Acid Together with Acetic Acid and the Scenario of Only Levulinic Acid in the Glucose-275 Scenario.*

Reaction Time (min)	Curve Fitting Using Superposition of Levulinic Acid and Acetic Acid HPLC Signals			Curve Fitting Using Levulinic Acid HPLC Signals Only		
	Minimum Mean Percent Error (%)	Minimum Mean Percent Error (%)	Maximum Mean Percent Error (%)	Minimum Mean Percent Error (%)	Minimum Mean Percent Error (%)	Maximum Mean Percent Error (%)
25.00	10.4154	8.8644	10.9544	11.6447	11.5319	11.6990
33.50	2.5155	0.0826	9.1673	8.0755	0.1928	20.8565
51.50	2.0291	0.0090	12.9324	3.5785	0.0067	13.7435
61.50	2.8921	0.0440	14.0446	3.3019	0.0411	13.7757
71.50	1.2871	0.0057	7.1054	3.1071	0.0116	11.8862
86.50	0.8871	0.0024	7.1645	3.2412	0.0083	12.1925
101.50	1.9824	0.0120	11.7057	3.1874	0.0109	12.1130
116.50	1.6228	0.0155	10.0063	3.7585	0.0202	13.4044

***Table 78**: Observed and Expected Peak Features of the Peaks of Lactic Acid HPLC Signals in the Glucose-275 Scenario.*

Reaction Time (min)	Retention Time of the First Peak (min)	First Peak Value in HPLC Signals	Expected Second Peak Value in HPLC Signals	Expected Major Peak Value in HPLC Signals	Expected Concentration of Lactic Acid (mM)
25.00	11.058	11315	36980	292440	411.34
33.50	11.067	10120	31490	249028	350.28
51.50	11.150	4854	10934	86471	121.63
61.50	11.158	2554	4338	34306	48.25
71.50	10.942	3775	7614	60211	84.69
86.50	10.917	3777	7620	60257	84.76
101.50	10.900	3133	5822	46039	64.76
116.50	10.892	2327	3794	30003	42.20

***Table 79**: Comparison between the Observed and Expected Peak Parameters at the Peaks of Lactic Acid HPLC Signals in the Glucose-275 Scenario.*

Reaction Time (min)	Retention Time of the Second Peak (min)	Observed Second Peak Value in HPLC Signals	Expected Concentration of Lactic Acid (mM)	Retention Time of the Major Peak Value in HPLC Signals	Observed Major Peak Value in HPLC Signals	Expected Concentration of Lactic Acid (mM)
25.00	11.583	4548	50.59	12.725	4008	5.64
33.50	12.092	17391	193.44	12.742	7883	11.09
51.50	12.250	5858	65.16	12.742	2890	4.06
61.50	12.250	3270	36.37	12.742	1113	1.57
71.50	12.250	5927	65.93	12.742	2033	2.86
86.50	12.250	6097	67.82	12.742	2122	2.98
101.50	12.250	5874	65.34	12.750	1866	2.62
116.50	12.250	4703	52.31	12.750	1542	2.17

Appendix C: HPLC Signal Modeling Results in Glucose-300 Scenario

***Table 80**: Simulated Area Values for Identified Species in HPLC Signals in the Glucose-300 Scenario at the reaction time of 0 min.*

Component	Mean Area Value	Minimum Area Value	Maximum Area Value
Cellotriose	41.5425	38.2363	45.1037
Cellobiose	210.1135	193.9818	235.1096
Glucose	238905.9763	227010.2864	250700.7442

***Table 81**: Simulated MPE Values for Identified Species in HPLC Signals in the Glucose-300 Scenario at the reaction time of 0 min.*

Component	Mean Value of MPE (%)	Minimum Value of MPE (%)	Maximum Value of MPE (%)
Cellotriose	10.3014	3.9745	18.0984
Cellobiose	13.0938	6.4734	20.7230
Glucose	1.1034	0.1908	4.6017

***Table 82**: Simulated Area Values for Identified Species in HPLC Signals in the Glucose-300 Scenario at the reaction time of 20 min.*

Component	Mean Area Value	Minimum Area Value	Maximum Area Value
Cellotriose	36.9802	33.8278	40.6205
Cellobiose	203.5827	185.7808	227.5828
Glucose	237653.0327	226294.5210	250010.6200

***Table 83**: Simulated MPE Values for Identified Species in HPLC Signals in the Glucose-300 Scenario at the reaction time of 20 min.*

Component	Mean Value of MPE (%)	Minimum Value of MPE (%)	Maximum Value of MPE (%)
Cellotriose	8.8168	3.8115	14.5298
Cellobiose	17.3564	6.2575	37.7011
Glucose	1.0585	0.1733	4.5377

***Table 84**: Simulated Area Values for Identified Species in HPLC Signals in the Glucose-300 Scenario at the reaction time of 40 min.*

Component	Mean Area Value	Minimum Area Value	Maximum Area Value
Cellobiose	240.1071	237.4787	241.8905
Glucose	14441.1404	14299.0882	14637.8224
Fructose	1581.3896	1486.9762	1630.7597
Glycolaldehyde	2187.4000	2117.2487	2245.7056
Formic acid	2945.2865	2888.9554	3018.8157
HMF	25303.0854	25027.1223	25489.0731
Furfural	6641.2675	6584.8495	6684.6508

***Table 85**: Simulated MPE Values for Identified Species in HPLC Signals in the Glucose-300 Scenario at the reaction time of 40 min.*

Component	Mean Value of MPE (%)	Minimum Value of MPE (%)	Maximum Value of MPE (%)
Cellobiose	19.5431	19.5006	19.5730
Glucose	0.3898	0.0125	2.2467
Fructose	7.0804	6.7867	7.9322
Glycolaldehyde	2.2474	0.6888	3.3069
Formic acid	5.0820	2.2273	8.7192
HMF	0.3497	0.0326	1.3399
Furfural	0.9782	0.0105	3.6782

***Table 86**: Simulated Area Values for Identified Species in HPLC Signals in the Glucose-300 Scenario at the reaction time of 60 min.*

Component	Mean Area Value	Minimum Area Value	Maximum Area Value
Glucose	2807.2672	2778.9885	2831.1138
Glycolaldehyde	1916.1887	1869.5027	1957.5611
Formic acid	2923.5162	2867.8458	3014.4127
HMF	21974.6667	21477.7031	22510.1631
Furfural	6419.6950	6336.7170	6533.7906

***Table 87**: Simulated MPE Values for Identified Species in HPLC Signals in the Glucose-300 Scenario at the reaction time of 60 min.*

Component	Mean Value of MPE (%)	Minimum Value of MPE (%)	Maximum Value of MPE (%)
Glucose	3.3216	0.1266	11.0301
Glycolaldehyde	1.4707	0.3715	2.2410
Formic acid	3.6618	1.7782	5.6397
HMF	0.6935	0.0161	3.6727
Furfural	0.5463	0.0100	2.7574

***Table 88**: Simulated Area Values for Identified Species in HPLC Signals in the Glucose-300 Scenario at the reaction time of 80 min.*

Component	Mean Area Value	Minimum Area Value	Maximum Area Value
Fructose	38.3662	32.3806	44.9821
Glycolaldehyde	824.3535	809.0761	831.4290
Formic acid	171.7697	165.7438	175.1860
Furfural	380.4665	365.6238	393.5756

***Table 89**: Simulated MPE Values for Identified Species in HPLC Signals in the Glucose-300 Scenario at the reaction time of 80 min.*

Component	Mean Value of MPE (%)	Minimum Value of MPE (%)	Maximum Value of MPE (%)
Fructose	9.3217	3.8830	15.4984
Glycolaldehyde	1.1478	0.8153	1.2982
Formic acid	4.0839	3.8915	4.4686
Furfural	2.3565	0.5180	4.6435

***Table 90**: Simulated Area Values for Identified Species in HPLC Signals in the Glucose-300 Scenario at the reaction time of 90 min.*

Component	Mean Area Value	Minimum Area Value	Maximum Area Value
Glucose	42.4824	41.0840	43.1824
Fructose	168.4048	164.3292	175.9065
Succinic acid	597.4778	596.3542	597.9135
Glycolaldehyde	905.3609	884.4129	920.2292
Furfural	478.9439	461.1338	488.5879

***Table 91**: Simulated MPE Values for Identified Species in HPLC Signals in the Glucose-300 Scenario at the reaction time of 90 min.*

Component	Mean Value of MPE (%)	Minimum Value of MPE (%)	Maximum Value of MPE (%)
Glucose	3.4549	3.2236	3.5992
Fructose	14.2852	9.9366	18.8794
Succinic acid	2.9192	2.8677	2.9392
Glycolaldehyde	1.7998	1.6514	1.9212
Furfural	5.2988	1.7258	7.8714

***Table 92**: Simulated Area Values for Identified Species in HPLC Signals in the Glucose-300 Scenario at the reaction time of 100 min.*

Component	Mean Area Value	Minimum Area Value	Maximum Area Value
Glucose	159.6149	157.8752	161.9179
Fructose	114.1283	94.9849	137.8607
Succinic acid	496.5750	493.6933	498.2461
Glycolaldehyde	666.4625	654.9639	676.6167

***Table 93**: Simulated MPE Values for Identified Species in HPLC Signals in the Glucose-300 Scenario at the reaction time of 100 min.*

Component	Mean Value of MPE (%)	Minimum Value of MPE (%)	Maximum Value of MPE (%)
Glucose	0.7284	0.0221	1.7721
Fructose	22.8655	13.8606	30.8041
Succinic acid	4.8667	4.7931	4.9325
Glycolaldehyde	2.7312	2.6486	2.8866

***Table 94**: Simulated Area Values for Identified Species in HPLC Signals in the Glucose-300 Scenario at the reaction time of 110 min.*

Component	Mean Area Value	Minimum Area Value	Maximum Area Value
Glucose	163.0756	160.4188	166.4616
Fructose	171.0961	124.3435	266.0052
Succinic acid	680.2522	673.1057	686.3095
Glycolaldehyde	834.2131	822.1665	843.5375

***Table 95**: Simulated MPE Values for Identified Species in HPLC Signals in the Glucose-300 Scenario at the reaction time of 110 min.*

Component	Mean Value of MPE (%)	Minimum Value of MPE (%)	Maximum Value of MPE (%)
Glucose	3.4129	0.1402	8.8224
Fructose	23.8517	13.8513	35.4793
Succinic acid	4.0009	3.8893	4.0849
Glycolaldehyde	2.5429	2.5018	2.5851

***Table 96**: Simulated Area Values for Identified Species in HPLC Signals in the Glucose-300 Scenario at the reaction time of 120 min.*

Component	Mean Area Value	Minimum Area Value	Maximum Area Value
Glucose	80.6292	79.0056	82.3684
Fructose	55.7476	47.1013	67.3566
Succinic acid	273.9020	272.2974	277.2289
Glycolaldehyde	372.0847	363.6968	377.8085

***Table 97**: Simulated MPE Values for Identified Species in HPLC Signals in the Glucose-300 Scenario at the reaction time of 120 min.*

Component	Mean Value of MPE (%)	Minimum Value of MPE (%)	Maximum Value of MPE (%)
Glucose	1.4062	0.4300	2.1230
Fructose	23.7406	14.4264	31.8858
Succinic acid	10.0265	9.8958	10.2974
Glycolaldehyde	1.5304	1.3469	1.6379

***Table 98**: Simulated Area Values for Identified Species in HPLC Signals in the Glucose-300 Scenario at the reaction time of 130 min.*

Component	Mean Area Value	Minimum Area Value	Maximum Area Value
Glucose	47.1063	45.1757	48.2866
Succinic acid	107.0620	104.7808	109.8879
Glycolaldehyde	231.2271	228.1598	232.4397

***Table 99**: Simulated MPE Values for Identified Species in HPLC Signals in the Glucose-300 Scenario at the reaction time of 130 min.*

Component	Mean Value of MPE (%)	Minimum Value of MPE (%)	Maximum Value of MPE (%)
Glucose	3.3846	1.1372	5.0115
Succinic acid	16.1425	12.0348	20.5508
Glycolaldehyde	0.9931	0.4415	1.1968

***Table 100**: Simulation Results of Area under the HPLC Curve in Deconvoluted HPLC Signals of Levulinic Acid and Acetic Acid in the Glucose-300 Scenario.*

Reaction Time (min)	Simulated Mean Value Area under the HPLC Curve of Levulinic Acid	Simulated Minimum Value Area under the HPLC Curve of Levulinic Acid	Simulated Maximum Value Area under the HPLC Curve of Levulinic Acid	Simulated Mean Value Area under the HPLC Curve of Acetic Acid	Simulated Minimum Value Area under the HPLC Curve of Acetic Acid	Simulated Maximum Value Area under the HPLC Curve of Acetic Acid
40.00	4680.8738	4666.5368	4695.2108	1179.6350	1151.0734	1208.1966
60.00	4778.4545	4761.2550	4795.6537	1145.9030	1073.1845	1218.6217
80.00	5915.0567	5839.8771	5991.7411	1242.4543	1120.4293	1322.3119
90.00	6200.8581	6166.2736	6252.1093	1346.4475	1261.8657	1414.6368
100.00	4801.3409	4763.7633	4844.2307	1046.4409	990.4549	1113.2830
110.00	6554.6252	6554.6252	6554.6253	1381.3823	1381.3823	1381.3823
120.00	2970.1469	2963.7787	2977.6552	1415.4101	1412.0911	1419.4796
130.00	2105.2885	2075.4755	2122.0185	1521.2939	1486.8522	1583.1399

***Table 101**: Comparison of Mean Percent Error Values Using EMG Model Between Superposition of Levulinic Acid Together with Acetic Acid and the Scenario of Only Levulinic Acid in the Glucose-300 Scenario.*

Reaction Time (min)	Curve Fitting Using Superposition of Levulinic Acid and Acetic Acid HPLC Signals			Curve Fitting Using Levulinic Acid HPLC Signals Only		
	Minimum Mean Percent Error (%)	Minimum Mean Percent Error (%)	Maximum Mean Percent Error (%)	Minimum Mean Percent Error (%)	Minimum Mean Percent Error (%)	Maximum Mean Percent Error (%)
40.00	0.3597	0.0226	1.5820	2.0529	0.0591	5.3747
60.00	1.4040	0.0026	7.8119	5.5214	0.0354	19.5759
80.00	0.8034	0.0033	6.3826	4.2731	0.0273	14.5317
90.00	0.6532	0.0032	5.8698	4.7067	0.0346	15.8526
100.00	0.4018	0.0031	1.8532	4.6026	0.0343	15.8365
110.00	0.8040	0.0041	3.2838	4.5709	0.0298	15.5239
120.00	0.4945	0.0034	3.8520	9.7125	0.2107	23.0406
130.00	0.0854	0.0165	0.1417	2.8435	2.7910	2.9625

***Table 102**: Observed and Expected Peak Features of the Peaks of Lactic Acid HPLC Signals in the Glucose-300 Scenario.*

Reaction Time (min)	Retention Time of the First Peak (min)	First Peak Value in HPLC Signals	Expected Second Peak Value in HPLC Signals	Expected Major Peak Value in HPLC Signals	Expected Concentration of Lactic Acid (mM)
40.00	11.183	7757	21474	169818	238.86
60.00	11.192	7373	19960	157848	222.02
80.00	10.883	3763	7579	59936	84.30
90.00	10.883	3596	7100	56144	78.97
100.00	11.400	1221	1499	11856	16.68
110.00	10.883	3177	5940	46973	66.07
120.00	10.867	1087	1268	10029	14.11
130.00	11.350	257	159	1258	1.77

***Table 103**: Comparison between the Observed and Expected Peak Parameters at the Peaks of Lactic Acid HPLC Signals in the Glucose-300 Scenario.*

Reaction Time (min)	Retention Time of the Second Peak (min)	Observed Second Peak Value in HPLC Signals	Expected Concentration of Lactic Acid (mM)	Retention Time of the Major Peak Value in HPLC Signals	Observed Major Peak Value in HPLC Signals	Expected Concentration of Lactic Acid (mM)
40.00	12.242	6090	67.74	12.750	5287	7.44
60.00	12.242	5594	62.22	12.742	4713	6.63
80.00	12.242	6140	68.30	12.742	2020	2.84
90.00	12.242	6409	71.29	12.742	2164	3.04
100.00	12.242	4912	54.64	12.742	1585	2.23
110.00	12.250	6607	73.49	12.750	1997	2.81
120.00	12.233	2701	30.04	12.742	900	1.27
130.00	12.242	1425	15.85	12.742	577	0.81

Appendix D: HPLC Signal Modeling Results in Levulinic-300 Scenario

***Table 104**: Simulated Area Values for Levulinic Acid in HPLC Signals in the Levulinic-300 Scenario.*

Reaction Time (min)	Mean Area Value	Minimum Area Value	Maximum Area Value
15.16	154199.4207	153390.3542	155876.5428
37.50	153485.4729	152673.2084	155083.6681
42.80	153492.7334	152727.9549	154036.7877
50.00	156725.6670	155857.6010	158318.5033
60.00	161001.4500	159782.3358	163811.5258
70.00	163415.0200	162486.0691	165397.1931
80.00	171347.1014	169558.3812	175597.8246

***Table 105**: Simulated MPE Values for Identified Species in HPLC Signals in the Levulinic-300 Scenario.*

Reaction Time (min)	Mean Value of MPE (%)	Minimum Value of MPE (%)	Maximum Value of MPE (%)
15.16	0.9919	0.5396	1.5127
37.50	0.9733	0.5305	1.4932
42.80	0.8674	0.4702	1.3938
50.00	1.0214	0.5489	1.5895
60.00	1.1455	0.6128	1.7473
70.00	1.1004	0.6055	1.6931
80.00	1.2964	0.6800	1.9649

Appendix E: Involved Chemical Reactions in the Reaction Pathway Schemes

***Table 106**: Summary of Reaction Kinetic Parameters Used in the Reaction Modeling in All Cases for the Hydrothermal Liquefaction Experimental Data.*

Reaction rate constant	Involved Chemical Reaction	Reference Reactant as Basis
$k_{G_4,G_3G_{11}}$	$G_4 \rightarrow G_3 + G_{11}$	G_4
$k_{G_4,G_2 2G_{11}}$	$G_4 \rightarrow G_2 + 2 \cdot G_{11}$	G_4
$k_{G_4,UDP}$	$G_4 \rightarrow UDP$	G_4
$k_{G_4,2G_2}$	$G_4 \rightarrow 2 \cdot G_2$	G_4
$k_{G_3G_{11},G_4}$	$G_3 + G_{11} \rightarrow G_4$	G_3
$k_{G_2 2G_{11},G_4}$	$G_2 + 2 \cdot G_{11} \rightarrow G_4$	G_2
k_{2G_2,G_4}	$2 \cdot G_2 \rightarrow G_4$	G_2
$k_{G_3,3G_{11}}$	$G_3 \rightarrow 3 \cdot G_{11}$	G_3
$k_{G_3,G_2G_{11}}$	$G_3 \rightarrow G_2 + G_{11}$	G_3
$k_{G_3,UDP}$	$G_3 \rightarrow UDP$	G_3
$k_{G_2G_{11},G_3}$	$G_2 + G_{11} \rightarrow G_3$	G_2
k_{3G_{11},G_3}	$3 \cdot G_{11} \rightarrow G_3$	G_{11}
k_{2G_{11},G_2}	$2 \cdot G_{11} \rightarrow G_2$	G_{11}
$k_{G_{12},G_{11}}$	$G_{12} \rightarrow G_{11}$	G_{12}

$k_{G_2,2G_{11}}$	$G_2 \rightarrow 2 \cdot G_{11}$	G_2
$k_{G_{11},ErGA}$	$G_{11} \rightarrow Er + GA$	G_{11}
$k_{G_{11},FA}$	$G_{11} \rightarrow FA + UDP$	G_{11}
$k_{G_{11},AA}$	$G_{11} \rightarrow AA + UDP$	G_{11}
$k_{G_{11},SA}$	$G_{11} \rightarrow SA + UDP$	G_{11}
$k_{G_{11},G_{12}}$	$G_{11} \rightarrow G_{12}$	G_{11}
$k_{G_{11},UDP}$	$G_{11} \rightarrow UDP$	G_{11}
$k_{G_{12},ErGA}$	$G_{12} \rightarrow Er + GA$	G_{12}
$k_{G_{12},FA}$	$G_{12} \rightarrow FA + UDP$	G_{12}
$k_{G_{12},AA}$	$G_{12} \rightarrow AA + UDP$	G_{12}
$k_{G_{12},HMF}$	$G_{12} \rightarrow HMF + 3 \cdot Water$	G_{12}
$k_{G_{12},UDP}$	$G_{12} \rightarrow UDP$	G_{12}
$k_{HMF,G_{12}}$	$HMF + 3 \cdot Water \rightarrow G_{12}$	HMF
$k_{GA,UDP}$	$GA \rightarrow UDP$	GA
$k_{SA,UDP}$	$SA \rightarrow UDP$	SA
$k_{LA,SA}$	$LA \rightarrow SA + UDP$	LA
$k_{LA,UDP}$	$LA \rightarrow UDP$	LA
$k_{HMF,LAFA}$	$HMF + 2 \cdot Water \rightarrow LA + FA$	HMF

$k_{LAFA,HMF}$	$LA + FA \rightarrow HMF + 2 \cdot Water$	LA
$k_{HMF,Fu}$	$HMF \rightarrow Fu + Fa$	HMF
$k_{HMF,UDP}$	$HMF \rightarrow UDP$	HMF
$k_{Fu,UDP}$	$Fu \rightarrow UDP$	Fu
$k_{FA,UDP}$	$FA \rightarrow UDP$	FA
k_{G_4,G_3G_1}	$G_4 \rightarrow G_3 + G_1$	G_4
$k_{G_4,G_2 2G_1}$	$G_4 \rightarrow G_2 + 2 \cdot G_1$	G_4
$k_{G_3G_1,G_4}$	$G_3 + G_1 \rightarrow G_4$	G_3
$k_{G_2 2G_1,G_4}$	$G_2 + 2 \cdot G_1 \rightarrow G_4$	G_2
$k_{G_3,3G_1}$	$G_3 \rightarrow 3 \cdot G_1$	G_3
k_{G_3,G_2G_1}	$G_3 \rightarrow G_2 + G_1$	G_3
$k_{G_2G_1,G_3}$	$G_2 + G_1 \rightarrow G_3$	G_2
k_{3G_1,G_3}	$3 \cdot G_1 \rightarrow G_3$	G_1
$k_{G_2,2G_1}$	$G_2 \rightarrow 2 \cdot G_1$	G_2
k_{2G_1,G_2}	$2 \cdot G_1 \rightarrow G_2$	G_1
$k_{G_1,ErGA}$	$G_1 \rightarrow Er + GA$	G_1
$k_{G_1,FA}$	$G_1 \rightarrow FA + UDP$	G_1

$k_{G_1,AA}$	$G_1 \rightarrow AA + UDP$	G_1
$k_{G_1,HMF}$	$G_1 \rightarrow HMF + 3 \cdot Water$	G_1
$k_{G_1,UDP}$	$G_1 \rightarrow UDP$	G_1
k_{HMF,G_1}	$HMF + 3 \cdot Water \rightarrow G_1$	HMF
$k_{AA,UDP}$	$AA \rightarrow UDP$	AA
$k_{G_1,SA}$	$G_1 \rightarrow SA + UDP$	G_1

Base Scenario

Case 1.1:

Cellulose-300

Cellotetraose:

$$\frac{\partial G_4}{\partial t} = -\left(k_{G_4,G_3G_{11}} + k_{G_4,G_22G_{11}} + k_{G_4,UDP}\right) \cdot G_4$$

Cellotriose:

$$\frac{\partial G_3}{\partial t} = k_{G_4,G_3G_{11}} \cdot G_4 - \left(k_{G_3,3G_{11}} + k_{G_3,G_2G_{11}} + k_{G_3,UDP}\right) \cdot G_3$$

Cellobiose:

$$\frac{\partial G_2}{\partial t} = k_{G_4,G_22G_{11}} \cdot G_4 + k_{G_3,G_2G_{11}} \cdot G_3 - \left(k_{G_2,2G_{11}} + k_{G_2,UDP}\right) \cdot G_2$$

Glucose:

$$\frac{\partial G_{11}}{\partial t} = \left(k_{G_4,G_3G_{11}} + 2 \cdot k_{G_4,G_22G_{11}}\right) \cdot G_4 + \left(k_{G_3,G_2G_{11}} + 3 \cdot k_{G_3,3G_{11}}\right) \cdot G_3 + 2 \cdot k_{G_2,2G_{11}} \cdot G_2 + k_{G_{12},G_{11}} \cdot G_{12} - \left(k_{G_{11},ErGA} + k_{G_{11},FA} + k_{G_{11},AA} + k_{G_{11},SA} + k_{G_{11},G_{12}} + k_{G_{11},UDP}\right) \cdot G_{11}$$

Fructose:

$$\frac{\partial G_{12}}{\partial t} = k_{G_{11},G_{12}} \cdot G_{11} - \left(k_{G_{12},ErGA} + k_{G_{12},FA} + k_{G_{12},AA} + k_{G_{12},G_{11}} + k_{G_{12},HMF} + k_{G_{12},UDP}\right) \cdot G_{12}$$

Glycolaldehyde:

$$\frac{\partial GA}{\partial t} = -k_{GA,UDP} \cdot GA + k_{G_{11},ErGA} \cdot G_{11} + k_{G_{12},ErGA} \cdot G_{12}$$

Succinic acid:

$$\frac{\partial SA}{\partial t} = -k_{SA,UDP} \cdot SA + k_{G_{11},SA} \cdot G_{11} + k_{LA,SA} \cdot LA$$

Levulinic acid:

$$\frac{\partial LA}{\partial t} = -(k_{LA,SA} + k_{LA,UDP}) \cdot LA + k_{HMF,LAFA} \cdot HMF$$

HMF:

$$\frac{\partial HMF}{\partial t} = -(k_{HMF,LAFA} + k_{HMF,Fu} + k_{HMF,UDP}) \cdot HMF + k_{G_{12},HMF} \cdot G_{12}$$

Furfural:

$$\frac{\partial Fu}{\partial t} = k_{HMF,Fu} \cdot HMF - k_{Fu,UDP} \cdot Fu$$

Formic acid:

$$\frac{\partial FA}{\partial t} = -k_{FA,UDP} \cdot FA + k_{G_{11},FA} \cdot G_{11} + k_{G_{12},FA} \cdot G_{12} + k_{HMF,LAFA} \cdot HMF$$

Acetic acid:

$$\frac{\partial AA}{\partial t} = -k_{AA,UDP} \cdot AA + k_{G_{11},AA} \cdot G_{11} + k_{G_{12},AA} \cdot G_{12}$$

Glucose 275:

Cellotetraose:

$$\frac{\partial G_4}{\partial t} = -\left(k_{G_4,G_3G_{11}} + k_{G_4,G_22G_{11}} + k_{G_4,UDP}\right) \cdot G_4$$

Cellotriose:

$$\frac{\partial G_3}{\partial t} = k_{G_4,G_3G_{11}} \cdot G_4 - \left(k_{G_3,3G_{11}} + k_{G_3,G_2G_{11}} + k_{G_3,UDP}\right) \cdot G_3$$

Cellobiose:

$$\frac{\partial G_2}{\partial t} = k_{G_4,G_22G_{11}} \cdot G_4 + k_{G_3,G_2G_{11}} \cdot G_3 - \left(k_{G_2,2G_{11}} + k_{G_2,UDP}\right) \cdot G_2$$

Glucose:

$$\frac{\partial G_{11}}{\partial t} = \left(k_{G_4,G_3G_{11}} + 2 \cdot k_{G_4,G_2 2G_{11}}\right) \cdot G_4 + \left(k_{G_3,G_2G_{11}} + 3 \cdot k_{G_3,3G_{11}}\right) \cdot G_3 + 2 \cdot k_{G_2,2G_{11}} \cdot G_2 + k_{G_{12},G_{11}} \cdot G_{12} - \left(k_{G_{11},ErGA} + k_{G_{11},FA} + k_{G_{11},AA} + k_{G_{11},G_{12}} + k_{G_{11},UDP}\right) \cdot G_{11}$$

Fructose:

$$\frac{\partial G_{12}}{\partial t} = k_{G_{11},G_{12}} \cdot G_{11} - \left(k_{G_{12},ErGA} + k_{G_{12},FA} + k_{G_{12},AA} + k_{G_{12},G_{11}} + k_{G_{12},HMF} + k_{G_{12},UDP}\right) \cdot G_{12}$$

Glycolaldehyde:

$$\frac{\partial GA}{\partial t} = -k_{GA,UDP} \cdot GA + k_{G_{11},ErGA} \cdot G_{11} + k_{G_{12},ErGA} \cdot G_{12}$$

Levulinic acid:

$$\frac{\partial LA}{\partial t} = -k_{LA,UDP} \cdot LA + k_{HMF,LAFA} \cdot HMF$$

HMF:

$$\frac{\partial HMF}{\partial t} = -(k_{HMF,LAFA} + k_{HMF,Fu} + k_{HMF,UDP}) \cdot HMF + k_{G_{12},HMF} \cdot G_{12}$$

Furfural:

$$\frac{\partial Fu}{\partial t} = k_{HMF,Fu} \cdot HMF - k_{Fu,UDP} \cdot Fu$$

Formic acid:

$$\frac{\partial FA}{\partial t} = -k_{FA,UDP} \cdot FA + k_{G_{11},FA} \cdot G_{11} + k_{G_{12},FA} \cdot G_{12} + k_{HMF,LAFA} \cdot HMF$$

Acetic acid:

$$\frac{\partial AA}{\partial t} = -k_{AA,UDP} \cdot AA + k_{G_{11},AA} \cdot G_{11} + k_{G_{12},AA} \cdot G_{12}$$

Glucose-300:

Cellotriose:

$$\frac{\partial G_3}{\partial t} = -\left(k_{G_3,3G_{11}} + k_{G_3,G_2G_{11}} + k_{G_3,UDP}\right) \cdot G_3$$

Cellobiose:

$$\frac{\partial G_2}{\partial t} = k_{G_3,G_2G_{11}} \cdot G_3 - \left(k_{G_2,2G_{11}} + k_{G_2,UDP}\right) \cdot G_2$$

Glucose:

$$\frac{\partial G_{11}}{\partial t} = \left(k_{G_3,G_2G_{11}} + 3 \cdot k_{G_3,3G_{11}}\right) \cdot G_3 + 2 \cdot k_{G_2,2G_{11}} \cdot G_2 + k_{G_{12},G_{11}} \cdot G_{12} - \left(k_{G_{11},ErGA} + k_{G_{11},FA} + k_{G_{11},AA} + k_{G_{11},SA} + k_{G_{11},G_{12}} + k_{G_{11},UDP}\right) \cdot G_{11}$$

Fructose:

$$\frac{\partial G_{12}}{\partial t} = k_{G_{11},G_{12}} \cdot G_{11} - \left(k_{G_{12},ErGA} + k_{G_{12},FA} + k_{G_{12},AA} + k_{G_{12},G_{11}} + k_{G_{12},HMF} + k_{G_{12},UDP}\right) \cdot G_{12}$$

Glycolaldehyde:

$$\frac{\partial GA}{\partial t} = -k_{GA,UDP} \cdot GA + k_{G_{11},ErGA} \cdot G_{11} + k_{G_{12},ErGA} \cdot G_{12}$$

Succinic acid:

$$\frac{\partial SA}{\partial t} = -k_{SA,UDP} \cdot SA + k_{G_{11},SA} \cdot G_{11} + k_{LA,SA} \cdot LA$$

Levulinic acid:

$$\frac{\partial LA}{\partial t} = -(k_{LA,SA} + k_{LA,UDP}) \cdot LA + k_{HMF,LAFA} \cdot HMF$$

HMF:

$$\frac{\partial HMF}{\partial t} = -(k_{HMF,LAFA} + k_{HMF,Fu} + k_{HMF,UDP}) \cdot HMF + k_{G_{12},HMF} \cdot G_{12}$$

Furfural:

$$\frac{\partial Fu}{\partial t} = k_{HMF,Fu} \cdot HMF - k_{Fu,UDP} \cdot Fu$$

Formic acid:

$$\frac{\partial FA}{\partial t} = -k_{FA,UDP} \cdot FA + k_{G_{11},FA} \cdot G_{11} + k_{G_{12},FA} \cdot G_{12} + k_{HMF,LAFA} \cdot HMF$$

Acetic acid:

$$\frac{\partial AA}{\partial t} = -k_{AA,UDP} \cdot AA + k_{G_{11},AA} \cdot G_{11} + k_{G_{12},AA} \cdot G_{12}$$

Case 2.1:

Cellulose-300

Cellotetraose:

$$\frac{\partial G_4}{\partial t} = -\left(k_{G_4,G_3G_{11}} + k_{G_4,G_22G_{11}} + k_{G_4,2G_2} + k_{G_4,UDP}\right) \cdot G_4$$

Cellotriose:

$$\frac{\partial G_3}{\partial t} = k_{G_4,G_3G_{11}} \cdot G_4 - \left(k_{G_3,3G_{11}} + k_{G_3,G_2G_{11}} + k_{G_3,UDP}\right) \cdot G_3$$

Cellobiose:

$$\frac{\partial G_2}{\partial t} = \left(k_{G_4,G_22G_{11}} + 2 \cdot k_{G_4,2G_2}\right) \cdot G_4 + k_{G_3,G_2G_{11}} \cdot G_3 - \left(k_{G_2,2G_{11}} + k_{G_2,UDP}\right) \cdot G_2$$

Glucose:

$$\frac{\partial G_{11}}{\partial t} = \left(k_{G_4,G_3G_{11}} + 2 \cdot k_{G_4,G_22G_{11}}\right) \cdot G_4 + \left(k_{G_3,G_2G_{11}} + 3 \cdot k_{G_3,3G_{11}}\right) \cdot G_3 + 2 \cdot k_{G_2,2G_{11}} \cdot G_2 + k_{G_{12},G_{11}} \cdot G_{12} - \left(k_{G_{11},ErGA} + k_{G_{11},FA} + k_{G_{11},AA} + k_{G_{11},SA} + k_{G_{11},G_{12}} + k_{G_{11},UDP}\right) \cdot G_{11}$$

Fructose:

$$\frac{\partial G_{12}}{\partial t} = k_{G_{11},G_{12}} \cdot G_{11} - \left(k_{G_{12},ErGA} + k_{G_{12},FA} + k_{G_{12},AA} + k_{G_{12},G_{11}} + k_{G_{12},HMF} + k_{G_{12},UDP}\right) \cdot G_{12}$$

Glycolaldehyde:

$$\frac{\partial GA}{\partial t} = -k_{GA,UDP} \cdot GA + k_{G_{11},ErGA} \cdot G_{11} + k_{G_{12},ErGA} \cdot G_{12}$$

Succinic acid:

$$\frac{\partial SA}{\partial t} = -k_{SA,UDP} \cdot SA + k_{G_{11},SA} \cdot G_{11} + k_{LA,SA} \cdot LA$$

Levulinic acid:

$$\frac{\partial LA}{\partial t} = -(k_{LA,SA} + k_{LA,UDP}) \cdot LA + k_{HMF,LAFA} \cdot HMF$$

HMF:

$$\frac{\partial HMF}{\partial t} = -(k_{HMF,LAFA} + k_{HMF,Fu} + k_{HMF,UDP}) \cdot HMF + k_{G_{12},HMF} \cdot G_{12}$$

Furfural:

$$\frac{\partial Fu}{\partial t} = k_{HMF,Fu} \cdot HMF - k_{Fu,UDP} \cdot Fu$$

Formic acid:

$$\frac{\partial FA}{\partial t} = -k_{FA,UDP} \cdot FA + k_{G_{11},FA} \cdot G_{11} + k_{G_{12},FA} \cdot G_{12} + k_{HMF,LAFA} \cdot HMF$$

Acetic acid:

$$\frac{\partial AA}{\partial t} = -k_{AA,UDP} \cdot AA + k_{G_{11},AA} \cdot G_{11} + k_{G_{12},AA} \cdot G_{12}$$

Glucose 275:

Cellotetraose:

$$\frac{\partial G_4}{\partial t} = -\left(k_{G_4,G_3G_{11}} + k_{G_4,G_22G_{11}} + k_{G_4,2G_2} + k_{G_4,UDP}\right) \cdot G_4$$

Cellotriose:

$$\frac{\partial G_3}{\partial t} = k_{G_4,G_3G_{11}} \cdot G_4 - \left(k_{G_3,3G_{11}} + k_{G_3,G_2G_{11}} + k_{G_3,UDP}\right) \cdot G_3$$

Cellobiose:

$$\frac{\partial G_2}{\partial t} = \left(k_{G_4,G_2 2G_{11}} + 2 \cdot k_{G_4,2G_2}\right) \cdot G_4 + k_{G_3,G_2G_{11}} \cdot G_3 - \left(k_{G_2,2G_{11}} + k_{G_2,UDP}\right) \cdot G_2$$

Glucose:

$$\frac{\partial G_{11}}{\partial t} = \left(k_{G_4,G_3G_{11}} + 2 \cdot k_{G_4,G_2 2G_{11}}\right) \cdot G_4 + \left(k_{G_3,G_2G_{11}} + 3 \cdot k_{G_3,3G_{11}}\right) \cdot G_3 + 2 \cdot k_{G_2,2G_{11}} \cdot G_2 + k_{G_{12},G_{11}} \cdot G_{12} - \left(k_{G_{11},ErGA} + k_{G_{11},FA} + k_{G_{11},AA} + k_{G_{11},G_{12}} + k_{G_{11},UDP}\right) \cdot G_{11}$$

Fructose:

$$\frac{\partial G_{12}}{\partial t} = k_{G_{11},G_{12}} \cdot G_{11} - \left(k_{G_{12},ErGA} + k_{G_{12},FA} + k_{G_{12},AA} + k_{G_{12},G_{11}} + k_{G_{12},HMF} + k_{G_{12},UDP}\right) \cdot G_{12}$$

Glycolaldehyde:

$$\frac{\partial GA}{\partial t} = -k_{GA,UDP} \cdot GA + k_{G_{11},ErGA} \cdot G_{11} + k_{G_{12},ErGA} \cdot G_{12}$$

Levulinic acid:

$$\frac{\partial LA}{\partial t} = -k_{LA,UDP} \cdot LA + k_{HMF,LAFA} \cdot HMF$$

HMF:

$$\frac{\partial HMF}{\partial t} = -\left(k_{HMF,LAFA} + k_{HMF,Fu} + k_{HMF,UDP}\right) \cdot HMF + k_{G_{12},HMF} \cdot G_{12}$$

Furfural:

$$\frac{\partial Fu}{\partial t} = k_{HMF,Fu} \cdot HMF - k_{Fu,UDP} \cdot Fu$$

Formic acid:

$$\frac{\partial FA}{\partial t} = -k_{FA,UDP} \cdot FA + k_{G_{11},FA} \cdot G_{11} + k_{G_{12},FA} \cdot G_{12} + k_{HMF,LAFA} \cdot HMF$$

Acetic acid:

$$\frac{\partial AA}{\partial t} = -k_{AA,UDP} \cdot AA + k_{G_{11},AA} \cdot G_{11} + k_{G_{12},AA} \cdot G_{12}$$

Glucose-300:

Cellotriose:

$$\frac{\partial G_3}{\partial t} = -\left(k_{G_3,3G_{11}} + k_{G_3,G_2G_{11}} + k_{G_3,UDP}\right) \cdot G_3$$

Cellobiose:

$$\frac{\partial G_2}{\partial t} = k_{G_3,G_2G_{11}} \cdot G_3 - \left(k_{G_2,2G_{11}} + k_{G_2,UDP}\right) \cdot G_2$$

Glucose:

$$\frac{\partial G_{11}}{\partial t} = \left(k_{G_3,G_2G_{11}} + 3 \cdot k_{G_3,3G_{11}}\right) \cdot G_3 + 2 \cdot k_{G_2,2G_{11}} \cdot G_2 + k_{G_{12},G_{11}} \cdot G_{12} - \left(k_{G_{11},ErGA} + k_{G_{11},FA} + k_{G_{11},AA} + k_{G_{11},SA} + k_{G_{11},G_{12}} + k_{G_{11},UDP}\right) \cdot G_{11}$$

Fructose:

$$\frac{\partial G_{12}}{\partial t} = k_{G_{11},G_{12}} \cdot G_{11} - \left(k_{G_{12},ErGA} + k_{G_{12},FA} + k_{G_{12},AA} + k_{G_{12},G_{11}} + k_{G_{12},HMF} + k_{G_{12},UDP}\right) \cdot G_{12}$$

Glycolaldehyde:

$$\frac{\partial GA}{\partial t} = -k_{GA,UDP} \cdot GA + k_{G_{11},ErGA} \cdot G_{11} + k_{G_{12},ErGA} \cdot G_{12}$$

Succinic acid:

$$\frac{\partial SA}{\partial t} = -k_{SA,UDP} \cdot SA + k_{G_{11},SA} \cdot G_{11} + k_{LA,SA} \cdot LA$$

Levulinic acid:

$$\frac{\partial LA}{\partial t} = -(k_{LA,SA} + k_{LA,UDP}) \cdot LA + k_{HMF,LAFA} \cdot HMF$$

HMF:

$$\frac{\partial HMF}{\partial t} = -(k_{HMF,LAFA} + k_{HMF,Fu} + k_{HMF,UDP}) \cdot HMF + k_{G_{12},HMF} \cdot G_{12}$$

Furfural:

$$\frac{\partial Fu}{\partial t} = k_{HMF,Fu} \cdot HMF - k_{Fu,UDP} \cdot Fu$$

Formic acid:

$$\frac{\partial FA}{\partial t} = -k_{FA,UDP} \cdot FA + k_{G_{11},FA} \cdot G_{11} + k_{G_{12},FA} \cdot G_{12} + k_{HMF,LAFA} \cdot HMF$$

Acetic acid:

$$\frac{\partial AA}{\partial t} = -k_{AA,UDP} \cdot AA + k_{G_{11},AA} \cdot G_{11} + k_{G_{12},AA} \cdot G_{12}$$

Case 1.2:

Cellulose-300

Cellotetraose:

$$\frac{\partial G_4}{\partial t} = -\left(k_{G_4,G_3G_1} + k_{G_4,G_22G_1} + k_{G_4,UDP}\right) \cdot G_4$$

Cellotriose:

$$\frac{\partial G_3}{\partial t} = k_{G_4,G_3G_1} \cdot G_4 - \left(k_{G_3,3G_1} + k_{G_3,G_2G_1} + k_{G_3,UDP}\right) \cdot G_3$$

Cellobiose:

$$\frac{\partial G_2}{\partial t} = k_{G_4,G_22G_1} \cdot G_4 + k_{G_3,G_2G_1} \cdot G_3 - \left(k_{G_2,2G_1} + k_{G_2,UDP}\right) \cdot G_2$$

Cellulo-monomers:

$$\frac{\partial G_1}{\partial t} = \left(k_{G_4,G_3G_1} + 2 \cdot k_{G_4,G_2 2G_1}\right) \cdot G_4 + \left(k_{G_3,G_2G_1} + 3 \cdot k_{G_3,3G_1}\right) \cdot G_3 + 2 \cdot k_{G_2,2G_1} \cdot G_2 - \left(k_{G_1,ErGA} + k_{G_1,FA} + k_{G_1,AA} + k_{G_1,SA} + k_{G_1,HMF} + k_{G_1,UDP}\right) \cdot G_1$$

Glycolaldehyde:

$$\frac{\partial GA}{\partial t} = -k_{GA,UDP} \cdot GA + k_{G_1,ErGA} \cdot G_1$$

Succinic acid:

$$\frac{\partial SA}{\partial t} = -k_{SA,UDP} \cdot SA + k_{G_1,SA} \cdot G_1 + k_{LA,SA} \cdot LA$$

Levulinic acid:

$$\frac{\partial LA}{\partial t} = -(k_{LA,SA} + k_{LA,UDP}) \cdot LA + k_{HMF,LAFA} \cdot HMF$$

HMF:

$$\frac{\partial HMF}{\partial t} = -(k_{HMF,LAFA} + k_{HMF,Fu} + k_{HMF,UDP}) \cdot HMF + k_{G_1,HMF} \cdot G_1$$

Furfural:

$$\frac{\partial Fu}{\partial t} = k_{HMF,Fu} \cdot HMF - k_{Fu,UDP} \cdot Fu$$

Formic acid:

$$\frac{\partial FA}{\partial t} = -k_{FA,UDP} \cdot FA + k_{G_1,FA} \cdot G_1 + k_{HMF,LAFA} \cdot HMF$$

Acetic acid:

$$\frac{\partial AA}{\partial t} = -k_{AA,UDP} \cdot AA + k_{G_1,AA} \cdot G_1$$

Glucose 275:

Cellotetraose:

$$\frac{\partial G_4}{\partial t} = -\left(k_{G_4,G_3G_1} + k_{G_4,G_22G_1} + k_{G_4,UDP}\right) \cdot G_4$$

Cellotriose:

$$\frac{\partial G_3}{\partial t} = k_{G_4,G_3G_1} \cdot G_4 - \left(k_{G_3,3G_1} + k_{G_3,G_2G_1} + k_{G_3,UDP}\right) \cdot G_3$$

Cellobiose:

$$\frac{\partial G_2}{\partial t} = k_{G_4,G_22G_1} \cdot G_4 + k_{G_3,G_2G_1} \cdot G_3 - \left(k_{G_2,2G_1} + k_{G_2,UDP}\right) \cdot G_2$$

Cellulo-monomers:

$$\frac{\partial G_1}{\partial t} = \left(k_{G_4,G_3G_1} + 2 \cdot k_{G_4,G_22G_1}\right) \cdot G_4 + \left(k_{G_3,G_2G_1} + 3 \cdot k_{G_3,3G_1}\right) \cdot G_3 + 2 \cdot k_{G_2,2G_1} \cdot G_2 - \left(k_{G_1,ErGA} + k_{G_1,FA} + k_{G_1,AA} + k_{G_1,HMF} + k_{G_1,UDP}\right) \cdot G_1$$

Glycolaldehyde:

$$\frac{\partial GA}{\partial t} = -k_{GA,UDP} \cdot GA + k_{G_1,ErGA} \cdot G_1$$

Levulinic acid:

$$\frac{\partial LA}{\partial t} = -k_{LA,UDP} \cdot LA + k_{HMF,LAFA} \cdot HMF$$

HMF:

$$\frac{\partial HMF}{\partial t} = -(k_{HMF,LAFA} + k_{HMF,Fu} + k_{HMF,UDP}) \cdot HMF + k_{G_1,HMF} \cdot G_1$$

Furfural:

$$\frac{\partial Fu}{\partial t} = k_{HMF,Fu} \cdot HMF - k_{Fu,UDP} \cdot Fu$$

Formic acid:

$$\frac{\partial FA}{\partial t} = -k_{FA,UDP} \cdot FA + k_{G_1,FA} \cdot G_1 + k_{HMF,LAFA} \cdot HMF$$

Acetic acid:

$$\frac{\partial AA}{\partial t} = -k_{AA,UDP} \cdot AA + k_{G_1,AA} \cdot G_1$$

Glucose-300:

Cellotriose:

$$\frac{\partial G_3}{\partial t} = -\left(k_{G_3,3G_1} + k_{G_3,G_2G_1} + k_{G_3,UDP}\right) \cdot G_3$$

Cellobiose:

$$\frac{\partial G_2}{\partial t} = k_{G_3,G_2G_1} \cdot G_3 - \left(k_{G_2,2G_1} + k_{G_2,UDP}\right) \cdot G_2$$

Cellulo-monomers:

$$\frac{\partial G_1}{\partial t} = \left(k_{G_3,G_2G_1} + 3 \cdot k_{G_3,3G_1}\right) \cdot G_3 + 2 \cdot k_{G_2,2G_1} \cdot G_2$$
$$- \left(k_{G_1,ErGA} + k_{G_1,FA} + k_{G_1,AA} + k_{G_1,SA} + k_{G_1,HMF} + k_{G_1,UDP}\right) \cdot G_1$$

Glycolaldehyde:

$$\frac{\partial GA}{\partial t} = -k_{GA,UDP} \cdot GA + k_{G_1,ErGA} \cdot G_1$$

Succinic acid:

$$\frac{\partial SA}{\partial t} = -k_{SA,UDP} \cdot SA + k_{G_1,SA} \cdot G_1 + k_{LA,SA} \cdot LA$$

Levulinic acid:

$$\frac{\partial LA}{\partial t} = -(k_{LA,SA} + k_{LA,UDP}) \cdot LA + k_{HMF,LAFA} \cdot HMF$$

HMF:

$$\frac{\partial HMF}{\partial t} = -(k_{HMF,LAFA} + k_{HMF,Fu} + k_{HMF,UDP}) \cdot HMF + k_{G_1,HMF} \cdot G_1$$

Furfural:

$$\frac{\partial Fu}{\partial t} = k_{HMF,Fu} \cdot HMF - k_{Fu,UDP} \cdot Fu$$

Formic acid:

$$\frac{\partial FA}{\partial t} = -k_{FA,UDP} \cdot FA + k_{G_1,FA} \cdot G_1 + k_{HMF,LAFA} \cdot HMF$$

Acetic acid:

$$\frac{\partial AA}{\partial t} = -k_{AA,UDP} \cdot AA + k_{G_1,AA} \cdot G_1$$

Case 2.2:

Cellulose-300

Cellotetraose:

$$\frac{\partial G_4}{\partial t} = -\left(k_{G_4,G_3G_1} + k_{G_4,G_22G_1} + k_{G_4,2G_2} + k_{G_4,UDP}\right) \cdot G_4$$

Cellotriose:

$$\frac{\partial G_3}{\partial t} = k_{G_4,G_3G_1} \cdot G_4 - \left(k_{G_3,3G_1} + k_{G_3,G_2G_1} + k_{G_3,UDP}\right) \cdot G_3$$

Cellobiose:

$$\frac{\partial G_2}{\partial t} = \left(k_{G_4,G_22G_1} + 2 \cdot k_{G_4,2G_2}\right) \cdot G_4 + k_{G_3,G_2G_1} \cdot G_3 - \left(k_{G_2,2G_1} + k_{G_2,UDP}\right) \cdot G_2$$

Cellulo-monomers:

$$\frac{\partial G_1}{\partial t} = \left(k_{G_4,G_3G_1} + 2 \cdot k_{G_4,G_22G_1}\right) \cdot G_4 + \left(k_{G_3,G_2G_1} + 3 \cdot k_{G_3,3G_1}\right) \cdot G_3 + 2 \cdot k_{G_2,2G_1} \cdot G_2 - \left(k_{G_1,ErGA} + k_{G_1,FA} + k_{G_1,AA} + k_{G_1,SA} + k_{G_1,HMF} + k_{G_1,UDP}\right) \cdot G_1$$

Glycolaldehyde:

$$\frac{\partial GA}{\partial t} = -k_{GA,UDP} \cdot GA + k_{G_1,ErGA} \cdot G_1$$

Succinic acid:

$$\frac{\partial SA}{\partial t} = -k_{SA,UDP} \cdot SA + k_{G_1,SA} \cdot G_1 + k_{LA,SA} \cdot LA$$

Levulinic acid:

$$\frac{\partial LA}{\partial t} = -(k_{LA,SA} + k_{LA,UDP}) \cdot LA + k_{HMF,LAFA} \cdot HMF$$

HMF:

$$\frac{\partial HMF}{\partial t} = -(k_{HMF,LAFA} + k_{HMF,Fu} + k_{HMF,UDP}) \cdot HMF + k_{G_1,HMF} \cdot G_1$$

Furfural:

$$\frac{\partial Fu}{\partial t} = k_{HMF,Fu} \cdot HMF - k_{Fu,UDP} \cdot Fu$$

Formic acid:

$$\frac{\partial FA}{\partial t} = -k_{FA,UDP} \cdot FA + k_{G_1,FA} \cdot G_1 + k_{HMF,LAFA} \cdot HMF$$

Acetic acid:

$$\frac{\partial AA}{\partial t} = -k_{AA,UDP} \cdot AA + k_{G_1,AA} \cdot G_1$$

Glucose 275:

Cellotetraose:

$$\frac{\partial G_4}{\partial t} = -\left(k_{G_4,G_3G_1} + k_{G_4,G_22G_1} + k_{G_4,2G_2} + k_{G_4,UDP}\right) \cdot G_4$$

Cellotriose:

$$\frac{\partial G_3}{\partial t} = k_{G_4,G_3G_1} \cdot G_4 - \left(k_{G_3,3G_1} + k_{G_3,G_2G_1} + k_{G_3,UDP}\right) \cdot G_3$$

Cellobiose:

$$\frac{\partial G_2}{\partial t} = (k_{G_4,G_22G_1} + 2 \cdot k_{G_4,2G_2}) \cdot G_4 + k_{G_3,G_2G_1} \cdot G_3 - \left(k_{G_2,2G_1} + k_{G_2,UDP}\right) \cdot G_2$$

Cellulo-monomers:

$$\frac{\partial G_1}{\partial t} = \left(k_{G_4,G_3G_1} + 2 \cdot k_{G_4,G_22G_1}\right) \cdot G_4 + \left(k_{G_3,G_2G_1} + 3 \cdot k_{G_3,3G_1}\right) \cdot G_3 + 2 \cdot k_{G_2,2G_1} \cdot G_2 - \left(k_{G_1,ErGA} + k_{G_1,FA} + k_{G_1,AA} + k_{G_1,HMF} + k_{G_1,UDP}\right) \cdot G_1$$

Glycolaldehyde:

$$\frac{\partial GA}{\partial t} = -k_{GA,UDP} \cdot GA + k_{G_1,ErGA} \cdot G_1$$

Levulinic acid:

$$\frac{\partial LA}{\partial t} = -k_{LA,UDP} \cdot LA + k_{HMF,LAFA} \cdot HMF$$

HMF:

$$\frac{\partial HMF}{\partial t} = -(k_{HMF,LAFA} + k_{HMF,Fu} + k_{HMF,UDP}) \cdot HMF + k_{G_1,HMF} \cdot G_1$$

Furfural:

$$\frac{\partial Fu}{\partial t} = k_{HMF,Fu} \cdot HMF - k_{Fu,UDP} \cdot Fu$$

Formic acid:

$$\frac{\partial FA}{\partial t} = -k_{FA,UDP} \cdot FA + k_{G_1,FA} \cdot G_1 + k_{HMF,LAFA} \cdot HMF$$

Acetic acid:

$$\frac{\partial AA}{\partial t} = -k_{AA,UDP} \cdot AA + k_{G_1,AA} \cdot G_1$$

Glucose-300:

Cellotriose:

$$\frac{\partial G_3}{\partial t} = -\left(k_{G_3,3G_1} + k_{G_3,G_2G_1} + k_{G_3,UDP}\right) \cdot G_3$$

Cellobiose:

$$\frac{\partial G_2}{\partial t} = k_{G_3,G_2G_1} \cdot G_3 - \left(k_{G_2,2G_1} + k_{G_2,UDP}\right) \cdot G_2$$

Cellulo-monomers:

$$\frac{\partial G_1}{\partial t} = \left(k_{G_3,G_2G_1} + 3 \cdot k_{G_3,3G_1}\right) \cdot G_3 + 2 \cdot k_{G_2,2G_1} \cdot G_2 - \left(k_{G_1,ErGA} + k_{G_1,FA} + k_{G_1,AA} + k_{G_1,SA} + k_{G_1,HMF} + k_{G_1,UDP}\right) \cdot G_1$$

Glycolaldehyde:

$$\frac{\partial GA}{\partial t} = -k_{GA,UDP} \cdot GA + k_{G_1,ErGA} \cdot G_1$$

Succinic acid:

$$\frac{\partial SA}{\partial t} = -k_{SA,UDP} \cdot SA + k_{G_1,SA} \cdot G_1 + k_{LA,SA} \cdot LA$$

Levulinic acid:

$$\frac{\partial LA}{\partial t} = -(k_{LA,SA} + k_{LA,UDP}) \cdot LA + k_{HMF,LAFA} \cdot HMF$$

HMF:

$$\frac{\partial HMF}{\partial t} = -(k_{HMF,LAFA} + k_{HMF,Fu} + k_{HMF,UDP}) \cdot HMF + k_{G_1,HMF} \cdot G_1$$

Furfural:

$$\frac{\partial Fu}{\partial t} = k_{HMF,Fu} \cdot HMF - k_{Fu,UDP} \cdot Fu$$

Formic acid:

$$\frac{\partial FA}{\partial t} = -k_{FA,UDP} \cdot FA + k_{G_1,FA} \cdot G_1 + k_{HMF,LAFA} \cdot HMF$$

Acetic acid:

$$\frac{\partial AA}{\partial t} = -k_{AA,UDP} \cdot AA + k_{G_1,AA} \cdot G_1$$

Condensation Scenario

Case 1.1:

Cellulose-300

Cellotetraose:

$$\frac{\partial G_4}{\partial t} = -\left(k_{G_4,G_3G_{11}} + k_{G_4,G_22G_{11}} + k_{G_4,UDP}\right) \cdot G_4 + k_{G_3G_{11},G_4} \cdot G_3 \cdot G_{11} + k_{G_22G_{11},G_4} \cdot G_2 \cdot G_{11}$$

Cellotriose:

$$\frac{\partial G_3}{\partial t} = k_{G_4,G_3G_{11}} \cdot G_4 - \left(k_{G_3,3G_{11}} + k_{G_3,G_2G_{11}} + k_{G_3,UDP}\right) \cdot G_3 - k_{G_3G_{11},G_4} \cdot G_3 \cdot G_{11} + k_{G_2G_{11},G_3} \cdot G_2 \cdot G_{11} + \frac{1}{3} \cdot k_{3G_{11},G_3} \cdot G_{11}$$

Cellobiose:

$$\frac{\partial G_2}{\partial t} = k_{G_4,G_22G_{11}} \cdot G_4 + k_{G_3,G_2G_{11}} \cdot G_3 - \left(k_{G_2,2G_{11}} + k_{G_2,UDP}\right) \cdot G_2 - k_{G_22G_{11},G_4} \cdot G_2 \cdot G_{11} - k_{G_2G_{11},G_3} \cdot G_2 \cdot G_{11} + \frac{1}{2} \cdot k_{2G_{11},G_2} \cdot G_{11}$$

Glucose:

$$\frac{\partial G_{11}}{\partial t} = \left(k_{G_4,G_3G_{11}} + 2 \cdot k_{G_4,G_22G_{11}}\right) \cdot G_4 + \left(k_{G_3,G_2G_{11}} + 3 \cdot k_{G_3,3G_{11}}\right) \cdot G_3 + 2 \cdot k_{G_2,2G_{11}} \cdot G_2 + k_{G_{12},G_{11}} \cdot G_{12} - \left(k_{G_{11},ErGA} + k_{G_{11},FA} + k_{G_{11},AA} + k_{G_{11},SA} + k_{G_{11},G_{12}} + k_{G_{11},UDP}\right) \cdot G_{11} - k_{G_3G_{11},G_4} \cdot G_3 \cdot G_{11} - 2 \cdot k_{G_22G_{11},G_4} \cdot G_2 \cdot G_{11} - k_{3G_{11},G_3} \cdot G_{11} - k_{G_2G_{11},G_3} \cdot G_2 \cdot G_{11} - k_{2G_{11},G_2} \cdot G_{11}$$

Fructose:

$$\frac{\partial G_{12}}{\partial t} = k_{G_{11},G_{12}} \cdot G_{11} - \left(k_{G_{12},ErGA} + k_{G_{12},FA} + k_{G_{12},AA} + k_{G_{12},G_{11}} + k_{G_{12},HMF} + k_{G_{12},UDP}\right) \cdot G_{12} + k_{HMF,G_{12}} \cdot HMF$$

Glycolaldehyde:

$$\frac{\partial GA}{\partial t} = -k_{GA,UDP} \cdot GA + k_{G_{11},ErGA} \cdot G_{11} + k_{G_{12},ErGA} \cdot G_{12}$$

Succinic acid:

$$\frac{\partial SA}{\partial t} = -k_{SA,UDP} \cdot SA + k_{G_{11},SA} \cdot G_{11} + k_{LA,SA} \cdot LA$$

Levulinic acid:

$$\frac{\partial LA}{\partial t} = -(k_{LA,SA} + k_{LA,UDP}) \cdot LA + k_{HMF,LAFA} \cdot HMF - k_{LAFA,HMF} \cdot LA \cdot FA$$

HMF:

$$\frac{\partial HMF}{\partial t} = -(k_{HMF,LAFA} + k_{HMF,Fu} + k_{HMF,UDP}) \cdot HMF + k_{G_{12},HMF} \cdot G_{12} - k_{HMF,G_{12}} \cdot HMF + k_{LAFA,HMF} \cdot LA \cdot FA$$

Furfural:

$$\frac{\partial Fu}{\partial t} = k_{HMF,Fu} \cdot HMF - k_{Fu,UDP} \cdot Fu$$

Formic acid:

$$\frac{\partial FA}{\partial t} = -k_{FA,UDP} \cdot FA + k_{G_{11},FA} \cdot G_{11} + k_{G_{12},FA} \cdot G_{12} + k_{HMF,LAFA} \cdot HMF - k_{LAFA,HMF} \cdot LA \cdot FA$$

Acetic acid:

$$\frac{\partial AA}{\partial t} = -k_{AA,UDP} \cdot AA + k_{G_{11},AA} \cdot G_{11} + k_{G_{12},AA} \cdot G_{12}$$

Glucose 275:

Cellotetraose:

$$\frac{\partial G_4}{\partial t} = -\left(k_{G_4,G_3G_{11}} + k_{G_4,G_22G_{11}} + k_{G_4,UDP}\right)\cdot G_4 + k_{G_3G_{11},G_4}\cdot G_3\cdot G_{11} + k_{G_22G_{11},G_4}\cdot G_2\cdot G_{11} + k_{G_3G_{11},G_4}\cdot G_3\cdot G_{11} + k_{G_22G_{11},G_4}\cdot G_2\cdot G_{11}$$

Cellotriose:

$$\frac{\partial G_3}{\partial t} = k_{G_4,G_3G_{11}}\cdot G_4 - \left(k_{G_3,3G_{11}} + k_{G_3,G_2G_{11}} + k_{G_3,UDP}\right)\cdot G_3 - k_{G_3G_{11},G_4}\cdot G_3\cdot G_{11} + k_{G_2G_{11},G_3}\cdot G_2\cdot G_{11} + \frac{1}{3}\cdot k_{3G_{11},G_3}\cdot G_{11}$$

Cellobiose:

$$\frac{\partial G_2}{\partial t} = k_{G_4,G_22G_{11}}\cdot G_4 + k_{G_3,G_2G_{11}}\cdot G_3 - \left(k_{G_2,2G_{11}} + k_{G_2,UDP}\right)\cdot G_2 - k_{G_22G_{11},G_4}\cdot G_2\cdot G_{11} - k_{G_2G_{11},G_3}\cdot G_2\cdot G_{11} + \frac{1}{2}\cdot k_{2G_{11},G_2}\cdot G_{11}$$

Glucose:

$$\frac{\partial G_{11}}{\partial t} = \left(k_{G_4,G_3G_{11}} + 2\cdot k_{G_4,G_22G_{11}}\right)\cdot G_4 + \left(k_{G_3,G_2G_{11}} + 3\cdot k_{G_3,3G_{11}}\right)\cdot G_3 + 2\cdot k_{G_2,2G_{11}}\cdot G_2 + k_{G_{12},G_{11}}\cdot G_{12} - \left(k_{G_{11},ErGA} + k_{G_{11},FA} + k_{G_{11},AA} + k_{G_{11},G_{12}} + k_{G_{11},UDP}\right)\cdot G_{11} - k_{G_3G_{11},G_4}\cdot G_3\cdot G_{11} - 2\cdot k_{G_22G_{11},G_4}\cdot G_2\cdot G_{11} - k_{3G_{11},G_3}\cdot G_{11} - k_{G_2G_{11},G_3}\cdot G_2\cdot G_{11} - k_{2G_{11},G_2}\cdot G_{11}$$

Fructose:

$$\frac{\partial G_{12}}{\partial t} = k_{G_{11},G_{12}}\cdot G_{11} - \left(k_{G_{12},ErGA} + k_{G_{12},FA} + k_{G_{12},AA} + k_{G_{12},G_{11}} + k_{G_{12},HMF} + k_{G_{12},UDP}\right)\cdot G_{12} + k_{HMF,G_{12}}\cdot HMF$$

Glycolaldehyde:

$$\frac{\partial GA}{\partial t} = -k_{GA,UDP}\cdot GA + k_{G_{11},ErGA}\cdot G_{11} + k_{G_{12},ErGA}\cdot G_{12}$$

Levulinic acid:

$$\frac{\partial LA}{\partial t} = -k_{LA,UDP} \cdot LA + k_{HMF,LAFA} \cdot HMF - k_{LAFA,HMF} \cdot LA \cdot FA$$

HMF:

$$\frac{\partial HMF}{\partial t} = -(k_{HMF,LAFA} + k_{HMF,Fu} + k_{HMF,UDP}) \cdot HMF + k_{G_{12},HMF} \cdot G_{12} + k_{LAFA,HMF} \cdot LA \cdot FA - k_{HMF,G_{12}} \cdot HMF$$

Furfural:

$$\frac{\partial Fu}{\partial t} = k_{HMF,Fu} \cdot HMF - k_{Fu,UDP} \cdot Fu$$

Formic acid:

$$\frac{\partial FA}{\partial t} = -k_{FA,UDP} \cdot FA + k_{G_{11},FA} \cdot G_{11} + k_{G_{12},FA} \cdot G_{12} + k_{HMF,LAFA} \cdot HMF - k_{LAFA,HMF} \cdot LA \cdot FA$$

Acetic acid:

$$\frac{\partial AA}{\partial t} = -k_{AA,UDP} \cdot AA + k_{G_{11},AA} \cdot G_{11} + k_{G_{12},AA} \cdot G_{12}$$

Glucose-300:

Cellotriose:

$$\frac{\partial G_3}{\partial t} = -\left(k_{G_3,3G_{11}} + k_{G_3,G_2G_{11}} + k_{G_3,UDP}\right) \cdot G_3 + k_{G_2G_{11},G_3} \cdot G_2 \cdot G_{11} + \frac{1}{3} \cdot k_{3G_{11},G_3} \cdot G_{11}$$

Cellobiose:

$$\frac{\partial G_2}{\partial t} = k_{G_3,G_2G_{11}} \cdot G_3 - \left(k_{G_2,2G_{11}} + k_{G_2,UDP}\right) \cdot G_2 - k_{G_2G_{11},G_3} \cdot G_2 \cdot G_{11} + \frac{1}{2} \cdot k_{2G_{11},G_2} \cdot G_{11}$$

Glucose:

$$\frac{\partial G_{11}}{\partial t} = \left(k_{G_3,G_2G_{11}} + 3 \cdot k_{G_3,3G_{11}}\right) \cdot G_3 + 2 \cdot k_{G_2,2G_{11}} \cdot G_2 + k_{G_{12},G_{11}} \cdot G_{12} - \left(k_{G_{11},ErGA} + k_{G_{11},FA} + k_{G_{11},AA} + k_{G_{11},SA} + k_{G_{11},G_{12}} + k_{G_{11},UDP}\right) \cdot G_{11} - k_{3G_{11},G_3} \cdot G_{11} - k_{G_2G_{11},G_3} \cdot G_2 \cdot G_{11} - k_{2G_{11},G_2} \cdot G_{11}$$

Fructose:

$$\frac{\partial G_{12}}{\partial t} = k_{G_{11},G_{12}} \cdot G_{11} - \left(k_{G_{12},ErGA} + k_{G_{12},FA} + k_{G_{12},AA} + k_{G_{12},G_{11}} + k_{G_{12},HMF} + k_{G_{12},UDP}\right) \cdot G_{12} + k_{HMF,G_{12}} \cdot HMF$$

Glycolaldehyde:

$$\frac{\partial GA}{\partial t} = -k_{GA,UDP} \cdot GA + k_{G_{11},ErGA} \cdot G_{11} + k_{G_{12},ErGA} \cdot G_{12}$$

Succinic acid:

$$\frac{\partial SA}{\partial t} = -k_{SA,UDP} \cdot SA + k_{G_{11},SA} \cdot G_{11} + k_{LA,SA} \cdot LA$$

Levulinic acid:

$$\frac{\partial LA}{\partial t} = -(k_{LA,SA} + k_{LA,UDP}) \cdot LA + k_{HMF,LAFA} \cdot HMF - k_{LAFA,HMF} \cdot LA \cdot FA$$

HMF:

$$\frac{\partial HMF}{\partial t} = -(k_{HMF,LAFA} + k_{HMF,Fu} + k_{HMF,UDP}) \cdot HMF + k_{G_{12},HMF} \cdot G_{12} - k_{HMF,G_{12}} \cdot HMF + k_{LAFA,HMF} \cdot LA \cdot FA$$

Furfural:

$$\frac{\partial Fu}{\partial t} = k_{HMF,Fu} \cdot HMF - k_{Fu,UDP} \cdot Fu$$

Formic acid:

$$\frac{\partial FA}{\partial t} = -k_{FA,UDP} \cdot FA + k_{G_{11},FA} \cdot G_{11} + k_{G_{12},FA} \cdot G_{12} + k_{HMF,LAFA} \cdot HMF - k_{LAFA,HMF} \cdot LA \cdot FA$$

Acetic acid:

$$\frac{\partial AA}{\partial t} = -k_{AA,UDP} \cdot AA + k_{G_{11},AA} \cdot G_{11} + k_{G_{12},AA} \cdot G_{12}$$

Case 2.1:

Cellulose-300

Cellotetraose:

$$\frac{\partial G_4}{\partial t} = -\left(k_{G_4,G_3G_{11}} + k_{G_4,G_22G_{11}} + k_{G_4,2G_2} + k_{G_4,UDP}\right) \cdot G_4 + k_{G_3G_{11},G_4} \cdot G_3 \cdot G_{11} + k_{G_22G_{11},G_4} \cdot G_2 \cdot G_{11} + \frac{1}{2} \cdot k_{2G_2,G_4} \cdot G_2$$

Cellotriose:

$$\frac{\partial G_3}{\partial t} = k_{G_4,G_3G_{11}} \cdot G_4 - \left(k_{G_3,3G_{11}} + k_{G_3,G_2G_{11}} + k_{G_3,UDP}\right) \cdot G_3 - k_{G_3G_{11},G_4} \cdot G_3 \cdot G_{11} + k_{G_2G_{11},G_3} \cdot G_2 \cdot G_{11} + \frac{1}{3} \cdot k_{3G_{11},G_3} \cdot G_{11}$$

Cellobiose:

$$\frac{\partial G_2}{\partial t} = \left(k_{G_4,G_22G_{11}} + 2 \cdot k_{G_4,2G_2}\right) \cdot G_4 + k_{G_3,G_2G_{11}} \cdot G_3 - \left(k_{G_2,2G_{11}} + k_{G_2,UDP}\right) \cdot G_2 - k_{G_22G_{11},G_4} \cdot G_2 \cdot G_{11} - k_{G_2G_{11},G_3} \cdot G_2 \cdot G_{11} + \frac{1}{2} \cdot k_{2G_{11},G_2} \cdot G_{11} - k_{2G_2,G_4} \cdot G_2$$

Glucose:

$$\frac{\partial G_{11}}{\partial t} = \left(k_{G_4,G_3G_{11}} + 2 \cdot k_{G_4,G_2 2G_{11}}\right) \cdot G_4 + \left(k_{G_3,G_2G_{11}} + 3 \cdot k_{G_3,3G_{11}}\right) \cdot G_3 + 2 \cdot k_{G_2,2G_{11}} \cdot G_2 + k_{G_{12},G_{11}} \cdot G_{12} - \left(k_{G_{11},ErGA} + k_{G_{11},FA} + k_{G_{11},AA} + k_{G_{11},SA} + k_{G_{11},G_{12}} + k_{G_{11},UDP}\right) \cdot G_{11} - k_{G_3G_{11},G_4} \cdot G_3 \cdot G_{11} - 2 \cdot k_{G_2 2G_{11},G_4} \cdot G_2 \cdot G_{11} - k_{3G_{11},G_3} \cdot G_{11} - k_{G_2G_{11},G_3} \cdot G_2 \cdot G_{11} - k_{2G_{11},G_2} \cdot G_{11}$$

Fructose:

$$\frac{\partial G_{12}}{\partial t} = k_{G_{11},G_{12}} \cdot G_{11} - \left(k_{G_{12},ErGA} + k_{G_{12},FA} + k_{G_{12},AA} + k_{G_{12},G_{11}} + k_{G_{12},HMF} + k_{G_{12},UDP}\right) \cdot G_{12} + k_{HMF,G_{12}} \cdot HMF$$

Glycolaldehyde:

$$\frac{\partial GA}{\partial t} = -k_{GA,UDP} \cdot GA + k_{G_{11},ErGA} \cdot G_{11} + k_{G_{12},ErGA} \cdot G_{12}$$

Succinic acid:

$$\frac{\partial SA}{\partial t} = -k_{SA,UDP} \cdot SA + k_{G_{11},SA} \cdot G_{11} + k_{LA,SA} \cdot LA$$

Levulinic acid:

$$\frac{\partial LA}{\partial t} = -(k_{LA,SA} + k_{LA,UDP}) \cdot LA + k_{HMF,LAFA} \cdot HMF - k_{LAFA,HMF} \cdot LA \cdot FA$$

HMF:

$$\frac{\partial HMF}{\partial t} = -(k_{HMF,LAFA} + k_{HMF,Fu} + k_{HMF,UDP}) \cdot HMF + k_{G_{12},HMF} \cdot G_{12} - k_{HMF,G_{12}} \cdot HMF + k_{LAFA,HMF} \cdot LA \cdot FA$$

Furfural:

$$\frac{\partial Fu}{\partial t} = k_{HMF,Fu} \cdot HMF - k_{Fu,UDP} \cdot Fu$$

Formic acid:

$$\frac{\partial FA}{\partial t} = -k_{FA,UDP} \cdot FA + k_{G_{11},FA} \cdot G_{11} + k_{G_{12},FA} \cdot G_{12} + k_{HMF,LAFA} \cdot HMF - k_{LAFA,HMF} \cdot LA \cdot FA$$

Acetic acid:

$$\frac{\partial AA}{\partial t} = -k_{AA,UDP} \cdot AA + k_{G_{11},AA} \cdot G_{11} + k_{G_{12},AA} \cdot G_{12}$$

Glucose 275:

Cellotetraose:

$$\frac{\partial G_4}{\partial t} = -\left(k_{G_4,G_3G_{11}} + k_{G_4,G_22G_{11}} + k_{G_4,2G_2} + k_{G_4,UDP}\right) \cdot G_4 + k_{G_3G_{11},G_4} \cdot G_3 \cdot G_{11} + k_{G_22G_{11},G_4} \cdot G_2 \cdot G_{11} + \frac{1}{2} \cdot k_{2G_2,G_4} \cdot G_2$$

Cellotriose:

$$\frac{\partial G_3}{\partial t} = k_{G_4,G_3G_{11}} \cdot G_4 - \left(k_{G_3,3G_{11}} + k_{G_3,G_2G_{11}} + k_{G_3,UDP}\right) \cdot G_3 - k_{G_3G_{11},G_4} \cdot G_3 \cdot G_{11} + k_{G_2G_{11},G_3} \cdot G_2 \cdot G_{11} + \frac{1}{3} \cdot k_{3G_{11},G_3} \cdot G_{11}$$

Cellobiose:

$$\frac{\partial G_2}{\partial t} = (k_{G_4,G_22G_{11}} + 2 \cdot k_{G_4,2G_2}) \cdot G_4 + k_{G_3,G_2G_{11}} \cdot G_3 - \left(k_{G_2,2G_{11}} + k_{G_2,UDP}\right) \cdot G_2 - k_{G_22G_{11},G_4} \cdot G_2 \cdot G_{11} - k_{G_2G_{11},G_3} \cdot G_2 \cdot G_{11} + \frac{1}{2} \cdot k_{2G_{11},G_2} \cdot G_{11} - k_{2G_2,G_4} \cdot G_2$$

Glucose:

$$\frac{\partial G_{11}}{\partial t} = \left(k_{G_4,G_3G_{11}} + 2 \cdot k_{G_4,G_2 2G_{11}}\right) \cdot G_4 + \left(k_{G_3,G_2G_{11}} + 3 \cdot k_{G_3,3G_{11}}\right) \cdot G_3 + 2 \cdot k_{G_2,2G_{11}} \cdot G_2 + k_{G_{12},G_{11}} \cdot G_{12} - \left(k_{G_{11},ErGA} + k_{G_{11},FA} + k_{G_{11},AA} + k_{G_{11},G_{12}} + k_{G_{11},UDP}\right) \cdot G_{11} - k_{G_3G_{11},G_4} \cdot G_3 \cdot G_{11} - 2 \cdot k_{G_2 2G_{11},G_4} \cdot G_2 \cdot G_{11} - k_{3G_{11},G_3} \cdot G_{11} - k_{G_2G_{11},G_3} \cdot G_2 \cdot G_{11} - k_{2G_{11},G_2} \cdot G_{11}$$

Fructose:

$$\frac{\partial G_{12}}{\partial t} = k_{G_{11},G_{12}} \cdot G_{11} - \left(k_{G_{12},ErGA} + k_{G_{12},FA} + k_{G_{12},AA} + k_{G_{12},G_{11}} + k_{G_{12},HMF} + k_{G_{12},UDP}\right) \cdot G_{12} + k_{HMF,G_{12}} \cdot HMF$$

Glycolaldehyde:

$$\frac{\partial GA}{\partial t} = -k_{GA,UDP} \cdot GA + k_{G_{11},ErGA} \cdot G_{11} + k_{G_{12},ErGA} \cdot G_{12}$$

Levulinic acid:

$$\frac{\partial LA}{\partial t} = -k_{LA,UDP} \cdot LA + k_{HMF,LAFA} \cdot HMF - k_{LAFA,HMF} \cdot LA \cdot FA$$

HMF:

$$\frac{\partial HMF}{\partial t} = -(k_{HMF,LAFA} + k_{HMF,Fu} + k_{HMF,UDP}) \cdot HMF + k_{G_{12},HMF} \cdot G_{12} - k_{HMF,G_{12}} \cdot HMF + k_{LAFA,HMF} \cdot LA \cdot FA$$

Furfural:

$$\frac{\partial Fu}{\partial t} = k_{HMF,Fu} \cdot HMF - k_{Fu,UDP} \cdot Fu$$

Formic acid:

$$\frac{\partial FA}{\partial t} = -k_{FA,UDP} \cdot FA + k_{G_{11},FA} \cdot G_{11} + k_{G_{12},FA} \cdot G_{12} + k_{HMF,LAFA} \cdot HMF - k_{LAFA,HMF} \cdot LA \cdot FA$$

Acetic acid:

$$\frac{\partial AA}{\partial t} = -k_{AA,UDP} \cdot AA + k_{G_{11},AA} \cdot G_{11} + k_{G_{12},AA} \cdot G_{12}$$

Glucose-300:

Cellotriose:

$$\frac{\partial G_3}{\partial t} = -\left(k_{G_3,3G_{11}} + k_{G_3,G_2G_{11}} + k_{G_3,UDP}\right) \cdot G_3 + k_{G_2G_{11},G_3} \cdot G_2 \cdot G_{11} + \frac{1}{3} \cdot k_{3G_{11},G_3} \cdot G_{11}$$

Cellobiose:

$$\frac{\partial G_2}{\partial t} = k_{G_3,G_2G_{11}} \cdot G_3 - \left(k_{G_2,2G_{11}} + k_{G_2,UDP}\right) \cdot G_2 - k_{G_2G_{11},G_3} \cdot G_2 \cdot G_{11} + \frac{1}{2} \cdot k_{2G_{11},G_2} \cdot G_{11}$$

Glucose:

$$\frac{\partial G_{11}}{\partial t} = \left(k_{G_3,G_2G_{11}} + 3 \cdot k_{G_3,3G_{11}}\right) \cdot G_3 + 2 \cdot k_{G_2,2G_{11}} \cdot G_2 + k_{G_{12},G_{11}} \cdot G_{12} - \left(k_{G_{11},ErGA} + k_{G_{11},FA} + k_{G_{11},AA} + k_{G_{11},SA} + k_{G_{11},G_{12}} + k_{G_{11},UDP}\right) \cdot G_{11} - k_{3G_{11},G_3} \cdot G_{11} - k_{G_2G_{11},G_3} \cdot G_2 \cdot G_{11} - k_{2G_{11},G_2} \cdot G_{11}$$

Fructose:

$$\frac{\partial G_{12}}{\partial t} = k_{G_{11},G_{12}} \cdot G_{11} - \left(k_{G_{12},ErGA} + k_{G_{12},FA} + k_{G_{12},AA} + k_{G_{12},G_{11}} + k_{G_{12},HMF} + k_{G_{12},UDP}\right) \cdot G_{12} + k_{HMF,G_{12}} \cdot HMF$$

Glycolaldehyde:

$$\frac{\partial GA}{\partial t} = -k_{GA,UDP} \cdot GA + k_{G_{11},ErGA} \cdot G_{11} + k_{G_{12},ErGA} \cdot G_{12}$$

Succinic acid:

$$\frac{\partial SA}{\partial t} = -k_{SA,UDP} \cdot SA + k_{G_{11},SA} \cdot G_{11} + k_{LA,SA} \cdot LA$$

Levulinic acid:

$$\frac{\partial LA}{\partial t} = -(k_{LA,SA} + k_{LA,UDP}) \cdot LA + k_{HMF,LAFA} \cdot HMF - k_{LAFA,HMF} \cdot LA \cdot FA$$

HMF:

$$\frac{\partial HMF}{\partial t} = -(k_{HMF,LAFA} + k_{HMF,Fu} + k_{HMF,UDP}) \cdot HMF + k_{G_{12},HMF} \cdot G_{12} - k_{HMF,G_{12}} \cdot HMF + k_{LAFA,HMF} \cdot LA \cdot FA$$

Furfural:

$$\frac{\partial Fu}{\partial t} = k_{HMF,Fu} \cdot HMF - k_{Fu,UDP} \cdot Fu$$

Formic acid:

$$\frac{\partial FA}{\partial t} = -k_{FA,UDP} \cdot FA + k_{G_{11},FA} \cdot G_{11} + k_{G_{12},FA} \cdot G_{12} + k_{HMF,LAFA} \cdot HMF - k_{LAFA,HMF} \cdot LA \cdot FA$$

Acetic acid:

$$\frac{\partial AA}{\partial t} = -k_{AA,UDP} \cdot AA + k_{G_{11},AA} \cdot G_{11} + k_{G_{12},AA} \cdot G_{12}$$

Case 1.2:

Cellulose-300

Cellotetraose:

$$\frac{\partial G_4}{\partial t} = -\left(k_{G_4,G_3G_1} + k_{G_4,G_22G_1} + k_{G_4,UDP}\right) \cdot G_4 + k_{G_3G_1,G_4} \cdot G_3 \cdot G_1 + k_{G_22G_1,G_4} \cdot G_2 \cdot G_1$$

Cellotriose:

$$\frac{\partial G_3}{\partial t} = k_{G_4,G_3G_1} \cdot G_4 - \left(k_{G_3,3G_1} + k_{G_3,G_2G_1} + k_{G_3,UDP}\right) \cdot G_3 - k_{G_3G_1,G_4} \cdot G_3 \cdot G_1 + k_{G_2G_1,G_3} \cdot G_2 \cdot G_1 + \frac{1}{3} \cdot k_{3G_1,G_3} \cdot G_1$$

Cellobiose:

$$\frac{\partial G_2}{\partial t} = k_{G_4,G_2 2G_1} \cdot G_4 + k_{G_3,G_2G_1} \cdot G_3 - \left(k_{G_2,2G_1} + k_{G_2,UDP}\right) \cdot G_2 - k_{G_2 2G_1,G_4} \cdot G_2 \cdot G_1 - k_{G_2G_1,G_3} \cdot G_2 \cdot G_1 + \frac{1}{2} \cdot k_{2G_1,G_2} \cdot G_1$$

Cellulo-monomers:

$$\frac{\partial G_1}{\partial t} = \left(k_{G_4,G_3G_1} + 2 \cdot k_{G_4,G_2 2G_1}\right) \cdot G_4 + \left(k_{G_3,G_2G_1} + 3 \cdot k_{G_3,3G_1}\right) \cdot G_3 + k_{G_2,2G_1} \cdot G_2 - \left(k_{G_1,ErGA} + k_{G_1,FA} + k_{G_1,AA} + k_{G_1,SA} + k_{G_1,HMF} + k_{G_1,UDP}\right) \cdot G_1 - k_{G_3G_1,G_4} \cdot G_3 \cdot G_1 - 2 \cdot k_{G_2 2G_1,G_4} \cdot G_2 \cdot G_1 - k_{3G_1,G_3} \cdot G_1 - k_{G_2G_1,G_3} \cdot G_2 \cdot G_1 - k_{2G_1,G_2} \cdot G_1 + k_{HMF,G_1} \cdot HMF$$

Glycolaldehyde:

$$\frac{\partial GA}{\partial t} = -k_{GA,UDP} \cdot GA + k_{G_1,ErGA} \cdot G_1$$

Succinic acid:

$$\frac{\partial SA}{\partial t} = -k_{SA,UDP} \cdot SA + k_{G_1,SA} \cdot G_1 + k_{LA,SA} \cdot LA$$

Levulinic acid:

$$\frac{\partial LA}{\partial t} = -(k_{LA,SA} + k_{LA,UDP}) \cdot LA + k_{HMF,LAFA} \cdot HMF - k_{LAFA,HMF} \cdot LA \cdot FA$$

HMF:

$$\frac{\partial HMF}{\partial t} = -(k_{HMF,LAFA} + k_{HMF,Fu} + k_{HMF,UDP}) \cdot HMF + k_{G_1,HMF} \cdot G_1 - k_{HMF,G_1} \cdot HMF + k_{LAFA,HMF} \cdot LA \cdot FA$$

Furfural:

$$\frac{\partial Fu}{\partial t} = k_{HMF,Fu} \cdot HMF - k_{Fu,UDP} \cdot Fu$$

Formic acid:

$$\frac{\partial FA}{\partial t} = -k_{FA,UDP} \cdot FA + k_{G_1,FA} \cdot G_1 + k_{HMF,LAFA} \cdot HMF - k_{LAFA,HMF} \cdot LA \cdot FA$$

Acetic acid:

$$\frac{\partial AA}{\partial t} = -k_{AA,UDP} \cdot AA + k_{G_1,AA} \cdot G_1$$

Glucose 275:

Cellotetraose:

$$\frac{\partial G_4}{\partial t} = -\left(k_{G_4,G_3G_1} + k_{G_4,G_22G_1} + k_{G_4,UDP}\right) \cdot G_4 + k_{G_3G_1,G_4} \cdot G_3 \cdot G_1 + k_{G_22G_1,G_4} \cdot G_2 \cdot G_1$$

Cellotriose:

$$\frac{\partial G_3}{\partial t} = k_{G_4,G_3G_1} \cdot G_4 - \left(k_{G_3,3G_1} + k_{G_3,G_2G_1} + k_{G_3,UDP}\right) \cdot G_3 - k_{G_3G_1,G_4} \cdot G_3 \cdot G_1 + k_{G_2G_1,G_3} \cdot G_2 \cdot G_1 + \frac{1}{3} \cdot k_{3G_1,G_3} \cdot G_1$$

Cellobiose:

$$\frac{\partial G_2}{\partial t} = k_{G_4,G_22G_1} \cdot G_4 + k_{G_3,G_2G_1} \cdot G_3 - \left(k_{G_2,2G_1} + k_{G_2,UDP}\right) \cdot G_2 - k_{G_22G_1,G_4} \cdot G_2 \cdot G_1 - k_{G_2G_1,G_3} \cdot G_2 \cdot G_1 + \frac{1}{2} \cdot k_{2G_1,G_2} \cdot G_1$$

Cellulo-monomers:

$$\frac{\partial G_1}{\partial t} = \left(k_{G_4,G_3G_1} + 2 \cdot k_{G_4,G_22G_1}\right) \cdot G_4 + \left(k_{G_3,G_2G_1} + 3 \cdot k_{G_3,3G_1}\right) \cdot G_3 + 2 \cdot k_{G_2,2G_1} \cdot G_2 - \left(k_{G_1,ErGA} + k_{G_1,FA} + k_{G_1,AA} + k_{G_1,HMF} + k_{G_1,UDP}\right) \cdot G_1 - k_{G_3G_1,G_4} \cdot G_3 \cdot G_1 - 2 \cdot k_{G_22G_1,G_4} \cdot G_2 \cdot G_1 - k_{3G_1,G_3} \cdot G_1 - k_{G_2G_1,G_3} \cdot G_2 \cdot G_1 - k_{2G_1,G_2} \cdot G_1 + k_{HMF,G_1} \cdot HMF$$

Glycolaldehyde:

$$\frac{\partial GA}{\partial t} = -k_{GA,UDP} \cdot GA + k_{G_1,ErGA} \cdot G_1$$

Levulinic acid:

$$\frac{\partial LA}{\partial t} = -k_{LA,UDP} \cdot LA + k_{HMF,LAFA} \cdot HMF - k_{LAFA,HMF} \cdot LA \cdot FA$$

HMF:

$$\frac{\partial HMF}{\partial t} = -(k_{HMF,LAFA} + k_{HMF,Fu} + k_{HMF,UDP}) \cdot HMF + k_{G_1,HMF} \cdot G_1 - k_{HMF,G_1} \cdot HMF + k_{LAFA,HMF} \cdot LA \cdot FA$$

Furfural:

$$\frac{\partial Fu}{\partial t} = k_{HMF,Fu} \cdot HMF - k_{Fu,UDP} \cdot Fu$$

Formic acid:

$$\frac{\partial FA}{\partial t} = -k_{FA,UDP} \cdot FA + k_{G_1,FA} \cdot G_1 + k_{HMF,LAFA} \cdot HMF - k_{LAFA,HMF} \cdot LA \cdot FA$$

Acetic acid:

$$\frac{\partial AA}{\partial t} = -k_{AA,UDP} \cdot AA + k_{G_1,AA} \cdot G_1$$

Glucose-300:

Cellotriose:

$$\frac{\partial G_3}{\partial t} = -\left(k_{G_3,3G_1} + k_{G_3,G_2G_1} + k_{G_3,UDP}\right) \cdot G_3 + k_{G_2G_1,G_3} \cdot G_2 \cdot G_1 + \frac{1}{3} \cdot k_{3G_1,G_3} \cdot G_1$$

Cellobiose:

$$\frac{\partial G_2}{\partial t} = k_{G_3,G_2G_1} \cdot G_3 - \left(k_{G_2,2G_1} + k_{G_2,UDP}\right) \cdot G_2 - k_{G_2G_1,G_3} \cdot G_2 \cdot G_1 + \frac{1}{2} \cdot k_{2G_1,G_2} \cdot G_1$$

Cellulo-monomers:

$$\frac{\partial G_1}{\partial t} = \left(k_{G_3,G_2G_1} + 3 \cdot k_{G_3,3G_1}\right) \cdot G_3 + 2 \cdot k_{G_2,2G_1} \cdot G_2 - \left(k_{G_1,ErGA} + k_{G_1,FA} + k_{G_1,AA} + k_{G_1,SA} + k_{G_1,HMF} + k_{G_1,UDP}\right) \cdot G_1 - k_{3G_1,G_3} \cdot G_1 - k_{G_2G_1,G_3} \cdot G_2 \cdot G_1 - k_{2G_1,G_2} \cdot G_1 + k_{HMF,G_1} \cdot HMF$$

Glycolaldehyde:

$$\frac{\partial GA}{\partial t} = -k_{GA,UDP} \cdot GA + k_{G_1,ErGA} \cdot G_1$$

Succinic acid:

$$\frac{\partial SA}{\partial t} = -k_{SA,UDP} \cdot SA + k_{G_1,SA} \cdot G_1 + k_{LA,SA} \cdot LA$$

Levulinic acid:

$$\frac{\partial LA}{\partial t} = -(k_{LA,SA} + k_{LA,UDP}) \cdot LA + k_{HMF,LAFA} \cdot HMF - k_{LAFA,HMF} \cdot LA \cdot FA$$

HMF:

$$\frac{\partial HMF}{\partial t} = -(k_{HMF,LAFA} + k_{HMF,Fu} + k_{HMF,UDP}) \cdot HMF + k_{G_1,HMF} \cdot G_1 - k_{HMF,G_1} \cdot HMF + k_{LAFA,HMF} \cdot LA \cdot FA$$

Furfural:

$$\frac{\partial Fu}{\partial t} = k_{HMF,Fu} \cdot HMF - k_{Fu,UDP} \cdot Fu$$

Formic acid:

$$\frac{\partial FA}{\partial t} = -k_{FA,UDP} \cdot FA + k_{G_1,FA} \cdot G_1 + k_{HMF,LAFA} \cdot HMF - k_{LAFA,HMF} \cdot LA \cdot FA$$

Acetic acid:

$$\frac{\partial AA}{\partial t} = -k_{AA,UDP} \cdot AA + k_{G_1,AA} \cdot G_1$$

Case 2.2:

Cellulose-300

Cellotetraose:

$$\frac{\partial G_4}{\partial t} = -\left(k_{G_4,G_3G_1} + k_{G_4,G_22G_1} + k_{G_4,2G_2} + k_{G_4,UDP}\right) \cdot G_4 + k_{G_3G_1,G_4} \cdot G_3 \cdot G_1 + k_{G_22G_1,G_4} \cdot G_2 \cdot G_1 + \frac{1}{2} \cdot k_{2G_2,G_4} \cdot G_2$$

Cellotriose:

$$\frac{\partial G_3}{\partial t} = k_{G_4,G_3G_1} \cdot G_4 - \left(k_{G_3,3G_1} + k_{G_3,G_2G_1} + k_{G_3,UDP}\right) \cdot G_3 - k_{G_3G_1,G_4} \cdot G_3 \cdot G_1 + k_{G_2G_1,G_3} \cdot G_2 \cdot G_1 + \frac{1}{3} \cdot k_{3G_1,G_3} \cdot G_1$$

Cellobiose:

$$\frac{\partial G_2}{\partial t} = \left(k_{G_4,G_22G_1} + 2 \cdot k_{G_4,2G_2}\right) \cdot G_4 + k_{G_3,G_2G_1} \cdot G_3 - \left(k_{G_2,2G_1} + k_{G_2,UDP}\right) \cdot G_2 - k_{G_22G_1,G_4} \cdot G_2 \cdot G_1 - k_{G_2G_1,G_3} \cdot G_2 \cdot G_1 + \frac{1}{2} \cdot k_{2G_1,G_2} \cdot G_1 - k_{2G_2,G_4} \cdot G_2$$

Cellulo-monomers:

$$\frac{\partial G_1}{\partial t} = \left(k_{G_4,G_3G_1} + 2 \cdot k_{G_4,G_22G_1}\right) \cdot G_4 + \left(k_{G_3,G_2G_1} + 3 \cdot k_{G_3,3G_1}\right) \cdot G_3 + 2 \cdot k_{G_2,2G_1} \cdot G_2 - \left(k_{G_1,ErGA} + k_{G_1,FA} + k_{G_1,AA} + k_{G_1,SA} + k_{G_1,HMF} + k_{G_1,UDP}\right) \cdot G_1 - k_{G_3G_1,G_4} \cdot G_3 \cdot G_1 - 2 \cdot k_{G_22G_1,G_4} \cdot G_2 \cdot G_1 - k_{3G_1,G_3} \cdot G_1 - k_{G_2G_1,G_3} \cdot G_2 \cdot G_1 - k_{2G_1,G_2} \cdot G_1 + k_{HMF,G_1} \cdot HMF$$

Glycolaldehyde:

$$\frac{\partial GA}{\partial t} = -k_{GA,UDP} \cdot GA + k_{G_1,ErGA} \cdot G_1$$

Succinic acid:

$$\frac{\partial SA}{\partial t} = -k_{SA,UDP} \cdot SA + k_{G_1,SA} \cdot G_1 + k_{LA,SA} \cdot LA$$

Levulinic acid:

$$\frac{\partial LA}{\partial t} = -(k_{LA,SA} + k_{LA,UDP}) \cdot LA + k_{HMF,LAFA} \cdot HMF - k_{LAFA,HMF} \cdot LA \cdot FA$$

HMF:

$$\frac{\partial HMF}{\partial t} = -(k_{HMF,LAFA} + k_{HMF,Fu} + k_{HMF,UDP}) \cdot HMF + k_{G_1,HMF} \cdot G_1 - k_{HMF,G_1} \cdot HMF + k_{LAFA,HMF} \cdot LA \cdot FA$$

Furfural:

$$\frac{\partial Fu}{\partial t} = k_{HMF,Fu} \cdot HMF - k_{Fu,UDP} \cdot Fu$$

Formic acid:

$$\frac{\partial FA}{\partial t} = -k_{FA,UDP} \cdot FA + k_{G_1,FA} \cdot G_1 + k_{HMF,LAFA} \cdot HMF - k_{LAFA,HMF} \cdot LA \cdot FA$$

Acetic acid:

$$\frac{\partial AA}{\partial t} = -k_{AA,UDP} \cdot AA + k_{G_1,AA} \cdot G_1$$

Glucose 275:

Cellotetraose:

$$\frac{\partial G_4}{\partial t} = -\left(k_{G_4,G_3G_1} + k_{G_4,G_22G_1} + k_{G_4,2G_2} + k_{G_4,UDP}\right) \cdot G_4 + k_{G_3G_1,G_4} \cdot G_3 \cdot G_1 + k_{G_22G_1,G_4} \cdot G_2 \cdot G_1 + \frac{1}{2} \cdot k_{2G_2,G_4} \cdot G_2$$

Cellotriose:

$$\frac{\partial G_3}{\partial t} = k_{G_4,G_3G_1} \cdot G_4 - \left(k_{G_3,3G_1} + k_{G_3,G_2G_1} + k_{G_3,UDP}\right) \cdot G_3 - k_{G_3G_1,G_4} \cdot G_3 \cdot G_1 + k_{G_2G_1,G_3} \cdot G_2 \cdot G_1 + \frac{1}{3} \cdot k_{3G_1,G_3} \cdot G_1$$

Cellobiose:

$$\frac{\partial G_2}{\partial t} = (k_{G_4,G_2 2G_1} + 2 \cdot k_{G_4,2G_2}) \cdot G_4 + k_{G_3,G_2G_1} \cdot G_3 - \left(k_{G_2,2G_1} + k_{G_2,UDP}\right) \cdot G_2 - k_{G_2 2G_1,G_4} \cdot G_2 \cdot G_1 - k_{G_2G_1,G_3} \cdot G_2 \cdot G_1 + \frac{1}{2} \cdot k_{2G_1,G_2} \cdot G_1 - k_{2G_2,G_4} \cdot G_2$$

Cellulo-monomers:

$$\frac{\partial G_1}{\partial t} = \left(k_{G_4,G_3G_1} + 2 \cdot k_{G_4,G_2 2G_1}\right) \cdot G_4 + \left(k_{G_3,G_2G_1} + 3 \cdot k_{G_3,3G_1}\right) \cdot G_3 + 2 \cdot k_{G_2,2G_1} \cdot G_2 - \left(k_{G_1,ErGA} + k_{G_1,FA} + k_{G_1,AA} + k_{G_1,HMF} + k_{G_1,UDP}\right) \cdot G_1 - k_{G_3G_1,G_4} \cdot G_3 \cdot G_1 - 2 \cdot k_{G_2 2G_1,G_4} \cdot G_2 \cdot G_1 - k_{3G_1,G_3} \cdot G_1 - k_{G_2G_1,G_3} \cdot G_2 \cdot G_1 - k_{2G_1,G_2} \cdot G_1 + k_{HMF,G_1} \cdot HMF$$

Glycolaldehyde:

$$\frac{\partial GA}{\partial t} = -k_{GA,UDP} \cdot GA + k_{G_1,ErGA} \cdot G_1$$

Levulinic acid:

$$\frac{\partial LA}{\partial t} = -k_{LA,UDP} \cdot LA + k_{HMF,LAFA} \cdot HMF - k_{LAFA,HMF} \cdot LA \cdot FA$$

HMF:

$$\frac{\partial HMF}{\partial t} = -(k_{HMF,LAFA} + k_{HMF,Fu} + k_{HMF,UDP}) \cdot HMF + k_{G_1,HMF} \cdot G_1 - k_{HMF,G_1} \cdot HMF + k_{LAFA,HMF} \cdot LA \cdot FA$$

Furfural:

$$\frac{\partial Fu}{\partial t} = k_{HMF,Fu} \cdot HMF - k_{Fu,UDP} \cdot Fu$$

Formic acid:

$$\frac{\partial FA}{\partial t} = -k_{FA,UDP} \cdot FA + k_{G_1,FA} \cdot G_1 + k_{HMF,LAFA} \cdot HMF - k_{LAFA,HMF} \cdot LA \cdot FA$$

Acetic acid:

$$\frac{\partial AA}{\partial t} = -k_{AA,UDP} \cdot AA + k_{G_1,AA} \cdot G_1$$

Glucose-300:

Cellotriose:

$$\frac{\partial G_3}{\partial t} = -\left(k_{G_3,3G_1} + k_{G_3,G_2G_1} + k_{G_3,UDP}\right) \cdot G_3 + k_{G_2G_1,G_3} \cdot G_2 \cdot G_1 + \frac{1}{3} \cdot k_{3G_1,G_3} \cdot G_1$$

Cellobiose:

$$\frac{\partial G_2}{\partial t} = k_{G_3,G_2G_1} \cdot G_3 - \left(k_{G_2,2G_1} + k_{G_2,UDP}\right) \cdot G_2 - k_{G_2G_1,G_3} \cdot G_2 \cdot G_1 + \frac{1}{2} \cdot k_{2G_1,G_2} \cdot G_1$$

Cellulo-monomers:

$$\begin{aligned}\frac{\partial G_1}{\partial t} = {} & \left(k_{G_3,G_2G_1} + 3 \cdot k_{G_3,3G_1}\right) \cdot G_3 + 2 \cdot k_{G_2,2G_1} \cdot G_2 \\ & - \left(k_{G_1,ErGA} + k_{G_1,FA} + k_{G_1,AA} + k_{G_1,SA} + k_{G_1,HMF} + k_{G_1,UDP}\right) \cdot G_1 - k_{3G_1,G_3} \cdot G_1 \\ & - k_{G_2G_1,G_3} \cdot G_2 \cdot G_1 - k_{2G_1,G_2} \cdot G_1 + k_{HMF,G_1} \cdot HMF\end{aligned}$$

Glycolaldehyde:

$$\frac{\partial GA}{\partial t} = -k_{GA,UDP} \cdot GA + k_{G_1,ErGA} \cdot G_1$$

Succinic acid:

$$\frac{\partial SA}{\partial t} = -k_{SA,UDP} \cdot SA + k_{G_1,SA} \cdot G_1 + k_{LA,SA} \cdot LA$$

Levulinic acid:

$$\frac{\partial LA}{\partial t} = -(k_{LA,SA} + k_{LA,UDP}) \cdot LA + k_{HMF,LAFA} \cdot HMF - k_{LAFA,HMF} \cdot LA \cdot FA$$

HMF:

$$\begin{aligned}\frac{\partial HMF}{\partial t} = {} & -(k_{HMF,LAFA} + k_{HMF,Fu} + k_{HMF,UDP}) \cdot HMF + k_{G_1,HMF} \cdot G_1 - k_{HMF,G_1} \cdot HMF \\ & + k_{LAFA,HMF} \cdot LA \cdot FA\end{aligned}$$

Furfural:

$$\frac{\partial Fu}{\partial t} = k_{HMF,Fu} \cdot HMF - k_{Fu,UDP} \cdot Fu$$

Formic acid:

$$\frac{\partial FA}{\partial t} = -k_{FA,UDP} \cdot FA + k_{G_1,FA} \cdot G_1 + k_{HMF,LAFA} \cdot HMF - k_{LAFA,HMF} \cdot LA \cdot FA$$

Acetic acid:

$$\frac{\partial AA}{\partial t} = -k_{AA,UDP} \cdot AA + k_{G_1,AA} \cdot G_1$$

Appendix G: Simulated Concentration Plots of Chemical Species via Kinetic Modeling

Cellulose-300 HTL Experiment:

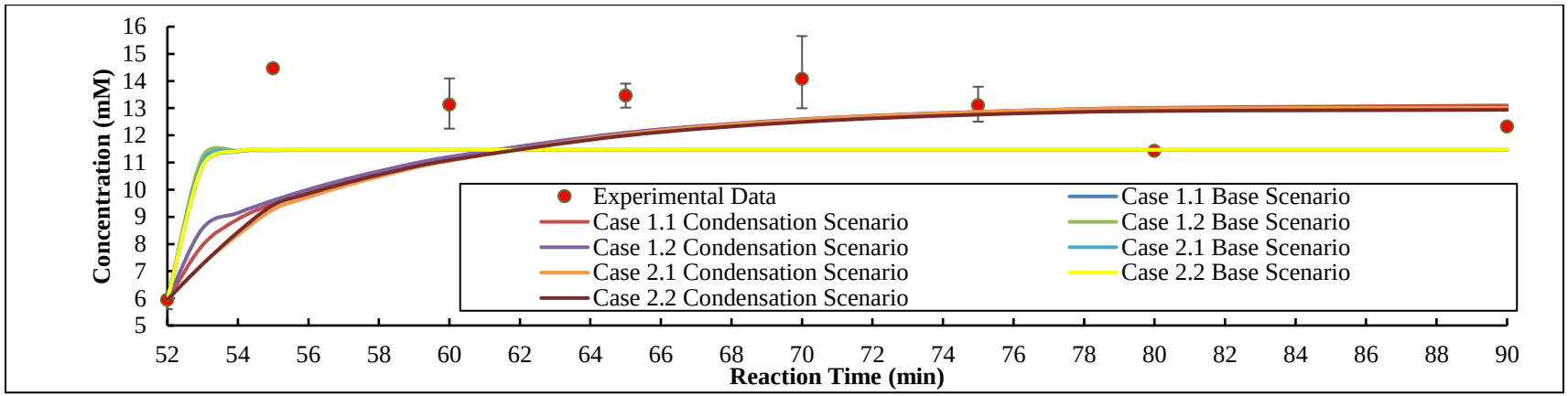

***Figure 41**: Simulated Concentration Profile of Acetic Acid in the Cellulose-300 HTL Experiment.*

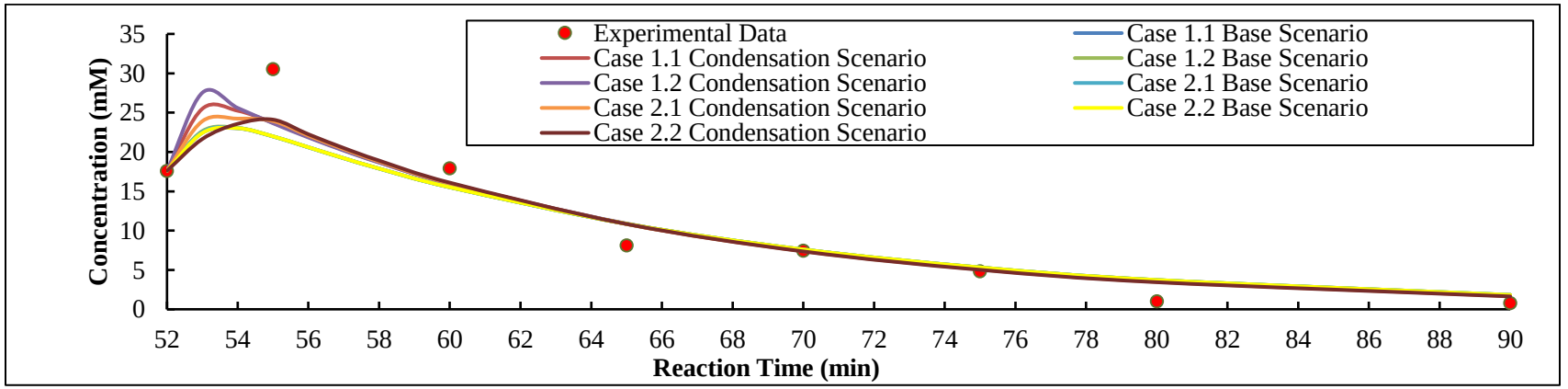

***Figure 42**: Simulated Concentration Profile of Formic Acid in the Cellulose-300 HTL Experiment.*

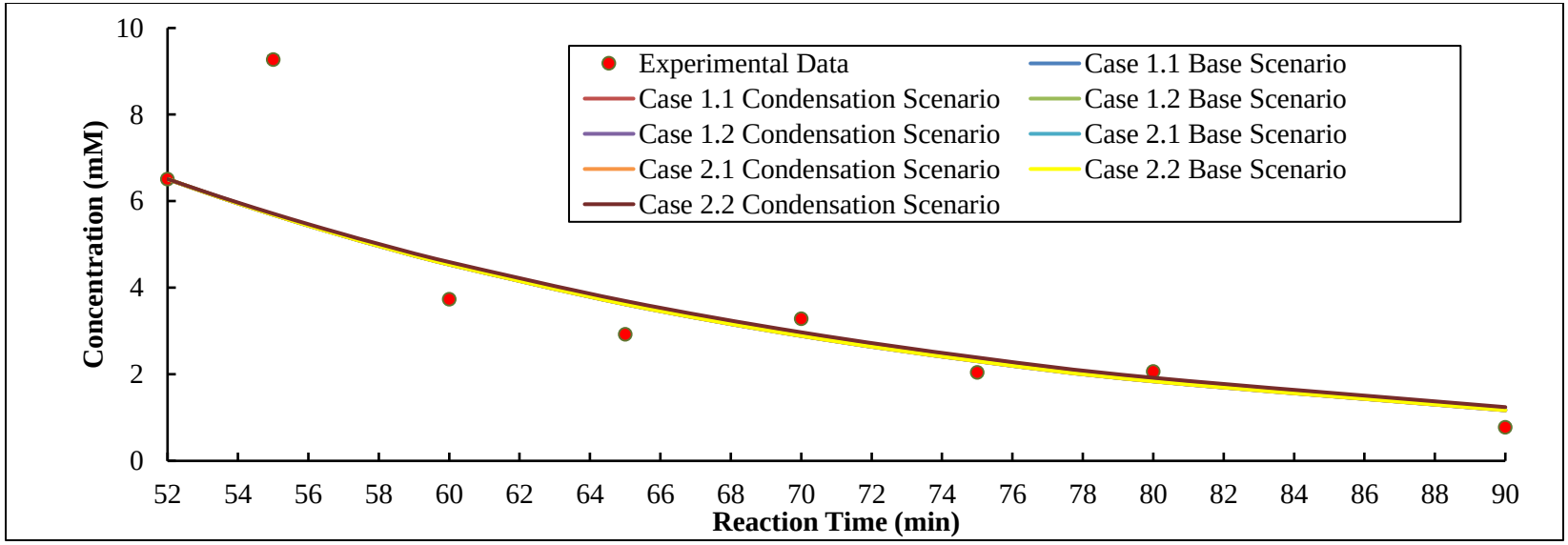

***Figure 43**: Simulated Concentration Profile of Furfural in the Cellulose-300 HTL Experiment.*

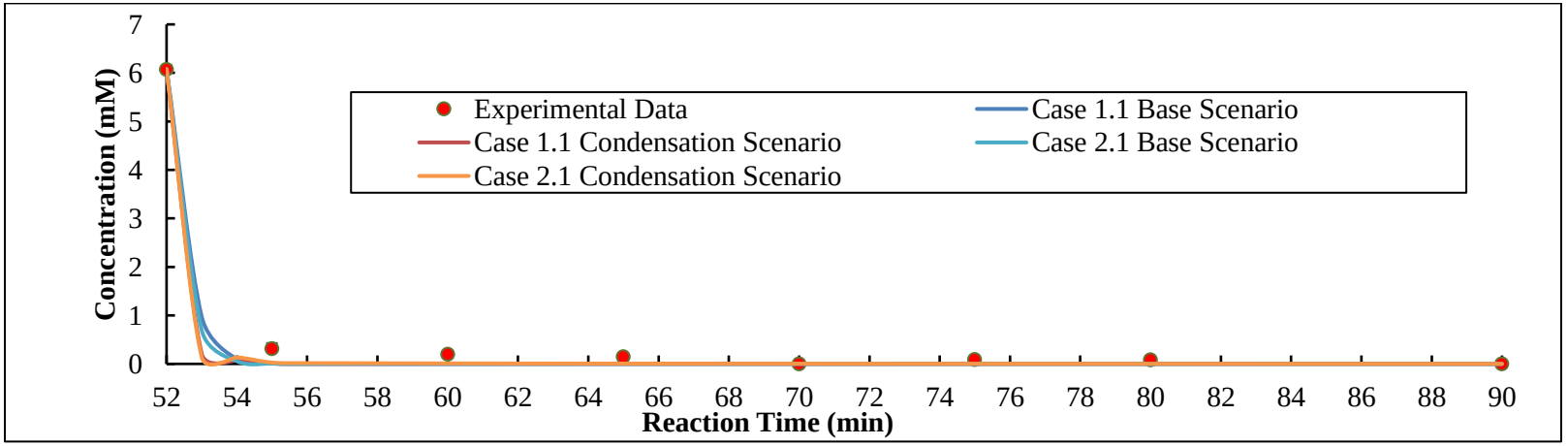

***Figure 44**: Simulated Concentration Profile of Glucose in the Cellulose-300 HTL Experiment.*

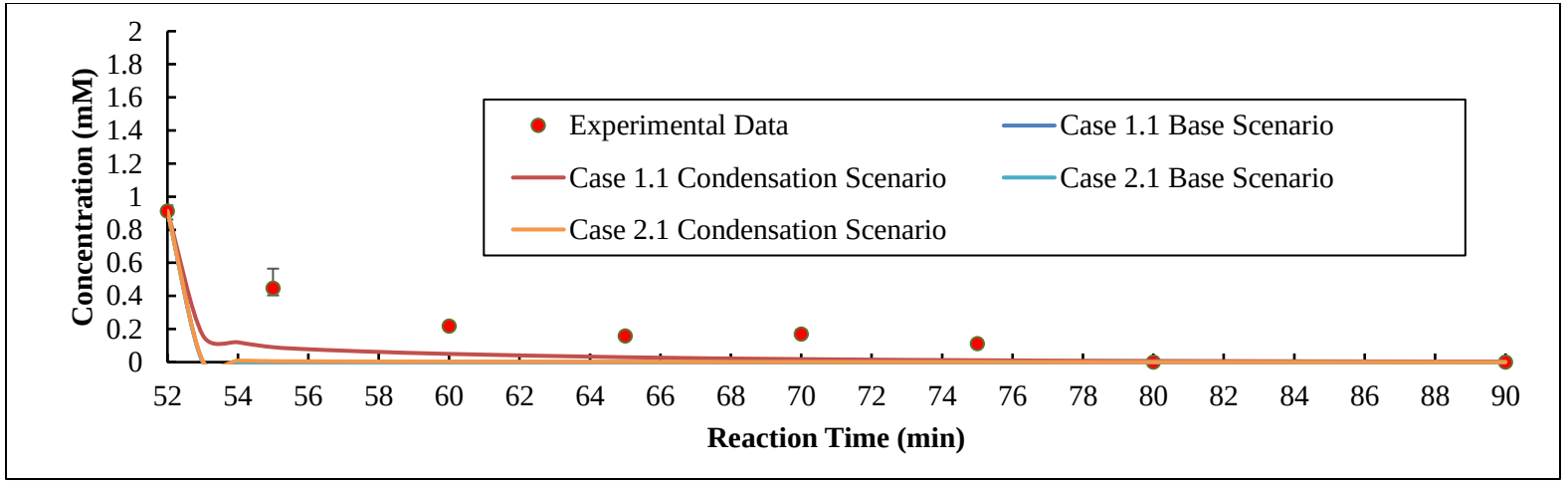

***Figure 45**: Simulated Concentration Profile of Fructose in the Cellulose-300 HTL Experiment.*

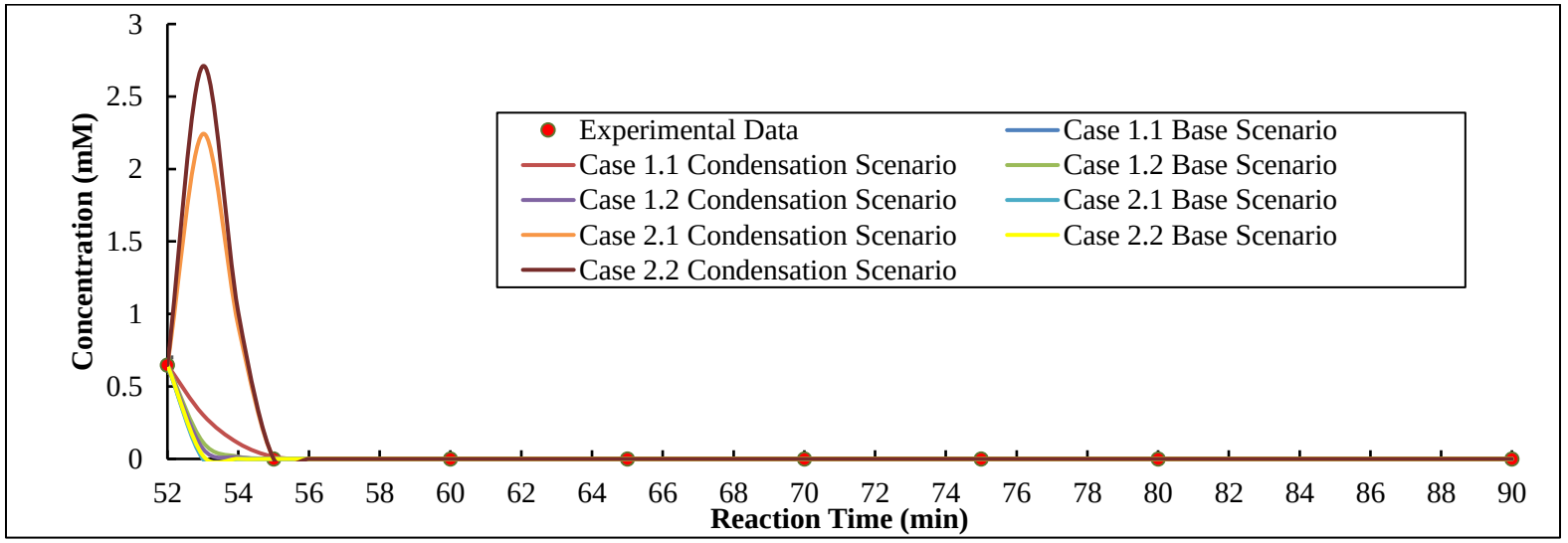

***Figure 46**: Simulated Concentration Profile of Cellobiose in the Cellulose-300 HTL Experiment.*

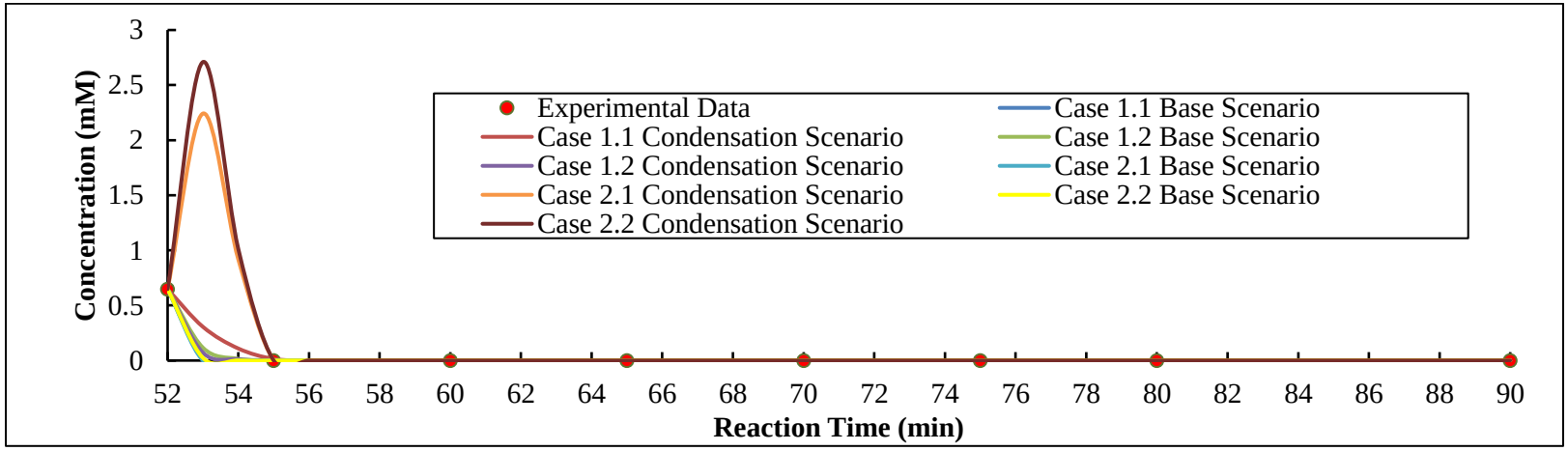

***Figure 47**: Simulated Concentration Profile of Cellotriose in the Cellulose-300 HTL Experiment.*

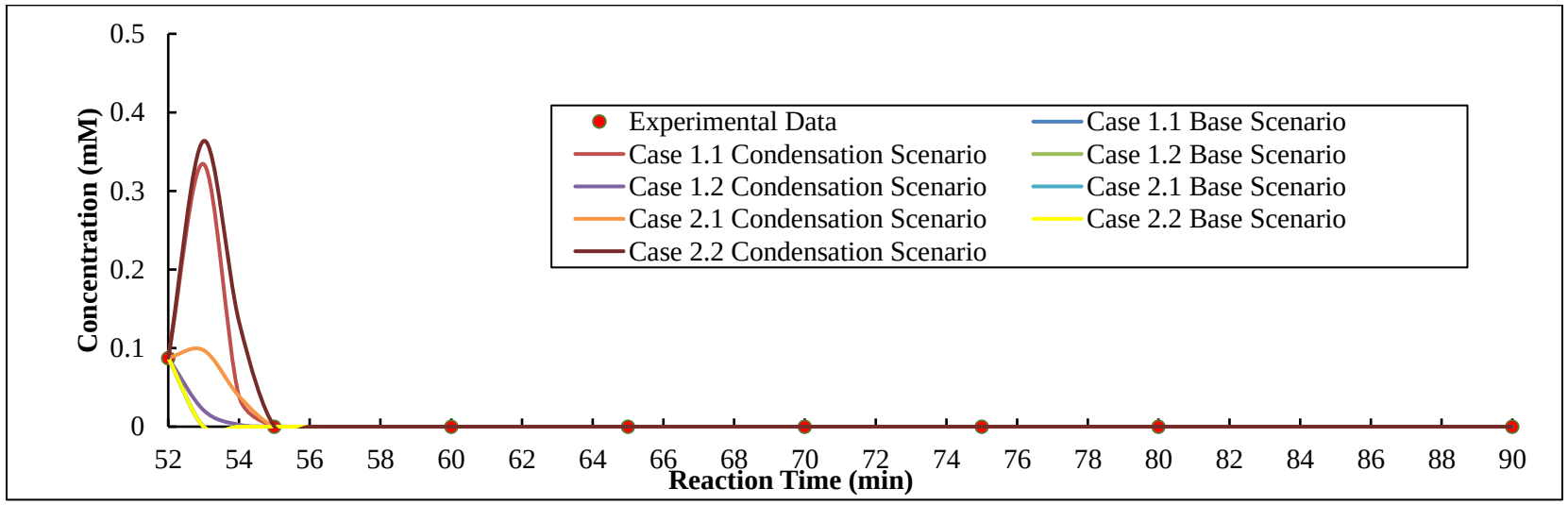

***Figure 48**: Simulated Concentration Profile of Cellotetraose in the Cellulose-300 HTL Experiment.*

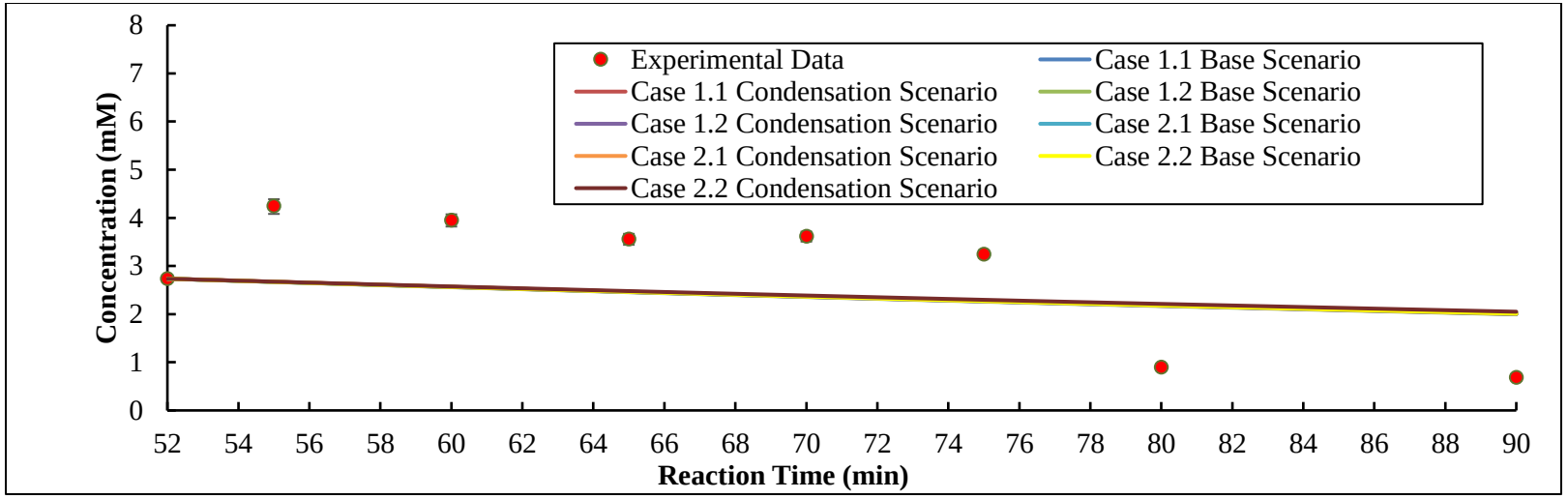

***Figure 49**: Simulated Concentration Profile of Glycolaldehyde in the Cellulose-300 HTL Experiment.*

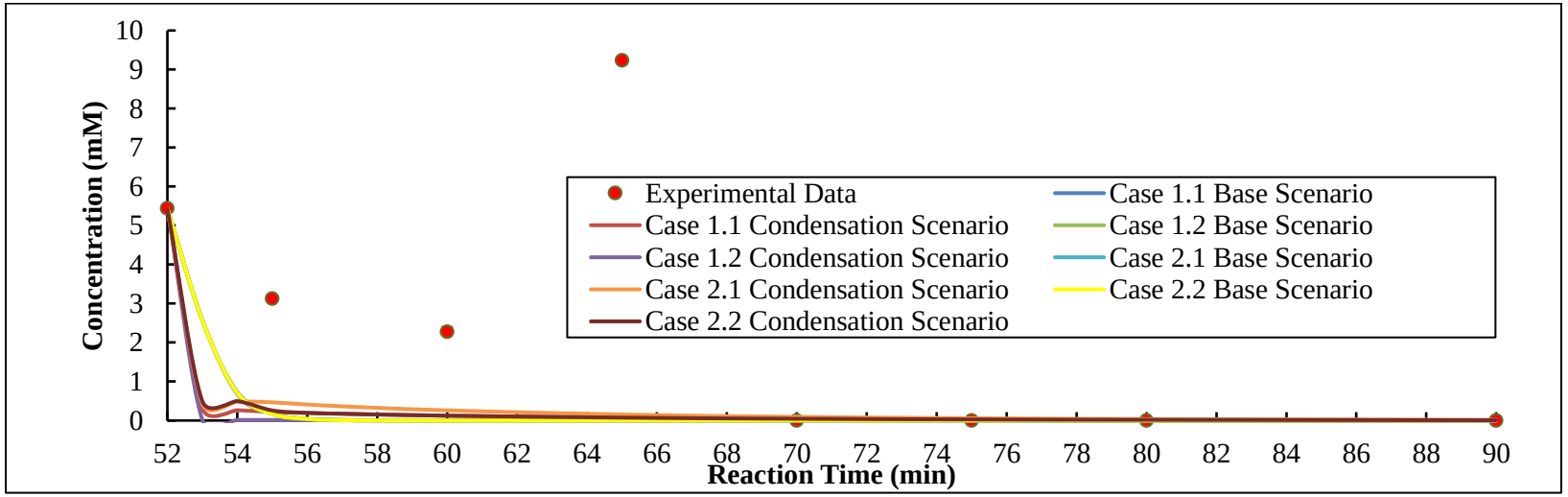

***Figure 50**: Simulated Concentration Profile of 5-HMF in the Cellulose-300 HTL Experiment.*

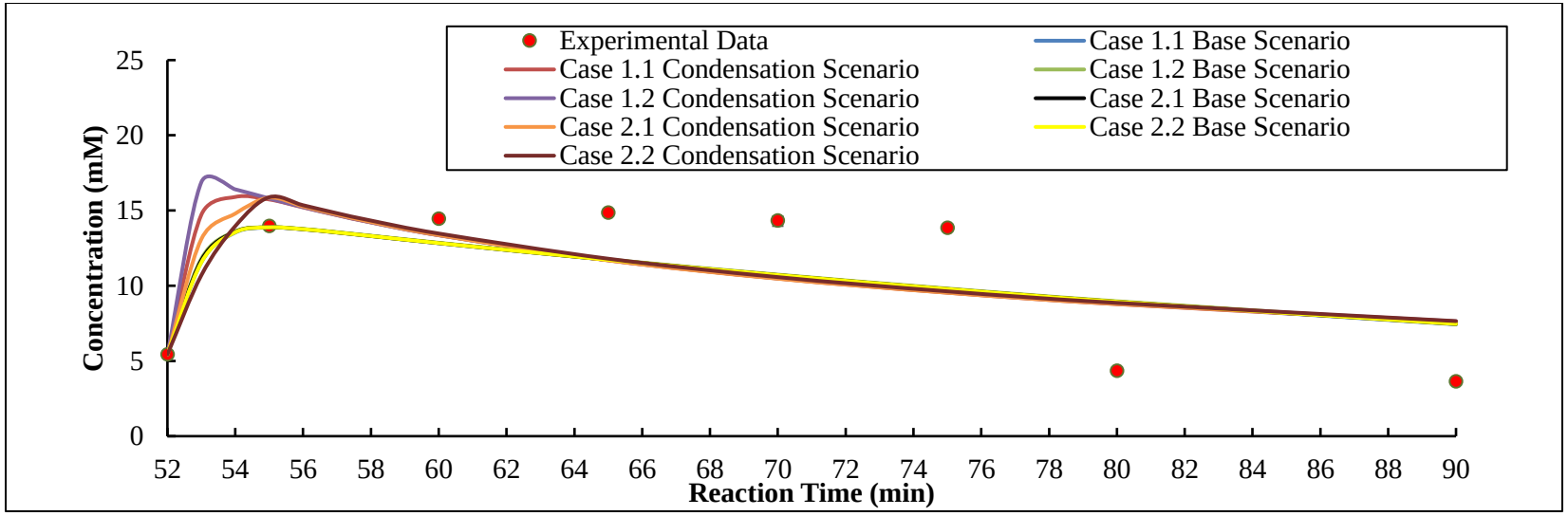

***Figure 51**: Simulated Concentration Profile of Levulinic Acid in the Cellulose-300 HTL Experiment.*

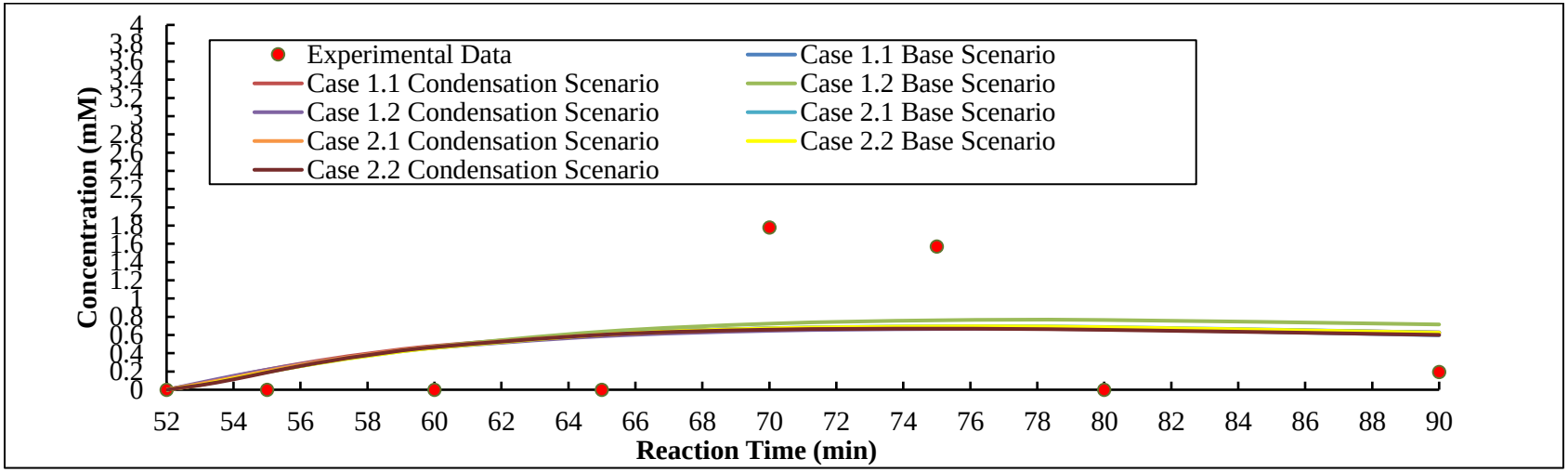

***Figure 52**: Simulated Concentration Profile of Succinic Acid in the Cellulose-300 HTL Experiment.*

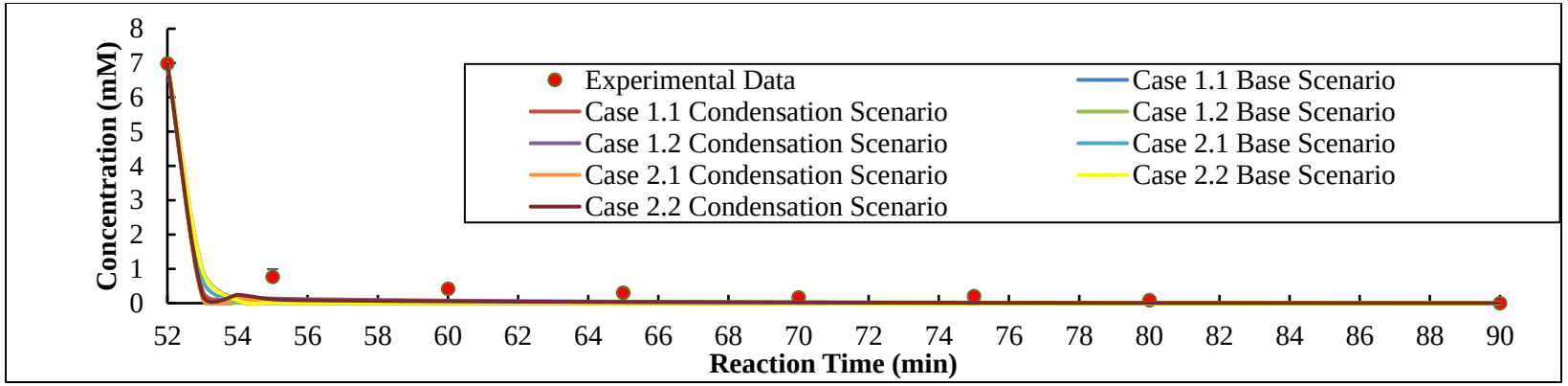

***Figure 53**: Simulated Concentration Profile of Cellulo-Monomers in the Cellulose-300 HTL Experiment.*

Glucose-275 HTL Experiment:

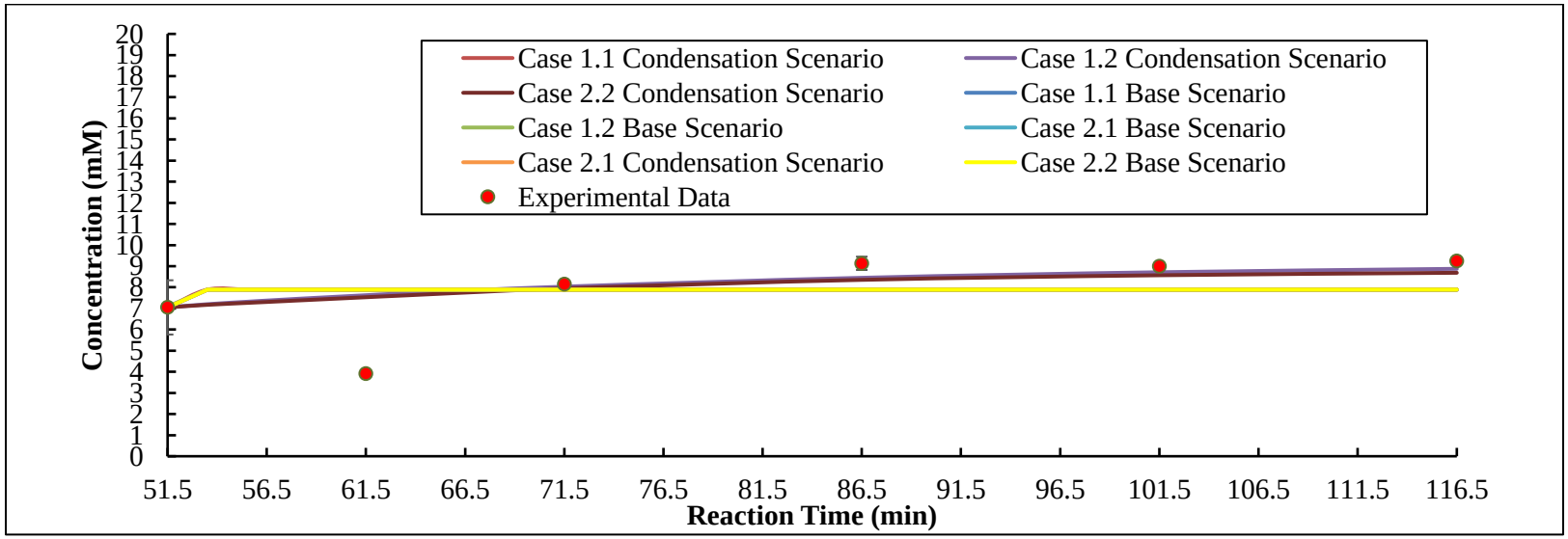

***Figure 54**: Simulated Concentration Profile of Acetic Acid in the Glucose-275 HTL Experiment.*

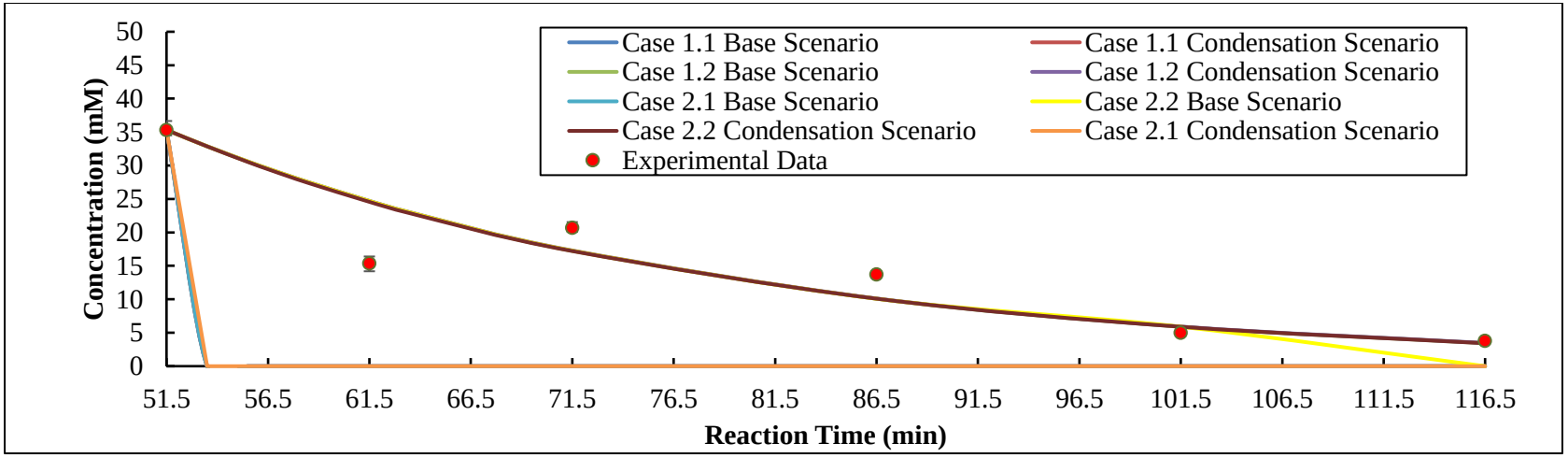

***Figure 55**: Simulated Concentration Profile of Formic Acid in the Glucose-275 HTL Experiment.*

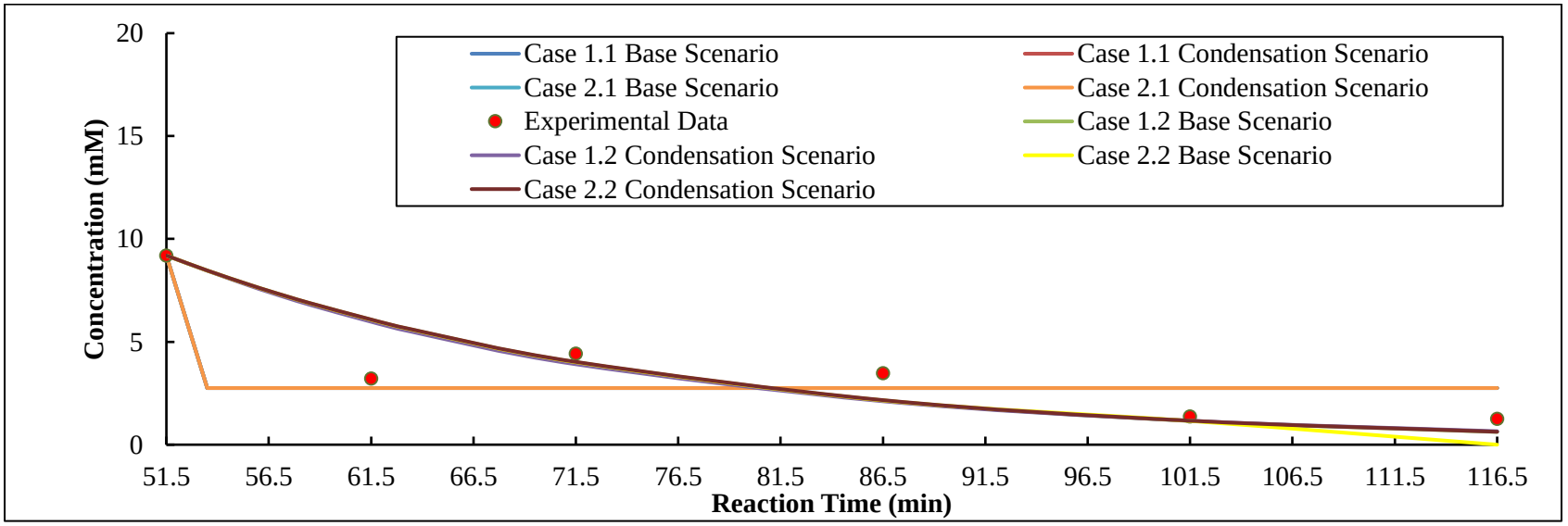

***Figure 56**: Simulated Concentration Profile of Furfural in the Glucose-275 HTL Experiment.*

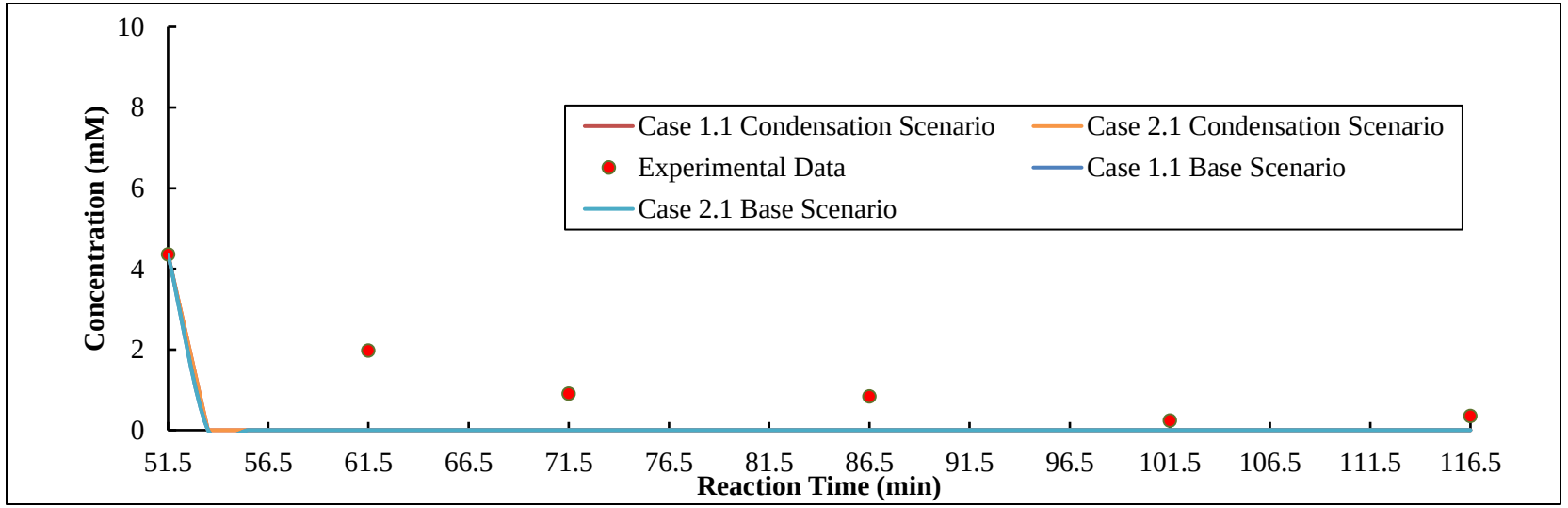

***Figure 57**: Simulated Concentration Profile of Glucose in the Glucose-275 HTL Experiment.*

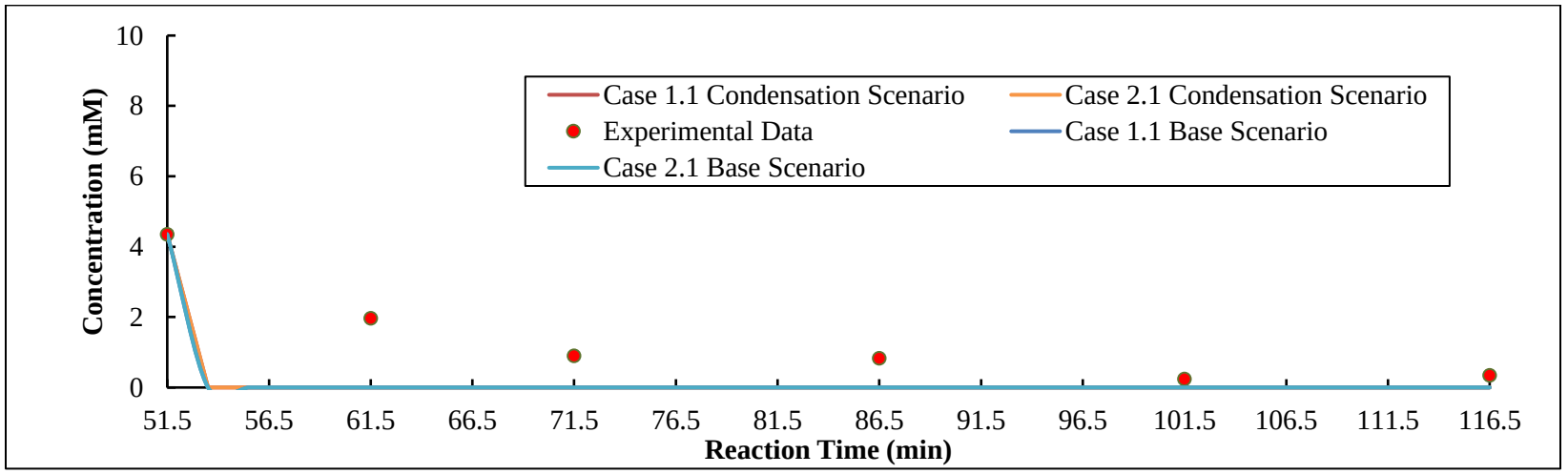

***Figure 58**: Simulated Concentration Profile of Fructose in the Glucose-275 HTL Experiment.*

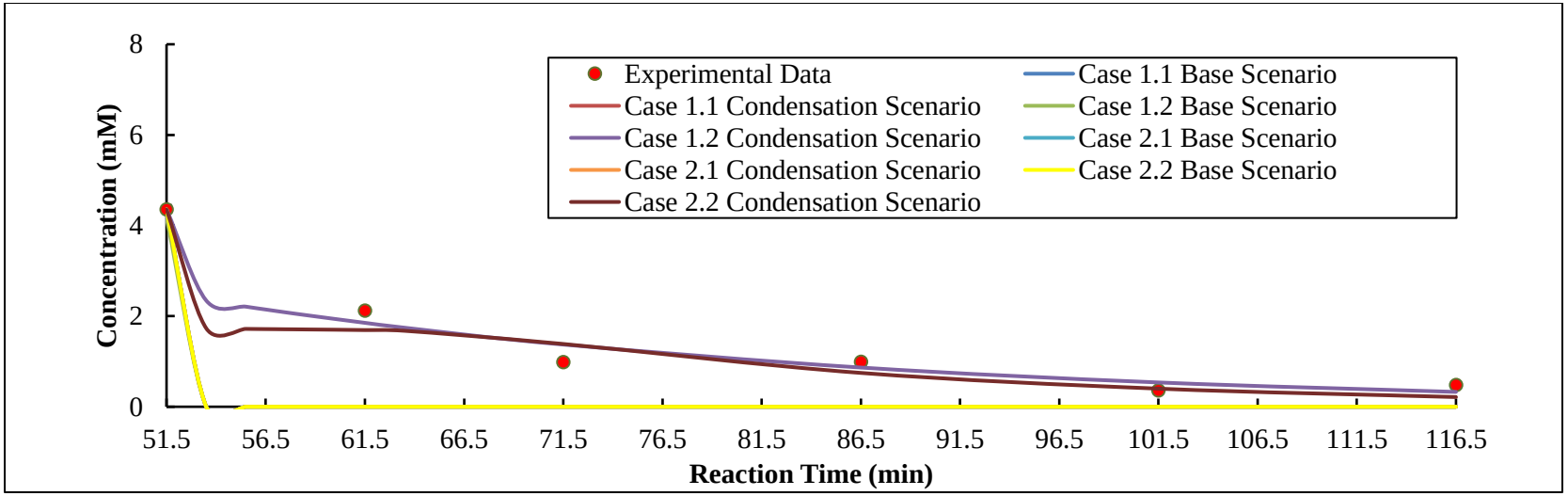

***Figure 59**: Simulated Concentration Profile of Cellulo-Monomers in the Glucose-275 HTL Experiment.*

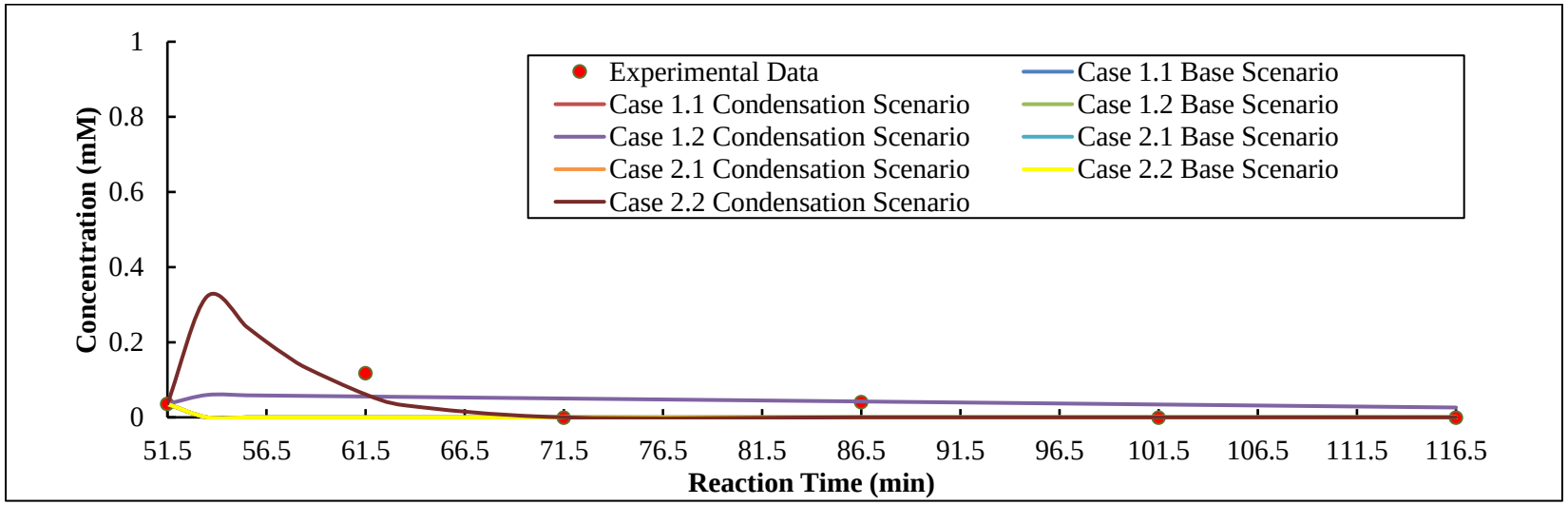

***Figure 60**: Simulated Concentration Profile of Cellubiose in the Glucose-275 HTL Experiment.*

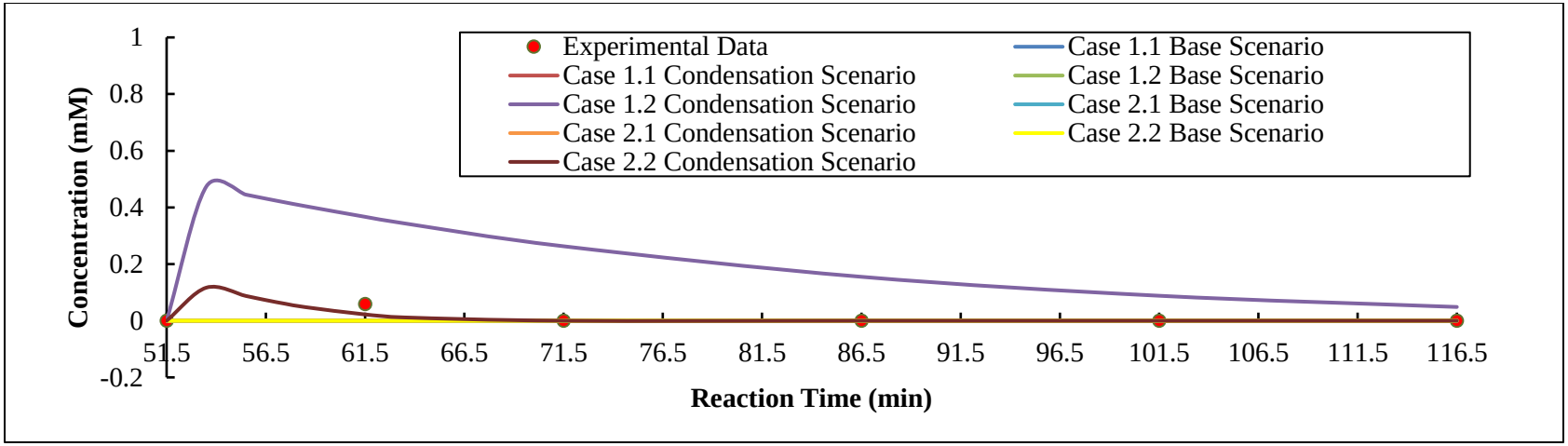

***Figure 61**: Simulated Concentration Profile of Cellotriose in the Glucose-275 HTL Experiment.*

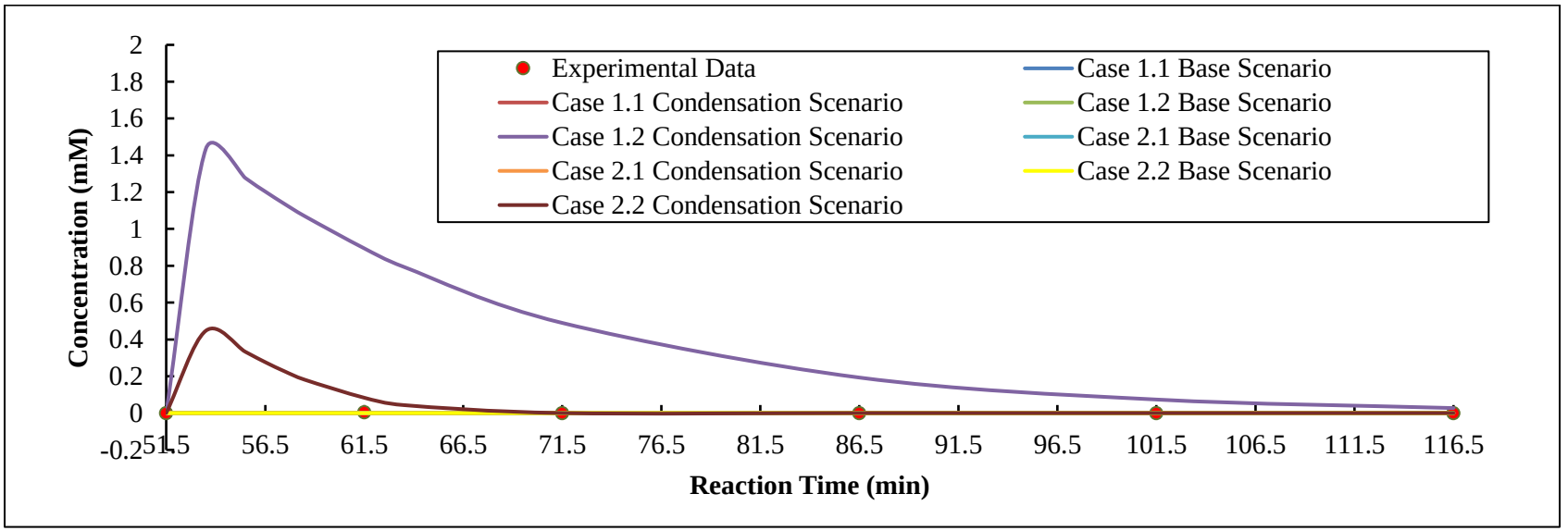

***Figure 62**: Simulated Concentration Profile of Cellotetraose in the Glucose-275 HTL Experiment.*

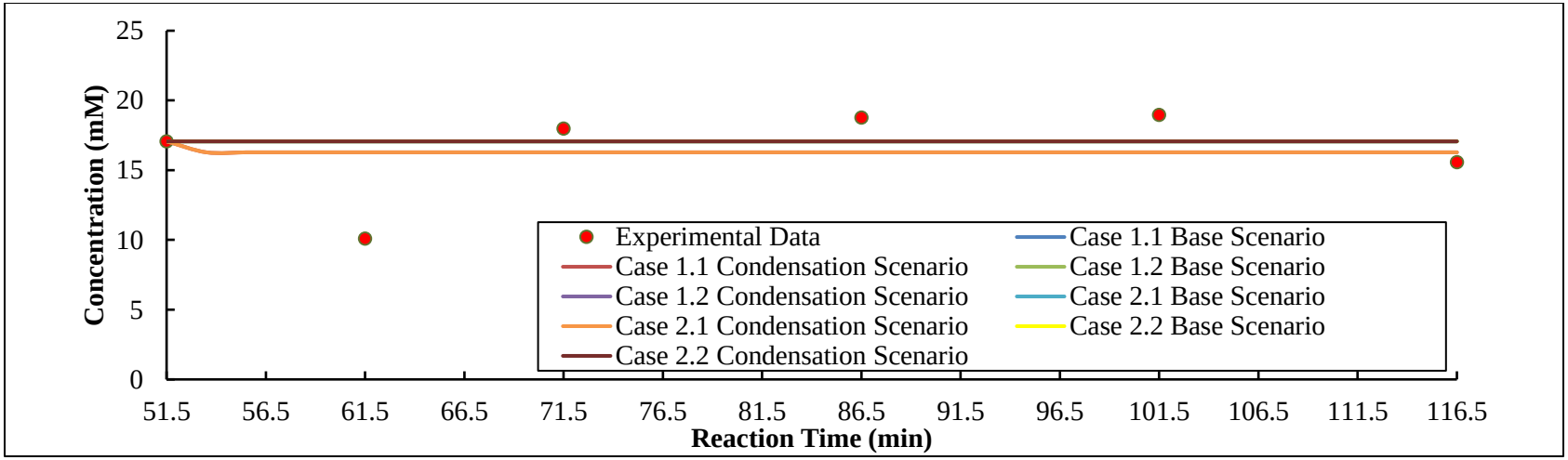

***Figure 63**: Simulated Concentration Profile of Levulinic Acid in the Glucose-275 HTL Experiment.*

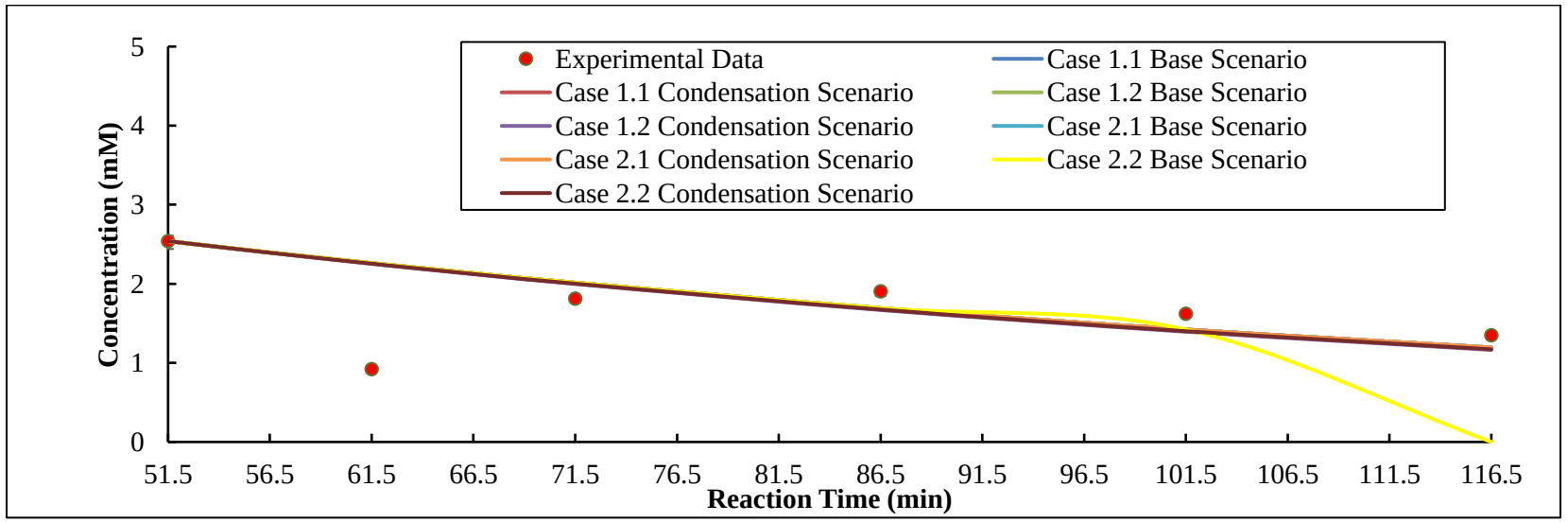

***Figure 64**: Simulated Concentration Profile of Glycolaldehyde in the Glucose-275 HTL Experiment.*

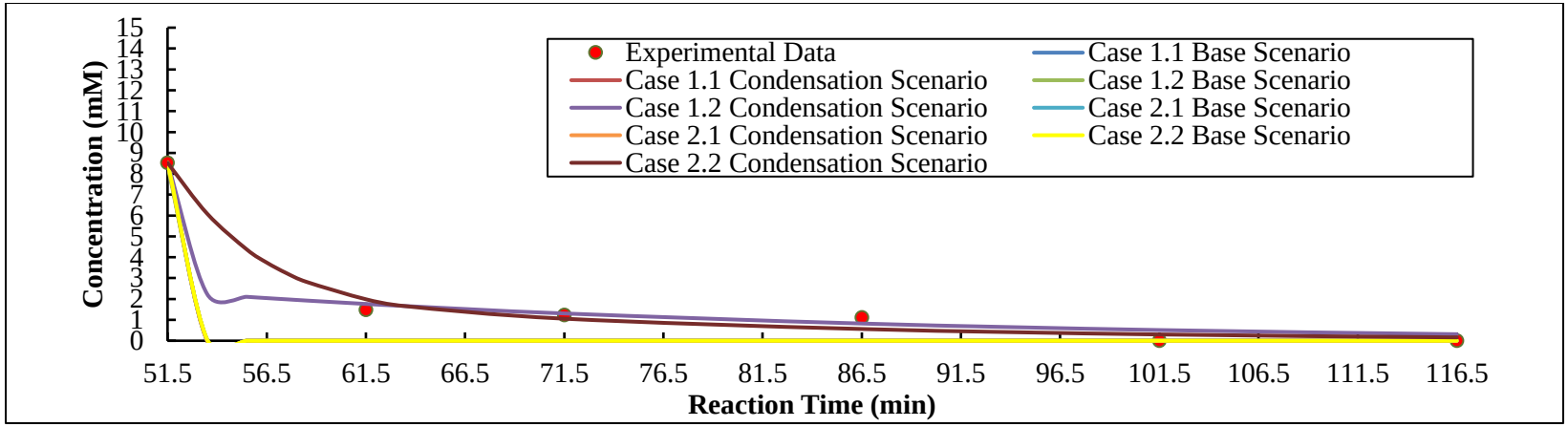

***Figure 65**: Simulated Concentration Profile of 5-HMF in the Glucose-275 HTL Experiment.*

Glucose-300 HTL Experiment:

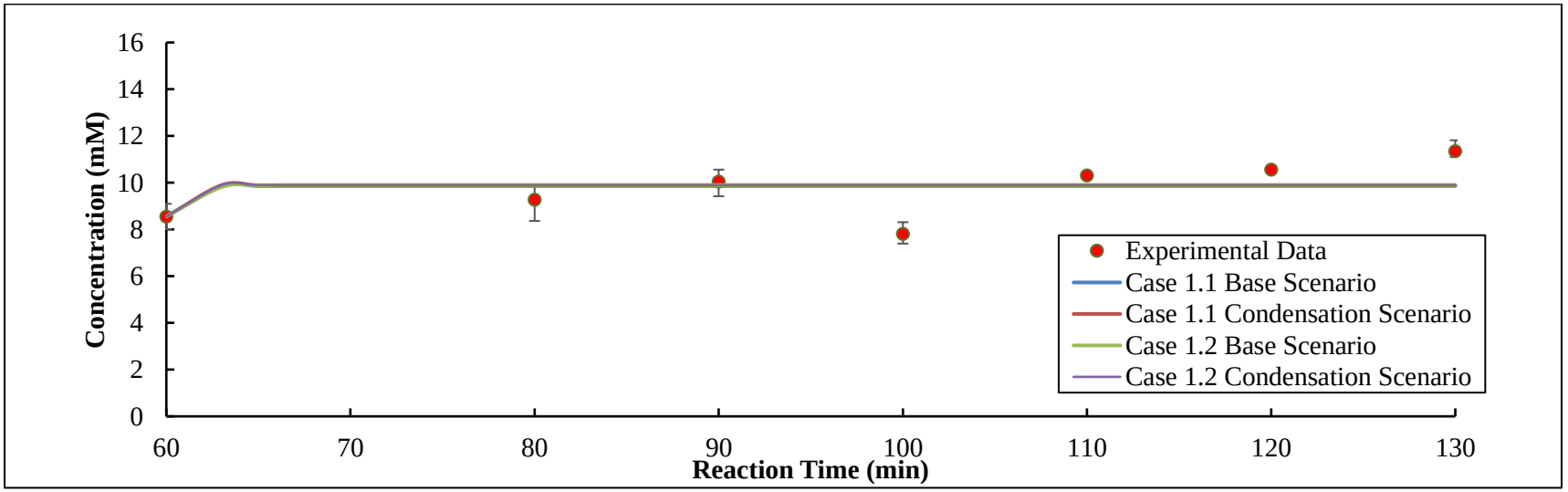

***Figure 66**: Simulated Concentration Profile of Acetic Acid in the Glucose-300 HTL Experiment.*

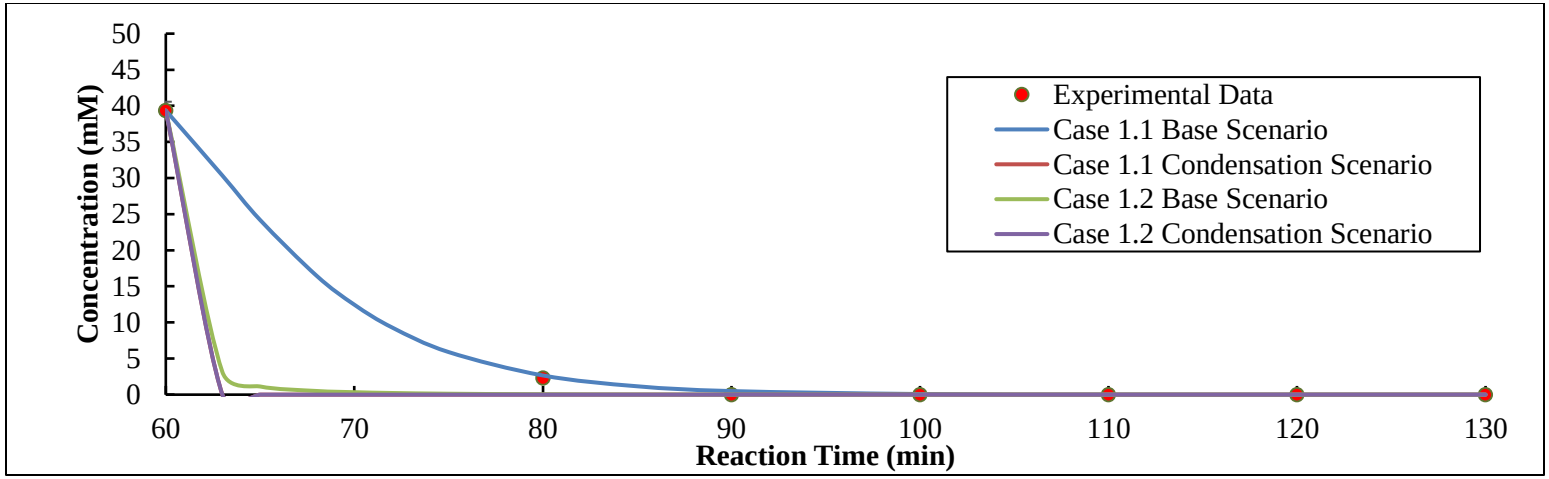

***Figure 67**: Simulated Concentration Profile of Formic Acid in the Glucose-300 HTL Experiment.*

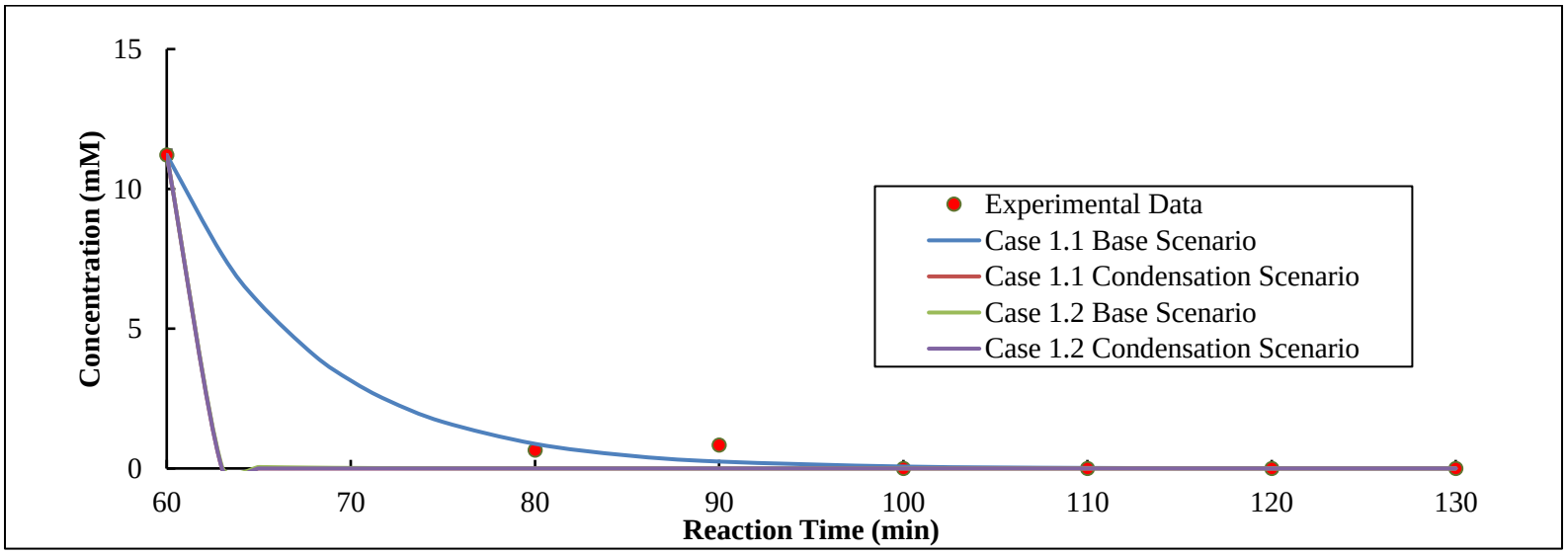

***Figure 68**: Simulated Concentration Profile of Furfural in the Glucose-300 HTL Experiment.*

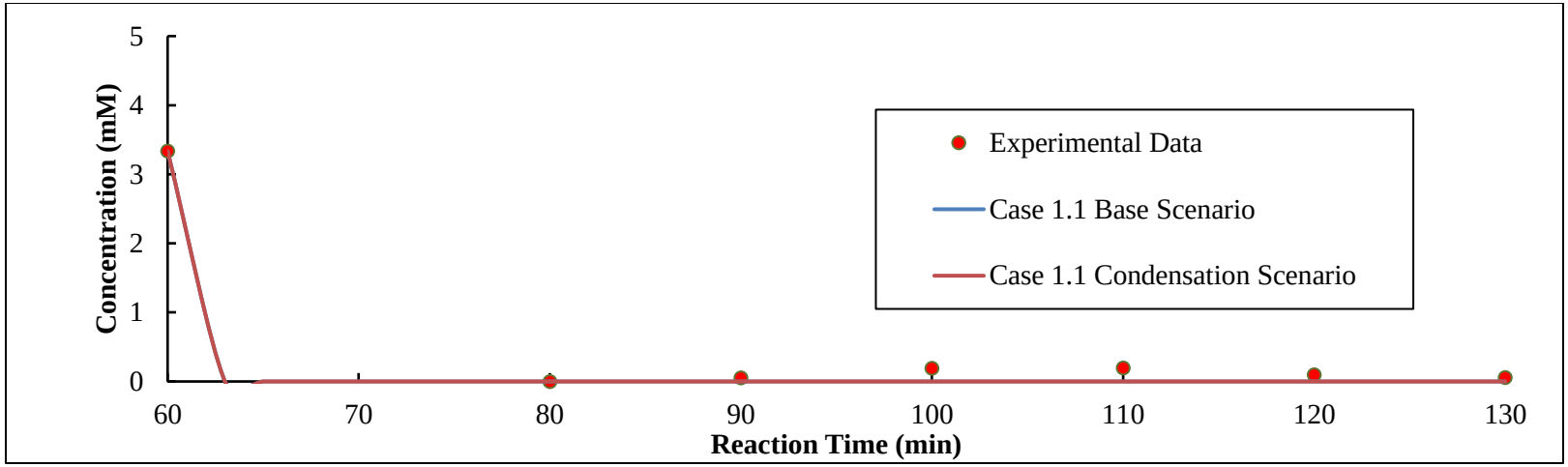

***Figure 69**: Simulated Concentration Profile of Glucose in the Glucose-300 HTL Experiment.*

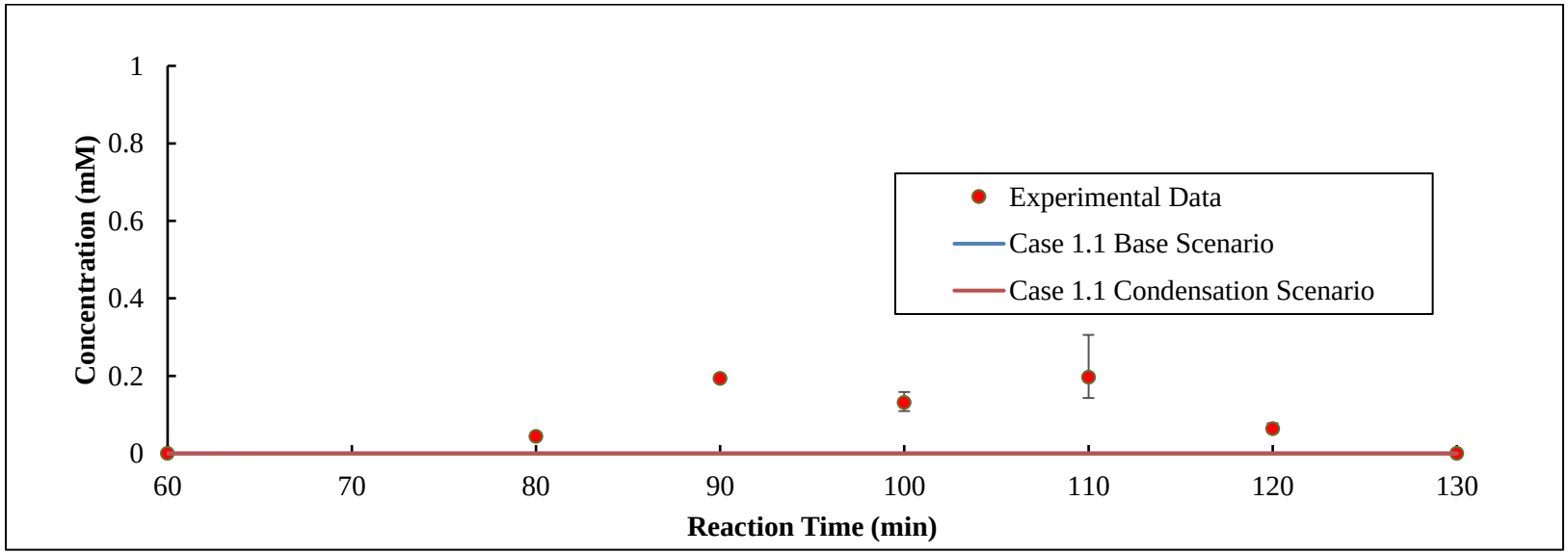

***Figure 70**: Simulated Concentration Profile of Fructose in the Glucose-300 Hydrothermal Experiment.*

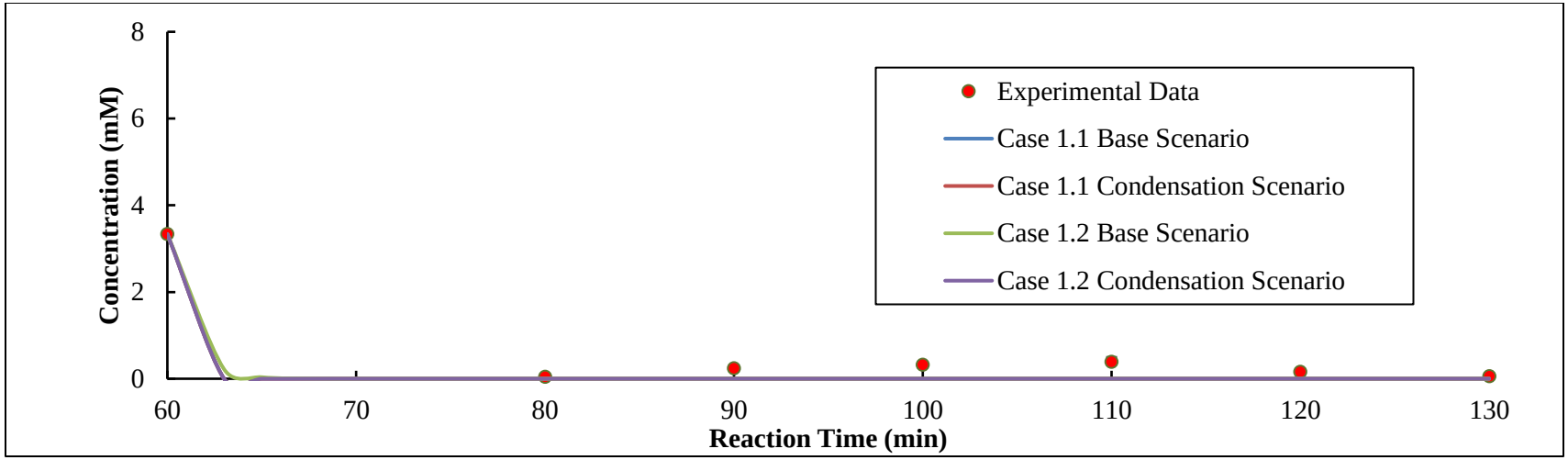

***Figure 71**: Simulated Concentration Profile of Cellulo-Monomers in the Glucose-300 HTL Experiment.*

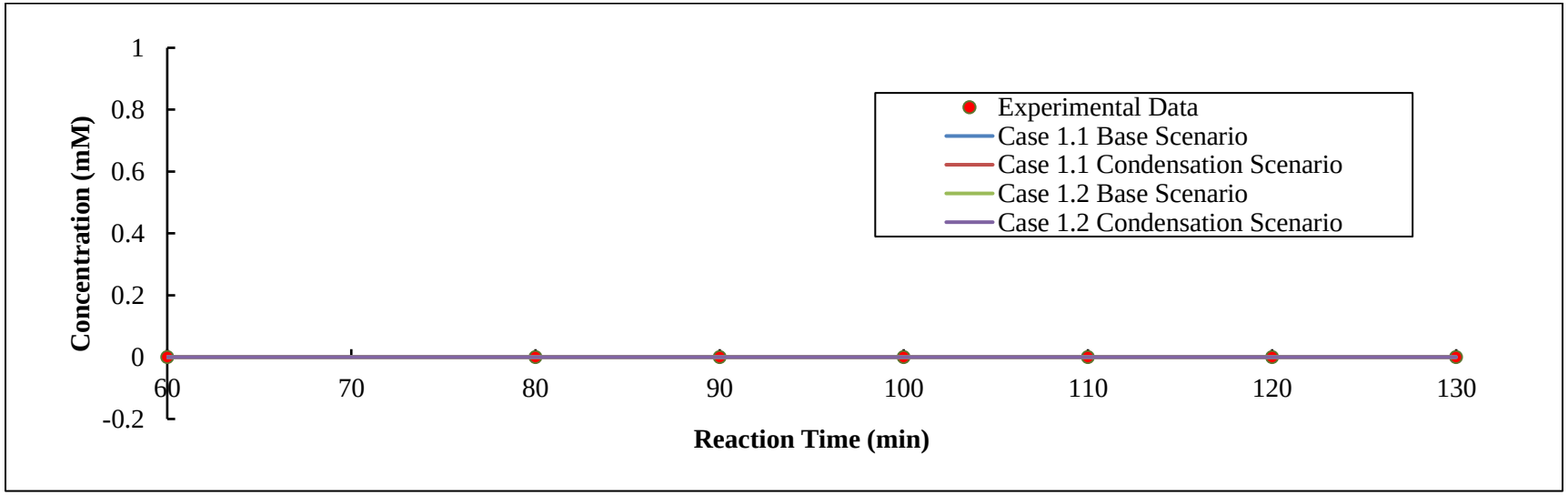

***Figure 72**: Simulated Concentration Profile of Cellobiose in the Glucose-300 HTL Experiment.*

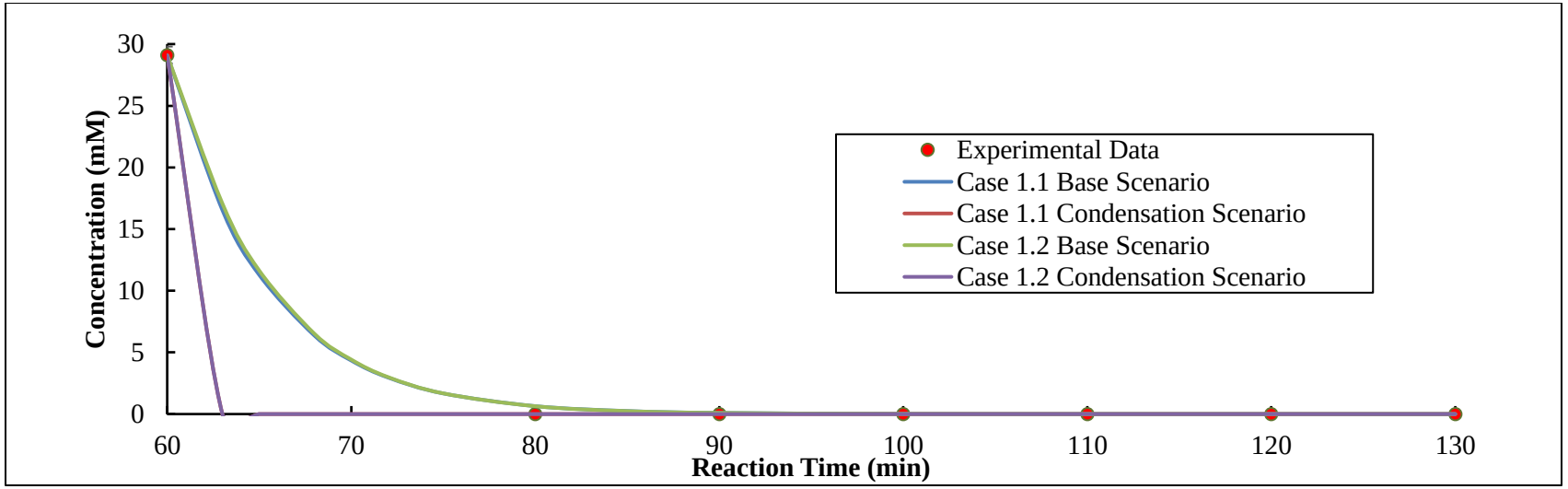

***Figure 73**: Simulated Concentration Profile of 5-HMF in the Glucose-300 HTL Experiment.*

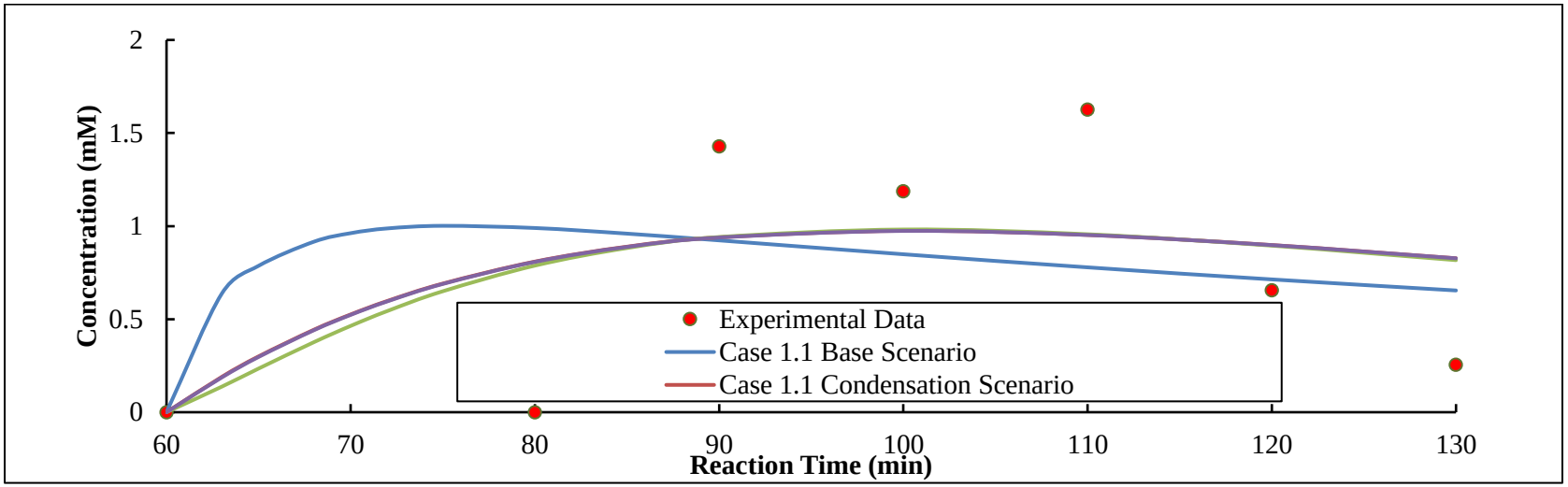

***Figure 74**: Simulated Concentration Profile of Succinic Acid in the Glucose-300 HTL Experiment.*

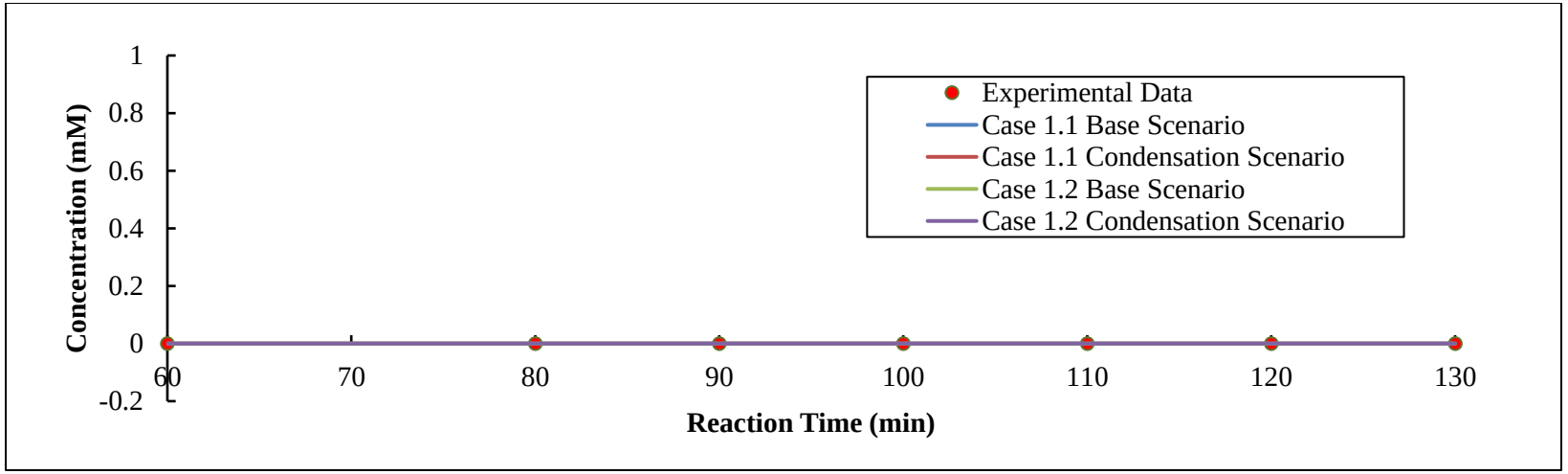

***Figure 75**: Simulated Concentration Profile of Cellotriose in the Glucose-300 HTL Experiment.*

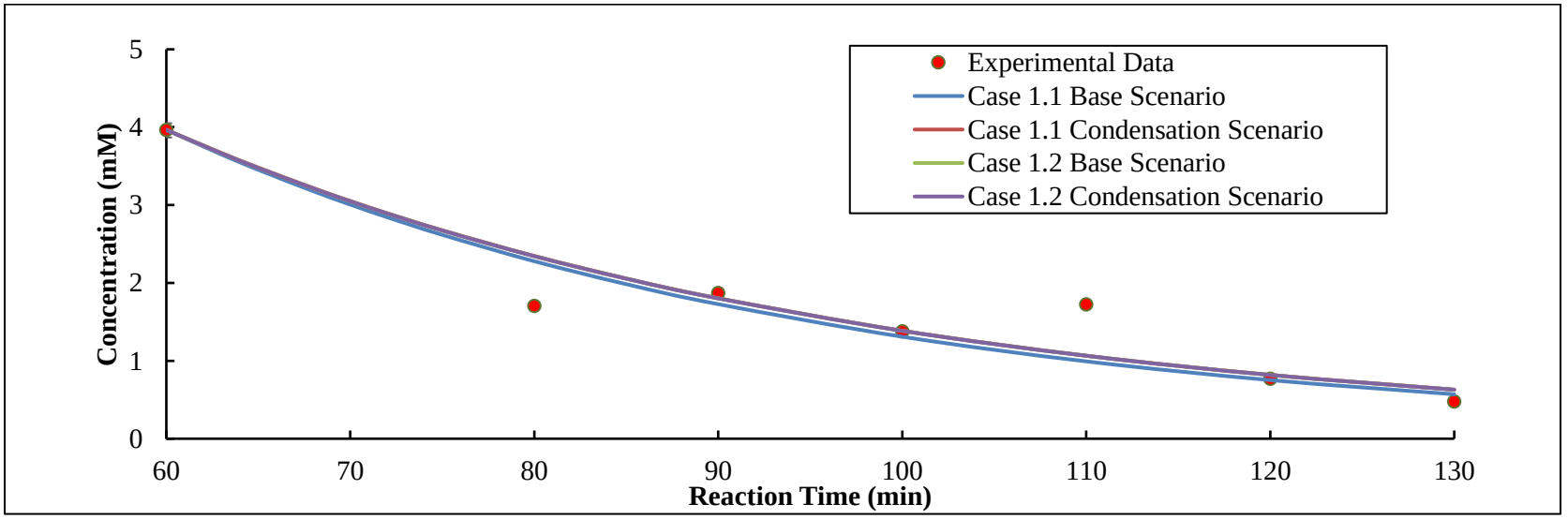

***Figure 76**: Simulated Concentration Profile of Glycolaldehyde in the Glucose-300 HTL Experiment.*

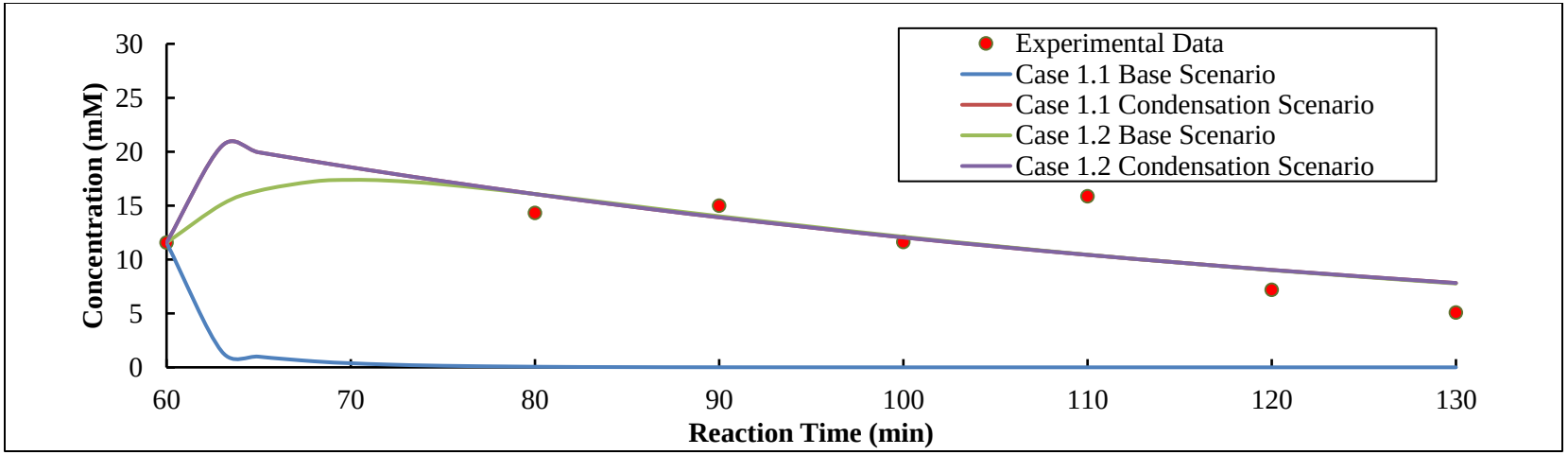

***Figure 77**: Simulated Concentration Profile of Levulinic Acid in the Glucose-300 HTL Experiment.*

REFERENCES

Albanez, R., Lovato, G., Zaiat, M., Ratusznei, S., & Rodrigues, J. A. (2016). Optimization, metabolic pathways modeling and scale-up estimative of an AnSBBR applied to biohydrogen production by co-digestion of vinasse and molasses. *International Journal of Hydrogen Energy*, 20473-20484.

Amarasekara, A., & Wiredu, B. (2014). Acidic Ionic Liquid Catalyzed One-Pot Conversion of Cellulose to Ethyl Levulinate and Levulinic Acid in Ethanol-Water Solvent System. *BioEnergy Research*, 1237-1243.

Antal Jr, M. J., Mok, W. S., & Richards, G. N. (1990). Four-carbon model compounds for the reactions of sugars in water at high temperature. *Carbohydrate Research*, 111-115.

Antal Jr, M. J., Mok, W. S., & Richards, G. N. (1990). Mechanism of formation of 5-(hydroxymethyl)-2-furaldehyde from d-fructose and sucrose. *Carbohydrate Research*, 91-109.

Archer, D., & Wang, P. (1990). The Dielectric Constant of Water and Debye-Hückel Limiting Law Slopes. *Journal of Physical and Chemical Reference Data*, 371-411.

Artemenko S., M. V. (2014). Phase Behavior of Biomass Components in Supercritical Water. In X. C. Fang Z., *Near-critical and Supercritical Water and Their Applications for Biorefineries* (p. 42). Dordrecht: Springer Netherlands.

Asghari, F. S., & Yoshida, H. (2007). Kinetics of the Decomposition of Fructose Catalyzed by Hydrochloric Acid in Subcritical Water: Formation of 5-Hydroxymethylfurfural, Levulinic, and Formic Acids. *Industrial and engineering chemistry research*, 7703-7710.

Baeza-Baeza, J., Torres-Lapasió, J., & García-Álvarez-Coque, M. (2011). Approaches to estimate the time and height at the peak maximum in liquid chromatography based on a modified Gaussian model. *Journal of Chromatography A*, 1385-1392.

Bandura, A., & Lvov, S. (2006). The Ionization Constant of Water over Wide Ranges of Temperature and Density. *Journal of Physical and Chemical Reference Data*, 15-30.

Bhatia, S., Kim, S. H., Yoon, J. J., & Yang, Y. H. (2017). Current status and strategies for second generation biofuel production using microbial systems. *Energy Conversion and Management*, 1142-1156.

Bonn, G., Rinderer, M., & Bobleter, O. (2006). Hydrothermal Degradation and Kinetic Studies of 1,3-Dihydroxy-2-Propanone and 2,3-Dihydroxypropanal. *Journal of Carbohydrate Chemistry*, 67-77.

Cantero-Tubilla, B. (2017, August). *Valorization of Residues from Agricultural and Food Industries towards Biofuels and Bioproducts Using Biochemical and Thermochemical Technologies.* Retrieved April 9, 2018, from ProQuest: https://search.proquest.com/docview/1964276841?pq-origsite=gscholar

Cantero-Tubilla, B., Cantero, D. A., Martinez, C. M., Tester, J. W., Walker, L. P., & Posmanik, R. (2017). Characterization of the solid products from hydrothermal liquefaction of waste feedstocks from food and agricultural industries. *The Journal of Supercritical Fluids*, 665-673.

Cavanillas, S., Serrano, N., Di´az-Cruz, J., Ariño, C., & Esteban, M. (2016). Parametric signal fitting of highly asymmetric voltammograms by using the exponentially modified Gaussian (EMG) function. *Chemometrics and Intelligent Laboratory Systems*, 80-87.

Croce, A., Battistel, E., Chiaberge, S., Spera, S., De Angelis, F., & Reale, S. (2017). A Model Study to Unravel the Complexity of Bio-Oil from Organic Wastes. *Chemistry & Sustainability*, 171-181.

Croce, A., Battistel, E., Chiaberge, S., Spera, S., Reale, S., & de Angelis, F. (2015). Mass Spectrometry and Nuclear Magnetic Resonance Spectroscopy Study of Carbohydrate Decomposition by Hydrothermal Liquefaction Treatment: A Modeling Approach on Bio-oil Production from Organic Wastes. *Energy & Fuels*, 5847-5856.

Daker, M. (n.d.). *Challenges of Ethanol Production from Lignocellulosic Biomass.* Retrieved April 8, 2018, from Katzen International, Inc.: http://www.katzen.com/ethanol101/Lignocellulosic%20Biomass.pdf

de Caprariis, B., De Filippis, P., Petrullo, A., & Scarsella, M. (2017). Hydrothermal liquefaction of biomass: Influence of temperature and biomass composition on the bio-oil production. *Fuel*, 618-625.

Dias, G. S., Luz Jr., L. F., Mitchell, D. A., & Krieger, N. (2017). Scale-up of biodiesel synthesis in a closed-loop packed-bed bioreactor system using the fermented solid produced by Burkholderia lata LTEB11. *Chemical Engineering Journal*, 341-349.

Dote, Y., Sawayama, S., Inoue, S., Minowa, T., & Yokoyama, S. (1994). Recovery of liquid fuel from hydrocarbon-rich microalgae by thermochemical liquefaction. *Fuel*, 1855-1857.

Duan, P., & Savage, P. (2011). Hydrothermal Liquefaction of a Microalga with Heterogeneous Catalysts. *Industrial and Engineering Chemistry Research*, 52-61.

Engineering Toolbox. (2003). *Fuels - Higher and Lower Calorific Values.* Retrieved April 6, 2018, from https://www.engineeringtoolbox.com/fuels-higher-calorific-values-d_169.html

Felinger, A. (1994). Deconvolution of Overlapping Skewed Peaks. *Analytical Chemistry*, 3066–3072.

Garcı´a Alba, L., Torri, C., Samori, C., van der Spek, J., Fabbri, D., & Kersten, S. (2012). Hydrothermal Treatment (HTT) of Microalgae: Evaluation of the Process As Conversion Method in an Algae Biorefinery Concept. *Energy & Fuels*, 642-657.

Goodman, K., & Brenna, J. (1994). Curve Fitting for Restoration of Accuracy for Overlapping Peaks in Gas Chromatography/Combustion Isotope Ratio Mass Spectrometry. *Analytical Chemistry*, 1294-1301.

IPCC. (2014). *Climate Change 2014: Synthesis Report. Contribution of Working Groups I, II and III to the Fifth Assessment Report of the Intergovernmental Panel on Climate Change.* Geneva, Switzerland: IPCC.

Jin, F., Zhou, Z., Enomoto, H., Moriya, T., & Higashijima, H. (2004). Conversion Mechanism of Cellulosic Biomass to Lactic Acid in Subcritical Water and Acid–Base Catalytic Effect of Subcritical Water. *Chemistry Letters*, 126-127.

Jin, G., Xue, X., Zhang, F., Zhang, X., Xu, Q., Jin, Y., & Liang, X. (2008). Prediction of retention times and peak shape parameters of unknown compounds in traditional Chinese medicine under gradient conditions by ultra performance liquid chromatography. *Analytica Chimica Acta*, 95-103.

Kabyemela, B., Adschiri, T., Malaluan, R., & Arai, K. (1999). Glucose and Fructose Decomposition in Subcritical and Supercritical Water: Detailed Reaction Pathway, Mechanisms, and Kinetics. *Industrial & Engineering Chemistry Research*, 2888-2895.

Kawasumi, R., Narita, S., Miyamoto, K., Tominaga, K., Takita, R., & Uchiyama, M. (2017). One-step Conversion of Levulinic Acid to Succinic Acid Using I2/t-BuOK System: The Iodoform Reaction Revisited. *Scientific Reports*, 17967.

Knez, Ž., Škerget, M., & Pavlovič, I. (2013). Subcritical Water - a Perspective Reaction Media for Biomass Processing to Chemicals: Study on Cellulose Conversion as a Model for Biomass. *Chemical and Biochemical Engineering Quarterly*, 73-82.

Kong, H., Ye, F., Lu, X., Guo, L., Tian, J., & Xu, G. (2005). Deconvolution of overlapped peaks based on the exponentially modified Gaussian model in comprehensive two-dimensional gas chromatography. *Journal of Chromatography A*, 160-164.

Koomyart, I., Nagamizu, H., Khuwijitjaru, P., Kobayashi, T., Shiga, H., Yoshii, H., & Adachi, S. (2016). Using severity factor as a parameter to optimize krill treatment under subcritical water conditions. *Bioscience, Biotechnology, and Biochemistry*, 2192-2197.

Krishna, R., Kallury, M., Ambidge, C., Tidwell, T. T., Boocock, D. G., Agblevor, F. A., & Stewart, D. J. (1986). Rapid hydrothermolysis of cellulose and related carbohydrates. *Carbohydrate Research*, 253-261.

Kröger, M., Hartmann, F., & Klemm, M. (2013). Hydrothermal Treatment of Carboxy-methyl Cellulose Salt: Formation and Decomposition of Furans, Pentenes and Benzenes. *Chemical Engineering & Technology*, 287-294.

Kumar, S., & Gupta, R. B. (2009). Biocrude Production from Switchgrass Using Subcritical Water. *Energy & Fuels*, 5151-5159.

Li, J. (2002). Comparison of the capability of peak functions in describing real chromatographic peaks. *Journal of Chromatography A*, 63-70.

Li, R., Xie, Y., Yang, T., Li, B., Zhang, Y., & Kai, X. (2016). Characteristics of the products of hydrothermal liquefaction combined with cellulosic bio-ethanol process. *Energy*, 862-867.

Lin, R., Cheng, J., Ding, L., Song, W., Qi, F., Zhou, J., & Cen, K. (2015). Subcritical water hydrolysis of rice straw for reducing sugar production with focus on degradation by-products and kinetic analysis. *Bioresource Technology*, 8-14.

López Barreiro, D., Prins, W., Ronsse, F., & Brilman, W. (2013). Hydrothermal liquefaction (HTL) of microalgae for biofuel production: State of the art review and future prospects. *Biomass and Bioenergy*, 113-127.

Luijkx, G. C., van Rantwijk, F., & van Bekkum, H. (1993). Hydrothermal formation of 1,2,4-benzenetriol from 5-hydroxymethyl-2-furaldehyde and d-fructose. *Carbohydrate Research*, 131-139.

Marshall, W., & Franck, E. (1981). Ion product of water substance, 0–1000 °C, 1–10,000 bars New International Formulation and its background. *Journal of Physical and Chemical Reference Data*, 295-304.

Matsugami, M., Yoshida, N., & Hirata, F. (2014). Theoretical characterization of the "ridge" in the supercritical region in the fluid phase diagram of water. *Journal of Chemical Physics*, 104511.

Matsui, T., Nishihara, A., Ueda, C., Ohtsuki, M., Ikenaga, N., & Suzuki, T. (1997). Liquefaction of micro-algae with iron catalyst. *Fuel*, 1043-1048.

Minowa, T., Yokoyama, S., Kishimoto, M., & Okakura, T. (1995). Oil production from algal cells of Dunaliella tertiolecta by direct thermochemical liquefaction. *Fuel*, 1735-1738.

Ogihara, Y. S. (2005). Direct observation of cellulose dissolution in subcritical and supercritical water over a wide range of water densities (550–1000 kg/m3). *Cellulose*, 595–606.

Patwardhan, P. R., Timko, M. T., Class, C. A., Bonomi, R. E., Kida, Y., Hernandez, H. H., . . . Green, W. H. (2013). Supercritical Water Desulfurization of Organic Sulfides Is Consistent with Free-Radical Kinetics. *Energy & Fuels*, 6108-6117.

Peterson, A., Vogel, F., Lachance, R., Froling, M., Antal, M. J., & Tester, J. (2008). Thermochemical biofuel production in hydrothermal media: A review of sub- and supercritical water technologies. *Energy, Environmental Science*, 32-65.

Podolean, I., Rizescu, C., Bala, C., Rotariu, L., Parvulescu, V. I., Coman, S. M., & Garcia, H. (2016). Unprecedented Catalytic Wet Oxidation of Glucose to Succinic Acid Induced by the Addition of n-Butylamine to a RuIII Catalyst. *Chemistry and Sustainability*, 2307-2311.

Posmanik, R., Cantero, D. A., Malkani, A., Sills, D. L., & Tester, J. (2017). Biomass conversion to bio-oil using sub-critical water: Study of model compounds for food processing waste. *The Journal of Supercritical Fluids*, 26-35.

Posmanik, R., Martinez, C., Cantero-Tubilla, B., Cantero, D., Sills, D., Cocero, M., & Tester, J. (2018). Acid and Alkali Catalyzed Hydrothermal Liquefaction of Dairy Manure Digestate and Food Waste. *ACS Sustainable Chemical Engineering*, 2724-2732.

Roman-Leshkov, Y., Barrett, C. J., Liu, Z., & Dumesic, J. A. (2007). Production of dimethylfuran for liquid fuels from biomass-derived carbohydrates. *Nature*, 982-985.

Shen, D. K., & Gu, S. (2009). The mechanism for thermal decomposition of cellulose and its main products. *Bioresource Technology*, 6496-6504.

Singh, R., Prakash, A., Balagurumurthy, B., Singh, R., Saran, S., & Bhaskar, T. (2015). Hydrothermal liquefaction of agricultural and forest biomass residue: comparative study. *Journal of Material Cycles and Waste Management*, 442-452.

SriBala, G., & Vinu, R. (2014). Unified Kinetic Model for Cellulose Deconstruction via Acid Hydrolysis. *Industrial & Engineering Chemistry Research*, 8714-8725.

Srokol, Z., Bouche, A., Van Estrik, A., Strik, R. C., Maschmeyer, T., & Peters, J. A. (2004). Hydrothermal upgrading of biomass to biofuel; studies on some monosaccharide model compounds. *Carbohydrate Research*, 1717-1726.

Thekkudan, D. F., Rutan, S. C., & Carr, P. W. (2010). A study of the precision and accuracy of peak quantification in comprehensive two-dimensional liquid chromatography in time. *Journal of Chromatography A*, 4313-4327.

Tripodi, A., Compagnoni, M., Martinazzo, R., Ramis, G., & Rossetti, I. (2017). Process Simulation for the Design and Scale Up of Heterogeneous Catalytic Process: Kinetic Modelling Issues. *Catalysts*, 159-191.

Wagner, W., & Pruss, A. (2002). The IAPWS Formulation 1995 for the Thermodynamic Properties of Ordinary Water Substance for General and Scientific Use. *Journal of Physical and Chemical Reference Data*, 387-535.

Wahab, M. F., Patel, D. C., & Armstrong, D. W. (2017). Total peak shape analysis: detection and quantitation of concurrent fronting, tailing, and their effect on asymmetry measurements. *Journal of Chromatography A*, 163-170.

Xiang, Q., Lee, Y., & Torget, R. (2004). Kinetics of glucose decomposition during dilute-acid hydrolysis of lignocellulosic biomass. *Applied Biochemistry and Biotechnology*, 1127-1138.

Yang, Y., & Li, B. (1999). Subcritical Water Extraction Coupled to High-Performance Liquid Chromatography. *Analytical Chemistry*, 1491–1495.

Yang, Y., Feng, C., Inamori, Y., & Maekawa, T. (2004). Analysis of energy conversion characteristics in liquefaction of algae. *Resources, Conservation and Recycling*, 21-33.

Yin, S., & Tan, Z. (2012). Hydrothermal liquefaction of cellulose to bio-oil under acidic, neutral and alkaline conditions. *Applied Energy*, 234-239.

Zhang, Y., & Cremer, P. S. (2006). Interactions between macromolecules and ions: the Hofmeister series. *Current Opinion in Chemical Biology*, 658-663.

Zhou, Y., Schideman, L., Yu, G., & Zhang, Y. (2013). A synergistic combination of algal wastewater treatment and hydrothermal biofuel production maximized by nutrient and carbon recycling. *Energy & Environmental Science*, 3765-3779.